

**PROTEOMIC ANALYSIS OF CELLULAR  
MODELS OF NEURODEGENERATION  
AND MITOCHONDRIAL DYSFUNCTION**

Florence Burté

A thesis submitted in partial fulfillment of the  
requirements of Nottingham Trent University  
for the degree of Doctor of Philosophy

October 2009

## **DECLARATION**

This work is the intellectual property of the author, and may also be owned by the research sponsor(s) and/or Nottingham Trent University. You may copy up to 5% of this work for private study, or personal, non-commercial research. Any re-use of the information contained within this document should be fully referenced, quoting the author, title, university, degree level and pagination. Queries or requests for any other use, or if a more substantial copy is required, should be directed in the first instance to the author."

## ACKNOWLEDGMENTS

Firstly, I would like to express my sincere thanks and gratitude to my supervisors Professor Ellen Billet, Dr Alan Hargreaves and Dr Luigi de Girolamo for their support, technical and moral help and encouragements throughout my PhD.

I also would like to acknowledge Professor Hartmut Kuhn at Charité, Humbolt University, Berlin for inviting me to work in his laboratory, under the supervision of Dr Christoph Ufer, who I sincerely thank for his help with molecular biology and for his tour of Berlin.

My work environment was made pleasant by all past and present colleagues from lab 106, namely, Asli, Heidi, Cheryl, Lyndsey, Gino, Christoph, David, Wayne, Julia, Bego and Ricky. Thank you for your technical help and support and also for the wonderful times (professional or personal!).

Thanks to a bunch of fellow PhD student colleagues that have shared this PhD experience with me and who I am now happy to call friends.

I would like to express special thanks to my most closest friends Stéphanie Laversin who has been at my side, sharing this experience all along, and well before; and Amélie Finelle who has been my dearest friend for so many years even thousands of kilometres away.

I am grateful to the Wells family, particularly Pat Wells, for their support and for the relaxing Sunday afternoons.

Finally, I would like to express my dearest love to my family and thank them for their support through the years, not only the last four ones. Thanks to mum, dad (merci maman et papa), Caroline, Robert, Muriel, Arnaud and my dear little niece Romane Stauffer.

I could not finish without thanking the person who has been putting up with my long hours of working and my stressful moods these last three years: thank you Gary Wells.

**ABSTRACT**

Mitochondrial dysfunction is thought to contribute to neurodegenerative processes. As an example, dysfunction of complex I of the electron transport chain has been observed in Parkinson's disease patients and 1-methyl-4-phenyl-1,2,3,6 tetrahydropyridine (MPTP), a complex I inhibitor, produces a Parkinsonian state in mammals. The aims of the present study were to determine the effects of MPTP on the mitochondrial proteome in a cellular model using mouse N2a neuroblastoma cells and to identify novel biomarkers of MPTP-induced toxicity.

The enrichment of mitochondria and the presence of cross-contamination from other subcellular components were monitored using a range of molecular markers. Mitochondrial proteins were then fractionated using an optimised 2-dimensional gel electrophoresis (2DE) protocol and the reproducibility of the method was investigated. A preliminary study comparing the mitochondrial proteome profile from two different states of mouse N2a neuroblastoma cells, mitotic and differentiated, was undertaken to establish whether differentiation of cells had major effects on the mitochondrial proteome. Since nine proteins showed changes in levels, which included stress-70 protein and aconitase, it was decided that differentiation did affect the mitochondrial proteome: hence, differentiated cells were used for further studies.

The effects of different concentrations (0 to 5 mM) and time-points (0 to 48 hours) of MPTP on plasma membrane integrity, cellular metabolic activity, cellular ATP concentration, mitochondrial potential, cytochrome c release and a variety of caspase activities were investigated. From this study, sub-cytotoxic and cytotoxic concentrations were defined and 1 mM MPTP for 24 hours was chosen as an example of a sub-cytotoxic concentration for further analysis. Using the previously optimised protocol for 2DE, mitochondrial preparations from differentiated N2a neuroblastoma cells treated with 1 mM MPTP for 24 hours were fractionated and compared to controls. Up to 32 proteins showed changes in protein levels, of which 10 were identified by peptide mass fingerprinting. Increases in the levels of 60 kDa heat shock protein (Hsp60), heat shock cognate 71 kDa protein (Hsc70), glutamate oxaloacetate 2 (GOT2) and voltage-dependent anion channel 1 (VDAC1) were validated as potential markers of MPTP-induced toxicity using western blot analysis. In parallel, a study of the mitochondrial phosphoproteome was undertaken. Despite the limitations of detection methods, a change in the phosphorylation status of a few mitochondrial proteins was observed following MPTP treatment, notably potential increased phosphorylation of Hsc70 and Hsp60.

Further analysis was undertaken in order to gain a better understanding of the increase in VDAC1 levels following sub-cytotoxic treatments with MPTP. Although VDAC1 protein levels were increasing in a dose- and time-dependent manner, no mRNA upregulation was observed. Similarly, the use of other inhibitors of the electron transfer chain led to increased VDAC1 protein levels but no change in mRNA. Finally, modulations in VDAC1 phosphorylation were observed following MPTP-induced toxicity, further implicating the channel in mitochondrial dysfunction.

To conclude, studies with this cellular model implicate the involvement of several mitochondrial pathways in the MPTP-induced Parkinsonian syndrome. In particular, alterations to VDAC1 may represent a novel target of neurodegeneration.

**LIST OF ABBREVIATIONS**

2DE: 2-dimensional gel electrophoresis  
3-NP: 3-nitropropionic acid  
ACN: Acetonitrile  
AD: Alzheimer's disease  
APS: Ammonium persulfate  
ASB-14: Aminosulfobetaine-14  
ATP: Adenosine triphosphate  
BCA: Bicinchoninic acid  
Bp: Base pair  
Bcl<sub>2</sub>: B-cell lymphoma 2  
BSA: Bovine serum albumine  
cDNA: Cyclic deoxyribonucleic acid  
CHAPS: 3-[(3-Cholamidopropyl)dimethylammonio]-1-propanesulfonate  
CHCA:  $\alpha$ -Cyano-4-hydroxycinnamic acid  
CK: creatine kinase  
DAT: Dopamine transporter  
dbcAMP: Dibutryl (DB) adenosine 3',5'-cyclic monophosphate  
DMEM: Dulbecco's Modified Eagle Medium  
DMSO: Dimethyl sulfoxide  
L-DOPA: 3,4-dihydroxy-L-phenylalanine  
DTT: Dithiothreitol  
EB: Extraction buffer  
ECL: Enhanced luminol-based chemiluminescent  
EDTA: Ethylene diamine tetraacetic acid  
EGTA: Ethylene glycol tetraacetic acid  
ER: Endoplasmic reticulum  
ERK: Extracellular signal-regulated kinase  
ETC: Electron transfer chain  
FBS: Foetal bovine serum  
GABA:  $\gamma$ -aminobutyric acid  
GAPDH: Glyceraldehyde-3-phosphate dehydrogenase  
GOT2: Glutamate oxaloacetate transaminase 2  
H<sub>2</sub>O<sub>2</sub>: Hydrogen peroxide  
HD: Huntington's disease  
HEPES: 4-(2-hydroxyethyl)-1-piperazineethanesulfonic acid  
HK: Hexokinase  
HRP: Horseradish peroxidase  
Hsp: Heat shock protein  
IEF: Isoelectrofocusing  
IMM: Inner mitochondrial membrane  
IMS: Intermembrane space  
INT: Iodonitrotetrazolium  
IPG: Immobilized pH gradient  
JNK: c-Jun N-terminal kinase  
LAMP2: Lysosomal-associated membrane protein 2

LC-MS: Liquid chromatography – mass spectrometry  
LDH: Lactate dehydrogenase  
LRRK2: Leucine-rich repeat kinase 2  
MALDI-TOF: Matrix-assisted laser desorption/ionisation – time-of-flight  
MAPK: Mitogen-activated protein kinase  
MAO: Monoamine oxidase  
MDH: Malate dehydrogenase  
MEK: Mitogen-activated protein kinase kinase 1  
MgCl<sub>2</sub>: Magnesium chloride  
MPTP: 1-methyl-4-phenyl-1,2,3,6-tetrahydropyridine  
mtDNA: Mitochondrial deoxyribonucleic acid  
MTT: 3-(4,5-Dimethylthiazol-2-yl)-2,5-diphenyltetrazolium bromide  
MW: Molecular weight  
NAC: N-acetyl-cysteine  
NaCl: Sodium chloride  
NADH: Nicotinamide adenine dinucleotide  
NADPH: Nicotinamide adenine dinucleotide phosphate  
NF-M: Neurofilament-medium  
NGF: Nerve growth factor  
NMDA: N-methyl-D-aspartate  
NOS: Nitric oxide synthase  
Nurr1: Nuclear receptor related 1  
O<sub>2</sub><sup>•-</sup>: superoxide anion  
OMM: Outer mitochondrial membrane  
PBS: Phosphate buffer saline  
PD: Parkinson's disease  
pI: Isoelectric point  
PINK1: PTEN induced putative kinase 1  
PSD: Post-source decay  
PTEN: phosphatase and tensin homolog  
RT-PCR: Reverse transcriptase – polymerase chain reaction  
RNA: Ribonucleic acid  
ROS: Reactive oxygen species  
SDH: Succinate dehydrogenase  
SDS-PAGE: Sodium dodecyl-sulfate  
SEM: Standard error of the mean  
SFM: Serum free medium  
siRNA: Silenced RNA  
STS: Staurosporine  
tBid: truncated Bid  
TBS: Tris buffer saline  
TCA: Trichloroacetic acid  
TEMED: Tetramethylethylene diamine  
TFA: trifluoroacetic acid  
UCHL-1: Ubiquitin carboxyl-terminal esterase L1  
UPS: Ubiquitin proteasome system  
VDAC: Voltage-dependent anion channel  
v/v: volume / volume  
w/v: weight / volume

## LIST OF CONTENTS

<b>ACKNOWLEDGMENTS</b> .....	<b>i</b>
<b>ABSTRACT</b> .....	<b>ii</b>
<b>LIST OF ABBREVIATIONS</b> .....	<b>iii</b>
<b>LIST OF CONTENTS</b> .....	<b>v</b>
<b>LIST OF FIGURES</b> .....	<b>xi</b>
<b>LIST OF TABLES</b> .....	<b>xiv</b>
<b>CHAPTER I:</b> .....	<b>1</b>
1.1 PARKINSON'S DISEASE AND OTHER NEURODEGENERATIVE CONDITIONS .....	2
1.1.1 Background to Parkinson's disease.....	2
1.1.2 Pathological features of Parkinson's disease .....	3
1.1.3 Pathological features of other neurodegenerative diseases.....	5
1.1.3.1 Alzheimer's disease .....	5
1.1.3.2 Huntington's disease.....	7
1.1.3.3 Amyotrophic lateral sclerosis.....	8
1.1.4 Common pathological features in neurodegenerative diseases.....	8
1.2 MITOCHONDRIA .....	9
1.2.1 General features .....	9
1.2.2 Mitochondrial cycle of life.....	10
1.2.3 Principal cellular roles of mitochondria.....	10
1.2.4 Mitochondria and neuronal cells.....	12
1.2.5 Mitochondrial dysfunction due to oxidative stress .....	13
1.3 CELL DEATH .....	14
1.3.1 Apoptotic cell death .....	14
1.3.1.1 Cysteine-dependent aspartate-directed proteases (caspases) .....	14
1.3.1.2 Bcl <sub>2</sub> family proteins.....	15
1.3.1.3 Molecular pathways of apoptosis.....	16
1.3.1.4 Regulation of apoptotic molecules by signaling kinases .....	19
1.3.2 Necrotic cell death .....	20
1.3.3 Autophagic cell death.....	20
1.3.4 Cell death and mitochondria .....	21
1.4 MPTP AS A MODEL FOR PARKINSON'S DISEASE .....	22
1.4.1 1-methyl-4-phenyl-1,2,3,6-tetrahydropyridine (MPTP) emergence as a toxin .....	22
1.4.2 MPTP as a model of Parkinson's disease .....	22
1.4.3 MPTP metabolism.....	23
1.4.4 Inhibition of complex I of the electron transfer chain.....	24
1.4.5 MPTP and generation of reactive oxygen species .....	24
1.4.6 Excitotoxicity and calcium homeostasis disruption.....	25
1.4.7 Proteolysis dysfunction .....	26
1.5 AIMS OF THE PROJECT .....	26

<b>CHAPTER II MATERIALS AND METHODS.....</b>	<b>28</b>
2.1 MATERIALS.....	29
2.1.1 Specialised equipment.....	29
2.1.2 Plastic ware .....	30
2.1.3 Glass ware .....	30
2.1.4 Laboratory reagents.....	30
2.1.4.1 Cell culture reagents.....	30
2.1.4.2 Laboratory reagents.....	30
2.1.5 Antibodies .....	30
2.1.5.1 Primary antibodies .....	31
2.1.5.2 Secondary antibodies .....	31
2.2 METHODS .....	32
2.2.1 Cell culture of mouse N2a neuroblastoma cells.....	32
2.2.1.1 Maintenance of N2a neuroblastoma cells .....	32
2.2.1.2 Subculture of N2a neuroblastoma .....	32
2.2.1.3 Cell seeding.....	32
2.2.1.4 Cryo-preservation of cells .....	33
2.2.1.5 Resuscitation of cryo-preserved cells.....	33
2.2.1.6 Differentiation of N2a cells.....	33
2.2.1.7 MPTP treatment .....	34
2.2.1.8 Staurosporine (STS) treatments .....	34
2.2.1.9 Caspase-3/7 inhibitor treatment .....	34
2.2.2 Cell viability.....	35
2.2.2.1 Morphology of the cells .....	35
2.2.2.2 Trypan blue exclusion assay .....	35
2.2.2.3 MTT assay.....	35
2.2.2.4 JC-1 fluorescent stain.....	36
2.2.2.5 Cellular ATP assay.....	36
2.2.3 Protein estimation of samples .....	38
2.2.4 Differential centrifugation.....	38
2.2.4.1 Cell harvesting .....	38
2.2.4.2 Homogenisation of the sample.....	39
2.2.4.3 Differential centrifugation protocol .....	39
2.2.5 SDS-PAGE.....	41
2.2.5.1 Preparation of resolving gel .....	41
2.2.5.2 Preparation of stacking gel.....	42
2.2.5.3 Preparation of samples and loading .....	42
2.2.5.4 Running the gel .....	42
2.2.6 Immunoblotting.....	43
2.2.6.1 Wet western blotting .....	43
2.2.6.2 Immunoprobng.....	43
2.2.6.3 Stripping and re-probing of western blot .....	45
2.2.6.4 Quantification of bands detected on western blot.....	46
2.2.7 Purity assessment of subcellular fractions using activity assays .....	47
2.2.7.1 Succinate dehydrogenase activity assay.....	47
2.2.7.2 NADPH-cytochrome c reductase (NADPH-CR)activity assay .....	47
2.2.7.3 Marker protein detection by western blot analysis .....	48
2.2.8 2-Dimensional-SDS-PAGE (2DE).....	48
2.2.8.1 First dimension: the IEF step .....	48

2.2.8.2	Equilibration of strips.....	50
2.2.8.3	Second dimension: SDS-PAGE .....	50
2.2.8.4	Gel staining .....	50
2.2.8.5	2D-SDS-PAGE image analysis.....	52
2.2.9	Spot picking and trypsinisation.....	53
2.2.10	Mass spectrometry and database searching.....	54
2.2.11	Phosphorylated amino acid co-localisation with VDAC detection using 2D- blot analysis.....	54
2.2.12	Caspase-3 activity assay.....	55
2.2.12.1	Fluorimetric activity assay .....	55
2.2.12.2	Bicinchoninic (BCA) protein assay .....	56
2.2.12.3	Data analysis .....	57
2.2.13	RT-PCR.....	57
2.2.13.1	RNA isolation from cells .....	57
2.2.13.2	Reverse transcription.....	58
2.2.13.3	Polymerase chain reaction (PCR) .....	58
2.2.13.4	Agarose gel electrophoresis .....	59
2.2.14	Real-time RT PCR .....	60
2.2.14.1	Sample preparation.....	60
2.2.14.2	DNA standards preparation.....	60
2.2.14.3	Standard dilutions .....	61
2.2.14.4	Real-time PCR .....	61
2.2.14.5	Data analysis .....	62

### **CHAPTER III: ESTABLISHING METHODS FOR THE ANALYSIS OF THE MITOCHONDRIAL PROTEOME ..... 63**

3.1	INTRODUCTION .....	64
3.1.1	Pre-differentiated mouse neuroblastoma cells: a model to investigate Parkinson's disease .....	64
3.1.1.1	Experimental models of study for Parkinson's disease .....	64
3.1.1.2	<i>In vitro</i> cultured cells .....	65
3.1.1.3	Mouse N2a neuroblastoma and their differentiation.....	65
3.1.2	Isolation of mitochondria using subcellular fractionation .....	66
3.1.2.1	Subcellular fractionation methods .....	66
3.1.3	Studying the mitochondrial proteome using a proteomic approach.....	68
3.1.3.1	Proteomics techniques.....	68
3.1.3.2	The mitochondrial proteome.....	69
3.1.4	Aims of the chapter .....	69
3.2.1	Comparison of protein recovery in the mitochondrial fraction following subcellular fractionation in mitotic N2a and SH-SY5Y neuroblastoma cells.....	71
3.2.2	Subcellular fractionation using mitotic and differentiated mouse N2a neuroblastoma cells.....	72
3.2.2.1	Comparison of protein recovery in the mitochondrial fraction following subcellular fractionation in mitotic and differentiated mouse N2a cells.....	72
3.2.2.2	Mitochondrial markers in fractions from mitotic and differentiated cells.....	73
3.2.2.3	Cytoplasmic marker in fractions from differentiated cells .....	75
3.2.2.4	Nuclear marker in fractions from differentiated cells.....	75
3.2.2.5	Lysosomal markers in fractions from differentiated cells.....	75

3.2.2.6	Microsomal marker .....	75
3.2.3	Optimisation of 2D-gel electrophoresis .....	78
3.2.3.1	Sample preparation.....	78
3.2.3.2	Equilibration conditions.....	83
3.2.4	Reproducibility of mini 2D-gel electrophoresis.....	84
3.2.4.1	Intra-sample reproducibility.....	84
3.2.4.2	Inter-sample reproducibility.....	87
3.2.5	Reproducibility of large 2D-gel electrophoresis.....	90
3.2.6	Choice of staining method .....	90
3.2.7	Summary of 2D-gel electrophoresis optimisation.....	92
3.2.8	Mass Spectrometry.....	94
3.2.9	Mitochondrial proteome changes between mitotic and differentiated phenotypes.....	94
3.2.9.1	Morphological changes.....	94
3.2.9.2	Changes in the mitochondrial proteome .....	99
3.3	DISCUSSION .....	102
3.3.1	Purity of subcellular fractions .....	102
3.3.2	2DE: optimization and reproducibility.....	103
3.3.3	Integrity of mitochondrial fractions on 2DE.....	106
3.3.4	Changes in the mitochondrial proteome following cell differentiation .....	107

#### **CHAPTER IV: EFFECTS OF MPTP ON CELL VIABILITY OF DIFFERENTIATED MOUSE N2A NEUROBLASTOMA CELLS ..... 110**

4.1	INTRODUCTION .....	111
4.1.1	Effects of MPTP on cell viability and mitochondrial activity in mouse N2a neuroblastoma cells.....	111
4.1.1.1	MPTP-mediated sub-cytotoxic effects.....	111
4.1.1.2	Monitoring cell viability following MPTP treatment in mouse N2a neuroblastoma cells.....	111
4.1.1.3	Monitoring mitochondrial activity following MPTP treatment in mouse N2a neuroblastoma cells .....	112
4.1.2	Investigation of cell death pathways.....	113
4.1.2.1	Cellular markers of necrosis.....	113
4.1.2.2	Cellular markers of apoptosis .....	114
4.1.3	Aims of the chapter .....	115
4.2	RESULTS .....	116
4.2.1	Assessment of effects of MPTP on N2a neuroblastoma cell viability.....	116
4.2.1.1	Cellular morphology .....	116
4.2.1.2	Cell membrane integrity.....	119
4.2.1.3	MTT reduction assay .....	119
4.2.1.4	Cellular ATP content .....	121
4.2.1.5	Mitochondrial potential.....	121
4.2.2	Effects of MPTP on apoptosis markers.....	124
4.2.2.1	Apoptotic morphology .....	124
4.2.2.2	Pro-caspase-2 cleavage.....	126
4.2.2.3	Cytochrome c release .....	126
4.2.2.4	Cleaved caspase-3 .....	126
4.2.2.5	Caspase-3/7 activation .....	128

4.3	DISCUSSION .....	132
4.3.1	MPTP effects on cell viability and mitochondrial activity of N2a neuroblastoma .....	132
4.3.1.1	Establishment of MPTP sub-cytotoxic concentrations .....	132
4.3.1.2	Effects of MPTP on mitochondrial activity .....	134
4.3.2	Markers of MPTP-induced cell death in mouse N2a neuroblastoma .....	136

## **CHAPTER V: EFFECTS OF MPTP ON THE MITOCHONDRIAL PROTEOME .**

5.1	INTRODUCTION .....	142
5.1.1	Proteomic approaches to a study of the mitochondrial proteome .....	142
5.1.2	Molecular markers linking mitochondrial dysfunction and Parkinson's disease .....	142
5.1.3	Signaling pathways in Parkinson's disease .....	143
5.1.4	Study of the mitochondrial phosphoproteome .....	144
5.1.5	Approaches to the study of the phosphoproteome .....	145
5.1.6	Aims of the chapter .....	145
5.2	RESULTS .....	147
5.2.1	MPTP effects on the mitochondrial proteome from differentiated mouse N2a neuroblastoma cells .....	147
5.2.1.1	pI 3-10 analysis .....	147
5.2.1.2	pI 5-8 analysis .....	148
5.2.1.3	pI 7-10 .....	153
5.2.1.4	Validation of markers .....	153
5.2.2	Effects of MPTP on the phosphoproteome .....	160
5.2.2.1	Study of the phosphoproteome using western blot analysis .....	160
5.2.2.2	Study of the phosphoproteome using SDS-PAGE analysis .....	167
5.3.1	Effects of MPTP on N2a neuroblastoma mitochondrial proteome .....	176
5.3.2	Effects of MPTP toxicity on phosphorylating pathways .....	178
5.3.3	Mitochondrial markers of MPTP-induced toxicity .....	179
5.3.3.1	Chaperone and co-chaperone proteins sensitive to MPTP-induced toxicity .....	179
5.3.3.2	Metabolic enzyme protein levels .....	182
5.3.3.3	Proteins linked to oxidative phosphorylation .....	185
5.3.3.4	Voltage-dependent-anion channel 1 .....	186

## **CHAPTER VI: MODIFIED EXPRESSION OF VOLTAGE-DEPENDENT ANION CHANNEL FOLLOWING MPTP TREATMENT .....**

6.1	INTRODUCTION .....	188
6.1.1	The voltage-dependent anion channel .....	188
6.1.1.1	Structure and general functions .....	188
6.1.1.2	The role of VDAC in cell death .....	190
6.1.1.3	The role of VDAC in glycolysis .....	192
6.1.2	Electron transfer chain inhibitors .....	192
6.1.2.1	Rotenone: a complex I inhibitor .....	192
6.1.2.2	3-nitropropionic acid: a complex II inhibitor .....	193
6.1.2.3	Antimycin A: a complex III inhibitor .....	193
6.1.2.4	Sodium azide: a complex IV inhibitor .....	193

6.1.3	Aims of the chapter .....	194
6.2	RESULTS .....	195
6.2.1	Effects of neurotoxins on VDAC expression.....	195
6.2.1.1	Identification of VDAC1 from 2DE using MALDI-TOF mass spectrometry.....	195
6.2.1.2	Concentration and time-dependent MPTP effects on VDAC levels.....	195
6.2.1.3	Effects of other complex inhibitors on VDAC protein levels.....	200
6.2.1.4	VDAC1 mRNA expression.....	200
6.2.2	VDAC post-translational modifications.....	204
6.2.2.1	Multiple forms of VDAC1 identified on 2D-western blot analysis.....	204
6.2.2.2	..... Serine phosphorylation of VDAC1 increased following MPTP treatment .....	208
6.2.2.3	Threonine phosphorylation of VDAC1 decreased following MPTP treatment .....	208
6.2.2.4	Potential phosphorylated peptides observed using peptide mass fingerprinting .....	210
6.3	DISCUSSION .....	212
6.3.1	Identification of VDAC1 isoforms in the mitochondrial proteome .....	212
6.3.2	Changes in VDAC1 protein levels following MPTP treatment.....	213
6.3.2.1	Links between increased VDAC1 levels and cell death markers .....	213
6.3.2.2	..... Effects of other inhibitors of the electron transfer chain on VDAC1 levels .....	213
6.3.2.3	Significance of increased levels of VDAC1 .....	214
6.3.3	Phosphorylation state of VDAC1 following MPTP treatment .....	218
<b>CHAPTER VII: GENERAL DISCUSSION.....</b>		<b>220</b>
7.1	STUDY OF THE MITOCHONDRIAL PROTEOME .....	221
7.1.1	Mitochondrial enrichment and purity following subcellular fractionation .....	221
7.1.2	Mitochondrial proteome resolved on mini-2DE .....	221
7.1.3	Limitations of 2DE protocol and further recommendations .....	221
7.1.4	Study of the mitochondrial phosphoproteome: limitations and future recommendations .....	222
7.2	MPTP EFFECTS ON MOUSE N2a NEUROBLASTOMA .....	223
7.2.1	Cellular effects .....	223
7.2.2	MPTP effects on the mitochondrial proteome .....	224
7.3	VDAC .....	225
7.3.1	The role of VDAC in neurodegeneration.....	225
7.3.2	Future recommendations for VDAC studies.....	226
7.4	CONCLUSION.....	228
<b>CHAPTER VIII: REFERENCES .....</b>		<b>229</b>

## LIST OF FIGURES

## CHAPTER I

Figure 1.1: Schematic overview of molecular pathways involved PD neurodegeneration ...	6
Figure 1.2: Electron micrograph of a typical mitochondrion.....	10
Figure 1.3: Schematic diagram of the electron transfer chain .....	11
Figure 1.4: ROS production from oxygen .....	13
Figure 1.5: Schematics representing the molecular events involved in the extrinsic pathway in mitochondria-independent and mitochondria dependent pathways.....	17
Figure 1.6: Schematics representing molecular events involved in the intrinsic pathway. .	18
Figure 1.7: MPTP metabolism .....	24

## CHAPTER II

Figure 2.1: Typical standard calibration graph for ATP using the ViaLight HS bioluminescent method. ....	37
Figure 2.2: Scheme of the subcellular fractionation protocol.....	40
Figure 2.3: Copper stained western blots showing total protein staining of different samples.....	46
Figure 2.4: Copper stained 2D-blots showing total protein staining and VDAC1 location	55

## CHAPTER III

Figure 3.1: Succinate dehydrogenase activity and cytochrome c protein level in each fraction compared to total extract from mitotic and differentiated cells.....	74
Figure 3.2: GAPDH and lamin A/C protein levels present in each fraction compared to total extract.....	76
Figure 3.3: LAMP 2 protein level and NADPH-cytochrome c reductase activity in each fraction compared to total extract from differentiated cells.....	77
Figure 3.4: Differences in spot detection using three different detergents (CHAPS, Triton-X-100 and ASB-14) in the IEF buffer in 2DE analysis .....	80
Figure 3.5: Influence of acetone precipitation prior to fractionation by 2DE and of thiourea inclusion in the IEF buffer on spot detection .....	82
Figure 3.6: Triplicate gels electrophoresed in parallel.....	85
Figure 3.7: Map of a 2DE showing expression changes between replicates of the same sample electrophoresed on different days .....	88
Figure 3.8: Map of a 2DE showing expression changes between replicates of different samples electrophoresed in parallel .....	89
Figure 3.9: Large-scale 2DE of mitochondrial proteins from differentiated mouse N2a neuroblastoma .....	91
Figure 3.10: 3-dimensional image of two different spots from a large 2DE .....	93
Figure 3.11: Differences in spot detection using silver stain compared to SyproRuby .....	93
Figure 3.12: 2DE (pI 3-10) stained with SyproRuby showing spots identified following peptide mass fingerprinting.....	95
Figure 3.13: Example of MALDI-TOF analysis and protein identification of spot 9 from figure 3.12 .....	98

Figure 3.14: Differentiated mouse N2a neuroblastoma cell morphology compared to mitotic cell morphology .....	99
Figure 3.15: Large-2DE (pI 3-10) stained with silver stain showing spots changing in levels when cells are differentiated compared to mitotic cells.....	100

#### CHAPTER IV

Figure 4.1: Morphological changes of mouse N2a neuroblastoma cells following exposure to MPTP for 24 hours.....	117
Figure 4.2: Morphological changes of mouse N2a neuroblastoma cells following exposure to MPTP for 48 hours.....	118
Figure 4.3: Effects of different concentrations of MPTP on cell viability using two different assays in differentiated N2a cells following 24 hour and 48 hour treatments .....	120
Figure 4.4: Effects of different concentrations of MPTP on ATP levels in differentiated N2a cells following 24 hour and 48 hour treatments.....	122
Figure 4.5: Effects of different concentrations of MPTP on mitochondrial membrane potential in mouse N2a neuroblastoma cells following 24 hours treatment .....	123
Figure 4.6: Time-course of morphological changes of N2a neuroblastoma cells due to 1 mM MPTP treatment as compared to staurosporine, inducer of apoptosis. ....	125
Figure 4.7: Detection of apoptotic markers in differentiated N2a neuroblastoma cells by western blot analysis .....	127
Figure 4.8: Effects of different concentrations and time-points of MPTP on caspase-3/7 activity in differentiated N2a cells .....	129
Figure 4.9: Effects of different concentrations of caspase-3/7 inhibitor on cell viability in differentiated N2a cells following 25 hours exposure .....	130
Figure 4.10: Inhibition of caspase-3/7 activity due to MPTP neurotoxicity.....	131

#### CHAPTER V

Figure 5.1: Mini 2D-electrophoretogram (pI 3-10) stained with SyproRuby showing spots changing in levels in MPTP treated differentiated N2a cells.....	149
Figure 5.2: Mini 2D-electrophoretogram (pI 5-8) stained with SyproRuby showing spots changing in levels in MPTP treated differentiated N2a cells.....	151
Figure 5.3: Mini 2D-electrophoretogram (pI 7-10) stained with SyproRuby showing spots changing in levels in MPTP treated differentiated N2a cells.....	154
Figure 5.4: Changes in 60 kDa heat shock protein (Hsp60) levels in various subcellular fractions following 1 mM MPTP treatment for 24 hours .....	155
Figure 5.5: Changes in heat shock cognate 71 kDa protein (Hsc70) in various subcellular fractions following 1 mM MPTP treatment for 24 hours .....	157
Figure 5.6: Changes in glutamate oxaloacetate transaminase 2 (GOT2) in various subcellular fractions following 1 mM MPTP treatment for 24 hours.....	158
Figure 5.7: Changes in voltage-dependent anion channel 1 (VDAC1) levels in various subcellular fractions following 1 mM MPTP treatment for 24 hours.....	159
Figure 5.8: Detection of proteins phosphorylated via a serine amino acid in various subcellular fractions in cells treated with 1 mM MPTP compared to controls.....	162
Figure 5.9: 2D-blot detection of proteins phosphorylated via a phosphoserine amino acid in mitochondrial fractions from cells treated with 1 mM MPTP for 24 hours compared to controls.....	164

Figure 5.10: Detection of proteins phosphorylated via a threonine amino acid in various subcellular fractions in cells treated with 1 mM MPTP compared to controls .....	166
Figure 5.11: Detection of proteins phosphorylated via a tyrosine amino acid in various subcellular fractions in cells treated with 1 mM MPTP compared to controls .....	169
Figure 5.12: Detection of phosphorylated proteins in mitochondrial fractions following 1 mM MPTP treatment for 24 hours using 1D-SDS-PAGE .....	170
Figure 5.13: Detection of phosphorylated proteins in mitochondrial fractions using 2DE (pI 3-10) .....	172
Figure 5.14: Detection of phosphorylated proteins in mitochondrial fractions using 2DE (pI 5-8 range strips) .....	175
Figure 5.15: Biochemical reactions involved in the TCA cycle and the link with the first enzyme of amino acid synthesis, GOT2 .....	183

## CHAPTER VI

Figure 6.1: VDAC folding pattern in the OMM as deduced by functional studies .....	188
Figure 6.2: 2D-gel electrophoretogram (pI 3-10) stained with SyproRuby showing spots identified as VDAC isoforms following peptide mass fingerprinting .....	196
Figure 6.3: MALDI-TOF analysis and protein identification of VDAC1 spot .....	197
Figure 6.4: VDAC1 protein expression following exposure to different MPTP concentrations for 24 hours .....	198
Figure 6.5: VDAC protein expression following exposure to 1 mM MPTP treatment over 24 hour time-course .....	199
Figure 6.6: Sub-cytotoxic and cytotoxic concentrations of various complex inhibitors measured by MTT reduction assay .....	201
Figure 6.7: Effects of subcytotoxic concentrations of complex inhibitors on VDAC1 protein levels using western blot analysis .....	202
Figure 6.8: Effects of 1 mM MPTP for 24 hours VDAC1 mRNA expression as measured by semi-quantitative RT-PCR .....	203
Figure 6.9: Example of quantitative analysis of VDAC1 mRNA expression using real-time PCR .....	205
Figure 6.10: Effects of electron transfer inhibitors on VDAC1 mRNA expression as measured by real-time PCR .....	206
Figure 6.11: Detection of VDAC isoforms on 2D-blot analysis using pI 3-10 and pI 7-10 strips .....	207
Figure 6.12: Co-localisation of phosphorylated residues and VDAC1 using 2D-blot analysis .....	209
Figure 6.13: Mouse VDAC1 amino acid sequence showing 2 phosphopeptides identified by MALDI-TOF PMF with potential kinase phosphorylation sites on each peptide .....	211
Figure 6.14: Hypothetic molecular events of MPTP effects leading to cell death .....	217

## CHAPTER VII

Figure 7.1: Schematic representation of MPTP effects on mitochondrial processes and cellular consequences .....	227
---	-----

## LIST OF TABLES

### CHAPTER II

Table 2.1: ATP stock concentrations used to produce an ATP calibration graph. ....	37
Table 2.2: ATP Concentration for each standard used to produce a calibration graph. ....	37
Table 2.3: Preparation of BSA standards and samples prior Bio-Rad protein estimation... ..	38
Table 2.4: Preparation of 10 ml polyacrylamide resolving gels for mini gels. ....	41
Table 2.5: Preparation of polyacrylamide stacking gels. ....	42
Table 2.6: Epitope and species specificity for each antibody used for immunoblotting. ....	45
Table 2.7: Silver staining steps .....	51
Table 2.8: SyproRuby staining steps.....	52
Table 2.9: ProQ Diamond staining steps. ....	52
Table 2.10: Serial dilutions of BSA standards using the provided 2 mg/ml BSA stock.....	56
Table 2.11: Sequences of primers used.....	58
Table 2.12: Master mix containing SensiMix SYBR for real-time PCR.....	61

### CHAPTER III

Table 3.1: Protein recovery in the mitochondrial fractions from mitotic mouse N2a and human SH-SY5Y cells .....	72
Table 3.2: Protein recovery in the mitochondrial fractions from mitotic and differentiated mouse N2a neuroblastoma cells.....	73
Table 3.3: Effects of CHAPS and triton-X-100 detergents on spot number and total spot volume resolved on 2DE.....	79
Table 3.4: Effects of CHAPS and triton-X-100 detergents on spot number and total spot volume resolved on 2DE.....	81
Table 3.5: Gel properties of the same sample electrophoresed by 2DE in parallel .....	86
Table 3.6: Reproducibility between triplicates of the same sample electrophoresed by 2DE in parallel.....	86
Table 3.7: Summary of the results for the optimisation of 2D-gel electrophoresis .....	92
Table 3.8: Protein identification of spots from 2DE (gel image in figure 3.12).....	97
Table 3.9: Quantitative analysis of spots showing significant changes in differentiated cell profiles compared to mitotic cells .....	101

### CHAPTER IV

Table 4.1: Summary of the toxicity assays used to assess MPTP effects on differentiated N2a neuroblastoma cells .....	133
---	-----

### CHAPTER V

Table 5.1: Quantitative analysis of spots showing significant changes in MPTP treated profiles compared to controls (pI 3-10 analysis).....	150
Table 5.2: Quantitative analysis of spots showing significant changes in MPTP treated profiles compared to controls (pI 5-8 analysis).....	152
Table 5.3: Identified proteins showing changes in levels following sub-cytotoxic MPTP concentrations .....	177

# **CHAPTER I:**

## **GENERAL INTRODUCTION**

## 1.1 PARKINSON'S DISEASE AND OTHER NEURODEGENERATIVE CONDITIONS

### 1.1.1 Background to Parkinson's disease

Parkinson's disease (PD) was first described by James Parkinson in 1817. It is the second most common neurodegenerative disorder after Alzheimer's disease (Palacino *et al.*, 2004). It affects 0.2 % of the population worldwide (Smith, 2002), and around 1 % of individuals over 50 years-old (Huang *et al.*, 2004); the incidence is increasing as the world's elderly population grows. The mean age of onset is 55 years-old with the risk of developing the disease increasing five-fold by 70 years-old (Hald and Lotharius, 2005). However, in rare cases, an early onset of the disease is observed in patients below 40 years-old (Golbe, 1990).

Parkinson's disease is a disorder with neurological impairment in controlling movement. The clinical features appear progressively; starting commonly by tremors in the hand, that can progress to bradykinesia, akinesia and postural instability (reviewed in Lane *et al.*, 2008).

The aetiology of the disease has not been completely resolved but the origin of the disorder is the selective degeneration of dopaminergic neurons, mainly in the substantia nigra *pars compacta*, but also in other parts of the brain such as the locus coeruleus, nucleus basalis, hypothalamus, cerebral cortex, cranial nerve motor nuclei, and central and peripheral components of the autonomic nervous system (Olanow and Tatton, 1999). The substantia nigra was first described by Trétiakoff in 1919. Its name reflects a particular dark pigmentation due to the presence of neuromelanin in the cells. The function of nigral cells is mainly attributed to the regulation of motility and movement. Nigral cells secrete dopamine and their axons provide a dense innervation to the corpus striatum; nearly 80 % of all dopamine in the brain is found in the striatum (and dopamine modulates striatal  $\gamma$ -aminobutyric acid-producing (GABAergic) neurons).

In PD patients, symptoms appear following the degeneration of over 50 % of the nigral dopaminergic neurons and corresponding to a reduction to 20 % of the levels of dopamine in the striatum (Deumens *et al.*, 2002). Consequently, the balance between dopamine and other neurotransmitters, such as acetylcholine, is disturbed, resulting in dysfunction in muscle motility.

Over 90 % of PD cases are thought to be sporadic, the rest being linked to genetic causes (Huang *et al.*, 2004). Sporadic cases may be caused by several factors, including environmental factors. Examples of environmental factors are pesticides such as rotenone (Zhou *et al.*, 2004) or paraquat (Brown *et al.*, 2006). Several mutated genes have been linked to PD; the most common mutated protein and first to be discovered was  $\alpha$ -synuclein (Golbe *et al.*, 1990; for other examples see section 1.1.2).

Although treatments are available to alleviate the symptoms, there is currently no treatment to prevent neurodegeneration. The main treatment involves the use of 3,4-dihydroxy-L-phenylalanine (L-DOPA), a precursor of dopamine (Lane *et al.*, 2008). Monoamine oxidase (MAO) inhibitors can also be administered to block the breakdown of dopamine in neurons (Leung and Mok, 2005). Other treatments directed to stimulating the dopaminergic nervous system or inhibiting dopamine catabolism, as well as the use of antioxidants, are being trialled (Lane *et al.*, 2008).

Another treatment, called deep-brain stimulation, consists of implanting electrodes in the subthalamus. This stimulates the deep-brain nuclei, which can result instantly in the regression of the tremors (Lane *et al.*, 2008).

### **1.1.2 Pathological features of Parkinson's disease**

The exact aetiology has not been resolved yet but several pathological hallmarks of PD have been observed in patients. Observations in sporadic and genetic forms of the disease suggest that mitochondrial dysfunction is one of the main factors in the neurodegeneration. In particular, complex I activity of the electron transfer chain (ETC) is decreased by up to 30 % in brains, muscles and platelets from patients (Schapira *et al.*, 1990). The use of complex I inhibitors in models of study reproduces similar biochemical features to those observed in PD patients (Cardoso *et al.*, 2005). Coenzyme Q 10, an antioxidant improving the ETC function, is also impaired in patients (Cardoso *et al.*, 2005). These two factors can lead to increased intracellular oxidative stress, reduced ATP production and proton gradient impairment. Mutations in DJ-1, PTEN-induced putative kinase 1 (PINK1),  $\alpha$ -synuclein and the protease Htra2 / Omi have all been linked to genetic forms of the disease and also are all either localised in the mitochondria or linked to mitochondrial function (Fitzgerald and Plun-Favreau, 2008). Additionally, mitochondrial DNA (mtDNA) deletions have been observed at higher levels in aging substantia nigra, in particular in PD brains (Bender *et al.*,

2005 and Kraytsberg *et al.*, 2005). Whether this could be a cause of mitochondrial dysfunction in PD or a consequence of high levels of oxidative stress in mitochondria has not been resolved.

Another feature of PD is excitotoxicity of dopaminergic neurons, due to hyperstimulation of glutamate receptors, which can activate  $\text{Ca}^{2+}$  channels leading to increased intracellular  $\text{Ca}^{2+}$  concentrations. Disruption of calcium homeostasis could have effects on mitochondrial function and increase nitric oxide synthase (NOS) levels, contributing to increased oxidative stress (Brazilai and Melamed, 2003). Interestingly, complex I inhibition by specific inhibitors (e.g. rotenone and  $\text{MPP}^+$ ) was also found to cause excitotoxicity (Barzilai and Melamed, 2003).

A pathological hallmark of PD was observed in 1912 by Lewy, who observed intracytoplasmic inclusions (Lewy bodies) in post-mortem neurons from PD patients (described in Holdorff, 2002). Since then, these inclusions have been the subject of many studies and their formation is thought to be linked to proteolytic impairment, particularly in the ubiquitin-proteasome system (UPS). Indeed, mutations in the parkin gene leading to loss of ubiquitin ligase activity (Greenmyre and Hastings, 2004), the ubiquitin carboxyl-terminal esterase L1 (UCHL-1) gene, which encodes a neuronal specific deubiquitinating enzyme (Leroy *et al.*, 2003) and in the  $\alpha$ -synuclein gene, coding for a potential substrate of the UPS and also a major component of Lewy bodies (Zhang *et al.*, 2008), are all linked to genetic cases of PD patients. Decreased proteasome activity has been reported in the substantia nigra *pars compacta* of PD brains (McNaught and Jenner, 2001), suggesting the role of disrupted proteolytic pathways in the pathology.

Inflammation has also been linked to the disease. Indeed, activation of astrocytes and microglia was observed in the substantia nigra of PD patients (McGeer *et al.*, 1998). Astrocytes can be activated by inflammatory factors and C reactive protein, which was shown to be upregulated in PD patients and can in turn activate NOS and cyclooxygenase 2 (McGeer *et al.*, 1998). To support these observations, high levels of cytokines and antibodies against proteins oxidised by dopamine were found in cerebrospinal fluid and striatum (Hald and Lotharius, 2005). This activation may be due to neuronal cell death but it is not really known if the consequences would be protective or would exacerbate neurodegeneration (Hald and Lotharius, 2005).

The pathological features observed in PD patients seem to be all linked to a further biochemical hallmark: oxidative stress. The substantia nigra is a part of the brain that is

more particularly vulnerable to oxidative stress due to dopamine auto-oxidation and MAO-induced production of hydrogen peroxide ( $H_2O_2$ ) (Blum *et al.*, 2001). Indeed, PD patients have high levels of iron, NOS and lipid peroxidation coupled with a loss of antioxidant defences (Ghandi and Wood, 2005). Additionally, as noted earlier, in some genetic cases a mutation in DJ-1, which encodes a scavenger of  $H_2O_2$  and potential chaperone, has been observed. Causes of increased oxidative stress could be linked to the observed inflammation reaction but it could also be linked to mitochondrial dysfunction, for example, via mitochondrial calcium homeostasis impairment and complex I inhibition (Blum *et al.*, 2001). Consequences of oxidative stress could include disruption of calcium homeostasis, UPS impairment, aggregation of oxidised proteins and activation or inhibition of various signaling pathways (figure 1.1).

### **1.1.3 Pathological features of other neurodegenerative diseases**

#### **1.1.3.1 Alzheimer's disease**

Alzheimer's disease (AD) is the most common neurodegenerative disease (Butterfield *et al.*, 2006), affecting around 1.4 % of the population in the USA, and the leading cause of dementia worldwide (Conejero-Goldberg *et al.*, 2008). It is characterised by progressive impairment in language, skilled movement, recognition and decision making (Conejero-goldberg *et al.*, 2008). It is due to the degeneration of cholinergic neurons from the forebrain, hippocampal pyramidal and cortical neurons (Cassarino and Bennet, 2008).

The pathological hallmarks of the disease include the formation of intraneuronal fibrillary tangles, mainly composed of phosphorylated tau protein (cytoskeletal protein), and the formation of extracellular plaques, mainly composed of oxidised amyloid (Cassarino and Bennett, 1999). Increased intracellular levels of calcium are observed, contributing to an increase of reactive oxygen species (ROS) and the impairment of mitochondrial and endoplasmic reticulum calcium homeostasis.

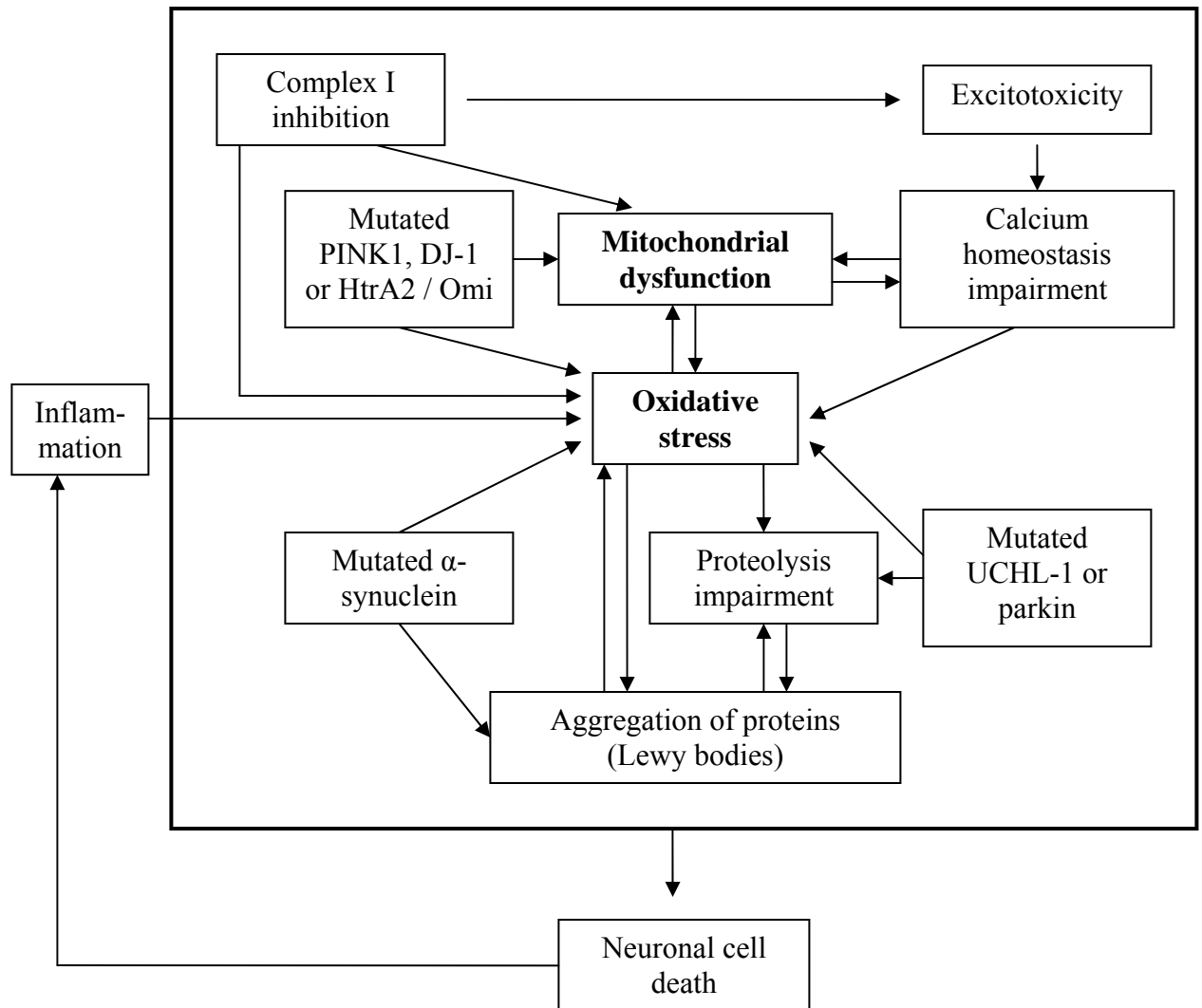


**Figure 1.1: Schematic overview of molecular pathways involved PD neurodegeneration**

Tightly linked to oxidative stress, mitochondrial dysfunction is also observed in AD patients, with complex IV of the ETC impaired (Atamna and Frey, 2007). Whether mitochondrial impairment is the cause or the consequence of increased oxidative stress has not been resolved. However, increased oxidative damage is associated with increased mtDNA mutations in AD brains (Cassarino and Bennet, 1999). Other markers of oxidative damage have been observed in AD brains such as increased levels of iron and lipid peroxidation. Finally inflammatory reactions have also been observed in AD patients and may exacerbate oxidative stress in cholinergic neurons (McGeer and McGeer, 1998).

#### 1.1.3.2 Huntington's disease

Huntington's disease (HD) affects 7 in 100,000 people worldwide (Mitra and Finkbeiner, 2008). It is characterised by involuntary movement, dystonia, rigidity, lack of coordination of movements, saccadic eye movements and inability to voluntarily maintain muscle tone (Mitra and Finkbeiner, 2008). It is due to the degeneration of neurons from the basal ganglia and brain cortex caused by a mutation in the huntingtin gene leading to a polyglutamylation of the resultant protein (Mitra and Finkbeiner, 2008). The mutant protein is cleaved into fragments that deposit into large inclusion bodies found in the neuronal cytoplasm, nucleus and processes (Mitra and Finkbeiner, 2008). The UPS has been observed to be the major proteolytic pathway involved in huntingtin degradation and inclusion formation is reversed by increasing the proteasome activity indicating a key role of the latter in HD (Mitra and Finkbeiner, 2008). In addition to proteolytic dysfunction, mitochondrial dysfunction has also been implicated in HD. Indeed, complex II of the ETC is impaired in post-mortem brains from HD patients together with disruption of calcium signaling pathways and depolarisation of the mitochondrial membrane potential, decreased ATP production and reduced cellular metabolism (Perez-de la Cruz and Santamaria, 2007). Consistent with mitochondrial dysfunction and protein accumulation, high levels of oxidative stress were observed, exacerbated by microglial activation, a marker of inflammation (Perez-de la Cruz and Santamaria, 2007).

### 1.1.3.3 Amyotrophic lateral sclerosis

Amyotrophic lateral sclerosis is another motor disease due to the progressive degeneration of anterior horn cells of the spinal cord and of cortical motor neurons (Baron *et al.*, 2007). One of the identified causes is a mutation in the  $\text{Cu}^{2+} / \text{Zn}^{2+}$  superoxide dismutase 1 gene (Baron *et al.*, 2007). The consequent hallmarks of this mutation observed in the antioxidant scavenging system include increased oxygen radical damage in patients' brains, glutamate excitotoxicity, formation of proteinaceous inclusions containing mutated superoxide dismutase, neurofilaments and ubiquitin, as well as mitochondrial damage (Baron *et al.*, 2007), including mtDNA mutations, ETC impairment (complex I activity was decreased in brains and muscles from patients) and decreased ATP production (Dupuis *et al.*, 2004).

### 1.1.4 Common pathological features in neurodegenerative diseases

Although these four neurodegenerative conditions affect different parts of the brain and lead to different symptoms in patients, they show certain similarities in their pathological features. Indeed, oxidative stress is a major hallmark in all four diseases and is linked to all the other biochemical features found in neurodegeneration (Butterfield *et al.*, 2006). In all cases, post-translationally modified proteins accumulate to form proteinaceous inclusions, associated with dysfunction of proteolysis (Rubinsztein, 2006; Cassarino and Bennett, 1999). Mitochondrial dysfunction has also been strongly related to the four neurodegenerative diseases, as indicated by the impairment of ETC complexes and the loss of mitochondrial potential (Cassarino and Bennett, 1999; Perez-de la Cruz and Santamaria, 2007). Whether the impairment of oxidative phosphorylation is the cause or consequence of increased levels of ROS has not yet been resolved. However, decreased mitochondrial antioxidant defences and increased levels of ROS, contributing to mtDNA oxidative damage is common to all four neurodegenerative diseases (Howell *et al.*, 2005; Dupuis *et al.*, 2004; Kasraie *et al.*, 2008).

## 1.2 MITOCHONDRIA

### 1.2.1 General features

Mitochondria are referred as the “power-house” organelles of the cells, with reference to their important role in energy production but they also have roles in cell survival and death. In 1963, Nass was the first to discover that mitochondria contained their own DNA (Reviewed in Chinnery and Schon, 2003). It is thought that these eukaryotic organelles are of bacterial descent derived from a symbiotic relationship with a primitive eukaryotic organism, explaining the presence of mtDNA, but have a high dependence on nuclear gene products (Gabaldon and Huymen, 2004).

The DNA of mitochondria is a circular double stranded DNA that contains around 16.6 kbp, which represents 0.1 to 2 % of total cellular DNA (Druzhyina *et al.*, 2003). Two of its genes encode ribosomal RNAs, 22 encode transfer RNAs, and 13 encode protein subunits of the ETC complexes (Chinnery and Schon, 2003). Each mitochondrion can contain from 1,000 to 100,000 copies of mtDNA that continuously replicate independently of the cell cycle state and that are all maternally transmitted (Chinnery and Schon, 2003). Contrary to nuclear DNA, mtDNA does not associate with histone proteins and has a much simpler repair mechanism. Consequently, it is less well protected against oxidative stress and other types of damage compared to nuclear DNA (Pieczenik and Neustadt, 2007).

Although mitochondria contain their own DNA, they are composed of an estimated 800 to 1,500 proteins (Liebler, 2002; Taylor *et al.*, 2003a), virtually all imported from the cytoplasm (apart from the 13 complex subunits encoded by the mtDNA). An extremely well regulated import mechanism is then required for the entry of these proteins into mitochondria (For a review see Bolender *et al.*, 2008).

The mitochondrion is a membrane-rich organelle composed of 4 compartments: the matrix, the inner mitochondrial membrane (IMM), the outer mitochondrial membrane (OMM) and the intermembrane space (IMS); all participating in the integrity and functions of the organelle, such as its role in survival and death (Bolender *et al.*, 2008) (Figure 1.2).



**Figure 1.2: Electron micrograph of a typical mitochondrion**

Electron microscopy from Fawcett (1994)

### 1.2.2 Mitochondrial cycle of life

Mitochondria are grouped in networks that continuously undergo fusion and fission states (Twig *et al.*, 2008). Both mechanisms are important in the maintenance of mitochondrial integrity, electrical and biochemical connectivity, regulation of mitochondrial turnover, segregation, stabilisation and protection of mtDNA (Van Laar and Berman, 2009). Mitochondria are degraded by an autophagic pathway that is thought to be activated via a decrease of mitochondrial potential (Twig *et al.*, 2008). However, degradation of unfolded and misfolded IMM and matrix proteins involves proteases associated with the IMM (Twig *et al.*, 2008). E3-ubiquitin ligase has been associated with a few outer mitochondrial membrane proteins, suggesting a potential role of the proteasome in the degradation of at least some OMM proteins (reviewed in Twig *et al.*, 2008).

### 1.2.3 Principal cellular roles of mitochondria

Overall, mitochondria are responsible for up to 90% of the total cellular energy production (Mootha *et al.*, 2003). They are the centre of many catabolic pathways including fatty acid oxidation and the Krebs cycle, which drives both carbohydrate and fatty acid metabolism (Mootha *et al.*, 2003). These pathways lead to the formation of some ATP energy but also the reduction of cofactors. The ETC situated in the IMM is responsible for the oxidation of reduced cofactors allowing the formation of ATP via proton transfer through the IMM.

The ETC is composed of five enzymatic complexes (Figure 1.3). Complex I is composed of 40 subunits that form the enzyme called NADH dehydrogenase (or NADH:ubiquinone oxidoreductase). It is responsible for the oxidation of NADH cofactor and transfer of electrons to coenzyme Q, carrying the electrons to complex III. Complex II is composed of 4 subunits and is called succinate dehydrogenase (or succinate:ubiquinone oxidoreductase) and forms part of the Krebs cycle. It is responsible for the transfer of electrons from FADH to coenzyme Q that also carries electrons to complex III. Complex III is composed of 11 subunits and is also called the bcl complex (or ubiquinone cytochrome c oxidoreductase). It transfers electrons from coenzyme Q to cytochrome c carrier. Electrons are then carried to complex IV, which is composed of 13 subunits and is called cytochrome c oxidase (or reduced cytochrome c: oxygen oxidoreductase). It transfers electrons to reduce oxygen into water. Complexes I, III and IV pump protons from the matrix to the inter-membrane space of the mitochondria for each electron transferred. This flow of protons creates a proton gradient that drives the protons back to the mitochondria through complex V (or ATP synthase), which synthesizes ATP (Schapira, 2006; Pieczenik and Neustadt, 2007, Kidd, 2005 and figure 1.3).

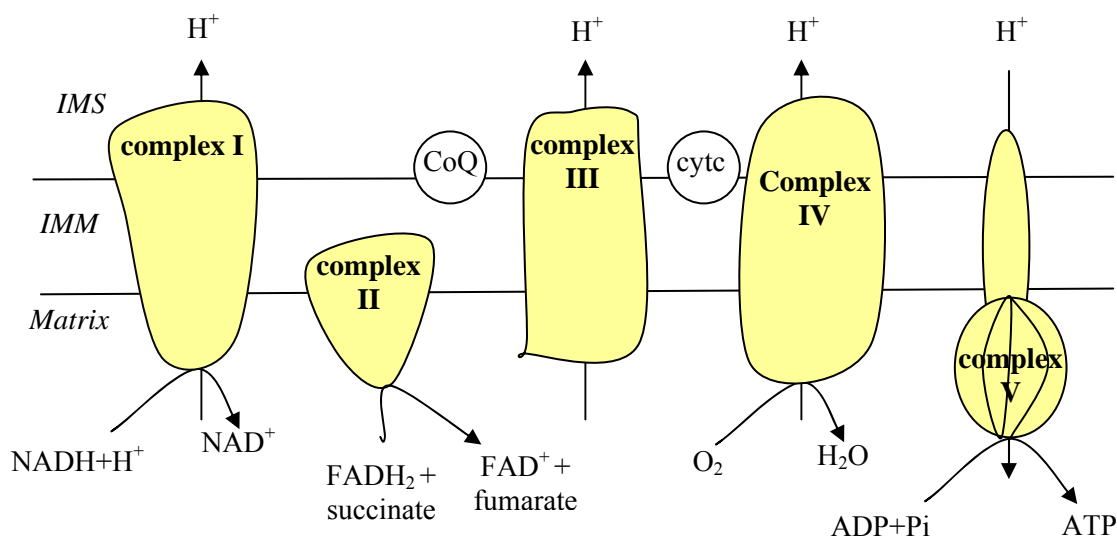


**Figure 1.3: Schematic diagram of the electron transfer chain**

coQ: coenzyme Q; cytc: cytochrome c

Mitochondria also contain key enzymes of other metabolic pathways such as the urea cycle, heme biosynthesis, ketone body generation, and hormone synthesis (Mootha *et al.*, 2003). Apart from their metabolic roles, mitochondria have a variety of other functions. They participate in calcium homeostasis, regulating calcium signaling. They are the centre of many other signaling pathways including guanine, GTP-related proteins, Ras-related proteins, kinases and phosphatases, protease inhibitors and signaling receptors (Taylor *et al.*, 2003b).

Mitochondria are the main producer of ROS in conjunction with highly regulated antioxidant defences to protect against these oxidative molecules (Mootha *et al.*, 2003).

Finally, one of the crucial functions of mitochondria includes their role in cell death via housing key regulators of programmed cell death in the IMS and their OMM interaction with B-cell lymphoma 2 (Bcl<sub>2</sub>) family proteins (originally found in B-cell lymphoma), including pro- and anti-apoptotic molecules that lead to or prevent the release of proapoptotic regulators into the cytoplasm (Suen *et al.*, 2008).

#### **1.2.4 Mitochondria and neuronal cells**

Neuronal cells have been observed to have different characteristics compared to other cell types. They are terminally differentiated in the adult brain, being unable to divide and regenerate in case of brain injury. Moreover, they are unable to survive anaerobically, meaning that if there is no oxygen provided to neurons, cells can die within a few minutes. Finally, they have a particular asymmetrical morphology due to the outgrowth of axonal processes and dendrites from their cell body (Dowling, 2001). Protein synthesis mostly occurs in the cell body and axons need a particular mechanism for the transport of molecules such as proteins, lipids and carbohydrates to and from the synapse. Axonal transport occurs along networks of cytoskeletal proteins (Dowling, 2001). Maintenance of neuronal integrity needs to be highly regulated. Because of their energy requirements and to ensure cell survival, neurons contain a high number of mitochondria per cell compared to other cell types. Moreover, mitochondria are transported along axons to bring ATP energy to the synapses and throughout the cell. Mitochondrial fusion and fission dynamics have been found to be crucial for axon development and survival (Berman *et al.*, 2008). Another reason why mitochondria are especially important in neurons is their capacity for

scavenging oxidative insult. Maintenance of oxidant production and antioxidant system is important in the normal functioning and survival of neurons.

### 1.2.5 Mitochondrial dysfunction due to oxidative stress

Mitochondria are efficient organelles in the production of up to 90 % of ATP by using  $O_2$  as a substrate (Mootha *et al.*, 2003). However,  $O_2$  is highly reactive and has a high affinity for electrons, with approximately 2 % being converted to superoxide anion ( $O_2^{\bullet-}$ ) (Boegarts *et al.*, 2008).  $O_2^{\bullet-}$  is a ROS and the precursor of most other ROS molecules. Indeed, it can be converted to  $H_2O_2$  by the antioxidant enzyme superoxide dismutase (Boegarts *et al.*, 2008).  $H_2O_2$  can, in turn, be converted to water by diverse antioxidant enzymes (figure 1.4). However, when ROS molecules accumulate in the mitochondria (e.g. over time during aging), the antioxidant defence system does not scavenge all the oxidative molecules, which are converted to other free radical molecules that cause oxidative damage to biological molecules such as lipid, protein and DNA oxidation (figure 1.4). The consequences can be numerous; examples are damage to the ETC leading to a decrease in ATP production, malfunction of proteins, decreased enzyme activities (e.g. proteolytic enzymes leading to protein accumulation). There is also an increased risk of mutations and deletions in the mtDNA, exacerbating the above mentioned effects. The accumulation of all these events can eventually lead to cell death (Kidd, 2005; Fukui and Morales, 2008).

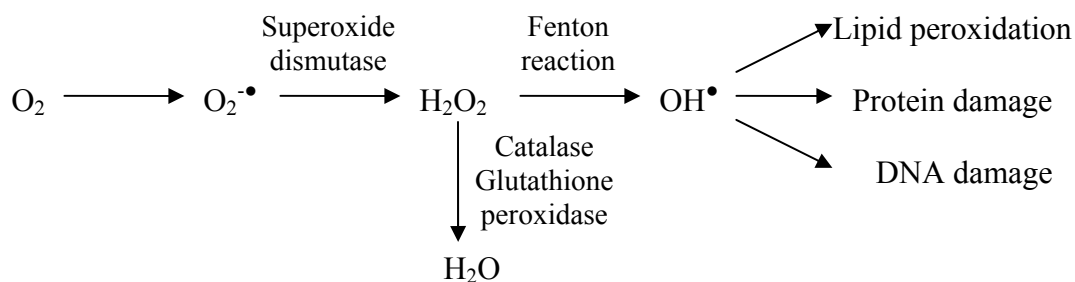


**Figure 1.4: ROS production from oxygen**

Modified schematic inspired by Boegarts *et al.* (2008).

### 1.3 CELL DEATH

Many different cell death pathways have been described in different cell types, distinct by morphological, enzymological, functional and immunological features (reviewed in Kroemer *et al.*, 2009). However, three main types of cell death, termed necrosis, apoptosis and autophagy, have been more commonly observed in neuronal cells (Yuan *et al.*, 2003)

#### 1.3.1 Apoptotic cell death

Apoptotic cell death was first described by Kerr *et al.* in 1972, who observed that cells could undergo different cell death pathways of which apoptosis was programmed by the cell itself, as opposed to necrosis (reviewed in Boujrad *et al.*, 2007). The morphological features of apoptosis include rounding of cells, loosening from surroundings, shrinkage, chromatin condensation and DNA fragmentation. The peculiarity of this type of cell death is that the plasma membrane remains intact, allowing the formation of apoptotic bodies (vesicles containing parts of cellular content) that are engulfed by macrophages without the release of toxic cellular content in the environment and without activation of inflammatory processes (Boujrad *et al.*, 2007; Han *et al.*, 2008b).

Apoptosis is an active process, also called “suicide of the cell” occurring naturally in development and homeostasis of neurons and requiring ATP energy and the regulation of a number of molecules involved in the process (Han *et al.*, 2008b). Such molecules belong to different protein families and have different characteristics, as discussed below.

##### 1.3.1.1 Cysteine-dependent aspartate-directed proteases (caspases)

Caspases are cysteinyl proteases able to cleave other proteins, including other caspases, on aspartate residues (Parone *et al.*, 2002). There are around 12 different proteins in this family. They are all found as inactive pro-enzymes, which upon stimulus, can be activated by cleavage via extra- or intra-cellular stimuli or via other caspases. Active caspases can activate other molecules, including caspases of the same or different groups (Orrenius, 2004).

There are two groups of caspases: the initiators (caspase-2, -8, -9 and -10) and the effectors (caspase-3, -6 and -7). The initiator caspases are generally activated by the formation of a

complex requiring initiator caspase binding for its activation. Activated caspases can then activate effector caspases, which in turn can activate other caspases and also cleave specific substrates that will lead to cell death.

### 1.3.1.2 Bcl<sub>2</sub> family proteins

Another group of proteins known to regulate apoptosis is the Bcl<sub>2</sub> family, which includes at least 17 members that can be either pro-apoptotic or anti-apoptotic (Han *et al.*, 2008b). They contain 4 sequence motifs called Bcl<sub>2</sub> homology (BH) domains and they all share one of them (BH3), while the other domains are shared between groups of proteins. Anti-apoptotic Bcl<sub>2</sub> molecules share the four domains (BH1 to 4; e.g. Bcl<sub>2</sub> and Bcl-x<sub>L</sub>), whereas pro-apoptotic molecules share three domains (BH1 to 3; e.g. Bax and Bak). Another group of Bcl<sub>2</sub> molecules only contains the BH3 domain, called BH3-only molecules (e.g. Bid, Bim, Bad, NOXA, PUMA); these promote cell death by interaction with and activation of pro-apoptotic Bcl<sub>2</sub> molecules and by inhibition of anti-apoptotic Bcl<sub>2</sub> molecules (Han *et al.*, 2008b).

Their localisation in healthy cells differs depending on the protein. For example, Bcl<sub>2</sub> localises to membranes, particularly of the endoplasmic reticulum but also nuclear and mitochondrial membranes (Krawjeski *et al.*, 1993); however, Bax and Bcl-x<sub>L</sub> are found in the cytoplasm of healthy cells and translocate to mitochondria following apoptotic stimulus (Hsu *et al.*, 1997).

The pro-apoptotic process of Bcl<sub>2</sub> molecules is thought to involve permeabilisation of the outer mitochondrial membrane (OMM), leading to the release of proteins from the intermembrane space (IMS) to the cytosol; this can then lead to toxicity and apoptotic cell death. The molecular events by which Bcl<sub>2</sub> molecules permeabilise the OMM have not yet been resolved. Several hypotheses have been proposed including the formation of a channel composed of Bax, tBid and Bak themselves or composed of a mitochondrial channel, voltage-dependent-anion channel (VDAC); the diameter of the latter is thought to increase upon interaction with Bax and Bak or following physical rupture of the OMM induced by osmotic swelling (process reviewed in Garrido *et al.*, 2006).

### 1.3.1.3 Molecular pathways of apoptosis

Depending on the stimulus, two different pathways of apoptosis have been distinguished. The extrinsic pathway, also called receptor-mediated death pathway, is activated in response to an extracellular stimulus by ligand binding (e.g. TRAIL, TRADD, FasL or TNF $\alpha$ ) and activation of cell surface death receptors (e.g. Fas, DR4/DR5, TNF $\alpha$ -receptor 1). Following this interaction, an adaptor protein (Fas associated death domain, FADD) binds to the receptor on the cytosolic side which leads to the cleavage of an initiator procaspase, which is mainly procaspase-8 but can also be procaspase-10 depending in the death receptor activated. Activated caspase-8 and -10 can directly cleave caspase-3 and -7, the effector caspases, which will lead to cell death (figure 1.5), or caspase-8 can cleave Bid to truncated Bid (tBid) which will associate with Bax on the OMM and activate the mitochondria-dependent apoptotic pathway (figure 1.5) (reviewed in Rossi and Gaidano, 2003; Han *et al.*, 2008b).

The intrinsic pathway is activated by an intracellular trigger, for example activation of initiator procaspase-2 (e.g. due to intracellular stimuli such as irradiation, withdrawal of serum, survival stimulus; Rossi and Gaidano, 2003). This leads to the activation of the mitochondria-dependent apoptotic pathway (figure 1.6). Whether via intrinsic or extrinsic pathway, the OMM loses its permeability leading to the release of molecules found in the IMS, such as cytochrome c, apoptosis-inducing factor and pro-caspases. Following its release, cytochrome c binds to Apaf1, ATP and procaspase-9 to form a complex called the apoptosome leading to the activation of caspase-9, an initiator caspase that will subsequently activate effector caspase-3, -6 and -7 (figure 1.6; Rossi and Gaidano, 2003). Caspase-3 is the main effector caspase, although caspase-7 is thought to have a similar role (Thornbery *et al.*, 1997). Caspase 3 activation leads to the cleavage of many protein substrates including caspase-3 itself and caspase-6 and -7, which will lead to the apoptotic morphology and eventually cell death (Rossi and Gaidano, 2003).

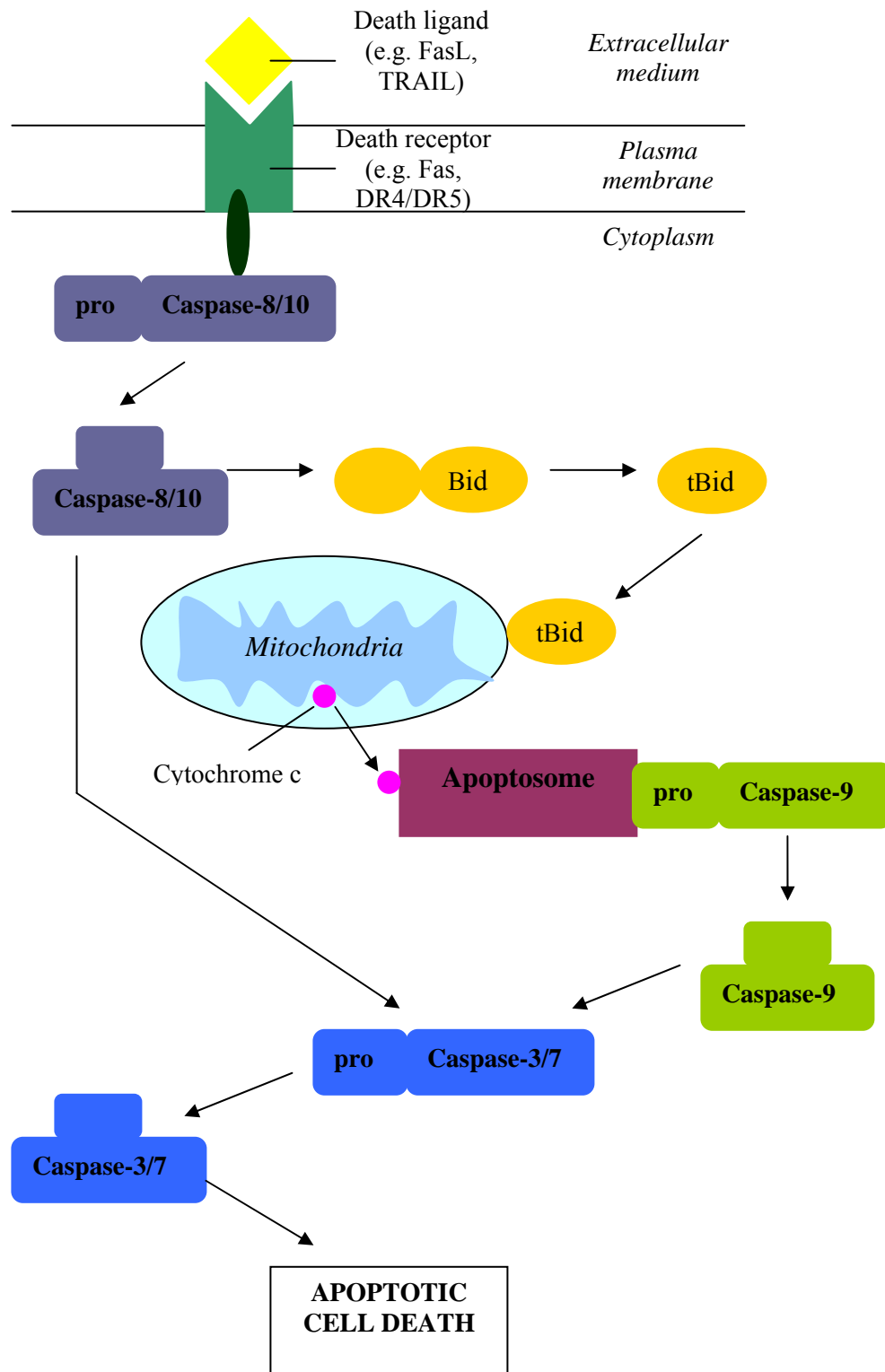


**Figure 1.5: Schematics representing the molecular events involved in the extrinsic pathway in mitochondria-independent and mitochondria dependent pathways.**

Figure inspired by Rossi and Gaidano, 2003

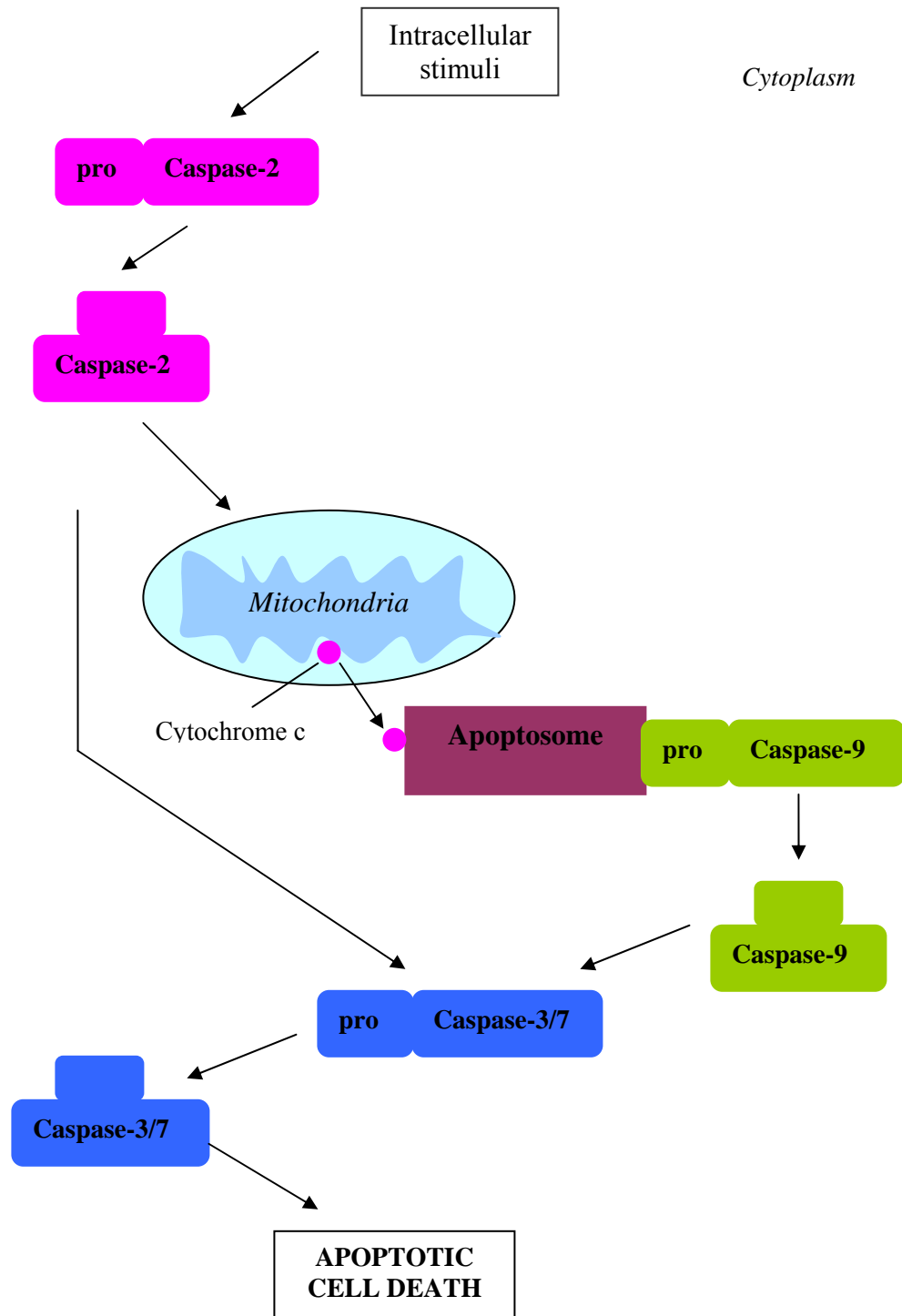


**Figure 1.6: Schematics representing molecular events involved in the intrinsic pathway.**

Figure inspired by Rossi and Gaidano, 2003

Caspase-7 was originally observed by Duan and colleagues (1996). It was found in a range of tissues and can be activated *in vitro* by activation of cell death receptors such as Fas/APO-1 (also called CD95) or TNFR-1. Caspase-7 has a substrate sequence for caspase-3, -6, -8 and -9 and for granzyme B (Thornberry *et al.*, 1997). As already mentioned, it has also been shown to have a similar substrate specificity to caspase-3 (Thornberry *et al.*, 1997) although it might have a different subcellular localisation (Chandler *et al.*, 1997). Indeed, both caspases are observed in the cytosol; however, only caspase-7 is found in microsomes and its activated form is found in mitochondria (Chandler *et al.*, 1997).

#### 1.3.1.4 Regulation of apoptotic molecules by signaling kinases

The apoptotic pathway, involving many pro- and anti-apoptotic molecules has been observed to be regulated by phosphorylation. Although many kinases have been linked to the apoptotic process, all pathways have not yet been resolved and only the most studied will be discussed here.

Protein kinase B, also called Akt, a serine-threonine kinase, has long been known to be linked to apoptosis (Datta *et al.*, 1997). Indeed, Akt was observed to phosphorylate Bad on its serine 136 residue. When phosphorylated in this way, Bad could not associate with and prevent the anti-apoptotic effects of Bcl<sub>2</sub> and Bcl-x<sub>L</sub> (Datta *et al.*, 1997). Since then, Akt has been shown to phosphorylate other molecules, for example the serine protease Htra2/Omi (preventing it from cleaving apoptotic inhibitor proteins; Yang *et al.*, 2007), caspase-9 (inactivating it in humans; Cardone *et al.*, 1998), and other proteins reviewed in Parcellier *et al.* (2008). Such findings show that Akt activation is associated with an anti-apoptotic phenotype. Moreover, Akt has been shown to inhibit the pro-apoptotic effects of both glycogen synthase kinase (GSK)-3 $\beta$  and c-Jun amino N-terminal kinase (JNK), a stress-activated protein kinase (SAPK) (Kajta, 2004). For example, JNK activation increases the phosphorylation and protein levels of transcription factor cJun, which led to the elevated transcription of pro-apoptotic molecules Bax and FasL. In parallel, JNK inhibits Bcl<sub>2</sub> and Bcl-x<sub>L</sub> by phosphorylating them. Moreover, GSK-3 $\beta$  inhibits by phosphorylation the anti-apoptotic molecule Mcl-1 (Kajta, 2004)

### 1.3.2 Necrotic cell death

Necrosis has long been thought to be a passive, accidental process but it has recently been shown that it can also be a programmed and physiological pathway (Boujrad *et al.*, 2007; Niquet *et al.*, 2006). Pathological causes of necrosis include DNA damage, tumor necrosis factor induction and cell-cell interactions (Han *et al.*, 2008b), although it has also been observed in developmental neuronal death (Golstein and Kroemer, 2006).

As opposed to apoptosis, necrosis is associated with a different cell morphology characterized by the swelling of organelles and the cell due to disruption of calcium homeostasis and to the disruption of the plasma membrane resulting from a combination of calcium overload, increased ROS production, damaging biological membranes, and depletion of ATP, leading to loss of integrity of the membranes (Golstein and Kroemer, 2006). The exact molecular pathways involved have not been completely resolved; however, there is evidence of activation of a few proteases including calpains, cathepsins and granzyme, further explaining the disruption of organelle membranes (Golstein and Kroemer, 2006). Disruption of the plasma membrane during necrosis leads to the release of cytoplasmic content to the extracellular environment, including release of cytokines, TNF- $\alpha$ , heat shock proteins and others, which can stimulate an inflammatory response when released and can lead to propagation of necrosis to surrounding cells (Han *et al.*, 2008b).

### 1.3.3 Autophagic cell death

Autophagy was first observed by Schweichel and Merker in 1973 (reviewed by Yuan *et al.*, 2003). It is characterised by the formation of double membrane vacuoles containing the cytoplasmic content or fragments of cellular organelles that will be digested by lysosomal hydrolases upon fusion of these vacuoles with lysosomes (reviewed by Kroemer *et al.*, 2007). There are three different types of autophagic processes: the chaperone-mediated autophagy involves delivering specific single proteins to the lysosomes for protein degradation; microautophagy is associated with engulfing cytosol portions or organelles to recycle damaged organelles; while macroautophagy involves forming sequestering vesicles in the cytoplasm containing intracellular organelles and portions of the cytoplasm, the latter process leads to cell death (Yuan *et al.*, 2003).

Autophagic cell death has been observed in neuronal development and also in cases of extracellular (e.g. nutrient deprivation or hypoxia) and intracellular (accumulation of damaged organelles and cytoplasmic components) stress conditions (Yuan *et al.*, 2003).

#### 1.3.4 Cell death and mitochondria

As previously mentioned, the involvement of mitochondria in cell death occurs at different levels through their involvement in ATP production and distribution,  $\text{Ca}^{2+}$  homeostasis, ROS production and also by the release of molecules toxic for the cytoplasm due to a loss of permeability of mitochondrial membranes (e.g. cytochrome c, apoptosis-inducing factor,...)

Following increased  $\text{Ca}^{2+}$  and ROS production or other intra- or extra-cellular stimuli, mitochondria are subjected to what is called the mitochondrial permeability transition, which is caused by a sudden increase in membrane permeability due to the opening of a pore through the OMM only or through the IMM at contact sites (Halestrap *et al.*, 2002). Such pores have been described to be composed of the protein cyclophilin D from the matrix, the adenine nucleotide translocator (ANT) from the IMM and VDAC from the OMM, although this complex composition has been challenged in the literature (Garrido *et al.*, 2006).

Permeabilisation of the mitochondrial membrane leads to the release of IMS proteins but also small molecules from the mitochondrial matrix, including cations such as  $\text{Ca}^{2+}$ . Additionally, the permeabilisation of the IMM has led to the uncoupling of the ETC leading to a drop in ATP production and even a reverse reaction of ATP synthase leading to ATP hydrolysis, further depleting ATP stores (Halestrap *et al.*, 2002). This phenomenon has been observed in both the apoptotic and necrotic pathways (Orrenius *et al.*, 2004).

## 1.4 MPTP AS A MODEL FOR PARKINSON'S DISEASE

### 1.4.1 1-methyl-4-phenyl-1,2,3,6-tetrahydropyridine (MPTP) emergence as a toxin

The first time MPTP was linked to PD occurred in the late 1970s when a graduate student, trying to reproduce a narcotic analogue of meperidine (analgesic drug), injected himself with the substance he made and started to develop PD-like symptoms. Analysis of the injected drug showed that it contained MPTP (Davis *et al.*, 1979). Another similar incident occurred a few years later when a group of addicted young people were taking some synthetic heroin supposed to contain the same narcotic analogue of meperidine. The analysis of the drug compounds showed that it also contained MPTP (Langston *et al.*, 1983). MPTP-induced symptoms included tremors, rigidity, slowness of movement, postural instability, freezing episodes similar to PD symptoms (Langston *et al.*, 1983). The symptoms were attenuated when treated with PD treatments such as L-DOPA and carbidopa (Langston *et al.*, 1983).

### 1.4.2 MPTP as a model of Parkinson's disease

MPTP became of particular interest when it was observed to reproduce symptomatic, pathological and biochemical features of PD in animal models. Interestingly, MPTP-induced symptoms in monkeys were virtually identical to human symptoms, more particularly in African green monkeys which reproduced resting tremors, the most similar to human PD (Tetrud and Langston, 1992). MPTP-induced damage to the nigrostriatal dopaminergic pathway with a larger damage in the substantia nigra than in the ventral tegmental area in both humans and monkeys (Seniuk *et al.*, 1990). MPTP-induced effects have been observed to be acute and although biochemical features are similar to PD in patients, MPTP did not show formation of Lewy bodies in both humans and monkeys (Bové *et al.*, 2001). Although higher concentrations were needed, MPTP also mimicked PD in mice. However, rats were much less sensitive to MPTP-induced toxicity (reviewed in Przedborski *et al.*, 2001). The differences observed in the different animals and between species of the same animal to MPTP-induced toxicity have not completely been explained.

The choice of administration showed different outcomes with a preference to systemic administration (Przedboski *et al.*, 2001). Moreover, as shown with mice models, the age, body weight, gender and strain are factors in MPTP-induced toxicity (Przedboski *et al.*, 2001); more particularly, the age of animals has been an important factor as aged mice and monkeys have been found to be more sensitive to MPTP (Gupta *et al.*, 1986; Forno *et al.*, 1988).

### 1.4.3 MPTP metabolism

MPTP is a neutral and highly lipophilic compound able to cross the blood brain barrier (see structure in figure 1.7; Beal, 2001). It can be taken up by the cells in a non-specific manner where it will be metabolized to an intermediate compound MPDP<sup>+</sup> (1-methyl-4-phenyl-2,3-dihydropyridinium ion), a reaction catalysed by the catecholaminergic enzyme MAO-B mainly and MAO-A to a lesser extent and involving two electron oxidation (Chiba *et al.*, 1985; Salach *et al.*, 1984). MPDP<sup>+</sup> being unstable it subsequently auto-oxidises into MPP<sup>+</sup> (1-methyl-4-phenylpyrimidium), also involving two electron oxidation. MAO-B levels were shown to be lower in catecholaminergic cells compared to glial and serotonergic cells (Levitt *et al.*, 1982), it was then shown that MPTP oxidation to MPP<sup>+</sup> was primarily occurring in glial cells (Brooks *et al.*, 1989). Following MPP<sup>+</sup> formation, the charged compound is released to the extracellular space where it will be specifically taken up by dopaminergic neurons via dopamine transporters (DAT) for which it has high affinity (Bezard *et al.*, 1999). Upon entry into dopaminergic neurons, MPP<sup>+</sup> can have three different outcomes: (a) MPP<sup>+</sup> is taken up by neuromelanin, a by-product of dopamine auto-oxidation (D'Amato *et al.*, 1987) delaying its release to the cytoplasm whereupon delaying its cytotoxicity; (b) MPP<sup>+</sup> is confined to synaptic vesicles via uptake by vesicular monoamine transporters (Takahashi *et al.*, 1997); (c) free MPP<sup>+</sup> present in the cytoplasm relocates to mitochondria where it will have its cytotoxic effects.

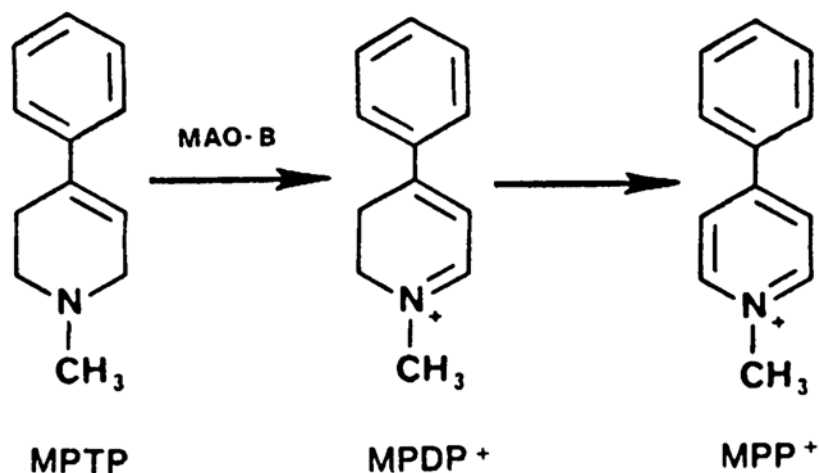


**Figure 1.7: MPTP metabolism**

Figure from Kopin, 1987.

#### 1.4.4 Inhibition of complex I of the electron transfer chain

MPP<sup>+</sup> was observed to accumulate in the mitochondria via an ATP-dependent uptake system, which was followed by the inhibition of oxidation of NAD<sup>+</sup> and of its linked substrates (e.g. pyruvate and glutamate oxidation; Nicklas *et al.*, 1985; Ramsay *et al.*, 1986). This was followed by ATP depletion (DiMonte *et al.*, 1986) accompanied by loss of mitochondrial potential, increase in ROS production and impairment of calcium homeostasis (reviewed in Blum *et al.*, 2001). Following these observations, Ramsay and colleagues (1987) found that MPP<sup>+</sup> was inhibiting the ETC by inhibiting the transfer of electrons from the iron-sulfur cluster of highest potential to the endogenous coenzyme Q10, from complex I to complex III, explaining the above mentioned effects.

#### 1.4.5 MPTP and generation of reactive oxygen species

The observation that MPTP caused increased production of ROS was noted by Johannessen *et al.* (1986). Since then, several modes of actions of MPTP to produce ROS have been uncovered. (a) The intermediate MPDP<sup>+</sup> was observed to induce O<sub>2</sub><sup>•-</sup> during its multi-step auto-oxidation to MPP<sup>+</sup> (Zang and Misra, 1992). (b) MPP<sup>+</sup> potentially can lead to the

formation of  $\text{MPP}^\bullet$  radical as an extra radical production (Adams *et al.*, 1993). (c) Inhibition of complex I increases  $\text{O}_2^\bullet$  production (Boegarts *et al.*, 2008).

Along with increased ROS production, a decrease in the antioxidant system was also observed following MPTP-induced toxicity, particularly a decrease in glutathione levels (Sriram *et al.*, 1997; Caneda-Ferron *et al.*, 2008). Overall deleterious consequences of increased oxidative stress to cellular processes have previously been described (section 1.3.5).

Following MPTP-induced toxicity, glial cells (microglia and astrocytes) have been shown to be activated (O'Callaghan *et al.*, 1990) leading to an inflammation response linked to further increased oxidative stress, as previously described in the pathology of Parkinson's disease description (section 1.1.2; figure 1.1).

#### 1.4.6 Excitotoxicity and calcium homeostasis disruption

Excitotoxicity has been linked to MPTP-induced effects as N-methyl-D-aspartate (NMDA) antagonists prevented MPTP-induced toxicity (Turski *et al.*, 1991). Moreover, a recent study showed that MPTP treatment of mice led to an increase in extracellular glutamate concentration in the substantia nigra and an increase in glutamate transporter affinity for the neurotransmitter (Meredith *et al.*, 2009), consistent with the idea that MPTP leads to excitotoxicity. This phenomenon was thought to happen due to ATP depletion and oxidative stress, consequent to complex I inhibition, leading to a decrease in plasma membrane potential and blockade of NMDA receptors becoming overexcited by glutamate. The direct consequence of this would lead to an excessive release of glutamate parallel to an excessive influx of  $\text{Ca}^{2+}$  into the cell (Sawada and Shimohama, 1999).  $\text{Ca}^{2+}$  overload can lead to activation of many  $\text{Ca}^{2+}$ -dependent enzymes of which NOS (participating in nitric oxide radical,  $\text{NO}^\bullet$ , production; Sawada and Shimohama, 1999), signaling kinases, proteases and endonucleases that can lead to activation of cell death pathways (Blum *et al.*, 2001).

Consistently, peroxynitrite ( $\text{ONOO}^-$ ) production has been also linked to MPTP-induced toxicity (Obata and Yamanaka, 2001; Obata, 2006). Indeed,  $\text{NO}^\bullet$ , a reactive nitrogen species important as an intracellular messenger can react with  $\text{O}_2^\bullet$  to form  $\text{ONOO}^-$  radical a powerful oxidant also linked with protein oxidation, lipid peroxidation and mtDNA damage, exacerbating the oxidative damage (Boegarts *et al.*, 2008).

### 1.4.7 Proteolysis dysfunction

Despite a lack of Lewy body formation using acute MPTP treatment in human and animal models, chronic treatments have led to the formation of intraneuronal proteinaceous inclusions resembling Lewy bodies in old monkeys (Forno *et al.*, 1988) and of nigral inclusions containing ubiquitin and  $\alpha$ -synuclein in MPTP-treated mice (Fornai *et al.*, 2005), further supporting MPTP as a model for PD. Parallel to the accumulation of proteins into inclusion bodies, a decrease in proteasome activity has also been observed following MPTP treatment in mice (Fornai *et al.*, 2004), in marmoset (decrease in activity of 20S- $\alpha$  subunit but not - $\beta$  subunit; Zeng *et al.*, 2006) and in human SH-SY5Y neuronal cells (Caneda-Ferron *et al.*, 2008).

## 1.5 AIMS OF THE PROJECT

As described above, mitochondrial dysfunction is thought to be an important factor in neurodegenerative pathways. The overall objective of the present study was to investigate changes in the mitochondrial proteome of cultured neuronal cells, of relevance to neurodegeneration, in particular PD, with the potential to uncover markers of mitochondrial dysfunction.

In order to further investigate the role of mitochondrial impairment in neurodegeneration, a protocol for the study of the mitochondrial proteome was optimised, including optimisation of mitochondrial isolation from cellular extracts and resolution of the mitochondrial proteome profile using 2DE followed by the use of peptide mass fingerprinting to attempt to identify proteins from the profile.

As neuronal cells are found in the post-mitotic state in the developed brain, mitochondrial profiles from differentiated neuroblastomas were compared to profiles from the mitotic state in order to evaluate the importance of differentiation in the mitochondrial proteome.

Due to MPTP's characteristics in mimicking PD and in mitochondrial impairment in humans and animal models, it was decided that it would be used as a model in the present study. To unravel markers of mitochondrial dysfunction prior cell death, cytotoxic and sub-cytotoxic concentrations of MPTP in mouse N2a neuroblastoma cells were defined using cell viability and mitochondrial activity assays. Early markers of cell death pathways, for example apoptosis, were then investigated following sub-cytotoxic concentrations of MPTP

in order to further characterise the cellular state under the treatments chosen for further study.

Using the optimised protocol for mitochondrial proteome study and the characterised model, the effects of MPTP on the mitochondrial proteome were investigated and potential mitochondrial markers of MPTP-induced toxicity were identified, followed by a validation process for some of them.

Finally, VDAC1, one of the proteins previously identified as changing in levels following MPTP-treatment was further analysed. This study included further insights on the changes in levels and also a comprehensive analysis of its phosphorylation states following treatment with the neurotoxin as compared to controls in order to further understand its role in mitochondrial dysfunction.

## **CHAPTER II**

### **MATERIALS AND METHODS**

## 2.1 MATERIALS

### 2.1.1 Specialised equipment

Aida image Analyser v.4.03 software, Raytek Scientific Ltd, Germany  
Axima CFR MALDI-TOF, Shimadzu UK Limited, UK  
Beckman Coulter DU 530 Life Science UV / VIS Spectrophotometer, Beckman, UK  
Bio-Rad mode 680 microplate reader, Bio-Rad Laboratories Ltd, UK  
CBS Isothermal liquid nitrogen storage system 2300 series, Sanyo Biomedical division, UK  
Consort Mini Power supply, Geneflow Ltd, UK  
Electro Blot mini, Geneflow Ltd, UK  
FLUOStar OPTIMA, BMG Labtech, UK  
Fujifilm FLA-5100 gel scanner, Fujifilm Life Sciences Products, UK  
Fujifilm Intelligent dark box, Fujifilm Life Sciences Products, UK  
Gilson pipettes (P10ml, P1000, P200, P100, P20, P10, P2), Anachem Ltd, UK  
Leica CLSM confocal laser microscope, Leica, Germany.  
MC1 Analytic AC2105 balance, Sarorius, UK  
MIKRO 22R microfuge, Hettich, Germany  
Mini-PROTEAN III system, Bio-Rad Laboratories Ltd, UK  
Nikon Digital Net camera DN100, Nikon, Japan  
Nikon Eclipse TS 100 inverted microscope, Nikon, Japan  
Ohaus Scout Pro balance, Fisher Scientific, UK  
OLYMPUS CK2 ULWCD light microscope, Olympus, Japan  
Philips pH meter – PW9409, Pye-Unicam, UK  
Power Pac 3000, Bio-Rad Laboratories Ltd, UK  
Power Pac Mini Power supply, Bio-Rad Laboratories Ltd, UK  
Protean IEF Cell, Bio-Rad Laboratories Ltd, UK  
Protean xi Vertical Electrophoresis Cells, Bio-Rad Laboratories Ltd, UK  
REVCO Ultima II -80°C freezer, Biocold Laboratories, UK  
Rotor-gene 3000 Thermal cycler, Corbett Research, Germany  
Sanyo CO<sub>2</sub> incubator MCO-17AIC, Sanyo Gallenkamp PLC, UK  
Sanyo Harrier 18/80 re Fridgerated centrifuge, Sanyo Gallenkamp PLC, UK  
SM1 magnetic stirrer, Stuart Scientific, UK  
Stuart Block Heater SBH130D, Geneflow Ltd, UK  
Stuart Orbital Shaker SSL1, Geneflow Ltd, UK  
Stuart SA7 vortex mix, Geneflow Ltd, UK  
Tecan SPECTRA Fluor plate reader, Tecan UK Ltd, UK  
Ultraflex III TOF / TOF, Bruker Daltonics Limited, UK  
Walker class II microbiological safety cabinet, Walker safety cabinets Ltd, UK  
Water bath 20-90°C, Grant, UK  
Water purification system, Millipore, USA

### 2.1.2 Plastic ware

All sterile plastic ware for tissue culture and of general laboratory use was supplied by Sarstedt, Leicester, UK

Cryotube vials (Nunc brand products), Merck Ltd. Leicester, UK

Disposable Haemocytometer C-Chip, Labtech International Ltd, UK

15 $\mu$  Slide 8-well for live cell analysis IbiTreat, Thistle Scientific, UK

### 2.1.3 Glass ware

Dounce All Glass 2 ml capacity Tissue Grinder, Apollo Scientific, UK

### 2.1.4 Laboratory reagents

All laboratory reagents were of the highest grade and purchased from Sigma-Aldrich Chemical Company, Poole, UK, unless otherwise specified.

#### 2.1.4.1 Cell culture reagents

1-methyl-4-phenyl-1,2,3,6-tetrahydropyridine hydrochloride (M0896), N<sub>6</sub>,2'-O-Dibutyryladenine 3',5'-cyclic monophosphate sodium salt (D0627), USA origin, sterile-filtered, cell culture tested, hybridoma tested Foetal bovine serum (FBS) (F2442), Hybri-Max™, sterile-filtered, hybridoma tested Dimethylsulfoxide (DMSO) (D2650), Trypan blue solution (0.4 %) (T8154), Sigma-Aldrich Chemical Company, UK

Dulbecco's Modified Eagles Medium (DMEM) (BE12-614F), L-Glutamine 200 mM (BE17-605E), Penicillin /streptomycin (DE17-603E), Lonza, UK

Dulbecco's Phosphate Buffer Saline (PBS) (H15-001), PAA laboratories, UK

#### 2.1.4.2 Laboratory reagents

Acetyl-Asp-Glu-Val-Asp-7-amido methyl Coumarin (260-031-M005), Acetyl-Asp-Glu-Val-Asp-CHO Alexis Biochemicals AXXORA Ltd, UK

Glycerol 99% (v/v) (158920025), ACROS organics, UK

RNaseZap (AM9780), Applied Biosystems, UK

Bromophenol blue, BDH Laboratory Chemicals Group, UK

7 cm pI 3-10 (163-2002), 7 cm pI 5-8 (163-2004), 7 cm pI 7-10 (163-2005), 17 cm pI 3-10

IPG strips (163-2007), BioLyte 3/10 ampholyte (163-2094), ReadyStrip 100X pI 7-10

Buffer (163-2093), Bio-Rad protein assay dye reagent concentrate (500-0006), Mineral Oil

(163-2129), Precision Plus Protein Dual Color Standards (161-0374), Precision Plus

Protein Unstained Standards (161-0363), ReadyPrep Overlay Agarose (163-2111), Bio-Rad

Laboratories Ltd, UK

3MM chromatography paper (CJF240090), Acetonitrile (A/0620/25), Dimethylsulfoxide

(DMSO) (D/4120/PB08), Ethanol 95% (v/v) (E/0500/17), Ethylacetate 99% GLC

(E/0850/17), Hydrochloric acid (H/1000/PB17), Methanol (M/3900/17), Sucrose

(S/8560/60), Trifluoroacetic acid (T/3258/04), Fisher Scientific, Leicestershire, UK

Accugel 29:1 (30% bis-acrylamide) (A20064), Geneflow, UK

Destreak reagent (17-6003-18), PlusOne Silver Stain kit (17.1150.01), GE Healthcare Life Sciences, UK

Nitrocellulose 0.22  $\mu$ M pore size (WP2HY00010), Genetic Research Instrumentation, Essex, UK.

Accuprime *Taq* DNA Polymerase System (12339-016), PeppermintStick phosphoprotein molecular weight standards (P27167), ProQ-Diamond Phosphoprotein Gel Stain (P-33300), Superscript II Reverse Transcriptase (18064-022), Sypro Ruby Protein Gel Stain (S-12000), Invitrogen, UK

Peptide calibration Mix 4 (Proteomix) (C104), Re-crystallized  $\alpha$ -cyano-4-hydroxycinnamic acid ( $\alpha$ CHCA) matrix (M101), LaserBio Labs, France

Vialight HS kit, (LT07-111), LumiTech Ltd, Nottingham UK

[3-[(3-Cholamidopropyl)-dimethylammonio]-1-propanesulfonate] (CHAPS) (B2006), Dithiothreitol (DTT) (MB1015), Melford Laboratories Ltd, UK

PCRSizer 100bp DNA Ladder (11400), Norgen Biotek, USA

Microplate BCA protein assay Kit-reducing agent compatible (23252), Pierce ECL Western Blotting Substrates (32106), Perbio Science UK Ltd, UK

dNTP mix, Sequencing Grade Trypsin (V5113), Promega UK, UK

RNeasy Mini Kit (74104), Qiashredder (79654), Qiagen House, UK

SensiMix SYBR (QT605), Quantace Ltd, UK

3-(4,5-dimethylthiazol-2-yl)-2,5-diphenyltetrazolium bromide (MTT) (M2128),

Oligonucleotides, Phosphatase inhibitor cocktail 2 (P5726), Protease inhibitor cocktail (P8340), Sigma-Aldrich Chemical Company, Poole, UK

3088S Syngene Gene Genius Bioimaging System, Syngene Europe, UK

## 2.1.5 Antibodies

### 2.1.5.1 Primary antibodies

Anti-Hsp60 antibody (ab46798), anti-LAMP2 antibody (ab37024), Abcam plc, UK

Anti-caspase-2 antibody (ALX-804-355), Alexis Biochemicals, UK

Anti-cleaved caspase-3 (9661), anti-GAPDH antibody (2118), anti-Lamin A/C antibody (2032), anti-phosphothreonine (42H4) (9386), anti-phosphotyrosine (P-Tyr-102) (9416), anti-VDAC antibody (4866), New England Biolabs, UK

Anti-AATM antibody (C-21) (sc-46704), anti-cytochrome c antibody (7H8) (sc-13560),

Anti-Heat Shock Protein 70 Clone BRM-22 (H5147), anti-phosphoserine antibody clone PSR-45 (P5747), Sigma-Aldrich Chemical Company, Poole, UK

### 2.1.5.2 Secondary antibodies

Goat anti-mouse immunoglobulin horseradish peroxidase conjugated (P0447), Goat anti-rabbit immunoglobulin horseradish peroxidase conjugated (P0447), DAKO Ltd, UK

Peroxidase-conjugated AffiniPure Bovine Anti-Goat IgG (H+L) (805-035-180), Stratech Scientific, UK

## 2.2 METHODS

### 2.2.1 Cell culture of mouse N2a neuroblastoma cells

Mouse N2a neuroblastoma cells were obtained from Flow Laboratories (Irving, UK).

#### 2.2.1.1 Maintenance of N2a neuroblastoma cells

N2a cells were maintained as monolayer in growth medium containing Dulbecco's modified Eagle's medium (DMEM), 10 % (v/v) fetal bovine serum (FBS), 2 mM 2-L-glutamine, 100 units/ml penicillin and 100 units/ml streptomycin. Cells were incubated at 37°C in a humidified atmosphere of 95 % air/5 % CO<sub>2</sub>.

#### 2.2.1.2 Subculture of N2a neuroblastoma

Cells were assessed via light microscopy to check viability and confluency. At 60-85 % confluence, cells were mechanically detached using a Pasteur pipette, aspirating medium and squirting it out on the wall of the flask to detach the cells. Medium containing the cells was transferred to a Sterilin tube. Cells were then passaged by centrifuging the medium 5 minutes at 300 g, re-suspending the pellet in 1 ml growth medium and transferring three to four drops to sterile flasks containing fresh medium. T25 flasks contained 8 ml; T75 flasks, 20 ml of and T175 flasks, 40 ml growth medium. Flasks containing passaged cells were incubated at 37°C in a humidified atmosphere of 95 % air/5 % CO<sub>2</sub> until 60-85 % confluency.

#### 2.2.1.3 Cell seeding

To seed the cells, a 1 in 20 dilution of cell suspension was prepared during sub-culture following harvesting by re-suspending the pellet in 1 ml growth medium. A count of visible cells was performed using a Haemocytometer (0.1 mm depth). Five fields of 1 mm<sup>2</sup> each were counted at a \* 100 magnification. The average of cells per field was calculated as well as the cell density per ml:

Cell density = average of cells per field \*  $10^4$  \* dilution factor

Cell density per ml was used to calculate the volume necessary to seed the cell at a required density. Mouse N2a cells were plated out in growth medium at a cell density of 5,000 cells/well in a 96-wells plate (100  $\mu$ l were added to each well) or 500,000 cells/T25 flask or  $4 \times 10^6$  cells/T75 flask or  $9 \times 10^6$  cells/T175. The cells were allowed to recover for 24 hour at 37°C in a humidified atmosphere of 95 % air/5 % CO<sub>2</sub>.

#### 2.2.1.4 Cryo-preservation of cells

For long-term storage preservation, cells were frozen in liquid nitrogen storage. Cells were seeded in a T25 flask. Following 24 hours incubation, cells were harvested and resuspended in 1ml ice-cold freezing medium containing 2.5 % FBS, 25 units/ml Penicillin / Streptomycin, 1 mM glutamine and 10 % DMSO in DMEM and transferred into freezing vials on ice. These vials were rapidly transferred to -80°C freezer overnight before being transferred to the liquid nitrogen storage.

#### 2.2.1.5 Resuscitation of cryo-preserved cells

A vial was removed from liquid nitrogen storage and quickly thawed in 37°C water bath. The content of the vial was transferred to a Sterilin tube containing 10 ml fresh growth medium previously warmed to 37°C. The tube was centrifuged at 300 g for 5 minutes and the supernatant was discarded. The pellet was re-suspended again in 10 ml growth medium and centrifuged the same way. Once the supernatant was discarded, the pellet was re-suspended in 1 ml growth medium and transferred to a T25 flask containing growth medium. Cells were allowed to recover at 37°C in a humidified atmosphere of 95 % air/5 % CO<sub>2</sub>.

#### 2.2.1.6 Differentiation of N2a cells

N2a cells were plated out in growth medium at a required cell density. The cells were allowed to recover for 24 hours at 37°C in a humidified atmosphere of 95 % air/5 % CO<sub>2</sub>. For the differentiation of cells, the growth medium was carefully removed. The cell

monolayer was carefully rinsed twice with DMEM to remove all traces of serum. The required volume of serum free medium (SFM) was then added, comprising 0.3 mM dibutiryl adenosine 3',5'-cyclic monophosphate (dbcAMP), 2 mM 2-L-glutamine, 100 units/ml penicillin and 100 units/ml streptomycin in DMEM. Cells were incubated at 37°C in a humidified atmosphere of 95 % air/5 % CO<sub>2</sub>.

#### 2.2.1.7 MPTP treatment

Following induction of differentiation, cells were incubated for 16 hours. The medium was then replaced by SFM containing 0.3 mM dbcAMP and the required concentration of MPTP (0 to 5 mM). Cells were incubated at 37°C in a humidified atmosphere of 95 % air/5 % CO<sub>2</sub> for the period of time required.

#### 2.2.1.8 Staurosporine (STS) treatments

Following induction of differentiation in T25 flask, cells were incubated for 16 hours. The medium was then replaced by 1 ml SFM containing 0.3 mM dbcAMP and 500 nM STS. Cells were incubated at 37°C in a humidified atmosphere of 95 % air/5 % CO<sub>2</sub> for the period of time required.

#### 2.2.1.9 Caspase-3/7 inhibitor treatment

For choosing the most adequate concentration of caspase-3/7 inhibitor (DEVD-CHO), mitotic cells were treated with different concentration of the inhibitor (0 to 50 µM) for 1 hour in parallel to controls. Following the incubation, different treatments were added to the cells in presence or absence of inhibitor.

For the effects of the inhibitor in conjunction with MPTP or STS treatments, 5 µM caspase-3/7 inhibitor was added to the medium following 16 hours differentiation in SFM supplemented with 0.3 mM dbcAMP. After 1 hour incubation, cell treatments were performed in the presence and absence of 5 µM inhibitor.

## 2.2.2 Cell viability

### 2.2.2.1 Morphology of the cells

Live cells were observed using phase contrast microscopy at a \* 400 magnification. Digital images of cells were then taken.

### 2.2.2.2 Trypan blue exclusion assay

Trypan blue is a dye that can enter non viable cells that have lost their membrane integrity. Following cell differentiation and MPTP treatment in T25 flasks, cells were harvested and resuspended in 1 ml growth medium. 20 µl of cell suspension were added to 100 µl trypan blue and 80 µl DMEM (cells were then diluted 1 in 10) in a 1.5 ml Eppendorf tube. The tube was vortex mixed thoroughly and left to stand for 2 minutes. A count of unstained cells (viable cells) was performed using a Haemocytometer as well as a count of total cells (refer to section 2.2.1.3). The percentage of viable cells was calculated as follows:

$$\% \text{ viable cell} = \text{number unstained cells} / \text{total number of cells} * 100.$$

### 2.2.2.3 MTT assay

3-(4,5-dimethylthiazol-2yl)-2,5-diphenyltetrazolium bromide (MTT) is a yellow substrate that is reduced by reductase enzymes. Once reduced to a purple formazan product, the product accumulates in the cells if the integrity of the cell membrane is intact (Mosmann, 1983).

Typically, differentiating cells were exposed to different concentrations of MPTP (0 to 5 mM) in 96-well plates. After 24 to 48 hours exposure (time points), 10 µl filtered MTT solution (5 mg/ml) were added to each well for 1 hour. The medium was then carefully removed from the wells and 100 µl dimethyl sulphoxide (DMSO) were added to each well. Plates were gently shaken on a plate shaker for 2 minutes. The absorbance in each well was read at 570 nm within 30 minutes. Results were expressed as a mean percentage cell viability compared to controls (untreated cells) ± SEM. Data were statistically analysed by a paired t-test using a two-tailed distribution.

#### 2.2.2.4 JC-1 fluorescent stain

Mouse N2a neuroblastoma cells were seeded at a density of 8,000 cells / 300  $\mu$ l growth medium on 15 micro-8-well Slides similarly as described in section 2.2.1.3 and differentiated and treated as described in sections 2.2.1.6-7. Following 24 hours treatment, the medium was removed. Three hundred microliters 10  $\mu$ M JC-1 staining (Molecular probes) diluted in DMEM were added to each well. The slide was incubated 3-5 minutes at 37°C in a humidified atmosphere of 95 % air/5 % CO<sub>2</sub>. The medium was then discarded, the cells were washed several times in DMEM and then incubated 30 minutes at 37°C in a humidified atmosphere of 95 % air/5 % CO<sub>2</sub> for recovery. The slide was observed on the laser confocal microscope. Using the Leica confocal software, the green signal and the red signal of ten cells present in a field of view were measured for each treatment. The data were expressed as a mean of green / red signal intensity per cell compared to the ratio in controls and statistically analysed by a paired t-test using a two-tailed distribution  $\pm$  SEM (n = 10).

#### 2.2.2.5 Cellular ATP assay

Cellular ATP presence was monitored using the Vialight HS kit's manufacturer's guidelines. The principle of the method relies on the ability of luciferase to catalyse the formation of light from ATP and luciferin. This light production is proportional to ATP concentration.

Known concentrations of ATP were used to build a standard curve as shown in table 2.2 using stock solutions previously made up as shown in table 2.1. Each standard was plated in triplicates. Cells were plated out in a 96-well plate at a 10,000 cells / well density, differentiated and treated as previously described (section 2.2.1). Each treatment was plated in triplicates. After the required time, the plate was removed from the incubator and left at room temperature for 5 minutes. Fifty microliters medium were removed from each well. A total of 25  $\mu$ l of Cell Lysing Reagent were added to each sample well and also to wells containing 50  $\mu$ l ATP standards previously prepared and the plate was left for 10 minutes. Fifty microliters of each cell lysate and ATP standards were transferred to wells in a white 96-well microplate. Then, 50  $\mu$ l of ATP monitoring reagent PLUS were added to each well

to generate the luminescence signal. The plate was incubated for 2 minutes. Luminescence of each well was read using a luminescence plate reader.

ATP concentration	ATP volume (stock used) ( $\mu$ l)	DMEM ( $\mu$ l)
<b>200 <math>\mu</math>M</b>	22 (10 mM)	980
<b>2 <math>\mu</math>M</b>	10 (200 $\mu$ M)	990
<b>0.1 <math>\mu</math>M</b>	50 (2 $\mu$ M)	950

**Table 2.1: ATP stock concentrations used to produce an ATP calibration graph.**

ATP concentration	ATP volume (stock used) ( $\mu$ l)	DMEM ( $\mu$ l)
<b>0 nM</b>	0 (0 mM)	1000
<b>5 nM</b>	50 (0.1 $\mu$ M)	950
<b>25 nM</b>	250 (0.1 $\mu$ M)	750
<b>100 nM</b>	50 (2 $\mu$ M)	950
<b>500 nM</b>	250 (2 $\mu$ M)	750
<b>1,000 nM</b>	5 (200 $\mu$ M)	995
<b>2,500 nM</b>	12.5 (200 $\mu$ M)	987.5

**Table 2.2: ATP Concentration for each standard used to produce a calibration graph.**

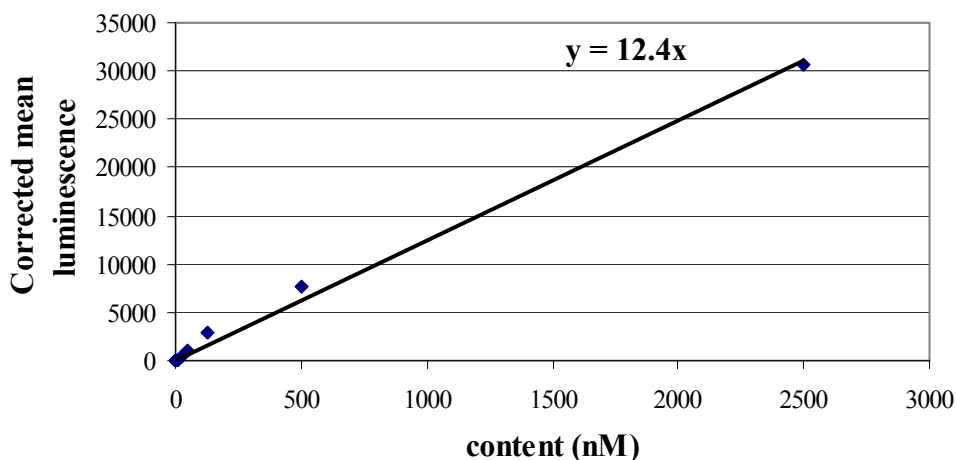


**Figure 2.1: Typical standard calibration graph for ATP using the ViaLight HS bioluminescent method.**

A typical standard calibration curve of mean luminescence for ATP standards (blanked to zero ATP) versus ATP concentration (nM) is shown in figure 2.1. Using the linear correlation, ATP concentration in each sample was estimated.

Results were also expressed as a mean percentage ATP presence compared to controls  $\pm$  SEM. Data were statistically analysed by a paired t-test using a two-tailed distribution.

### 2.2.3 Protein estimation of samples

Unless otherwise indicated, the protein content of each sample was estimated using the Bio-Rad protein assay based on the Bradford method (Bradford, 1976). This method is based on the particularity of Coomassie brilliant blue G-250 to shift in colour when binding to proteins. The assay was used in accordance with the manufacturer's specifications. Bovine serum albumin (BSA) standards ranging from 0 to 50  $\mu$ g were used to produce a calibration graph from which a linear correlation was calculated. Each BSA standards and samples were diluted as shown in table 2.3 in duplicates.

BSA concentration / sample ( $\mu$ g)	Volume of BSA stock (1 mg / ml) ( $\mu$ l)	Volume of extraction buffer / sample ( $\mu$ l)	Volume of water ( $\mu$ l)
0	0	10	790
5	5	10	785
10	10	10	780
15	15	10	775
20	20	10	770
25	25	10	765
30	30	10	760
40	40	10	750
50	50	10	740
Sample	0	10	790

**Table 2.3: Preparation of BSA standards and samples prior Bio-Rad protein estimation**

Each Eppendorf tube was vortex mixed. 200  $\mu$ l of Bio-Rad protein assay reagent were added to each tube. Each replicate was vortex mixed again. 100  $\mu$ l of each replicate were transferred onto a transparent 96-well plate. The plate was read within an hour at 570 nm. Protein content of each sample was calculated from the mean of duplicates using the linear correlation obtained from the BSA calibration curve.

## 2.2.4 Differential centrifugation

### 2.2.4.1 Cell harvesting

All the steps were undertaken on ice. Following seeding, differentiating and treatment, cells were detached from flasks and harvested at 300 g for 5 minutes. The supernatant was discarded and the pellet was resuspended into 1 ml sterile PBS buffer. This step was repeated three times, following which the pellet was resuspended in 500  $\mu$ l extraction buffer (EB) containing 10 mM HEPES, pH 7.5, 70 mM sucrose, 200 mM mannitol, 1 mM EGTA, 1 % protease inhibitors and 1 % phosphatase inhibitors.

### 2.2.4.2 Homogenisation of the sample

The homogeniser used was a Dounce All Glass 2 ml capacity Tissue Grinder accompanied with a Loose Pestle and a Tight Pestle (Apollo Scientific, UK). Following harvesting, the cell extract was transferred into the glass-glass homogeniser and homogenised ten times with the loose pestle and then ten times with the tight pestle. The cell lysate was then transferred to a 1.5 ml plastic tube.

### 2.2.4.3 Differential centrifugation protocol

Differential centrifugation was then carried out following a modified protocol from Lai and Clark (1979). Two initial low speed spins were used. The first centrifugation was at 1,000 g for 10 minutes and the second, using the resulting pellet resuspended in 200  $\mu$ l EB, for 5 minutes at 1,000 g. The resultant pellet was called “nuclear fraction”, which mainly contained nuclei. Supernatants from these spins were combined and centrifuged at 10,000 g for 15 minutes and the subsequent pellet was further centrifuged at 10,000 g for 10 minutes after resuspension in extraction buffer. The resultant pellet was called “mitochondrial pellet”, which contained mostly enriched mitochondria. Supernatants were combined and called “cytoplasmic fraction”, which contained mainly the cytoplasm and organelles except nuclei and mitochondria (figure 2.2). The fractions were protein estimated using the Bio-rad assay (section 2.2.3) and then stored at -80°C but for further analysis of purity assessment, fresh pellets were resuspended in extraction buffer.

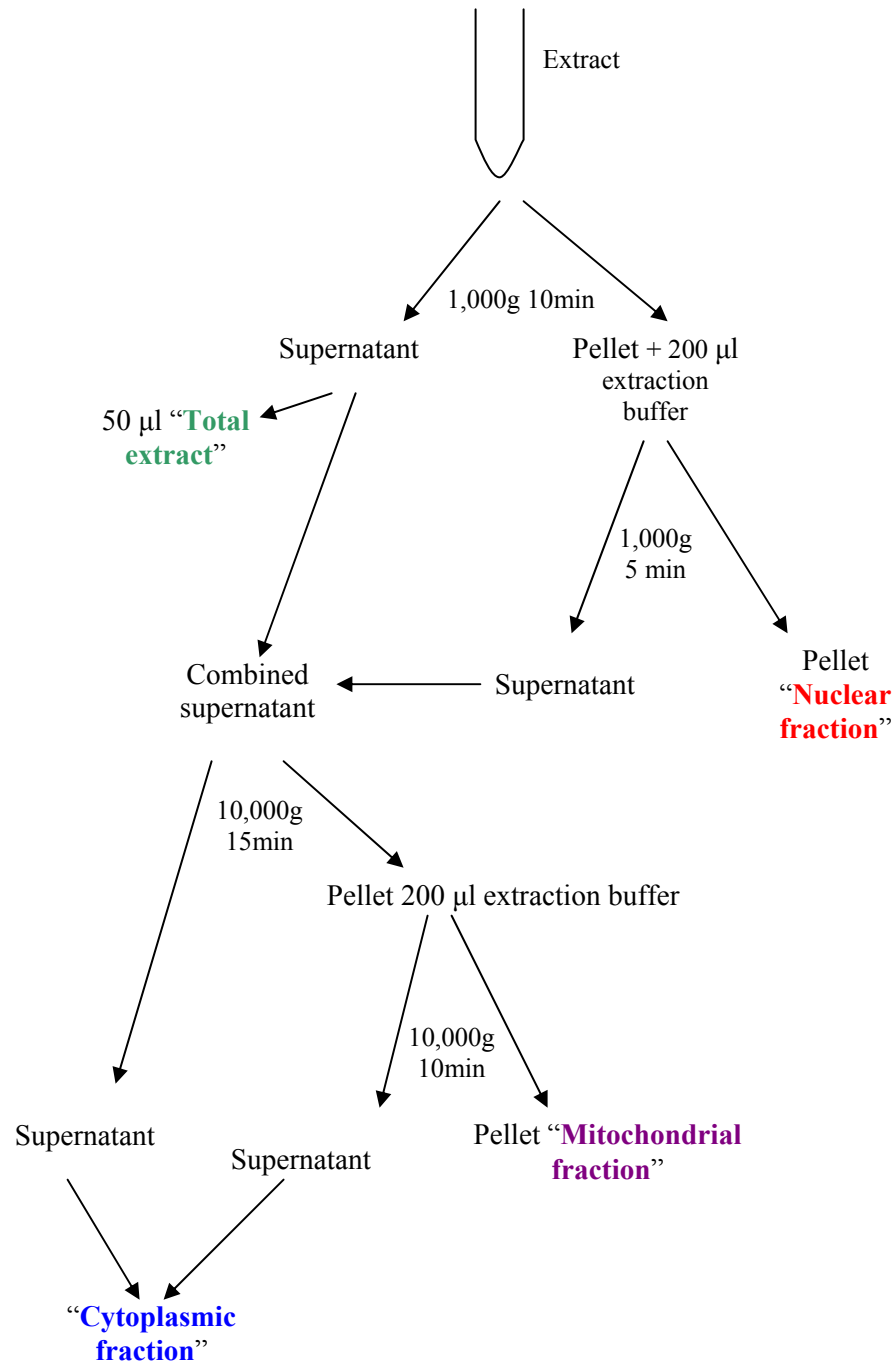


Figure 2.2: Schematic view of the subcellular fractionation protocol

### 2.2.5 SDS-PAGE

Proteins from samples were separated in accordance to their molecular weight using sodium dodecyl-sulfate polyacrylamide gel electrophoresis (SDS-PAGE).

#### 2.2.5.1 Preparation of resolving gel

The Bio-Rad mini-Protean III apparatus was used for mini-gels and the Bio-Rad Protean II XL Cell was used for large gels. Combs and spacer plates were generally 1.5 mm thick. For mini-gels, 10 ml resolving gel mix were prepared; while 60 ml were prepared for large gels. The percentage of polyacrylamide used was chosen in function of the molecular weights of the proteins of interest (refer to table 2.4 for mini gels as an example). Tetramethylethylene diamine (TEMED) and ammonium persulfate (APS) were added prior pouring the gel as they are catalyst and polymerising agents, respectively. 8 ml resolving gel were poured for mini gels and 50 ml for large gels. Distilled water was layered on top of the gel. The gel mix was allowed to polymerise at room temperature for approximately 30-45 minutes.

Reagent	7.5 % resolving gel	10 % resolving gel	12 % resolving gel	15 % resolving gel
<b>30 % acrylamide stock</b>	2.5 ml	3.3 ml	4.0 ml	5 ml
<b>1.5 M Tris, pH 8.8</b>	2.5 ml	2.5 ml	2.5 ml	2.5 ml
<b>10 % (w/v)SDS</b>	0.1 ml	0.1 ml	0.1 ml	0.1 ml
<b>Distilled water</b>	4.9 ml	4.1 ml	3.4 ml	2.4 ml
<b>TEMED (add to polymerise)</b>	10 µl	10 µl	10 µl	10 µl
<b>APS (add to polymerise)</b>	50 µl	50 µl	50 µl	50 µl

**Table 2.4: Preparation of 10 ml polyacrylamide resolving gels for mini gels.**

Those volumes were multiplied by 6 for large gels.

## 2.2.5.2 Preparation of stacking gel

Once the resolving gel was polymerised, the distilled water layer was removed. 1 ml 4 % acrylamide stacking gel (table 2.5) was added to the top of the plate for both mini and large-scale gels. The required comb was applied to the gel. The gel mixture was allowed to polymerise at room temperature for approximately 45-60 minutes.

Reagent	10 ml 4 % resolving gel
<b>30 % acrylamide stock</b>	1.33 ml
<b>0.65 M Tris, pH 6.8</b>	2.5 ml
<b>10 % (w/v)SDS</b>	0.1 ml
<b>Distilled water</b>	6.1 ml
<b>TEMED (add to polymerise)</b>	20 $\mu$ l
<b>APS (add to polymerise)</b>	50 $\mu$ l

**Table 2.5: Preparation of polyacrylamide stacking gels.**

## 2.2.5.3 Preparation of samples and loading

The required amount of sample was aliquoted and mixed with the same volume of sample buffer (0.125 M Tris pH6.8, 20 % (v/v) glycerol, 4 % (v/v) SDS, 0.004 % (w/v) bromophenol blue, 10 % (v/v)  $\beta$ -mercaptoethanol). When the volume of sample was too high (over 20  $\mu$ l), the sample was acetone precipitated by adding ten times the sample volume of ice-cold acetone and incubating at -20°C overnight. The samples were then centrifuged at 10,000 g for 15 minutes and acetone was removed. The appropriate sample buffer volume was added and samples were boiled for 10 minutes before being pulse-centrifuged for 10 seconds prior to analysis by SDS-PAGE.

## 2.2.5.4 Running the gel

Once the stacking gel was polymerised, the comb was carefully removed. The set-up was transferred to the tank. SDS-PAGE buffer (0.0265 M Tris, 0.192 M glycine, 0.1 % SDS (w/v), pH 8.3) was first added to the tank. Each sample was added to each lane and 5  $\mu$ l pre-stained molecular weight markers were added to a further lane. Separation of proteins was allowed at a constant voltage (180V). Voltage was stopped as the dye front was at the bottom level of the plates.

## 2.2.6 Immunoblotting

### 2.2.6.1 Wet western blotting

Separated proteins were then transferred to nitrocellulose membranes by wet blotting (Towbin *et al.*, 1979) using the manufacturer's instructions (Geneflow Electro Blot Mini). Two pieces of filter paper (9 cm \* 6 cm) pre-soaked in electroblotting buffer were laid onto a fibre pad over the black plastic side of the cassette. The gel was transferred onto it and overlaid by a nitrocellulose membrane (9 cm \* 6 cm) being careful to remove any air bubbles. And two other filter papers were added followed by a fibre pad and the whole "sandwich" was sealed in the cassette. Each cassette was transferred to the tank being careful to orientate the gel side towards the negative electrode. Electroblotting buffer (39 mM glycine, 48 mM tris, 0.0375 % (w/v) SDS, 20 % (v/v) methanol) was added up to the top of the cassettes and a constant voltage of 30V was applied overnight.

The following day, blotting efficiency was checked by staining with copper phthalocyanine 3,4',4'',4'''- tetrasulfonic acid tetrasodium salt in 12.5 mM HCl. Blots were destained in 12.5 mM NaOH prior to immunoprobng, after recording a digital image.

### 2.2.6.2 Immunoprobng

Membranes were incubated in blocking reagent to reduce non-specific binding. Two different blocking solutions were used depending on the primary antibody. Typically, 5 % (w/v) BSA in Tris buffer saline (TBS: 50 mM tris, 200 mM NaCl, pH 7.4) for 2 hours was used with anti-phosphorylated antibodies and 3 % (w/v) Marvel milk for 1 hour was used for other antibodies. Following blocking, nitrocellulose membranes were incubated in primary antibody overnight at 4°C with gentle shaking. Table 2.6 shows the details of which blocking reagent was used and the antibody working dilutions required for each antibody.

Unbound primary antibody was washed away by incubating the membrane in TBS containing 0.1 % (v/v) Tween 20 (TBS-tween) thoroughly shaking for 20 minutes at room temperature. This wash was repeated 3 times in total. The membrane was then incubated 2 hours at room temperature in secondary antibody corresponding to species specificity of the primary antibody used (table 2.6) and being conjugated with horseradish peroxidase (HRP)

while being gently shaken. The membrane was then washed as before 3\*20 minutes in TBS-tween and then 5 minutes in TBS for washing away the tween prior exposing the membrane. The membrane was incubated with HRP substrates for enhanced chemiluminescence (ECL) using the manufacturer's instructions (Pierce). The membrane was incubated for 1 minute in substrates. Excess of substrate was drained before exposing the membrane to chemiluminescence using the Fujifilm LAS 3100 from Raytek Scientific Limited. The exposure times used for each primary antibody are shown in table 2.6.

<b>Primary antibody specificity</b>	<b>Epitope specificity</b>	<b>Blocking reagent used</b>	<b>Working dilution</b>	<b>Secondary antibody working dilution</b>	<b>Exposure time to ECL</b>
Cytochrome c (7H8) monoclonal	Full length of human origin	3 % (w/v) marvel milk	1:500 in 5 % (w/v) BSA	1:1,000 anti-mouse	10 minutes
LAMP2 Polyclonal	17 amino acids from C-terminus of human origin	3 % (w/v) marvel milk	1:500 in 5 % (w/v) BSA	1:1,000 anti-rabbit	15 minutes
Lamin A/C polyclonal	Residues surrounding Asp230 of human origin	3 % (w/v) marvel milk	1:1,000 in 5 % (w/v) BSA	1:1,000 anti-rabbit	10 minutes
GAPDH (14C10) monoclonal	Full length of human origin	3 % (w/v) marvel milk	1:1,000 in 5 % (w/v) BSA	1:1,000 anti-rabbit	10 minutes
VDAC1 polyclonal	Amino terminus of human origin	3 % (w/v) marvel milk	1:1,000 in 5 % (w/v) BSA	1:1,000 anti-rabbit	10 minutes
AATM (GOT2) (C21) polyclonal	C-terminus of GOT2 of human origin	3 % (w/v) marvel milk	1:500 in 5 % (w/v) BSA	1:10,000 Anti-goat	8 minutes
Hsp60 polyclonal	Synthetic peptide of human origin	3% (w/v) marvel milk	1:5,000 in 5% (w/v) BSA	1:1,000 anti-rabbit	30 seconds
Hsp70 (BRM-22) monoclonal	Full length of bovine brain origin	3 % (w/v) marvel milk	1:10,000 in 5 % (w/v) BSA	1:1,000 anti-mouse	1 minute
Phosphoserine (PSR-45) monoclonal	N/A	5 % (w/v) BSA	1:500 in 5 % (w/v) BSA	1:1,000 anti-mouse	1 hour
Phosphothreonine	N/A	5 % (w/v)BSA	1:1,000 in 5 %	1:1,000 anti-mouse	10 minutes

(42H4) monoclonal			(w/v) BSA		
Phospho-tyrosine (P-Tyr-102) monoclonal	N/A	5% (w/v) BSA	1:500 in 5 % (w/v) BSA	1:1,000 anti-mouse	1 hour
Caspase-3	amino-terminal residues adjacent to (Asp175), human origin	3% (w/v) marvel milk	1:500 in 5 % (w/v) BSA	1:1,000 anti-rabbit	15-20 minutes
Caspase-2	Epitope of P19 subunit	3% (w/v) marvel milk	1:500 in 5 % (w/v) BSA	1:1,000 anti-rat	10-15 minutes

**Table 2.6: Epitope and species specificity and working dilutions for each primary antibody used for immunoblotting.**

### 2.2.6.3 Stripping and re-probing of western blot

Primary and secondary antibodies could be un-bound from the membrane by using stripping stringent conditions. The membrane was washed in TBS-tween for a few minutes to ensure that ECL substrates were removed. Nitrocellulose was bathed in 50 ml stripping buffer (62.5 mM Tris-HCl, pH 6.7, 2 % (w/v) SDS, 100 mM  $\beta$ -mercaptoethanol (added fresh)) at 55°C for 30 minutes. The membrane was then transferred to TBS-tween for 4\*10 minutes washes prior blocking in a suitable solution (see table 2.6). The membrane was then probed as explained in section 2.2.6.2.

## 2.2.6.4 Quantification of bands detected on western blot

To allow comparison between samples, band intensities were measured using AIDA software according to the manufacturer's instructions. Intensities of each band of interest were measured and corrected for background. Each band intensity was then also corrected for total protein using the corresponding copper stained full lane (figure 2.3). Each treatment was then expressed as a percentage compared to corresponding control  $\pm$  SEM. Data were statistically analysed by a paired t-test using a two-tailed distribution.

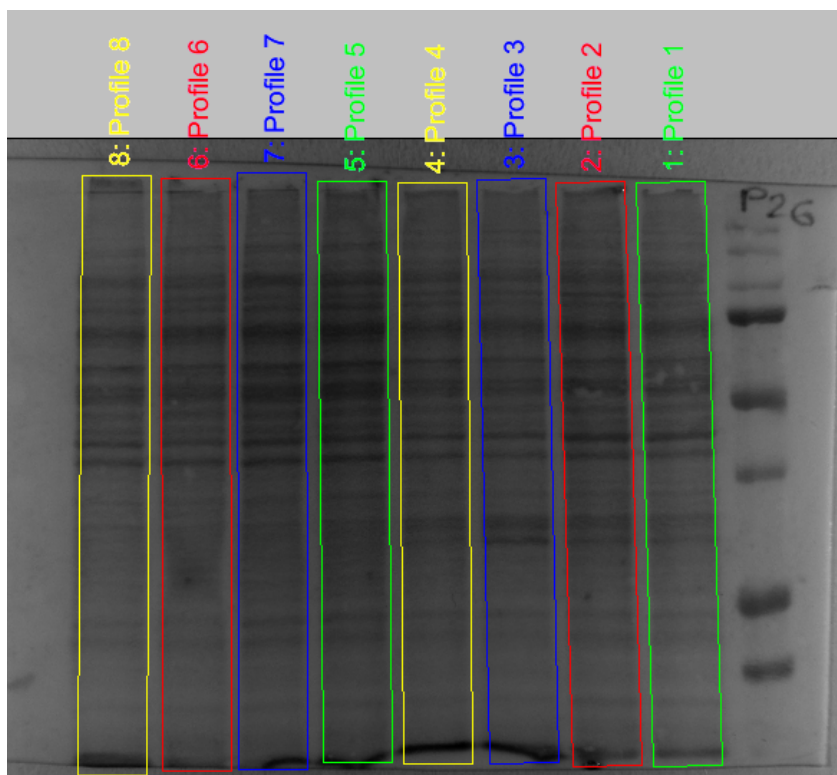


**Figure 2.3: Copper stained western blots showing total protein staining of different samples.** Cells were pre-differentiated for 16 hours in serum free medium supplemented with 0.3 mM dbcAMP. Following incubation, cells were treated or not with 1 mM MPTP for 24 hours. Subcellular fractionation was then carried out and 20  $\mu$ g protein from each fraction for each treatment were fractionated by 1D-SDS-PAGE (12 % resolving gel) and then transferred onto a nitrocellulose membrane. Blots were stained with copper pthalocyanine (section 2.2.6.1) to check for protein loading and efficiency of transfer. A typical digital image is shown here. Each lane intensity was quantified, using AIDA software. Each lane was labeled as profile 1 to 8.

### 2.2.7 Purity assessment of subcellular fractions using activity assays

#### 2.2.7.1 Succinate dehydrogenase activity assay

To assess the mitochondrial yield in the “mitochondrial fraction” and contamination in other fractions, a succinate dehydrogenase (SDH) activity assay was used. Following subcellular fractionation (refer to section 2.2.4), glass test tubes were prepared containing 1 % (w/v) iodonitrotetrazolium (INT), 100 µl SDH buffer (0.25 M sodium phosphate, 5 mg / ml bovine serum albumin (BSA), pH 7.4), 150 µl distilled water and 50 µl fraction sample. Tubes were equilibrated at 37°C in a water bath prior to the addition of 100 µl sodium succinate (100 mM). The tubes were incubated for 1 hour 30 minutes in a water bath at 37°C and the reaction was stopped by the addition of 500 µl trichloroacetic acid (TCA) (10 % (w/v)). 3 ml ethylacetate were added to each tube and thoroughly vortex mixed. Tubes were incubated overnight for the organic phase to separate from the aqueous phase. 100 µl of the top aqueous phase were transferred to a 96-well-plate and the absorbance was read at 490 nm. Absorbance versus time was plotted and the gradient of the plot was used to calculate the specific activity in each sample. Results were expressed as a mean specific activity per microgram protein (each fraction was protein estimated using the Bio-Rad reagent, refer to section 2.2.3); in order to check for enrichment, the specific activity values for various fractions were normalised against the specific activity of the total extract (given a value of 1). Data were expressed as mean  $\pm$  SEM and statistically analysed by a paired t-test using a two-tailed distribution.

#### 2.2.7.2 NADPH-cytochrome c reductase (NADPH-CR) activity assay

In a cuvette, 1 ml of NADPH-CR buffer (50 mM sodium phosphate, 0.1 mM EDTA, pH 7.7), 50µl cytochrome c (25 mg/ml) in NADPH-CR buffer and 50 µl fraction sample were added. 100 µl NADPH (2 mg/ml) in NADPH-CR buffer were added. Absorbance was recorded every 15 seconds for 3 minutes at 550 nm. Absorbance versus time was plotted and the gradient of the plot was used to calculate the specific activity in each sample. Results were expressed as a mean specific activity per microgram protein (each fraction was protein estimated using the Bio-Rad reagent, refer to section 2.2.3); in order to check for enrichment, the specific activity values for various fractions were normalised against

the specific activity of the total extract (given a value of 1). Data were expressed as mean  $\pm$  SEM and statistically analysed by a paired t-test using a two-tailed distribution.

### 2.2.7.3 Marker protein detection by western blot analysis

The different fractions and total extracts following subcellular fractionation (section 2.2.4) were further analysed by western blotting (section 2.2.5 and 6) using anti-cytochrome c, anti-lamin A/C, anti-GAPDH and anti-LAMP2 antibodies as specific markers of mitochondrial, nuclear, cytoplasmic and lysosomal fractions, respectively, as primary antibodies (for protocol refer to table 2.6). Intensities of each band were measured relative to copper stain band intensities as described in section 2.2.6.4. In order to check for enrichment, the corrected intensity values for various fractions were normalised against the corrected intensity of the total extract (given a value of 1). Data were expressed mean ratio  $\pm$  SEM and statistically analysed by a paired t-test using a two-tailed distribution.

## 2.2.8 2-Dimensional-SDS-PAGE (2DE)

To improve protein separation on a gel, proteins can be separated by their charge using isoelectrofocusing (IEF) prior to being separated by their molecular weight using SDS-PAGE (O'Farrell, 1975).

### 2.2.8.1 First dimension: the IEF step

#### - pI 3-10 large gels

Mitochondrial samples containing 150-200  $\mu$ g protein were pelleted as explained in section 2.2.4.3. 300  $\mu$ l (IEF) rehydration buffer (8 M urea, 4 % (w/v) CHAPS, 2 % (v/v) carrier ampholyte, 0.0002 % (w/v) bromophenol blue, 65 mM DTT (added freshly) in nanopure water) were added to the mitochondrial pellets and shaken for 2 hours at room temperature. Then, samples were transferred to the large IEF focusing tray (17 cm) along with a ReadyStrip immobilized pH gradient (IPG) strip (pH 3-10, 17 cm, Bio-Rad) and allowed to passively rehydrate for 1 hour before overlaying each strip with 4 ml mineral oil. Strips were then actively rehydrated for 13 hours 40 minutes at 50 V using a PROTEAN IEF cell followed by focusing (250 V for 20 min linear, 10,000 V for 2 hours 30 minutes linear,

10,000 V for 60,000 V/hour rapid). Strips were then transferred to a plastic equilibration tray and stored at -80°C or processed to equilibration immediately.

- pI 3-10 and pI 5-8 mini-gels

A similar protocol was used except that volumes and quantities were smaller. Mitochondrial samples containing 50-80 µg protein were pelleted or acetone precipitated. Up to 125µl sample IEF rehydration buffer were added to the mitochondrial pellets and shaken for 2 hours at room temperature. Then, samples were transferred to the small IEF focusing tray (7 cm) along with a ReadyStrip IPG strip (pH 3-10 or pH 5-8, 7 cm, Bio-Rad) and allowed to passively rehydrate for 1 hour before overlaying each strip with 2 ml mineral oil. Strips were then actively rehydrated for 13 hours 40 minutes at 50 V using a PROTEAN IEF cell followed by focusing (250 V for 15 min linear, 4,000 V for 2 hours linear, 4,000 V for 10,000 V/hour rapid). Strips were then transferred to a plastic equilibration tray and stored at -80°C or processed to equilibration immediately.

For optimisation purposes, different detergents were trialled in the IEF rehydration buffer: 4% CHAPS was replaced by 1.5 % triton or 4 % ASB-14. 8 M urea could also be replaced by 6 M urea and 2 M thiourea for the same purposes and acetone precipitation prior sample lysis was also tested.

- pI 7-10 mini gels

A different protocol had to be used for pI 7-10 mini-gels. 50-80 µg mitochondrial samples were acetone precipitated. Then, 1.5 % destreak reagent was added to pI 7-10 IEF rehydration buffer (6 M urea, 2 M thiourea, 4 % (w/v) CHAPS, 1X (v/v) pI 7-10 Bio-lyte, 0.0002 % (w/v) bromophenol blue in nanopure water) and mixed thoroughly. Then, 110 µl buffer were transferred to a small plastic equilibration tray (7 cm) along with a ReadyStrip IPG strip (pH 7-10, Bio-Rad) and allowed to passively rehydrate for 1 hour before overlaying each strip with 2 ml mineral oil. Strips were then passively rehydrated overnight on the bench. Strips were transferred to the IEF focusing tray. Wicks were added on both sides of the strips between the electrodes and the strips. Up to 65 mM DTT were added to 15 µl freshly thawed pI 7-10 IEF rehydration buffer and mixed for 1 hour with 50-80 µg acetone precipitated mitochondrial proteins. The samples were then added under the passively rehydrated strips on the positive side. Following a 30 minutes incubation, 2 ml mineral oil were overlaid and strips were focused (250 V for 15 min linear, 4,000 V for 2

hours linear, 4,000 V for 15,000 V/hour rapid). Strips were then transferred to a plastic equilibration tray and stored at -80°C or processed to equilibration immediately.

#### 2.2.8.2 Equilibration of strips

Following IEF, strips were equilibrated by shaking gently for 15 minutes in equilibration buffer I (6 M urea, 2 % (w/v) SDS, 20 % (v/v) glycerol, 50 mM Tris pH 8.8, in nanopure water and 2 % (w/v) DTT) and then 15 minutes in equilibration buffer II (6 M urea, 2 % (w/v) SDS, 20 % (v/v) glycerol, 50 mM Tris pH 8.8 in nanopure water and 2.5 % (w/v) iodoacetamide).

For optimisation purposes, a different concentration of glycerol (30 % (v/v)) was trialled in both equilibration buffers.

#### 2.2.8.3 Second dimension: SDS-PAGE

12 % (w/v) polyacrylamide resolving gels overlaid with a 1-2 cm 4 % (w/v) polyacrylamide stacking gel were prepared (refer to section 2.2.5). Strips were then rinsed in running buffer, inserted onto the SDS-PAGE stacking gel and overlaid with 1.5 % melted agarose. SDS-PAGE was then run as explained in section 2.2.5.4. Gels were then transferred onto a nitrocellulose membrane and probed as explained in section 2.2.6 or transferred to a plastic tray for staining.

#### 2.2.8.4 Gel staining

##### - Silver stain

PlusOne Silver staining kit was used to dye total proteins. The protocol was following the manufacturer's instructions (GE Healthcare) and is shown in table 2.7. Gels were then imaged using The Fujifilm FLA-5100 image scanner using digitising parameters.

<b>STEP</b>	<b>REAGENT</b>	<b>PROTOCOL</b>
<b>Fixation step</b>	50 % (v/v) ethanol, 10 % (v/v) acetic acid in ultra pure water	2 * 15 min Thorough shaking
<b>Washing step</b>	Ultrapure water	4 * 5 min Thorough shaking
<b>Sensitization step</b>	30 % (v/v) ethanol 0.2 % (v/v) sodium thiosulphate 500 $\mu$ M sodium acetate in ultrapure water	1 * 30 min Gentle shaking
<b>Washing step</b>	Ultrapure water	4 * 15 min Thorough shaking
<b>Silver stain step</b>	0.25 % (v/v) silver nitrate solution in ultrapure water	1 * 20 min Gentle shaking
<b>Washing step</b>	Ultrapure water	2 * 1 min Thorough shaking
<b>Developing step</b>	236 $\mu$ M sodium carbonate 0.148 % (v/v) Formaldehyde in ultrapure water	Until proteins appear Thorough shaking
<b>Stopping step</b>	183 $\mu$ M EDTA- $\text{Na}_2$	1 * 10 min Thorough shaking
<b>Wash step</b>	Ultrapure water	2 * 5 min Until pick spots Thorough shaking

**Table 2.7: Silver staining steps**

- SyproRuby

SyproRuby dye kit was also used to dye total proteins. The protocol was following the manufacturer's instructions (Invitrogen) and is shown in table 2.8. Gels were then imaged with The Fujifilm FLA-5100 image scanner using the following parameters: 1 image / 1 Laser, 473 nm laser, LPB filter at 600 V resolution.

If the gels were stained with ProQ Diamond dye prior SyproRuby, the fixation step was replaced by a 2 \* 5 minutes washing step in ultrapure water.

STEP	REAGENT	PROTOCOL
<b>Fixation step</b>	50 % (v/v) ethanol, 10 % (v/v) acetic acid in ultra pure water	2 * 15 min Thorough shaking
<b>Stain step</b>	SYPRO Ruby gel stain	Overnight (16 hours) Gentle shaking
<b>Background destain step</b>	10 % (v/v) methanol 7 % (v/v) acetic acid	30 min Thorough shaking
<b>Wash step</b>	Ultrapure water	2 * 5 min Thorough shaking

**Table 2.8: SyproRuby staining steps.**

- ProQ Diamond

ProQ Diamond dye kit was used to dye specifically phosphorylated proteins. The protocol was following the manufacturer's instructions (Invitrogen) and is shown in table 2.9. Gels were then imaged with The Fujifilm FLA-5100 image scanner using the following parameters: 1 image / 1 Laser, 532 nm laser, Cy3 filter at 600 V resolution.

STEP	REAGENT	PROTOCOL
<b>Fixation step</b>	50 % (v/v) methanol, 10 % (v/v) acetic acid	overnight 30 min
<b>Wash step</b>	Heated Ultrapure water	4 * 15 min
<b>Stain step</b>	ProQ diamond stain	3 hours
<b>Destain step</b>	20 % (v/v) acetonitrile 50 mM sodium acetate, pH4	4 * 1 hour
<b>Wash step</b>	Ultrapure water	5 min 5 min (image 1) 20 minutes (image 2)

**Table 2.9: ProQ Diamond staining steps.**

2.2.8.5 2D-SDS-PAGE image analysis

To allow comparison between 2D-gel electrophoretogram pictures, the SameSpots software from Progenesis was used. Images of each gel were taken using Fujifilm FLA-5100 image scanner. Pictures were transferred to Samespots software (Progenesis) and each gel image

was aligned to one chosen gel (called reference). The statistical package allowed choosing the best alignment features. Each isolated spot volume was normalised to the total volume spot calculated for the given gel. Each treatment gel was paired with its corresponding control gel and each aligned spot was compared for normalised volume in each gel and compared to other gels. The statistical analysis was included in the software. Any spot showing changes in level between controls and treatments with a  $p < 0.1$  using a paired student t-test was selected.

### 2.2.9 Spot picking and trypsinisation

Following image capture, gels were washed in ultrapure water. Selected spots (for 2DE) were picked using sterile tips with cut ends and transferred to 1.5 ml sterile Eppendorf tubes. These spots were incubated overnight in LC-MS grade water.

A solution of 25 mM ammonium bicarbonate was prepared fresh as well as 2:1 (v:v) acetonitrile (ACN): 25 mM ammonium bicarbonate. Water was removed from the tubes containing gel pieces, after which gel pieces were dehydrated in 50  $\mu$ l ACN: ammonium bicarbonate (2:1) for 15 minutes whilst shaking. Then, they were rehydrated in 50  $\mu$ l 25 mM ammonium bicarbonate for 10 minutes. Gel pieces were dehydrated again the same way as before for 15 minutes. Eppendorf tubes were pulsed centrifuged and supernatants removed. The gel pieces were left until dry. Then, 25  $\mu$ l 10 mM DTT in 25 mM ammonium bicarbonate were then added to each Eppendorf tube followed by 45 minutes incubation in 56°C. Supernatants were then removed and replaced by 25  $\mu$ l 55 mM iodoacetamide in 25 mM ammonium bicarbonate. Samples were incubated at room temperature in the dark for 30 minutes. Supernatants were then removed and gel pieces were then rehydrated as before, followed by a dehydration step, another rehydration step and a final dehydration step. Gel pieces were left to dry. When the spots were dry, 15  $\mu$ l 12.5 ng /  $\mu$ l trypsin were added to the gel pieces and left on ice for 2 minutes. Once the samples were fully rehydrated, the excess trypsin was removed and replaced by 15  $\mu$ l 25 mM ammonium bicarbonate. Eppendorf tubes were quickly spun to make sure the gel pieces were fully immersed in the solution. Samples were incubated at 37°C for 4 hours. Eppendorf tubes were transferred onto a shaker for 20 minutes. Supernatants were then transferred to 0.5 ml Eppendorf tubes leaving the used tip in the small tube. To improve peptide recovery, 10  $\mu$ l 4:1 ACN : LC-MS grade water (v/v) were added to the gel pieces and left for 15 minutes while shaking.

Tubes were pulsed centrifuged prior transferring the supernatant to the corresponding 0.5 ml tube using the tips used in the last transfer. Then, 5  $\mu$ l 0.1 % trifluoroacetic acid (TFA) were added to each tube. Finally, 1  $\mu$ l sample was plated on the MALDI plate followed by 1  $\mu$ l 10 mg CHCA matrix / ml in 50 % (v/v) ACN / 0.1% (v/v) TFA.

### **2.2.10 Mass spectrometry and database searching**

Peptide mass spectra were processed using Matrix-Assisted-Laser-Desorption ionisation-time-of-flight (MALDI-TOF) mass spectrometer (Axima mass spectrometer, Shimadzu). Proteins were then identified by transferring mass lists from mass spectra to the Mascot database. The Swiss-Prot database was chosen as well as carbamidomethylation as a fixed modification and oxidation (M) as a variable modification. Positive identity was given by scores over 54 (comparing Swiss-Prot database) and their molecular mass and pI were compared to the position of the spot on the original gel.

### **2.2.11 Phosphorylated amino acid co-localisation with VDAC detection using 2D-blot analysis**

Proteins separated by 2DE were transferred onto nitrocellulose membranes. Blots were stained with copper stain as described in section 2.2.6.1. The membrane was cut around the molecular weight level of VDAC1 according to the copper stain as compared to the spot previously identified as VDAC1 using silver stained gels by MALDI-TOF mass spectrometry (figure 2.5). Immunoprobings with anti-phosphoserine, anti-phosphothreonine or anti-phosphotyrosine antibodies was carried out as described in section 2.2.6.2 and table 2.6. Following visualisation, antibodies were stripped off the membrane and the blots were re-probed using the anti-VDAC1 antibody as described in section 2.2.6.3. Spots at the basic end of the blots co-localising with VDAC detection, following phosphoamino acid residue detection were considered to be phosphorylated forms of VDAC1 protein.

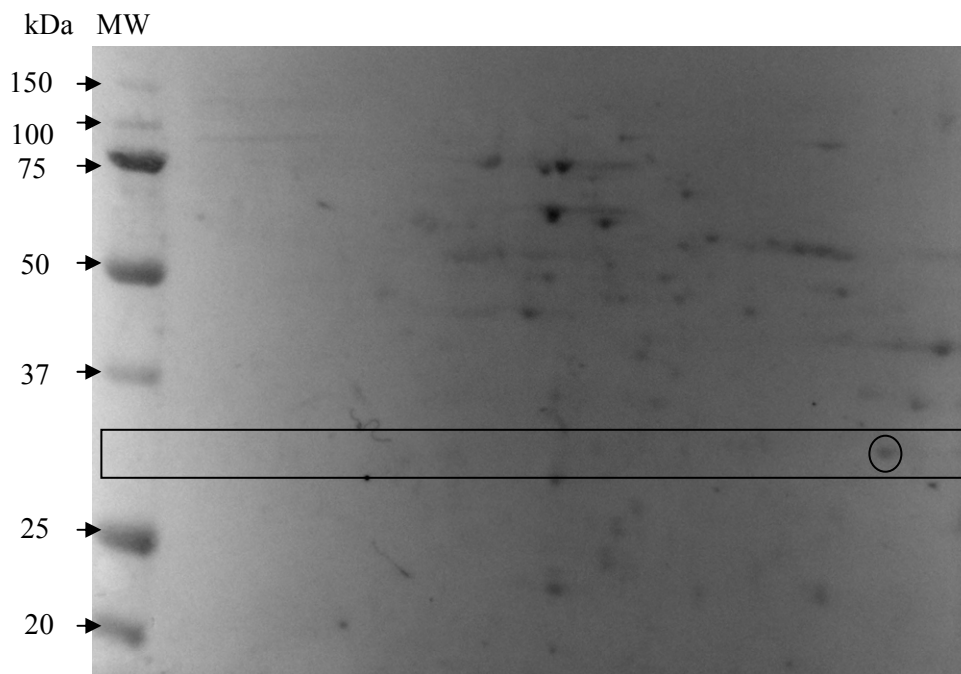


**Figure 2.4: Copper stained 2D-blots showing total protein staining and VDAC1 location**

50  $\mu$ g protein from mitochondrial fractions were fractionated by 1D-SDS-PAGE (12 % resolving gel) and then transferred onto a nitrocellulose membrane. Blots were stained with copper pthalocyanine (section 2.2.6.1) to check for protein loading and efficiency of transfer. The picture represents a typical digital image, in which VDAC1 is circled. The rectangle shows the part of the blot cut out for further antibody labeling with anti-phosphoamino acid antibodies followed by stripping the blot and VDAC1 detection.

## 2.2.12 Caspase-3 activity assay

### 2.2.12.1 Fluorimetric activity assay

Caspase-3 activity was determined using a fluorimetric assay by measuring the apparition of a fluorescent peptide product of caspase-3 cleavage.

Cell pellets were prepared from one T25 flask per treatment as explained in section 2.2.1. Pellets were resuspended in 100  $\mu$ l ice-cold lysis buffer (50 mM HEPES, pH7.4, 5 mM CHAPS, 5 mM DTT) and vortex mixed for 1 minute prior to centrifugation for 2 minutes at 13,000 g. Samples were then set up as follows in a black 96-well plate: 80  $\mu$ l assay buffer (20 mM HEPES, pH 7.4, 2 mM EDTA, 0.1% (w/v) CHAPS, 5 mM DTT) and 10  $\mu$ l sample supernatant. Two blanks were added as follows: 80  $\mu$ l assay buffer and 10  $\mu$ l lysis buffer. To start the reaction, 10  $\mu$ l peptide substrate (Ac-DVED-AMC) were added to each well to

start the reaction. The fluorescence was read every 5 minutes for 2 hours using 360 nm excitation and 460 nm emission wavelengths using a fluorimeter plate reader.

#### 2.2.12.2 Bicinchoninic (BCA) protein assay

Because reducing and detergent reagents were used in the caspase-3 lysis buffer, the Bio-Rad protein estimation reagent was not compatible. The BCA protein assay kit from Thermo Scientific was used following the manufacturer's instruction. BSA standards ranging from 0 to 2000  $\mu\text{g} / \text{ml}$  were used to produce a calibration graph from which a linear correlation was calculated. Duplicate BSA standards were prepared as shown in table 2.10.

Tube label	Concentration of BSA ( $\mu\text{g} / \text{ml}$ )	Source and volume BSA ( $\mu\text{l}$ )	Volume of lysis buffer ( $\mu\text{l}$ )
A	2,000	100 $\mu\text{l}$ 2mg / ml stock	0
B	1,500	100 $\mu\text{l}$ 2mg / ml stock	33
C	1,000	50 $\mu\text{l}$ tube A	50
D	750	50 $\mu\text{l}$ tube B	50
E	500	50 $\mu\text{l}$ tube C	50
F	250	50 $\mu\text{l}$ tube E	50
G	125	50 $\mu\text{l}$ tube F	50
H	0	0 $\mu\text{l}$	100

**Table 2.10: Serial dilutions of BSA standards using the provided 2 mg / ml BSA stock.**

Nine microliters of each sample and standards were added to the centre of the 96-well plate provided. Then, 260  $\mu\text{l}$  freshly prepared BCA working reagent (50:1 provided reagents A:B) were added to each well. The plate was then covered with foil and mixed on a shaker at medium speed for 1 minute. The plate was then incubated at 37°C for 30 minutes. The plate was then cooled at room temperature for 5 minutes prior to measuring the absorbance at 570 nm using a plate reader. The protein concentration of each sample was calculated from the mean of duplicates using the linear correlation obtained from the BSA calibration curve.

### 2.2.12.3 Data analysis

Results were expressed as the mean of specific caspase-3 activity (activity /  $\mu\text{g}$ )  $\pm$  SEM. Data were statistically analysed by a paired t-test using a two-tailed distribution.

## 2.2.13 RT-PCR

### 2.2.13.1 RNA isolation from cells

Isolating RNA from cells requires very clean, particularly ribonuclease-free, surfaces and equipment. All surfaces and equipment were therefore cleaned carefully with water, sprayed with 70 % (v/v) ethanol, followed by a RNaseZap spray. All steps were carried out at room temperature.

One T75 flask of mouse N2a neuroblastoma cells per treatment was grown as explained in section 2.2.1. RNA was extracted using the Qiagen RNeasy mini kit following the manufacturer's instructions. Cell pellets were then washed twice by centrifugation in PBS. The subsequent pellets were resuspended in 300  $\mu\text{l}$  RLT buffer (from kit) with 1% (v/v)  $\beta$ -mercaptoethanol. Suspensions were applied onto Qia-Shredder columns (Qiagen) followed by a 2 minute centrifugation at 10,000 g. Columns were then discarded and 300  $\mu\text{l}$  70 % (v/v) ethanol were added to the flow through and mixed by pipetting. Samples were then applied onto the RNeasy columns (from kit). They were centrifuged for 15 seconds at 10,000 g and flow throughs were discarded. 700  $\mu\text{l}$  RW1 buffer (from kit) were added to each column, which were centrifuged again at 10,000 g for 15 seconds. The flow-throughs were discarded. 500  $\mu\text{l}$  RPE buffer (from kit) were added and columns were centrifuged for 15 seconds at 10,000 g. These two steps (RPE buffer and spin) were repeated once more. Flow throughs were discarded and columns were centrifuged at 10,000 g for 2 minutes. Flow throughs were once more discarded. Columns were transferred onto fresh tubes, 35  $\mu\text{l}$  RNase free water (from kit) were applied, columns were left to stand for 5 minutes and then centrifuged at 10,000 g for 2 minutes. Columns were discarded. The flow through contained the RNA. RNA was kept at  $-80^{\circ}\text{C}$  or processed immediately.

RNA concentration of RNA dilutions was measured using the Beckman spectrophotometer. Absorbance at 260 nm ( $A_{260}$ ) was used for RNA concentration (should be over 0.2; if not, a lower dilution of the RNA was needed). Absorbance at 280 nm ( $A_{280}$ ) corresponded to the

DNA concentration. The  $A_{260} / A_{280}$  ratios were calculated. An adequate ratio should be over 1.6. RNA concentration was calculated for each sample as follows:

$$\text{RNA concentration (ng / } \mu\text{l)} = A_{260} * \text{dilution factor} * 44$$

### 2.2.13.2 Reverse transcription

Typically, 2  $\mu\text{g}$  RNA were used and diluted in autoclaved distilled water for a total of 10  $\mu\text{l}$  in 0.5 ml Eppendorf tubes. Two master mixes were prepared. Master mix 1 was containing 1  $\mu\text{l}$  dNTPs and 1  $\mu\text{l}$  oligo dT18 (TTTTTTTTTTTTTTTTTT primer from Sigma) per number of samples used. Master mix 2 contained 4  $\mu\text{l}$  5X first strand buffer (Invitrogen), 2  $\mu\text{l}$  0.1 M DTT (Invitrogen) and 1  $\mu\text{l}$  water per number of samples used. 2  $\mu\text{l}$  master mix 1 were added to each 10  $\mu\text{l}$  RNA sample. Tubes were vortex mixed, spun, left 5 minutes at 65°C and then transferred to melting ice for 2 minutes. Tubes were then quickly spun at 10,000 g (1 second). 7  $\mu\text{l}$  master mix 2 were added to each tube. Samples were vortex mixed, quickly spun and left 2 minutes at 42°C. 1  $\mu\text{l}$  SuperScript II enzyme (Invitrogen) was quickly added to each tube and mixed. Tubes were incubated at 42°C for 70 minutes followed by 15 minutes at 70°C. Resulting cDNA samples were then frozen at -20°C.

### 2.2.13.3 Polymerase chain reaction (PCR)

The sequences of the primers (Sigma) are shown in table 2.11. Paired forward and reverse primers were mixed together at a 10 mM concentration each. A master mix 3 was prepared as follows: 20  $\mu\text{l}$  water, 2.5  $\mu\text{l}$  10X Accuprime PCR buffer and 1  $\mu\text{l}$  primer mix per number of samples used. Two master mixes were prepared: one for VDAC1 DNA sequence amplification and one for GAPDH DNA sequence amplification. Then, 23.5  $\mu\text{l}$  master mix 3 were added to 1  $\mu\text{l}$  template. Templates were also aliquoted in duplicates: one for VDAC1 sequence and one for GAPDH amplifications. Tubes were vortex mixed and spun quickly. To start the reaction, 0.5  $\mu\text{l}$  Accuprime *Taq* polymerase (Invitrogen) were added. Tubes were mixed very gently and transferred to the PCR machine. The program was as follows: 2 minutes at 95°C, 30 cycles of [30 seconds at 95°C, 30 seconds at 59°C and 1 minute at 68°C], 2 minutes at 68°C and hold at 4°C.

Primer name	Sequence (5' - 3')	Annealing temperature
mVDAC1-forward	GGGTACAAGAGGGAGCACATCA	68°C
mVDAC1-reverse	CTCTGTCCCGTCATTCACATTAG	68°C
mGAPDH-forward	CTCATGACCACAGTCCATGC	64.4°C
mGAPDH-reverse	CACATTGGGGGTAGGAACAC	64°C

**Table 2.11: Sequences of primers used.**

#### 2.2.13.4 Agarose gel electrophoresis

Agarose (1.5 % w/v) was prepared in 100 ml Tris acetate EDTA (TAE) buffer (40 mM Tris, 0.1 % (v/v) acetic acid, 2 mM EDTA). The agarose was heated until completely melted. 4 µl ethidium bromide were added. Melted agarose was then cooled under tap water until the bottle could be held with bare hands. The agarose was poured onto the gel electrophoresis tray, a comb was added and gel was allowed to set. Then, 3 µl 10X loading buffer (0.025 % (w/v) bromophenol blue, 20 % (v/v) Ficoll, 1 % (w/v) SDS, 0.1 M EDTA, pH 8.0) were added to each 25 µl sample. When the gel was set, it was transferred to the tank, the comb was removed and the gel was immersed in TAE buffer. The required volume of sample was loaded onto each lane as well as the DNA ladder on the two lanes on both sides. The gel was run at 60 mA until samples were in the gel and 1 hour at 80 mA. The gel was stopped and imaged using the UV transilluminator.

To allow comparison between samples, band intensities were measured using AIDA software according to manufacturer's instructions. Intensities of each band resulting from VDAC1 and GAPDH gene amplifications were measured and corrected for background. Log intensities were plotted against log volumes. For the chosen volume (8 µl), each intensity was calculated from the linear equation. Then, VDAC1 band intensities were corrected to corresponding GAPDH intensities (calculated ones). Corrected values were then expressed as a percentage compared to the corresponding control ± SEM. Data were statistically analysed by a paired t-test using a two-tailed distribution.

### 2.2.14 Real-time RT PCR

#### 2.2.14.1 Sample preparation

RNA isolation from cell extracts and reverse transcription was undertaken as previously described in 2.2.13.1 and 2.2.13.2.

#### 2.2.14.2 DNA standards preparation

A PCR reaction was set up using two control samples with the primer pairs for GAPDH and VDAC1 amplification as described previously in section 2.2.13.3. A 1.5 % (w/v) agarose gel was prepared as described in section 2.2.13.4. Amplified DNA samples were applied onto the gel and electrophoresed as previously described. The resulting bands were excised using a scalpel and cDNA bands were extracted from the gel following the QIAquick gel extraction kit (Qiagen) manufacturer's instructions. The resultant samples, constituting the amplicons extracted from the gel, were then cloned into pCR-2.1-TOPO plasmid and transformed into TOP10 *E.coli* competent cells using TOPO TA cloning kit according to the manufacturer's instructions (Invitrogen). The plasmid DNA were then extracted from the bacteria using the QIAprep Spin Mini-prep kit (QIAGEN) followed by EcoRI digestion following the manufacturer's instructions (Qiagen digestion kit, QIAGEN). Clones showing a band corresponding to the molecular weight of VDAC1 or GAPDH inserts were selected for sequencing (MWG The Genomic Company, Eurofins MWG Operon, UK) for checking the insert sequences.

Positive sequencing was followed by plasmid DNA extraction from the bacteria using the QIAGEN Plasmid Midi kit (QIAGEN). The DNA concentration was measured by measuring the absorbance of a 1:200 dilution as carried out previously in section 2.2.13.1.

The DNA plasmids containing GAPDH and VDAC1 inserts were linearised by digesting 10 µg DNA with Hind III restriction enzyme following the manufacturer's instructions (Fermentas, Germany). An aliquot of linear vector (5 µl) was electrophoresed on agarose gel to check that only one band was present. The rest of the linear vector solutions were further purified using QIAquick PCR purification kit (QIAGEN).

## 2.2.14.3 Standard dilutions

The concentration in DNA of each linear vector was measured as previously described (section 2.2.13.1). The number of double-stranded DNA molecules per  $\mu\text{l}$  in the original solution (labelled UL) was calculated as follows:

$$\frac{c \left( DNA \left[ g / \mu l \right] \right)}{\left( Fragment \ length \left[ bp \right] \right) \times M_r} \times N_A = \text{Molecules} / \mu l$$

**c**: Concentration of DNA previously measured (g /  $\mu\text{l}$ )

**N<sub>A</sub>**: Avogadro's number =  $6.022 \times 10^{23}$  molecules / mol

**M<sub>r</sub>**: molecular weight of double stranded DNA = 660 g / mol  $\times$  bp

Serial standard solutions were prepared from the UL solution, containing  $10^{10}$ ,  $10^8$  and  $10^7$  as stocks of cDNA molecules, stored at  $-20^\circ\text{C}$ .

## 2.2.14.4 Real-time PCR

cDNA sample content was quantified using Rotor-gene 3000 Thermal cycler (Corbett Research, Germany). Dilutions of GAPDH cDNA samples were prepared (1 in 5 dilution in autoclaved water). A master mix containing SensiMixPlus SYBR was prepared following the manufacturer's instructions (Quantace Ltd, UK, table 2.12).

VDAC1 and GAPDH standard solutions from  $10^7$  to  $10^1$  molecules, were freshly prepared from the  $10^7$  solution previously obtained (section 2.2.14.3), using RT buffer (10 mM Tris, 15 mM KCl, 0.6 mM  $\text{MgCl}_2$ , pH 8.0) as a diluent.

<b>Solution</b>	<b>Volume * no. sample (<math>\mu\text{l}</math>)</b>
<b>SensiMix SYBR</b>	5
<b>Primer mix (5 <math>\mu\text{M}</math> each )</b>	0.4
<b>Autoclaved water</b>	3.6

**Table 2.12: Master mix containing SensiMix SYBR for real-time PCR**

Then, 9  $\mu$ l SensiMix SYBR master mix were transferred to Rotor-gene real-time PCR tubes, followed by addition of 1  $\mu$ l standard or sample to each tube. Tubes were transferred to the Rotor-gene Thermo cycler and run through the following program: 95°C for 10 minutes for initiation and enzyme activation, 35 cycles of [95°C for 15 seconds, 65°C for 30 seconds, 72°C at 66 bp /sec].

#### 2.2.14.5 Data analysis

Data were analysed using the Rotor-gene 6000 series software. Selecting all samples on the graph showing the fluorescent signal expansion as the cycle number increases, a threshold value was calculated automatically by the software. The cycle number reached at the threshold for each sample was called the Ct value. Each Ct value for standards was transferred onto a standard graph of Ct against concentrations as defined by the serial dilutions prepared. Sample Ct values could then be reported to the standard graph and the copy number for each sample calculated. Each triplicate sample was run in duplicate for each gene of interest, GAPDH and VDAC1. VDAC1 mRNA was expressed as molecules VDAC1 mRNA per 1,000 molecules GAPDH mRNA ratios  $\pm$  SEM for each sample. Data were statistically analysed by a paired t-test using a two-tailed distribution.

## **CHAPTER III:**

# **ESTABLISHING METHODS FOR THE ANALYSIS OF THE MITOCHONDRIAL PROTEOME**

### 3.1 INTRODUCTION

#### 3.1.1 Pre-differentiated mouse neuroblastoma cells: a model to investigate Parkinson's disease

##### 3.1.1.1 Experimental models of study for Parkinson's disease

To study neurodegeneration in Parkinson's disease (PD) different experimental models have been used, each exhibiting strengths and limitations. The choice of model often depends on the specific study carried out. Three different types of experimental models have been used to study Parkinsonism features; these are post-mortem observations of neurons, use of experimental animal models and various cell line cultures (Olanow and Taton, 1999).

Post-mortem neurons from patients are an important tool to observe changes that occurred in PD patient's brain. For example, Lewy bodies were discovered by the observation of post-mortem neuronal tissues of patients in 1912 (reviewed in Olanow *et al.*, 2004) and are, nowadays, an important hallmark of the disorder. However, as with most post-mortem studies, it is difficult to establish which changes are actively involved in the cell death process. (Olanow *et al.*, 2004). Moreover, it is difficult to obtain access to precious brain samples and only limited laboratories work with them.

An ideal animal model for PD should have the following characteristics. The animal should have normal health during development notably in respect to its neuronal development, until starting gradual neurodegeneration in adulthood. The disorder should have similar symptoms to the disease in humans and similar cellular characteristics such as mitochondrial dysfunction and formation of Lewy bodies. The period of the disease should be short to allow rapid screening of drugs for potential therapies (Beal, 2001). Animal models are useful for studying the pathological, behavioural and symptomatic reactions and are essential for curative treatment trials prior to human testing (Deumens *et al.*, 2002). However animal models have their limitations. For example, since the toxins or other methods of study lead to changes in several cell types, a detailed study of individual cell types is difficult (this is also the case using primary cell cultures). Moreover, the actual concentration of agent reaching dopaminergic neurons is not known. Finally, using animal models raises ethical issues (Deumens *et al.*, 2002).

Primary cultures are composed of neuronal and glial cells and are adequate for looking at the overall effects of treatment on brain cells and particularly the interaction between glial and neuronal cells. However, it is again difficult to separate astrocytes from neurons (Augusti-Tocco and Sato, 1969). Separation techniques used include gradient centrifugation (Subbalakshmi and Murphy, 1983) and flow cytometry (Rozental *et al.*, 1995) although the purity of each resulting cell line is not neat.

The most ethical experimental models are *in vitro* models. On the other hand, established cell lines are essentially composed of one clonal cell type and they provide a good model for understanding the particular molecular pathways involved in a non-metabolised treatment in a particular type of cell (Cappelletti *et al.*, 2001). Disadvantages include the introduction of spontaneous genetic recombinations following a number of passages and the lack of potential interactions between different cell types that could occur *in vivo*.

#### 3.1.1.2 *In vitro* cultured cells

A good cell line for studying PD features should express neuronal properties. Human and rodent neuroblastomas and central nervous system tumour cells are more commonly used for that purpose (Cappelletti *et al.*, 2001). An important characteristic of a good cell line would be a stable genotype and phenotype (Beal, 2001). Three types of cells have been mainly used for studying PD: human SH-SY5Y neuronal cells, rat PC12 cells and mouse N2a neuroblastoma cells. Human SH-SY5Y neuronal cells are cholinergic cells exhibiting a neuronal phenotype (Shindo *et al.*, 1996). Their main advantages are that they are of human origin and have properties similar to dopaminergic neurons (Hu *et al.*, 2005), whilst a disadvantage is that their differentiation is not always easy to achieve (Beck, 2004, PhD thesis).

PC12 cells are rat adrenal pheochromocytoma cells that are able to synthesise, store and secrete dopamine similarly to dopaminergic nigral cells (Greene and Tischler, 1976). They can be induced to differentiate by extending neurites and acquiring the appearance of neurons when treated with nerve growth factor (NGF) (Greene and Tischler, 1976) but this is an expensive process.

### 3.1.1.3 Mouse N2a neuroblastoma and their differentiation

Mouse N2a neuroblastoma cells derived from a mouse spontaneous neuronal tumour in Jackson's Laboratories that has been maintained from the 1940s (Schubert *et al.*, 1969). The N2a clone is an adrenergic clone that shows neuronal morphology characterised by cell bodies with a large number of elongated processes (Augusti-Tocco and Satto, 1969). The cell line contains high levels of tyrosine hydroxylase and also low levels of dopamine, norepinephrine, serotonin and monoamine oxidase (MAO) (Narotzsky and Bondareff, 1994). Mouse N2a neuroblastoma differentiation has been well characterised using dbcAMP and removing serum (Prashad and Rosenberg, 1978, De Girolamo *et al.*, 2000). Indeed, Prashad and colleagues observed that cyclic AMP (cAMP) promoted the organisation of microtubules and microfilaments, whilst Chang and Prasad (1976) reported that cAMP decreased cell division. DbcAMP induced significant increases in cAMP levels in N2a cells when treated with serum free medium (Prashad and Rosenberg, 1978). Additionally, mouse N2a neuroblastoma cells have widely been used in a wide range of studies. These include toxicological studies to investigate the effects of a range of neurotoxins on neuronal cells (Harris *et al.*, 2009; Flaskos *et al.*, 1998) and their use as a model of study for a range of neurodegenerative diseases such as Alzheimer's disease (Zhou *et al.*, 2009), Huntington's disease (Ye *et al.*, 2008) and PD (Amazzal *et al.*, 2007; De Girolamo *et al.*, 2001).

Disadvantages of this cell line are that it is not primarily noradrenergic and it does not contain dopamine transporters (DAT) that would take up MPP<sup>+</sup>, the metabolised active compound of MPTP (Song *et al.*, 1997). Nevertheless, the cells can take up MPTP, which is converted to MPP<sup>+</sup> by endogenous MAO activity (Mizuno *et al.*, 1987; De Girolamo *et al.*, 2001).

## 3.1.2 Isolation of mitochondria using subcellular fractionation

### 3.1.2.1 Subcellular fractionation methods

To enrich the mitochondrial proteome, the choice of method for mitochondrial isolation and enrichment is the most important step. Subcellular fractionation involves separating the cells into different fractions corresponding to single organelles or groups of organelles. It is

divided into two steps: cell homogenisation and cell fractionation (de Araújo and Huber, 2007). The choice of method for these two steps depends on the nature of the sample. Cultured cells need a softer homogenisation than animal tissues such as, for example, pig liver, to avoid disruption of organelle membranes. The cytoskeleton and interaction of cytoskeletal proteins with organelles was observed to vary with each different cell lines so the homogenisation protocol has to be optimised for each cell line (de Araújo and Huber, 2007). Different types of soft homogenisation techniques have been described in the past including mechanical techniques, such as the use of manual dounce homogeniser and sonication, physical methods (e.g. freeze/thaw method) and chemical techniques, such as hypotonic shock (Lizotte *et al.*, 2005). For each method, it is important to check if cells were efficiently broken and if the organelles are intact. This can be done using staining methods and microscopy or using electron microscopy (Huber *et al.*, 2003). Many laboratories have used different fractionation methods depending on the fraction of the cell wanted. Differential centrifugation (Lai and Clark, 1979; Fernandez-Vizarra *et al.*, 2002), use of detergents (Lizotte *et al.*, 2005), chemical gradients (Pertoft, 1999; Aubry and Klein, 2006) and, sometimes, antibody based techniques have been employed (Murray *et al.*, 2004). The most commonly used fractionation method for cultured cells is differential centrifugation (Cox and Emili, 2006), developed by Lai and Clark (1979) and modified by groups to suit the sample used. Gradient steps have been added to purify the crude mitochondrial extracts resulting from differential centrifugation. Sucrose, salts, polysucrose (for example Ficoll and dextran), percoll and iodinated compounds have all been used and each have advantages and disadvantages (Pertoft, 2000).

Enzyme assays, immunoprobng western blots and electron microscopy have been widely used to assess the purity of fractions resulting from subcellular fractionation and it is an important step to confirm that the fractionation method is suitable for a specific cell type (Huber *et al.*, 2003). For example, succinate dehydrogenase (SDH) is known to be an enzyme from the Krebs cycle and constitutes complex II of the ETC on the inner side of the IMM (Ackrell, 2000). Cytochrome c is a protein also bound to the IMM where it performs its role in the ETC; it is also found in the intermembrane space as a soluble protein (Garrido *et al.*, 2006). Due to these properties SDH and cytochrome c were chosen as suitable mitochondrial markers. Glyceraldehyde-3-phosphate dehydrogenase (GAPDH), an aerobic and anaerobic glycolytic enzyme is a cytosolic protein, although GAPDH has also been observed to translocate to the nucleus during apoptosis (Hara *et al.*, 2006). The nuclear

marker chosen was lamin, a cytoskeletal protein exclusively found in the nucleus of cells and cleaved in apoptosis (Goldberg *et al.*, 1999). Although the subcellular fractionation procedure adapted produced only three fractions (mitochondrial, cytoplasmic and nuclear), the presence of lysosomes and endoplasmic reticulum was also investigated. The lysosomal marker chosen was lysosomal-associated-membrane protein 2 (LAMP2), present on the membrane of lysosomes as revealed by their name (Chang *et al.*, 2002). The endoplasmic reticulum chosen marker was NADPH-cytochrome c reductase, which was used in a study by Fujiki and colleagues (1982).

### **3.1.3 Studying the mitochondrial proteome using a proteomic approach**

#### 3.1.3.1 Proteomics techniques

Proteomics is a large-scale study which involves making an inventory of all the proteins present in an organism and analysing the interaction between these proteins (Govorun and Archakov, 2002). The proteomics approach has four principal applications. The primary role is mining; that is, identifying all proteins present in a sample. Another application is protein expression profiling; that is, the identification of a protein in a particular sample given its function in a particular state of the organism or cell or under exposure to a certain drug, chemical or physical stimulus. Moreover, proteomics can be used to determine how proteins interact with each other in a living system. This approach is called protein-network mapping and can be used to discover certain protein involved in signal transduction pathways. The last application, is mapping protein modifications, which involves identifying and localizing different modified forms of proteins, usually studied under various chemical, drug or physical conditions (Liebler, 2002).

Proteomics includes a wide range of high throughput technologies devised to separate complex mixtures of proteins or digested peptides followed by protein identification by mass spectrometry (Govorun and Archakov, 2002). Gel based methods have been widely employed, for example, 2-dimensional-gel electrophoresis (2DE) or blue-native-PAGE, both combined with matrix-assisted-laser-desorption ionisation mass spectrometry (MALDI-TOF) (Scheffler *et al.*, 2001), or 1D-SDS-PAGE combined with liquid chromatography-mass spectrometry (LC-MS) (Gaucher *et al.* 2004). Two-dimensional gels were first devised by O'Farrell in 1975 and have since then been widely used over the

decades. Typically, proteins from a complex mixture are separated using isoelectrofocusing (IEF) as a first step followed by SDS-PAGE as a second dimension. Resolved spots are then eluted and subjected to proteolytic digestion (Aebersold *et al.*, 1987) or in-gel digested (Rosenfeld *et al.*, 1992). Digested peptides can then be processed through MALDI-TOF in order to get a mass list that should correspond to one protein peptide profile (Scheffler *et al.*, 2001). Other techniques also widely used consist of digesting the protein mixture first and then fractionating the peptides using a range of chromatographic techniques. Such methods are commonly called the Shotgun proteome techniques. These techniques normally involve 2-dimensional liquid chromatography combined with tandem mass spectrometry (2D-LC-MS/MS), also known as MudPit technology (Stasyk and Huber, 2004), or isotope coded affinity tags (ICAT) generally combined with LC-MS (Govorun and Archakov, 2002). Proteomics techniques generally allow the study of protein mixtures of up to 1,000 proteins. So, for cellular studies, it has then been well documented that fractionating the cell reduces the complexity of the sample and allows a more comprehensive analysis (Lopez and Melov, 2002).

#### 3.1.3.2 The mitochondrial proteome

Mitochondria have been one of the most widely studied organelles for proteomic research (Bailey *et al.*, 2005). This interest in the mitochondrial proteome is partly due to the fact that mitochondria are relatively easily separated, although with a certain level of contamination (Taylor *et al.*, 2003b). It was originally thought that there were about 1,000-1,500 proteins forming the mitochondrial proteome (Taylor *et al.*, 2003b). Although a wide variety of techniques have been used, and a combination of them all would probably be ideal, 2DE is the most commonly employed technique for studying the mitochondrial proteome, due to its high resolution capacity (Govorun and Archakov, 2002).

### 3.1.4 Aims of the chapter

The overall objective of this chapter was to develop methods for the analysis of the mitochondrial proteome of neuroblastoma cells. A study of changes to the proteome following treatment with toxins that could mimick some of the biochemical features of PD would then follow (see chapter V). Included in this objective was the choice of using mitotic versus differentiated cells.

First, a protocol for the isolation of mitochondria with acceptable enrichment and contamination with other organelles was optimised, based on subcellular fractionation using differential centrifugation. Enrichment and contamination levels were monitored using a range of enzymatic and antibody-based methods.

Once a satisfactory protocol was devised, the resultant mitochondrial fractions were resolved by 2DE following a protocol modified from O'Farrell (1975). Buffer conditions were optimised based on the resolution, solubility and staining of the mixture of proteins. The reproducibility of such gels was then analysed and measures to minimise variability devised.

A final aim was to evaluate protein profile changes in the mitochondrial proteome following differentiation of neuroblastoma cells. Thus, proteins in mitotic and differentiated cells were compared using 2DE followed by peptide mass fingerprinting for potential spot identification.

## 3.2 RESULTS

The first step was to optimise the mitochondria isolation protocol for neuroblastoma cells by optimising each step of the protocol. Preliminary experiments designed to measure the efficiency of homogenisation showed that a glass-glass homogeniser was more efficient than a teflon-glass homogeniser and that the percentage of lysed cells following homogenisation was 50 to 75 % total cells (lysed plus unlysed cells) in N2a mouse neuroblastoma cells and 65-80 % in human SH-SY5Y neuroblastoma cells (data not shown). This percentage lysis was considered as acceptable as increasing the number of homogenisation passages would lead to disruption of organelle membranes. Following homogenisation the same protocol for differential centrifugation was applied for the two cell lines.

### 3.2.1 Comparison of protein recovery in the mitochondrial fraction following subcellular fractionation in mitotic N2a and SH-SY5Y neuroblastoma cells

Mouse N2a and human SH-SY5Y cells were grown to 80 % confluency as observed by microscopy in growth medium and cells were counted (refer to section 2.2.1.3) prior to homogenisation using an haemocytometer and subcellular fractionation (refer to section 2.2.4). Protein recovery and the relative presence of mitochondrial marker protein in the mitochondrial fraction were determined (refer to sections 2.2.3, 2.2.4 and 2.2.7). The mitochondrial marker protein distribution, as measured by SDH activity, was normalised against the total cell extract in each case (given a value of 1) in order to assess enrichment. Table 3.1 compares the protein recovery in the mitochondrial fraction in the two different cell lines. The protein content per  $10^6$  cells recovered in the mitochondrial fraction of mouse N2a neuroblastoma cells was significantly higher than with SH-SY5Y cells. The enrichment of mitochondria in the mitochondrial fraction compared to total extract was 5.5-fold in the N2a cells and 3.5-fold in the SH-SY5Y cells, which was not significantly different between the two cell lines.

Because the recovery of mitochondrial proteins by subcellular fractionation was more than doubled in the mouse N2a cells, these cells were used in the following experiments using mitochondrial fractions.

	Mitochondrial protein recovery ( $\mu\text{g} / 10^6$ cells) <sup>1</sup>	Mitochondria enrichment compared to total extracts <sup>2</sup>
Mouse N2a cells	65.3 $\pm$ 12.1	5.5 $\pm$ 1.97
Human SH-SY5Y cells	23.9 $\pm$ 6.7 *	3.5 $\pm$ 1.24

**Table 3.1: Protein recovery in the mitochondrial fractions from mitotic mouse N2a and human SH-SY5Y cells**

Mitotic mouse N2a and Human SH-SY5Y neuroblastoma cells were detached and counted followed by subcellular fractionation as described in section 2.2.4. <sup>1</sup> Protein estimation of the resultant mitochondrial fraction was carried out (section 2.2.3). The protein content was divided by the number of  $10^6$  cells originally extracted ( $\mu\text{g} / 10^6$  cells). All \* values  $\pm$  SEM  $p < 0.05$  when compared to N2a cells using a paired t-test with a two-tail distribution ( $n \geq 7$ ). <sup>2</sup> SDH activity was measured in the mitochondrial fractions from each type of cells. Mitochondrial enrichment is expressed as mean specific activity normalised against the specific activity of the total extract (given a value of 1)  $\pm$  SEM. All \* values  $p < 0.05$  when compared to N2a cells using a paired t-test with a two-tail distribution ( $n \geq 5$ ).

### 3.2.2 Subcellular fractionation using mitotic and differentiated mouse N2a neuroblastoma cells

#### 3.2.2.1 Comparison of protein recovery in the mitochondrial fraction following subcellular fractionation in mitotic and differentiated mouse N2a cells

A comparison of subcellular fractionation in mitotic versus differentiated cell states was undertaken. Cells were seeded and left to recover for 24 hours in growth medium. For the next 24 hours, the cells were further incubated either in fresh growth medium (mitotic state), or in serum free medium supplemented with 0.3 mM dbcAMP (differentiated state, see section 2.2.1.3 and 2.2.1.6 for further details). Cells were then extracted and subjected to subcellular fractionation followed by protein estimation (section 2.2.3) of each resulting fraction (nuclear, cytoplasmic and mitochondrial).

Table 3.2 compares the protein recovery in the mitochondrial fraction from the two different cellular states. Protein recovered was similar for both states, being around 150-200  $\mu\text{g}$  protein /  $10^6$  seeded mitotic cells and a lower, but not significant, range of 130-180  $\mu\text{g}$  protein /  $10^6$  seeded differentiated cells.

	Nuclear protein recovery ( $\mu\text{g} / 10^6$ cells seeded) <sup>1</sup>	Cytoplasm protein recovery ( $\mu\text{g} / 10^6$ cells seeded) <sup>1</sup>	Mitochondria protein recovery ( $\mu\text{g} / 10^6$ cells seeded) <sup>1</sup>
Mitotic N2a cells	369 $\pm$ 28 (42 %)	332 $\pm$ 49 (38 %)	177 $\pm$ 28 (20 %)
Differentiated N2a cells	225 $\pm$ 27 (35 %)	258 $\pm$ 41 (40%)	157 $\pm$ 26 (25 %)

**Table 3.2: Protein recovery in the mitochondrial fractions from mitotic and differentiated mouse N2a neuroblastoma cells**

N2a cells were seeded as explained in section 2.2.1.3 followed by incubation of the cells in growth medium for 24 hours. Cells were either further incubated in growth medium for 24 hours, mitotic state, or incubated in serum free medium supplemented with 0.3 mM dbcAMP for 24 hours, differentiated state. Cells were then extracted and subjected to subcellular fractionation.<sup>1</sup> Protein estimation of the various fractions was carried out (section 2.2.3). The protein content was divided by the number of  $10^6$  cells originally seeded ( $\mu\text{g} / 10^6$  seeded cells). In brackets: protein content in the fraction as a percentage of the total in the three subfractions together. (n = 6 for nucleus; n = 10 for cytoplasm; n = 16 for mitochondria).

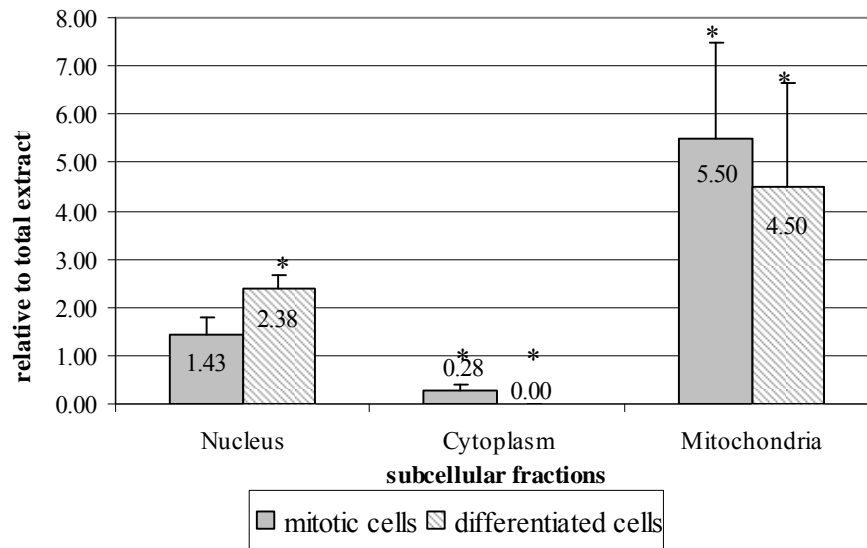
### 3.2.2.2 Mitochondrial markers in fractions from mitotic and differentiated cells

Figure 3.1A shows the presence of SDH activity in each subcellular fraction (nucleus, cytoplasm and mitochondria) normalised to corresponding total extract activities. There was a 5.5-fold enrichment of SDH in the mitochondrial fraction from mitotic cells and a 4.5-fold enrichment for differentiated cells. These enrichments were significant compared to total extracts for both cellular states and the enrichment was not significantly different between the two states.

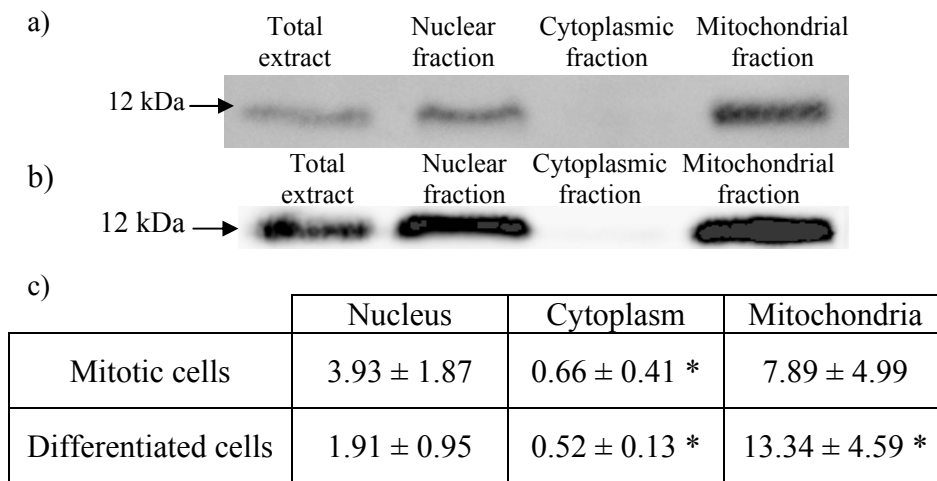
SDH activity in the cytoplasmic fraction was low (0.28) compared to total extract in mitotic cells and not detected in the differentiated cells. SDH activity was enriched 1.4 and 2.4-fold in the nuclear fraction compared to total extract in mitotic and differentiated cells, respectively.

Figure 3.1B shows the presence of another mitochondrial marker, cytochrome c, in the different subcellular fractions compared to total extract in both mitotic and differentiated cells. Cytochrome c was highly enriched in the mitochondrial fraction from both mitotic (7.9-fold increase) and differentiated cells (13.3-fold increase). For both cellular states, cytochrome c was found at very low levels in the cytoplasmic fraction. Finally, as for SDH activity, reactivity with the anti-cytochrome c antibody was slightly enriched in the nuclear fraction. No significant difference was observed between mitotic and differentiated cells.

### A. Succinate dehydrogenase activity in each fraction



### B. Western blot analysis showing cytochrome c detection in each fraction



**Figure 3.1: Succinate dehydrogenase activity and cytochrome c protein level in each fraction compared to total extract from mitotic and differentiated cells**

Mitotic and differentiated mouse N2a neuroblastoma cells were fractionated using differential centrifugation.

A. SDH activity was used as a mitochondrial marker. The graph shows the activity of SDH in the three subcellular fractions compared to total extract for both mitotic and differentiated cells. (mitotic: n = 11; differentiated = 4)

Enrichment = (specific enzyme activity of fraction / specific enzyme activity of total extract)  
enzyme specific activities were expressed in  $\Delta$ absorbance/minute/ $\mu$ g protein

B. Anti-cytochrome c antibody was used to detect the presence of cytochrome c in the different subcellular fractions and the total extract of a) mitotic cells and b) differentiated cells. The digitized blots were quantified using the AIDA image analyzer software and the average intensity in each fraction compared to the total extract  $\pm$  SEM for mitotic (n = 3) and differentiated (n = 18), tabulated in (c).

All \* values  $p < 0.05$  when compared to total extract using a paired t-test with a two-tail distribution

Following the observations showing that mitochondrial recovery and enrichment were similar in both mitotic and differentiated N2a cells, only the data for the differentiated cells are presented here as an example for the investigation of presence of contamination in the mitochondrial fraction.

#### 3.2.2.3 Cytoplasmic marker in fractions from differentiated cells

Glyceraldehydes-3-phosphate dehydrogenase (GAPDH) protein levels were higher in the cytoplasmic fraction compared to other fractions and were low in the mitochondrial and the nuclear fractions (figure 3.2A).

#### 3.2.2.4 Nuclear marker in fractions from differentiated cells

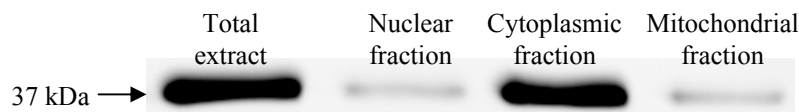
Figure 3.2B shows the presence of the nuclear marker lamin in each subcellular fraction from differentiated cells. Lamin was enriched in the nuclear fraction (35.5-fold) and was of low-abundance in the cytoplasmic and mitochondrial fractions.

#### 3.2.2.5 Lysosomal markers in fractions from differentiated cells

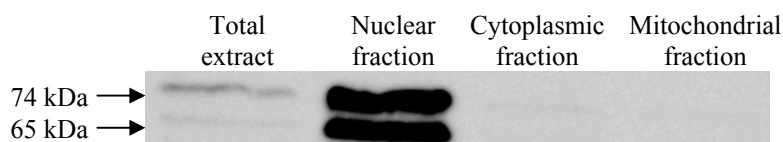
Figure 3.3A shows the presence of LAMP2 in the different fractions and indicates high lysosomal content in the cytoplasm (4.4-fold enrichment compared to the total extract). Lysosomes were also enriched in the mitochondria (2.3-fold) whilst depleted in the nuclear fraction.

#### 3.2.2.6 Microsomal marker

NADPH-cytochrome c reductase is an enzyme found in microsomes. Figure 3.3B shows that NADPH-cytochrome c reductase activity was mainly present in the cytoplasmic fraction compared to other subcellular fractions. The nuclear fraction was slightly contaminated with the microsomal marker. The specific activity of the microsomal marker was significantly reduced in the mitochondrial fraction compared to total extract showing a low level of contamination.

**A. Detection of GAPDH in each fraction**

	Nucleus	Cytoplasm	Mitochondria
Differentiated cells	$0.25 \pm 0.18 *$	$0.9 \pm 0.33$	$0.15 \pm 0.06 *$

**B. Detection of lamin in each fraction**

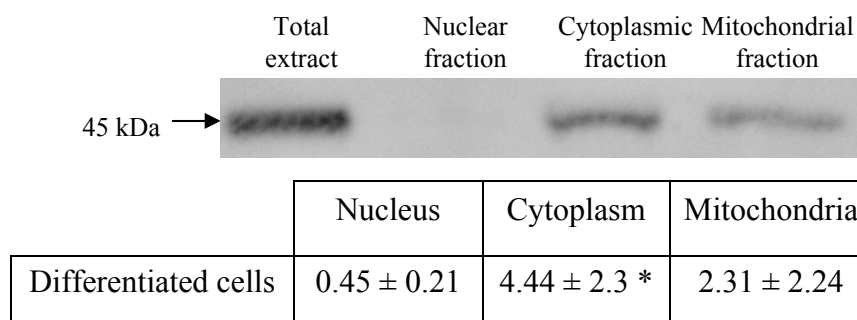
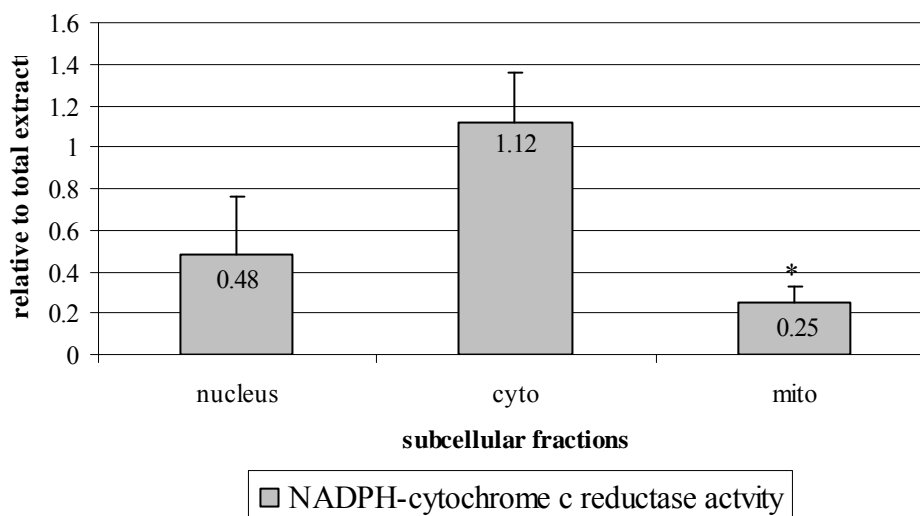
	Nucleus	Cytoplasm	Mitochondria
Lamin densitometry	$35.50 \pm 9.18 *$	$0.68 \pm 0.26$	$0.85 \pm 0.18$

**Figure 3.2: GAPDH and lamin A/C protein levels present in each fraction compared to total extract**

Differentiated mouse N2a neuroblastoma cells were fractionated using differential centrifugation and GAPDH and lamin were detected in the various subcellular fractions by probing western blots with anti-GAPDH antibody (A, n = 13) and anti-lamin A/C antibody (B, n = 14).

The digitized blots were quantified using the AIDA image analyzer software and expressed relative to total extract (given a value of 1). The tables show the average intensity change in each fraction compared to total extract  $\pm$  SEM.

All \* values  $p < 0.05$  when compared to total extracts using a paired t-test with a two-tail distribution.

**A. Detection of LAMP2 in each fraction****B. NADPH-cytochrome c reductase activity in each fraction**

**Figure 3.3: LAMP 2 protein level and NADPH-cytochrome c reductase activity in each fraction compared to total extract from differentiated cells**

Differentiated mouse N2a neuroblastoma cells were fractionated using differential centrifugation. A. LAMP2 was detected in the various subcellular fractions by probing western blots with anti-LAMP2 antibody (n =17). The digitized blots were quantified using the AIDA image analyzer software and expressed relative to total extract (given a value of 1). The table shows the average enrichment in each fraction compared to the total extract  $\pm$  SEM.

B. NADPH-cytochrome c reductase activity was used as an endoplasmic reticulum marker. The graph shows the specific activity of NADPH-cytochrome c reductase in the three subcellular fractions compared to the total extract (n = 9).

Specific enzyme activities are expressed in  $\Delta$ absorbance/minute/ $\mu$ g protein

All \* values  $p < 0.05$  when compared to total extract using a paired t-test with a two-tail distribution

### 3.2.3 Optimisation of 2D-gel electrophoresis

Following subcellular fractionation, proteins contained in the mitochondrial fraction were separated relative to their isoelectric point (pI) and their molecular weight (MW). This was performed using 2DE. Since many mitochondrial proteins are membrane proteins with a basic pI, the isoelectro-focusing (IEF) buffer prior to the first dimension conditions needed optimisation. As mitotic mitochondrial fractions showed similar biochemical marker enrichment to differentiated cells, all mitochondrial samples used for the optimisation of 2DE and its reproducibility were from untreated mitotic cells.

Pictures of each gel were taken using Fujifilm FLA-5100 image scanner. Pictures were transferred to Samespots software (Progenesis) and each gel image was aligned to one chosen gel (called reference). The statistical package allowed choosing the best alignment features. When the 2DE was based on a mini-gel system for detergent choice, 50 µg protein were chosen; nevertheless, for practicability, further analysis of sample preparation and buffer optimisation, lower amounts of proteins were used leading to two different groups of studies. The issue of protein loading will be discussed in section 3.2.3.3.

#### 3.2.3.1 Sample preparation

##### - Choice of detergent

The first step of 2DE is lysis of mitochondrial preparations prior to IEF protein separation. An important consideration is the choice of detergents, the precipitation method and the inclusion of chaotropic agents.

Three different detergents were tested for their ability to enhance separation of mitochondrial proteins. The non ionic detergent Triton-X-100 (1.5% [w/v]) was first compared to the zwitterionic detergent CHAPS (4% [w/v]), both in the presence of urea. Figures 3.4A and B show a representative profile for the triplicate gels and the spots that were exclusive to each group of gels. Table 3.3 shows the number of spots resolved on each gel and the total spot volume as calculated by the Samespot software. The two detergent buffers revealed approximately the same number of spots, but different profiles; using Triton-X-100, basic proteins were enriched but there was a reduced number of acidic proteins. When CHAPS was used as a detergent, proteins across the pI range were revealed, including a number of acidic proteins. Thus, for broad range, acidic and neutral pI

investigations, the zwitterionic detergent CHAPS seemed to be more suitable than Triton-X-100. The total spot volume as calculated by the Samespot software relates to how strong the staining was from one gel to another. As the total spot volume was much higher with replicate 3 from the CHAPS group (table 3.3) than the other replicates in the same group, it can be suggested that the staining was stronger; however the number of spots was similar for the 3 gels.

Sample preparation specification	Replicate no.	Total spot volume <sup>1</sup>	Spot no. detected <sup>2</sup>	Average spot no. $\pm$ SEM <sup>3</sup>
A. CHAPS	1	$6.8 \times 10^8$	395	$394 \pm 13$
	2	$5.8 \times 10^8$	376	
	3	$12.2 \times 10^8$	412	
B. Triton	1	$5.0 \times 10^8$	396	$375 \pm 43$
	2	$6.5 \times 10^8$	294	
	3	$4.3 \times 10^8$	403	

**Table 3.3: Effects of CHAPS and triton-X-100 detergents on spot number and total spot volume resolved on 2DE**

50  $\mu$ g mitochondria isolated from mitotic N2a neuroblastoma were fractionated by 2DE using IEF buffers containing A. 4% CHAPS / 8 M urea, B. 1.5% triton / 8 M urea in triplicates. One replicate of each group of gels is shown in figure 3.4.

<sup>1</sup> Total spot volume: Sum of the volume (calculated intensity) of each spot calculated by the Samespot software.

<sup>2</sup> Total number of spots detected in each gel using the Samespot software.

<sup>3</sup> Average number of spot in each group of samples (triplicates using CHAPS as detergent and using Triton-X-100 as detergent)  $\pm$  SEM (n = 3).

Another zwitterionic detergent, ASB-14, was tested compared to CHAPS. This is described by manufacturers (Calbiochem) as a more powerful agent for solubilising membrane proteins if used in combination with thiourea. Figure 3.4C shows a representative image for a set of triplicate gels. Although the basic pI range of the gel looked similar to the CHAPS gel, the acidic and neutral parts of the gel were fuzzy and weakly stained. Consequently, CHAPS remained the detergent of choice for broad spectrum, acidic and neutral pI analyses.

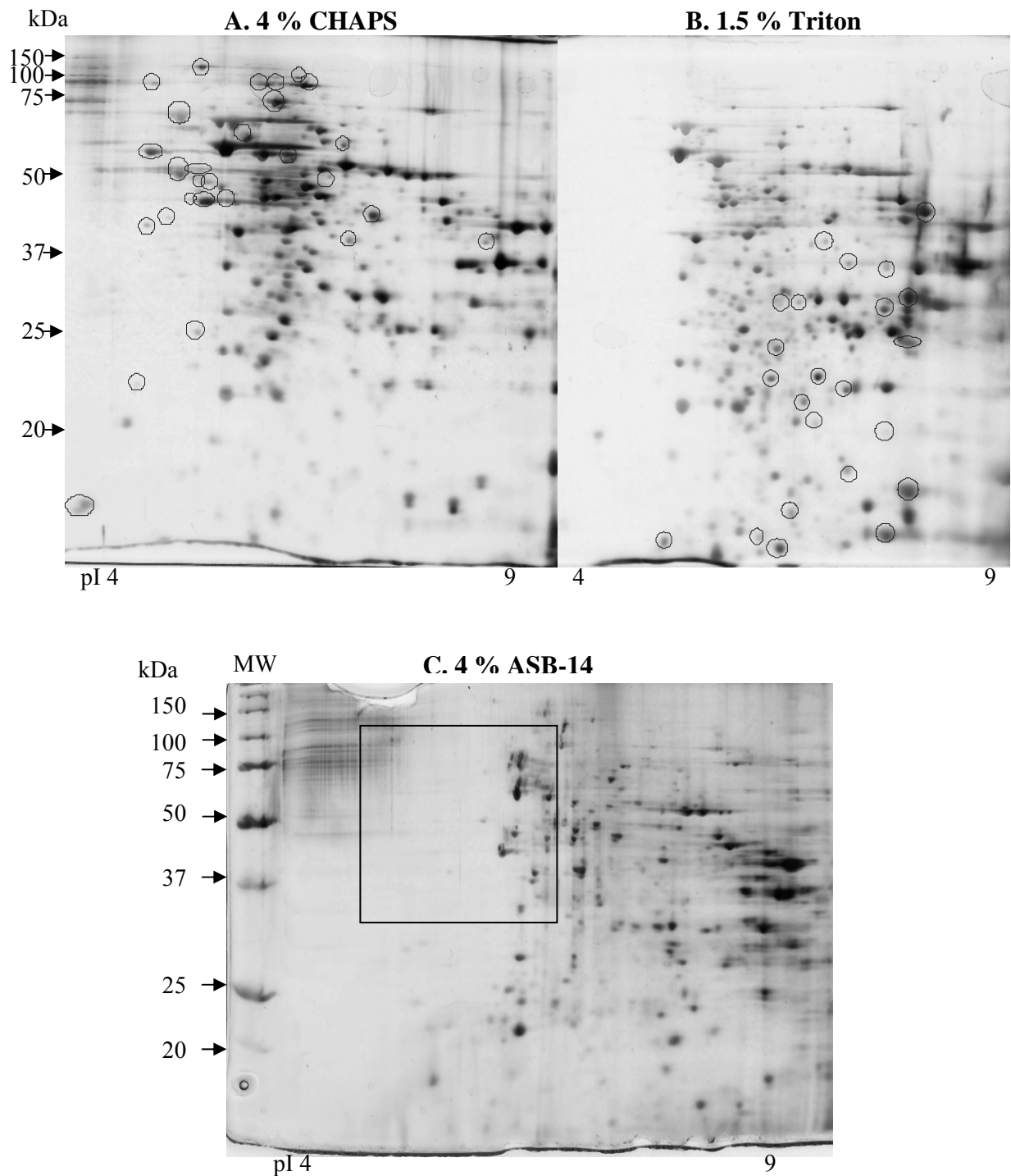


**Figure 3.4: Differences in spot detection using three different detergents (CHAPS, Triton-X-100 and ASB-14) in the IEF buffer in 2DE analysis**

50  $\mu$ g mitochondria isolated from mitotic N2a neuroblastoma were fractionated by 2DE using IEF buffers containing A. 4% CHAPS / 8 M urea, B. 1.5% triton / 8 M urea or C. 4% ASB-14 / 6 M urea / 2 M thiourea. Circled spots in A and B represents spots exclusive to each gel. The square in C shows the area where the most changes were observed between CHAPS (A) and ASB-14 gels (C). Representative gel shown here (n = 3). Total spot numbers and total spot volume resolved on each gel shown in table 3.3.

MW: Molecular weight markers. Only pI 4-9 ranges of the gels are shown here.

- Influence of acetone precipitation for sample preparation

Acetone precipitation has been widely used to concentrate proteins but also to remove excess detergents, lipids and salts (England and Seifter, 1990). Figure 3.5A and B and table 3.4 shows that acetone precipitation of samples prior to adding the IEF buffer had little effect on the resolution and spot number of proteins on 2DE. However, the total spot volume was decreased in the three replicates showing an effect on staining efficiency, which could be due to a decrease in protein recovery. For reproducible analysis, samples were not acetone precipitated as it could be a source of variability to add another step to the protocol.

Sample preparation specification	Replicate no.	Total spot volume <sup>1</sup>	Spot no. detected <sup>2</sup>	Average spot no. $\pm$ SEM <sup>3</sup>
A. CHAPS / urea	1	$5.5 \times 10^8$	395	$333 \pm 50$
	2	$6.3 \times 10^8$	257	
	3	$6.0 \times 10^8$	347	
C. Acetone precipitation / CHAPS / urea	1	$2.5 \times 10^8$	322	$328 \pm 12$
	2	$2.1 \times 10^8$	347	
	3	$2.8 \times 10^8$	316	
B. CHAPS / thiourea	1	$3.1 \times 10^8$	272	$266 \pm 32$
	2	$2.1 \times 10^8$	309	
	3	$6.8 \times 10^8$	218	

**Table 3.4: Effects of CHAPS and triton-X-100 detergents on spot number and total spot volume resolved on 2DE**

20  $\mu$ g mitochondria isolated from mitotic N2a neuroblastoma were fractionated by 2DE using IEF buffers containing A. 4% CHAPS / 8 M urea, (no acetone precipitation), or B. 4 %CHAPS / 8 M urea following acetone precipitation of mitochondrial pellet, or C. 4 % CHAPS / 6 M urea / 2 M thiourea (no acetone precipitation). One replicate of each group of gels is shown in figure 3.5.

<sup>1</sup> Total spot volume: Sum of the volume (calculated intensity) of each spot calculated by the Samespot software.

<sup>2</sup> Total number of spots detected in each gel using the Samespot software.

<sup>3</sup> Average number of spot in each group of samples  $\pm$  SEM (n = 3).

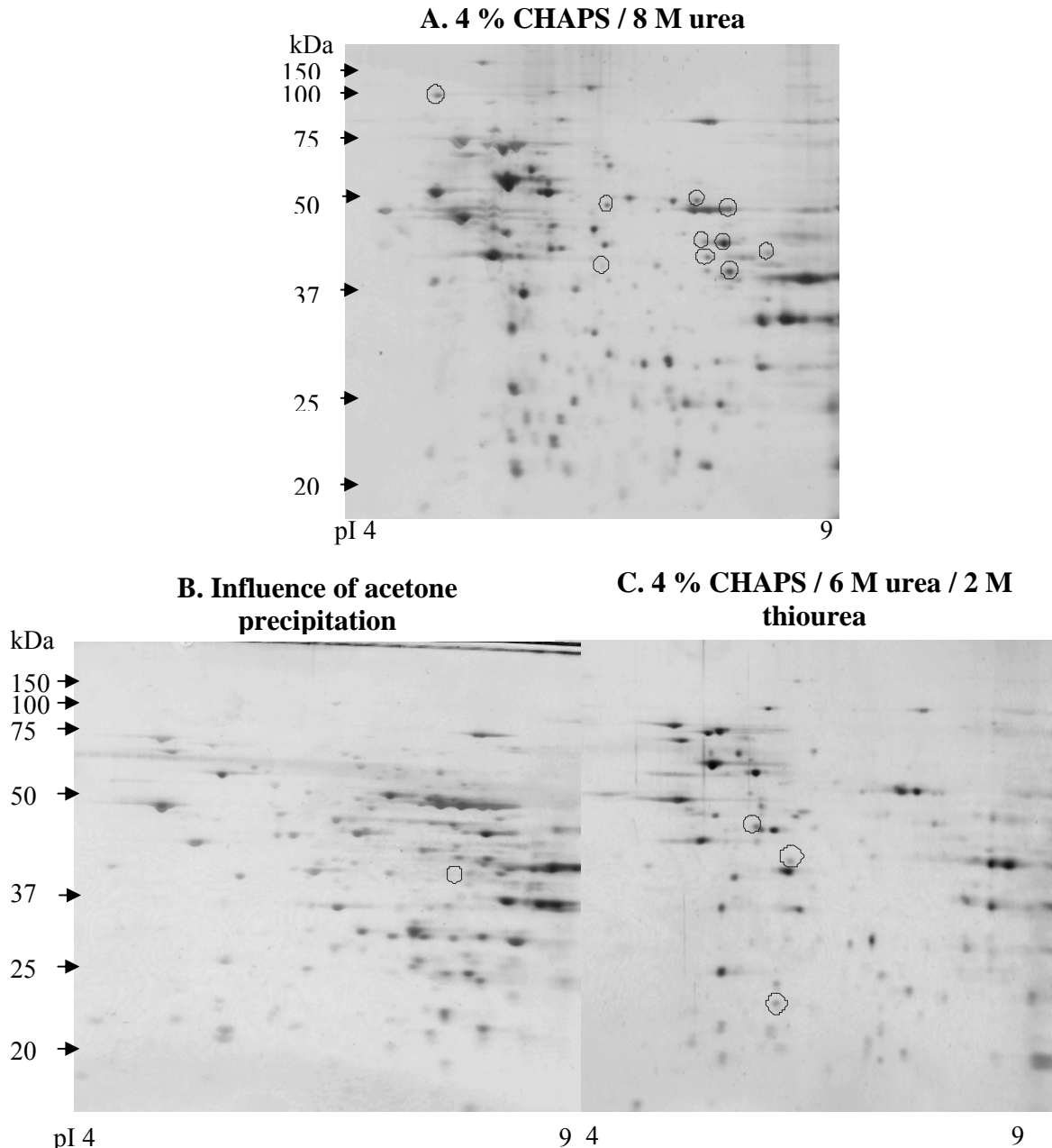


**Figure 3.5: Influence of acetone precipitation prior to fractionation by 2DE and of thiourea inclusion in the IEF buffer on spot detection**

20  $\mu$ g mitochondria isolated from mitotic N2a neuroblastoma were fractionated by 2DE using IEF buffers containing A. 4 % CHAPS / 8 M urea, B. 4 % CHAPS / 8 M urea following acetone precipitation of mitochondrial pellet or C. 4 % CHAPS / 6 M urea / 2 M thiourea (no acetone precipitation was performed for both groups). Circled spots in A to C represents spots exclusive to each gel. Representative gel shown for each group (n = 3). Spot numbers and total spot volume resolved on each gel shown in table 3.4. Only pI 4-9 ranges of the gels are shown here.

- Influence of thiourea

Thiourea is known to help the solubilisation of proteins. Figure 3.5A and C show images of representative gels using CHAPS / urea with or without thiourea. Several basic proteins seemed to be more enriched without thiourea. The main difference was a consistent horizontal streaking of acidic proteins when thiourea was present. Moreover, the number of spots resolved on each gel was lower with thiourea and the total spot volume was decreased in 2 out of the three replicates showing an effect on staining efficiency, which could be due to a decrease in protein recovery (table 3.4) during the 2DE protocol. Consequently, for broad pI 3-10 range and acidic to neutral pI ranges, urea without thiourea was chosen as the solubilising agent.

- Protein loading

Two different protein loadings were analysed using CHAPS / urea in the IEF buffer. The number of spot was slightly reduced when using less protein material (20 µg as opposed to 50 µg protein; compare table 3.3A and 3.4A), nevertheless, the total spot volume was similar in both groups.

### 3.2.3.2 Equilibration conditions

Glycerol was used to increase buffer viscosity in the equilibration buffer and to improve the transfer of proteins from the IPG strip to the second dimension. Too much glycerol led to fuzzy separation of the proteins in the second dimension (figure not shown). 20% (v/v) glycerol was then used in the subsequent protocol.

The decision was therefore to use no acetone precipitation, CHAPS combined with urea but no thiourea in the first dimension, and 20% glycerol in the equilibration buffer for optimal resolution of mitochondrial proteins.

### 3.2.4 Reproducibility of mini 2D-gel electrophoresis

Following optimisation of 2DE buffer conditions the reproducibility of the overall method needed to be assessed. To improve the reproducibility between gels, it was important to determine which steps were the most reproducible and which were the most variable. For these analyses silver staining was used and spots were not saturated (for significance of this, see section 3.2.5).

#### 3.2.4.1 Intra-sample reproducibility

In general each set of samples was composed of triplicates run in parallel with another set. (total of six gels). For practical reasons, duplicates of both sets were run in the same tank, leaving one replicate of each set in a separate tank. Nevertheless, both tanks were run in parallel linked to the same power pack. As discussed below, the variability between tanks was not discernable.

- Same sample, same day

Triplicates of a sample were electrophoresed the same day (figure 3.6). The volume of each spot was normalised to the total spot volume in each gel so that the normalised volume of each spot could be compared between gels. Figure 3.6 shows that replicate 1 was the most intensely stained gel and replicate 3 staining intensity was the lowest, reflected by the total spot volume calculated by Samespot software (shown in table 3.5); but spot number was not necessarily correlated with spot volume.

A gel to gel analysis was undertaken using Samespots software (Progenesis). The fold change of each spot between gels was calculated and comparative analysis between each gel is shown in table 3.6. Between 77 and 91 % of spots varied in relative intensity by less than 2-fold and between 92 and 97 % of the spots varied by less than 3-fold between gels. Interestingly, although there was a higher difference in staining intensity between replicate 1 and 3, the fold changes seemed to be smaller than between gels 1 and 2 showing that normalising to total spot volume was efficient. Additionally, replicate 3 was the replicate run on the different tank in parallel to the other replicates showing that the variability between tanks did not reflect on the reproducibility between gels.

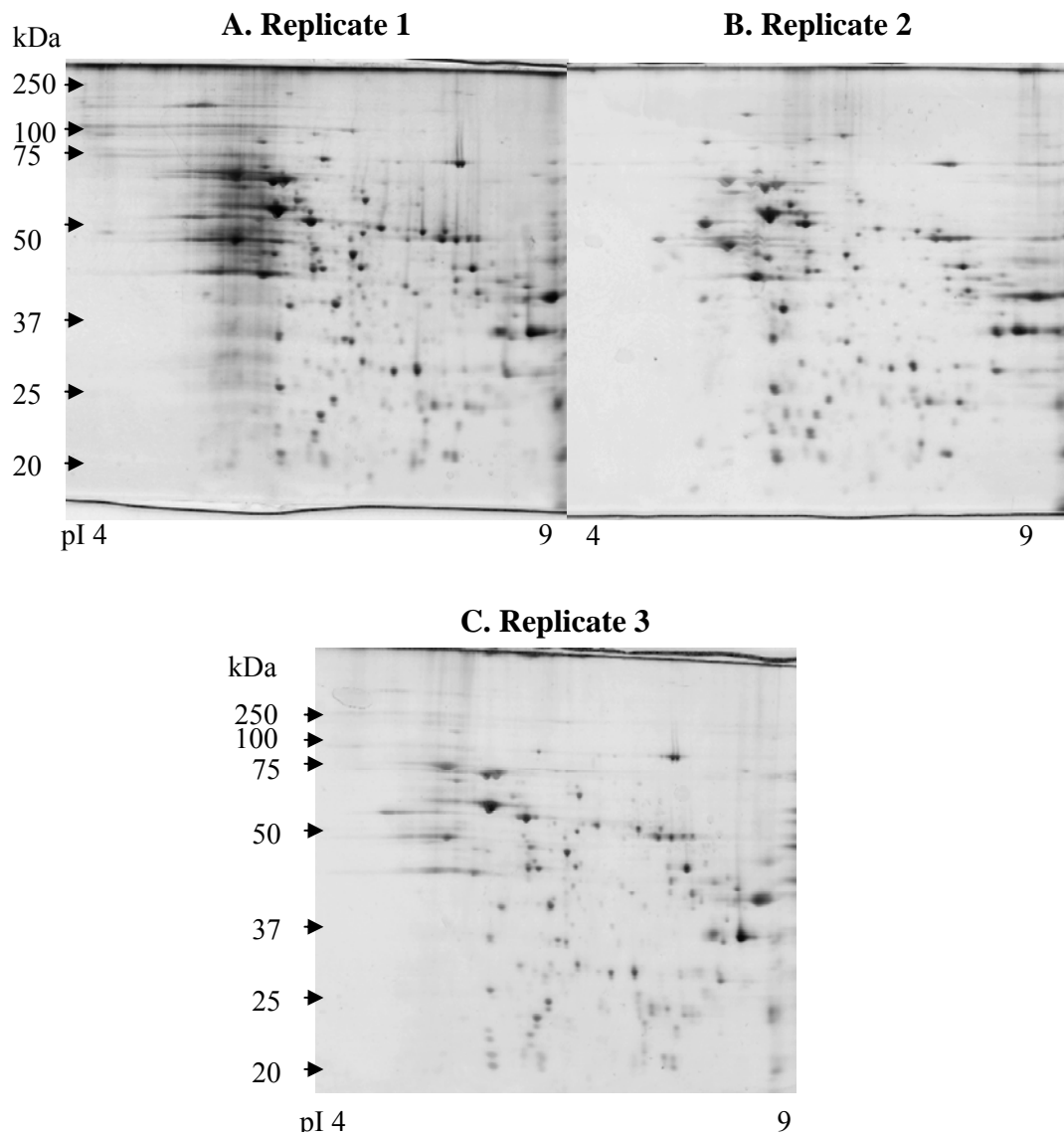


**Figure 3.6: Triplicate gels electrophoresed in parallel**

Mitochondria isolated from mitotic N2a neuroblastoma were fractionated by 2DE in triplicate in parallel using IEF buffer containing A. 4 % CHAPS / 8 M urea. Spot numbers and total spot volume resolved on each gel are shown in table 3.5 and comparative analysis between gels compared to the average reference gel is shown in table 3.6. Only pI 4-9 ranges of the gels are shown here

Replicate	Total volume spot <sup>1</sup>	Spot no. <sup>2</sup>	Average no. spot $\pm$ SEM <sub>3</sub>
1	$5.73 \times 10^8$	321	304 $\pm$ 40
2	$3.4 \times 10^8$	350	
3	$2.9 \times 10^8$	240	

**Table 3.5: Gel properties of the same sample electrophoresed by 2DE in parallel**

Mitochondria isolated from mitotic N2a neuroblastoma were fractionated in triplicate by 2DE using IEF buffer containing 4 % CHAPS / 8 M urea. Each replicate gel is shown in figure 3.6.

<sup>1</sup> Total spot volume: sum of the volume (calculated intensity) of each spot calculated by the Samespot software.

<sup>2</sup> Total number of spots detected in each gel using the Samespot software.

<sup>3</sup> Average number of spot  $\pm$  SEM (n = 3).

Gels compared	Min <sup>1</sup>	Max <sup>2</sup>	Average <sub>3</sub>	Median <sub>4</sub>	1-2-fold change <sub>5</sub>	2-3-fold change <sub>5</sub>	3-5-fold change <sub>5</sub>	> 5-fold change <sub>5</sub>
Gel 1 versus gel 2	1.003	7.23	1.68	1.39	78 %	15 %	6 %	1 %
Gel 2 versus gel 3	1.002	11.072	1.81	1.45	77 %	15 %	10 %	3 %
Gel 1 versus gel 3	1.017	4.48	1.48	1.36	91 %	6 %	3 %	0 %

**Table 3.6: Reproducibility between triplicates of the same sample electrophoresed by 2DE in parallel**

Mitochondria isolated from mitotic N2a neuroblastoma were fractionated in triplicate by 2DE using IEF buffer containing 4 % CHAPS / 8 M urea. Each replicate gel is shown in figure 3.6. The fold changes between each spot volume between 2 gels were calculated from the normalized volume as measured by Samespot software.

<sup>1</sup> Lowest –fold change calculated between the 2 gels compared

<sup>2</sup> Highest–fold change calculated between the 2 gels compared

<sup>3</sup> Average of all the –fold changes of each spot from one gel to another

<sup>4</sup> Median of all the –fold changes of each spot from one gel to another

<sup>5</sup> Percentage of spots that showed a –fold change in the range analysed between two gels

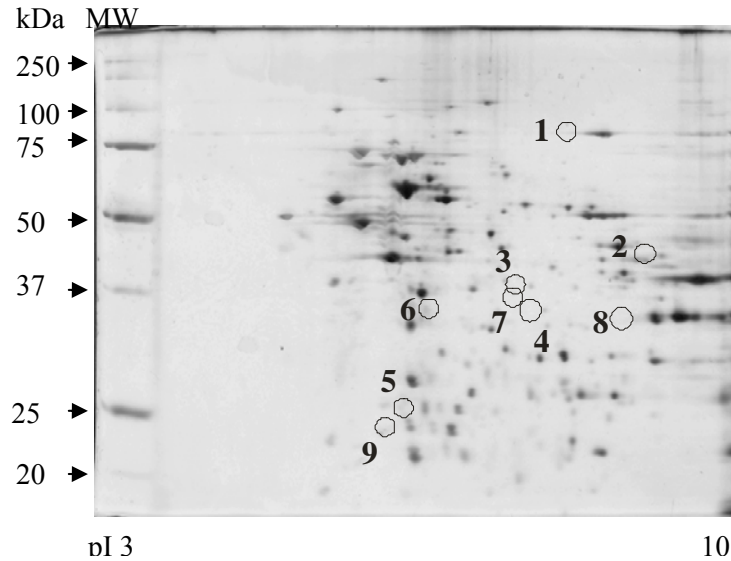
- Same sample run on a different day

2DE of two sets of triplicates of the same sample were electrophoresed on two separate days. Each set of three gels was grouped, the volumes of each group were averaged and averaged groups were analysed against each other using Samespots software. Since 92 to 97 % of the spots were previously shown to vary in relative intensity by less than 3-fold, only spots showing a change of more than 3-fold in intensity were annotated (Figure 3.7). Only 9 spots varied by more than 3-fold, these were of low intensity and differences between gels are likely to be due to detection limits.

#### 3.2.4.2 Inter-sample reproducibility

Two samples prepared on different days were subjected to 2DE in triplicate. The data were analysed in the same way as in the previous section. Figure 3.8A shows spots that varied in intensity by more than 3-fold, the numerical data are reported in figure 3.8B. Although 9 spots varied in relative intensity by more than 3-fold, as previously, the changes were smaller, not exceeding 5.3-fold change between spots.

From the latter results, the best way of analysing two different samples would be to run as many samples as possible in parallel.

**A. Changes between gels from same sample electrophoresed on a different day****B. Numerical data showing the changes between gels represented in A**

Spot number	Average of normal volumes of gels from day 1 <sup>1</sup>	Average of normal volumes of gels from day 2 <sup>1</sup>	Fold change
1	870 ± 146	271 ± 176	3.2 <sup>2*</sup>
2	232 ± 18	62 ± 9	3.8 <sup>2*</sup>
3	71 ± 7	11 ± 2	6.3 <sup>2*</sup>
4	57 ± 6	5 ± 2	10.6 <sup>2*</sup>
5	201 ± 113	58 ± 12	3.5 <sup>2</sup>
6	52 ± 9	184 ± 96	3.5 <sup>3</sup>
7	40 ± 5	197 ± 41	4.9 <sup>3</sup>
8	338 ± 50	1204 ± 65	3.6 <sup>3*</sup>
9	94 ± 51	355 ± 77	3.8 <sup>3*</sup>

**Figure 3.7: Map of a 2DE showing expression changes between replicates of the same sample electrophoresed on different days**

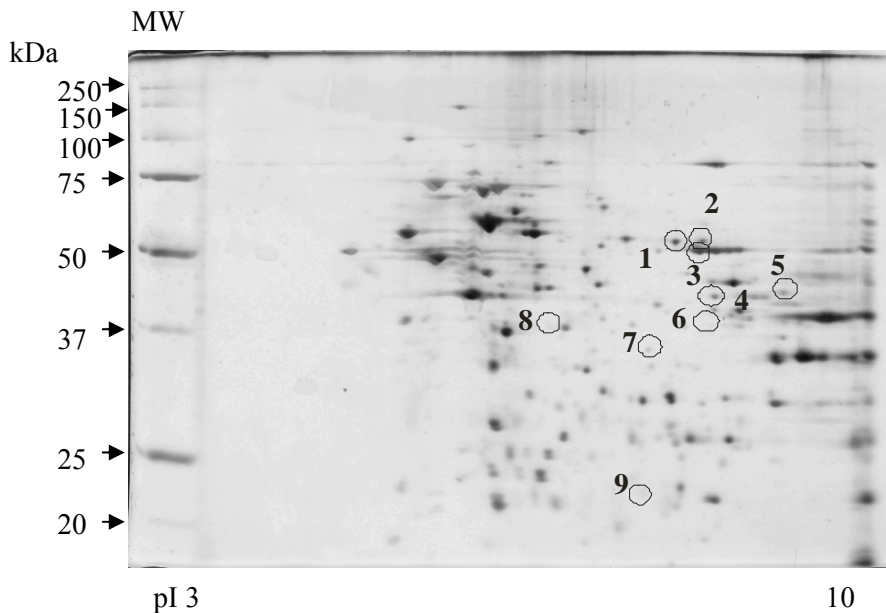
Six replicates of the same mitochondrial fraction from mitotic N2a cells were prepared. The triplicates were electrophoresed on 2DE (12 % polyacrylamide) on two different days. The six gels were analysed using Samespots software from Progenesis. The gel images were grouped and averaged per day. The two averages were compared showing the spots that changed by more than 3-fold (spots 1 to 9 in A). MW: Molecular weight markers. The numerical data are shown in B.

<sup>1</sup> Average of normalised volumes (n = 3) ± SEM.

<sup>2</sup> Fold decrease = Average of normalised volumes from sample 1 gels / Average of normalised volumes from sample 2 gels.

<sup>3</sup> Fold increase = Average of normalised volumes from sample 2 gels / Average of normalised volumes from sample 1 gels.

All \* values p<0.05 using ANOVA test.

**A. Changes between gels from different samples electrophoresed in parallel****B. Numerical data showing the changes between gels represented in A**

Spot number	Average of normal volumes of gels from sample 1 <sup>1</sup>	Average of normal volumes of gels from sample 2 <sup>1</sup>	Fold change
1	1139 ± 179	287 ± 63	4.0 <sup>2*</sup>
2	688 ± 86	187 ± 44	3.7 <sup>2</sup>
3	1519 ± 150	409 ± 139	3.7 <sup>2*</sup>
4	457 ± 68	128 ± 18	3.6 <sup>2*</sup>
5	232 ± 18	77 ± 11	3.0 <sup>2*</sup>
6	272 ± 21	83 ± 5	3.3 <sup>2*</sup>
7	57 ± 6	11 ± 2	5.3 <sup>2*</sup>
8	126 ± 36	402 ± 118	3.2 <sup>3*</sup>
9	112 ± 11	475 ± 193	4.2 <sup>3*</sup>

**Figure 3.8: Map of a 2DE showing expression changes between replicates of different samples electrophoresed in parallel**

Three replicates of the same mitochondrial fraction from mitotic N2a cells were prepared. This was repeated with a fraction prepared on a different day. The two pairs of triplicates were electrophoresed on 2DE (12 % polyacrylamide) in parallel. The six gels were analysed using Samespots software from Progenesis. The gel images were grouped and averaged per sample. The two averages were compared showing the spots that changed of more than 3-fold (spots 1 to 9 in A). MW: Molecular weight markers. The data is shown in table B.

<sup>1</sup> Average of normalised volumes (n = 3) ± SEM.

<sup>2</sup> Fold decrease = Average of normalised volumes from sample 1 gels / Average of normalised volumes from sample 2 gels.

<sup>3</sup> Fold increase = Average of normalised volumes from sample 2 gels / Average of normalised volumes from sample 1 gels.

All \* values p<0.05 using ANOVA test.

### 3.2.5 Reproducibility of large 2D-gel electrophoresis

Preliminary experiments were run using 17 cm IEF strips and 17 cm by 17 cm gels since it was expected that resolution would be better than when using the mini-system (7 cm strips). However, the latter was not found to be the case, so optimization experiments shown in section 3.2.2 and 3 were all undertaken using mini-gels (7 cm strips). The key reasons for using the mini-system for the main analyses are given below.

An example of large 2DE is shown in figure 3.9. Large gels often showed horizontal streaking, particularly at the basic end and vertical streaking, particularly with high molecular weight proteins. Moreover, some acidic proteins were sometimes absent on gels. In the present study, these gels were inconstant and did not show more spots than with mini-gels (up to 350 spots observed). Furthermore, the reproducibility of proteomic profiles on large gels tended to be lower than of mini-gels. For example, in a comparative analysis using Samespots software of one to one gel, the majority of the spots showed a 4 to 5-fold variability with large gels (data not shown) compared to 2 to 3-fold with mini gels (table 3.6). Because the large gels needed higher amount of proteins and for the above reasons, detailed comparisons in subsequent chapters involved the use of mini-gels.

### 3.2.6 Choice of staining method

Using mini-2DE gels instead of large-gels improved the staining pattern as the stain was more homogenous all over the gel. Nevertheless, despite the high sensitivity of the stain (0.2 to 0.6 ng), silver stain had a narrow linear range (1 to 10 ng) and saturated relatively quickly making quantitative analysis difficult.

Figure 3.10 shows 3-dimensional images of silver stained spots which are saturated (a) and non-saturated (b) with silver on the same gel. The saturated spot showed a truncated shape, showing that the intensity reported for this spot would be lower than what it should have been compared to other unsaturated spots.

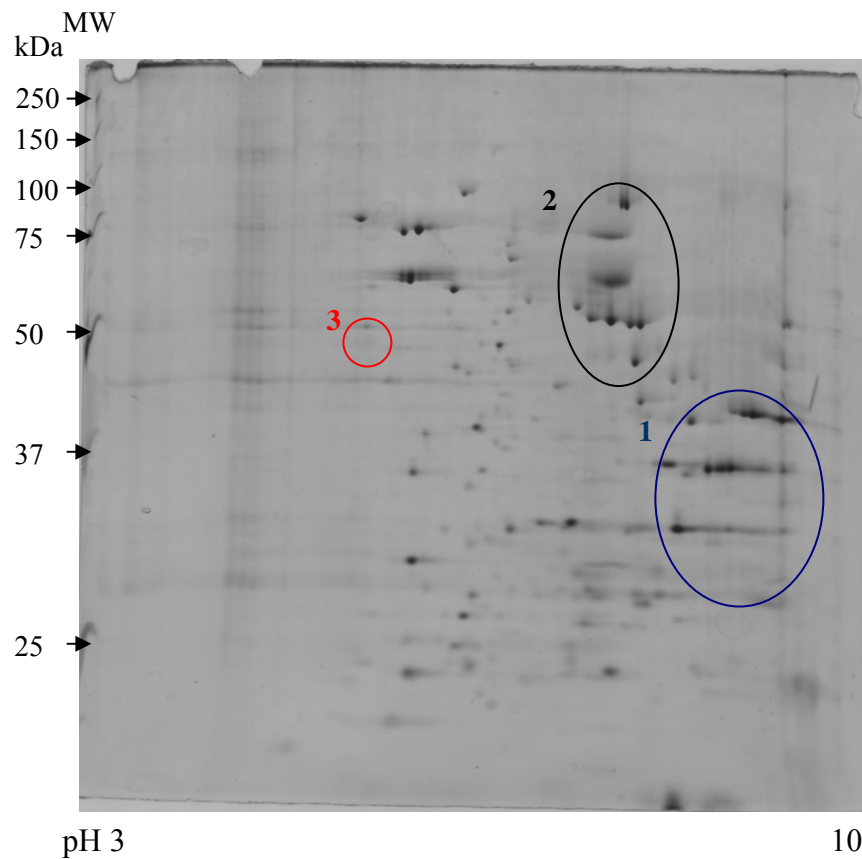


**Figure 3.9: Large-scale 2DE of mitochondrial proteins from differentiated mouse N2a neuroblastoma**

120  $\mu\text{g}$  of mitochondrial sample from differentiated N2a cells were resolved on a large 2D-gel electrophoretic system (17 cm by 17 cm). 1. Horizontal streaking of the basic spots, 2. vertical streaking of high molecular weight spots and 3. ATP synthase  $\beta$ -subunit is less abundant, whereas it has been shown in mini-gel studies to be highly abundant. MW: Molecular weight markers.

SyproRuby (Molecular Probes) is a fluorescent stain. It is said to be as sensitive as silver stain (0.25 ng to 0.5 ng) and has a greater linear range (0.25 ng to 1000 ng). Preliminary testing showed that staining with this dye was more homogenous over the whole gel and did not saturate as quickly as silver stain (data not shown). In order to compare the two stains, five gels of a sample were stained with SyproRuby followed by silver stain. Figure 3.11 shows one representative gel stained with both stains, consecutively. In the five gels, around 96 % of all spot intensities showed less than 2-fold difference, compared to 86 % from the silver stained gels (consistent with data from table 3.6, quantitative data not shown).

To conclude, silver staining was adequate for visualising spots but staining with SyproRuby was more reproducible for quantifying changes occurring between two different samples.

### 3.2.7 Summary of 2D-gel electrophoresis optimisation

Table 3.7 shows the optimised conditions used in the present project.

category	Optimisation	Comment
Detergent	CHAPS	Some acidic proteins did not stain with ASB-14 and Triton-X-100
Solubility	8M Urea	Thiourea increased the variability even though the solubility was better
Sample preparation	Sample not precipitated	Acetone precipitation did not improve gel profiles and adding a step could increase the variability
Equilibration	20 % glycerol	30 % glycerol made the spots fuzzy
Reproducibility	Different samples on the same run	Reproducibility was better when gels were run in parallel
Size	Mini gels	More reproducible, mass spectrometry efficiency equivalent, needed less sample
Stain	SyproRuby	Staining more homogenous, more reproducible, less saturation due to a larger linear range

**Table 3.7: Summary of the results for the optimisation of 2D-gel electrophoresis**

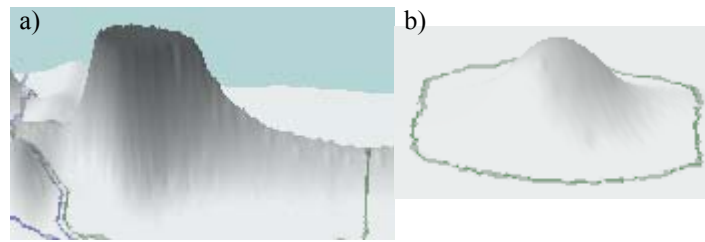


**Figure 3.10: 3-dimensional image of two different spots from a large 2DE**

120  $\mu$ g mitochondrial fractions from mitotic mouse N2a cells were run on a large 2DE followed by silver stain. 3-dimensional images from spots were observed using Progenesis Samespots software: a) a saturated spot of glutamate oxaloacetate transaminase 2 (41.2 kDa, pI 9.0) and b) a non saturated spot of ATP synthase  $\delta$ -subunit (19 kDa, pI 5.88) from a mitochondrial fraction from mouse N2a neuroblastoma resolved on 2DE.

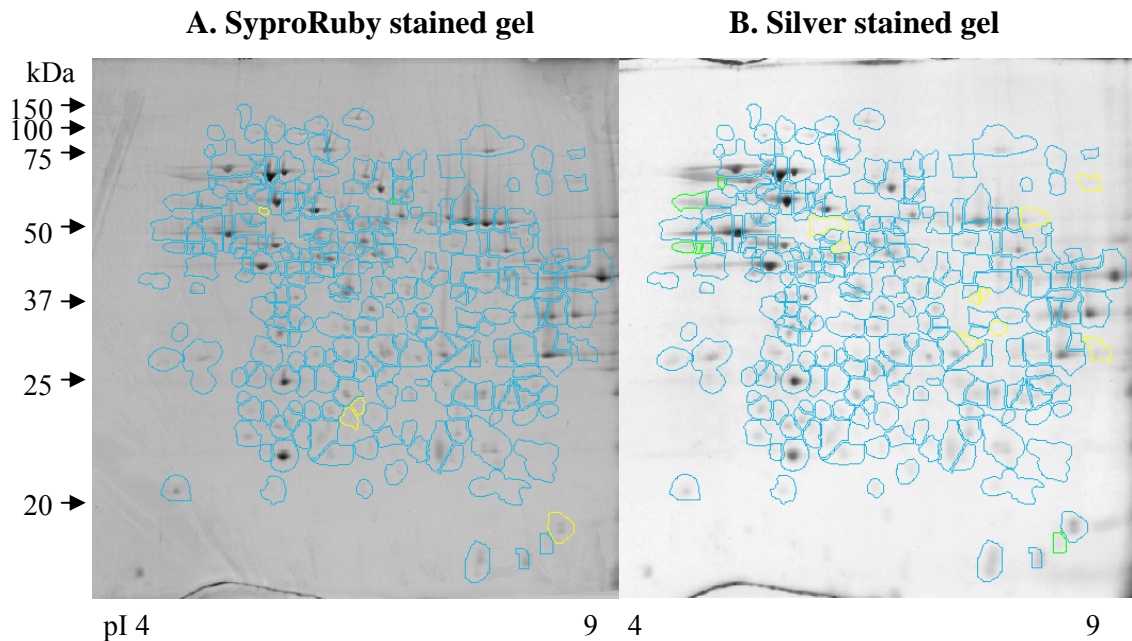


**Figure 3.11: Differences in spot detection using silver stain compared to SyproRuby**

Five different replicates of gels were consecutively stained with SyproRuby (A) followed by silver stain (B). The five replicates for each stain were grouped and spot densities were averaged using Progenesis Samespots software. The pictures show a representative profile. Yellow spots are spots that have densities decreasing by more than 2-fold compared to the average of the five gels. Green spots are spots that have densities increasing by more than 2-fold compared to the average. Blue spots are spots that are changed by less than 2-fold (increase or decrease) compared to the average gel.

### 3.2.8 Mass Spectrometry

Figure 3.12 and table 3.8 show the spots that have been identified from 2DE profiles using peptide mass fingerprinting. Sixteen out of twenty-one proteins were of mitochondrial origin, mainly matrix. Outer and inner membrane proteins were also present. Five of the identified proteins were not specific to mitochondria but three were ubiquitous in the cell and the other two were normally found in the endoplasmic reticulum. Figure 3.13 shows an example of protein identification using peptide mass fingerprinting, namely of spot 9 shown in figure 3.12. This spot had a positive match to ATP synthase, F1 complex  $\alpha$ -subunit isoform 1 with a significant identification score as calculated by the Mascot database (score > 54).

### 3.2.9 Mitochondrial proteome changes between mitotic and differentiated phenotypes

Cellular differentiation in mouse N2a neuroblastoma cells increased the variability of samples. This was due to the fact that not all cells differentiate at the same rate and only around 20-40 % of total cells in a sample actually produce axon-like processes (Flaskos *et al.*, 1998).

#### 3.2.9.1 Morphological changes

Mouse N2a neuroblastoma cells were differentiated and characterised in-house using 0.3 mM dbcAMP (De Girolamo *et al.*, 2000). Figure 3.14 shows the typical morphology of N2a neuroblastoma cells when they were differentiated with 0.3 mM dbcAMP in serum free medium for 24 hours compared to mitotic cells grown in growth medium (containing 10 % serum, refer to section 2.2.1.1 and 2.2.1.6). Differentiated cells expressed a different morphological phenotype from mitotic cells. Axon-like processes were extended from the cell body and cells were more ovoid in shape, typical of differentiated neuronal cells.

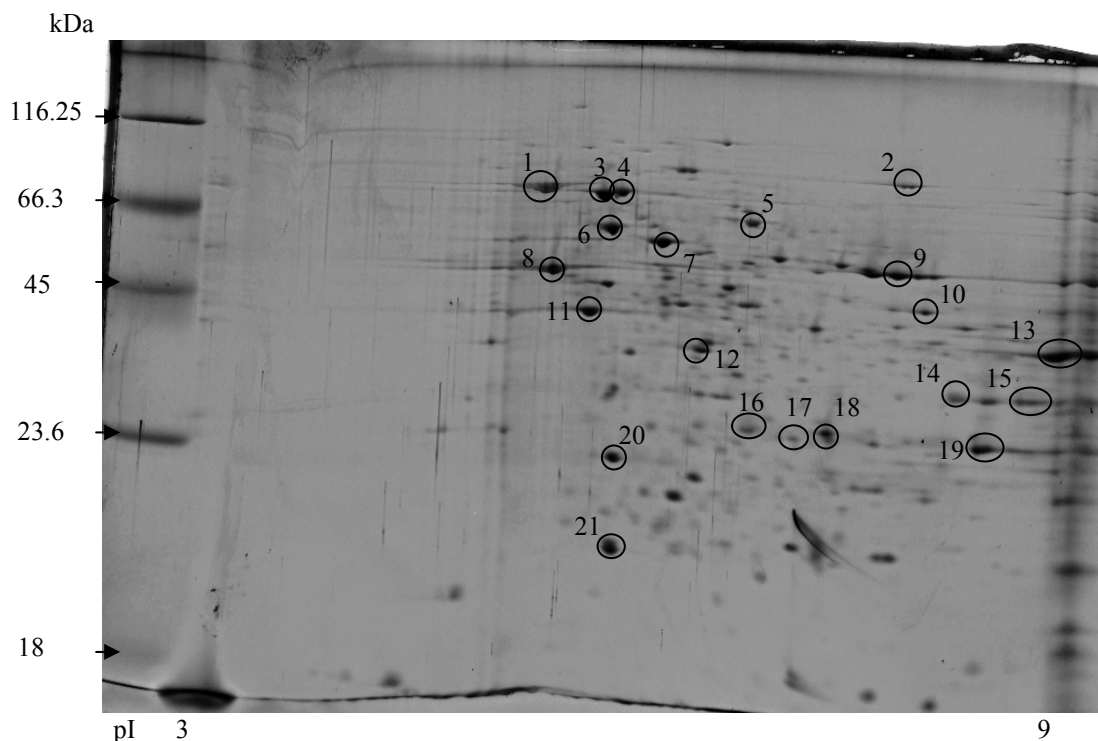


**Figure 3.12: 2DE (pI 3-10) stained with SyproRuby showing spots identified following peptide mass fingerprinting**

**Inner mitochondrial membrane proteins:**

- 8. ATP synthase, H<sup>+</sup> transporting mitochondrial F1 complex  $\beta$ -subunit (ATPase- $\beta$ )
- 9. ATP synthase, H<sup>+</sup> transporting mitochondrial F1 complex  $\alpha$ -subunit isoform 1 (ATPase- $\alpha$ )
- 21. ATP synthase, H<sup>+</sup> transporting mitochondrial F0 complex subunit d (ATPase- $\delta$ )
- 20. Prohibitin (BAP32 homolog)

**Outer mitochondrial proteins:**

- 16. Voltage-dependent-anion channel protein 2 (VDAC2)
- 19. Voltage-dependent-anion channel 1 (VDAC1)

**Mitochondrial matrix**

- 2. Aconitate hydratase, mitochondrial precursor
- 4. Stress-70 protein, mitochondrial precursor (GRP75)
- 6. 60 kDa Heat shock protein, mitochondrial precursor (Hsp60)
- 10. Fumarate hydratase, mitochondrial
- 12.  $\delta(3,5)$ - $\delta(2,4)$ -dienoylCoA isomerase, mitochondrial precursor
- 13. Glutamate oxaloacetate transaminase 2, mitochondrial (GOT2)
- 14. bifunctional methylenetetrahydrofolate dehydrogenase / cyclohydrolase, mitochondrial
- 15. Malate dehydrogenase, mitochondrial precursor (MDH)
- 17. Electron transfer flavoprotein subunit alpha, mitochondrial
- 18. Electron transfer flavoprotein subunit alpha, mitochondrial

**Outer membrane interacting proteins from other cellular compartments:**

- 1. 78 kDa glucose-regulated protein precursor (GRP 78)
- 7. Protein disulfide isomerase A3 precursor
- 11. Putative  $\beta$ -actin

**Ubiquitous proteins:**

- 3. Heat shock cognate 71 kDa protein (Hsc70)
- 5. Stress-induced-phosphoprotein 1 (STIP1)

<b>Spot symbol</b> <sup>1</sup>	<b>Protein identification</b> <sup>2</sup>	<b>Accession number</b> <sup>3</sup>	<b>Score</b> <sup>4</sup>	<b>% sequence coverage</b> <sup>5</sup>	<b>Molecular weight</b>	<b>Theoretical pI</b>	<b>Subcellular location</b>
1	78 kDa glucose-regulated precursor	P20029	142	29 %	72 kDa	5.07	ER-interacting with OMM
2	Aconitate hydratase, mitochondrial	Q99K10	69	23 %	86 kDa	8.08	Matrix
3	Heat shock cognate 71 kDa protein	P63017	83	27 %	71 kDa	5.37	Ubiquitous
4	Stress-70 protein, mitochondrial	P38647	57	18 %	74 kDa	5.91	Matrix
5	Stress-induced-phosphoprotein 1	Q60864	79	20 %	63 kDa	6.40	Ubiquitous
6	60 kDa Heat shock protein, mitochondrial	P63038	113	27 %	61 kDa	5.91	Matrix
7	Protein disulfide isomerase A3	P27773	134	36 %	57 kDa	5.88	ER-interacting with OMM
8	ATP synthase, H <sup>+</sup> transporting mitochondrial F1 complex $\beta$ -subunit	P56480	189	51 %	56 kDa	5.25	IMM
9	ATP synthase, F1 complex $\alpha$ -subunit isoform 1	Q03265	123	42 %	60 kDa	9.19	IMM
10	Fumarate hydratase, mitochondrial	P97807	103	43 %	54 kDa	9.12	Matrix
11	Putative $\beta$ -actin	P60710	120	24 %	42 kDa	5.78	Ubiquitous
12	$\delta(3,5)$ - $\delta(2,4)$ -dienoylCoA isomerase, mitochondrial	O35459	60	14 %	36 kDa	7.60	Matrix
13	Glutamate oxaloacetate	P05202	89	22 %	41 kDa	9.00	Matrix

	transaminase 2, mitochondrial						
14	bifunctional methylenetetrahydrofolate dehydrogenase / cyclohydrolase, mitochondrial	P18155	160	30 %	38 kDa	8.98	Matrix
15	Malate dehydrogenase	P08249	101	43 %	36 kDa	8.93	Matrix
16	Voltage-dependent-anion channel protein 2	Q60930	125	42 %	32 kDa	7.44	OMM
17-18	Electron transfer flavoprotein subunit alpha, mitochondrial	Q99LC5	65	17 %	35 kDa	8.62	Matrix
19	Voltage-dependent-anion channel 1	Q60932	196	81 %	30 kDa	8.62	OMM
20	Prohibitin (BAP32 homolog)	P67778	169	21 %	30 kDa	5.22	IMM
21	ATP synthase, H <sup>+</sup> transporting mitochondrial F0 complex subunit d	Q9DCX2	97	31 %	19 kDa	5.88	IMM

**Table 3.8: Protein identification of spots from 2DE (gel image in figure 3.12)**

<sup>1</sup> Refers to circled spots figure 3.12

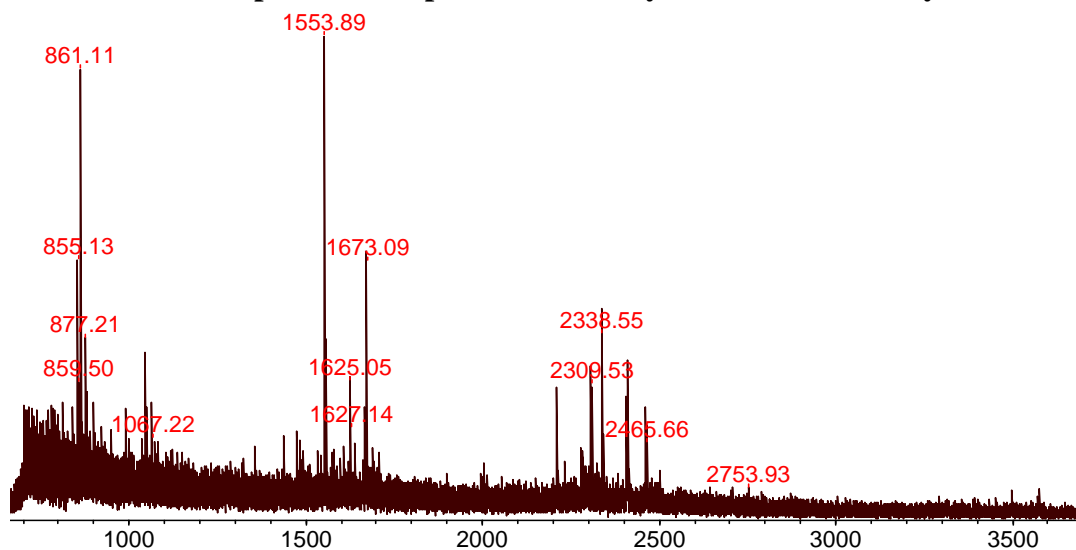
<sup>2</sup> Using the Mascot database <http://www.matrixscience.com>

<sup>3</sup> Accession number from the Protein Knowledgebase UniProtKb: <http://www.uniprot.org>

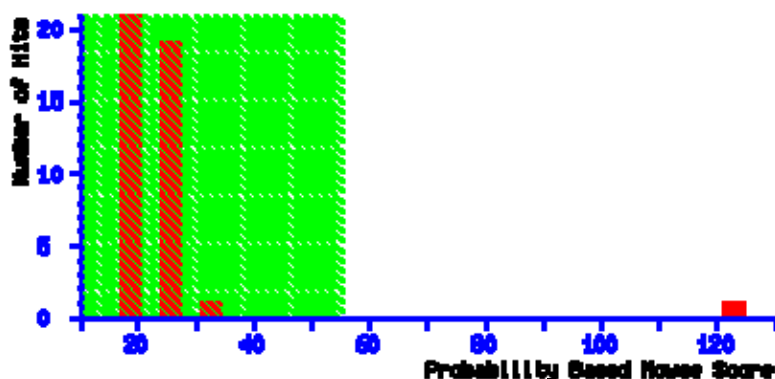
<sup>4</sup> Protein score greater than 54 are significant according to the Mascot database search software when comparing SwissProt database

<sup>5</sup> Coverage of all peptide sequences matched to the identified protein sequence

### A. Mass spectrum of spot 9 obtained by MALDI-TOF analysis



### B. Mascot database results for spot 9 identification



Match to: **ATPA\_MOUSE** Score: 123 Expect: 8.1e-09  
**ATP synthase subunit alpha, mitochondrial OS=Mus musculus GN=Atp5a1 PE=1**  
 Nominal mass ( $M_r$ ): 59830; Calculated pI value: 9.22  
 Number of mass values matched: 16  
 Sequence Coverage: 40%

**Figure 3.13: Example of MALDI-TOF analysis and protein identification of spot 9 from figure 3.12**

Mitochondrial fraction was electrophoresed by 2DE (pI 3-10) followed by silver staining. Spot 9 (figure 3.12) was picked, trypsinised and processed via MALDI-TOF mass spectrometry. The peptide mass list obtained was transferred to the Mascot database giving a significant positive identification. A. Mass spectrum obtained by MALDI-TOF. B. Identity probability of spot 9 as ATP synthase subunit alpha.

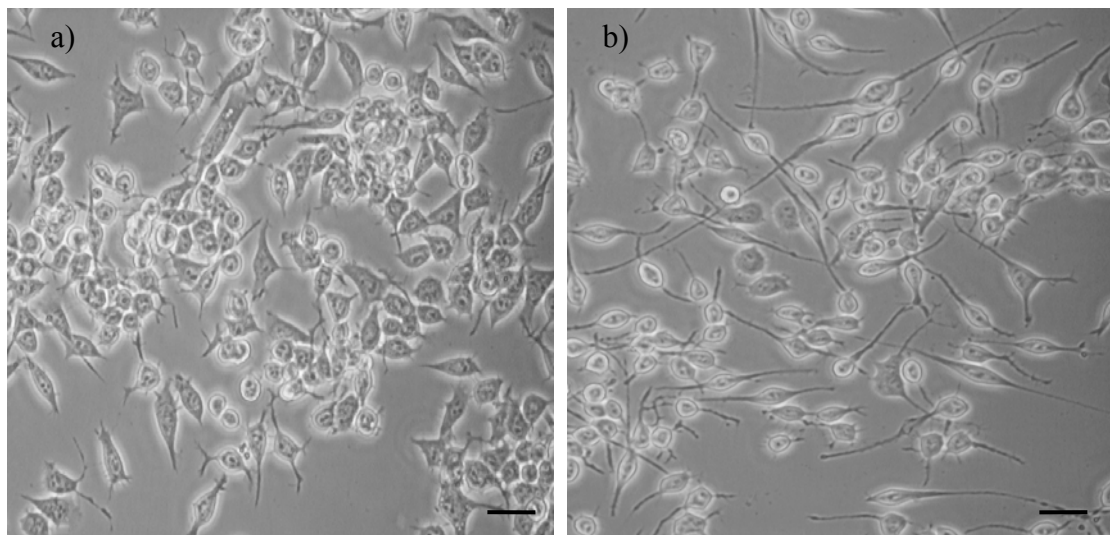


**Figure 3.14: Differentiated mouse N2a neuroblastoma cell morphology compared to mitotic cell morphology**

Mouse N2a neuroblastoma cells were seeded then grown for 24 hours. a) Growth medium was changed and cells incubated for 24 more hours: mitotic cells. b) Alternatively, growth medium was replaced by serum free medium with 0.3 mM dbcAMP for 24 hours: differentiated cells.

Objective x 400, bar = 20 $\mu$ m.

### 3.2.9.2 Changes in the mitochondrial proteome

Since mitochondria have been implicated in differentiation, it was interesting to investigate whether the mitochondrial proteome changed when mouse N2a neuroblastoma were differentiated. Figure 3.15 shows a representative mitochondrial proteome from a mitotic sample resolved on a large 2DE (please note – at this stage optimisation had not been conducted). Circles highlight spots that showed significant changes between differentiated and mitotic cells. These changes were quantified using the Samespots software and are shown in table 3.3. Nine spots showed significant changes. Most of them were decreasing in levels, indicating a lower level expression of those proteins in the post-mitotic state. Table 3.3 also shows that two of those proteins were identified. Stress-70 protein was significantly increased following differentiation. Moreover, aconitate hydratase level was significantly decreased.

### A. Protein mitochondrial profile following differentiation of N2a cells

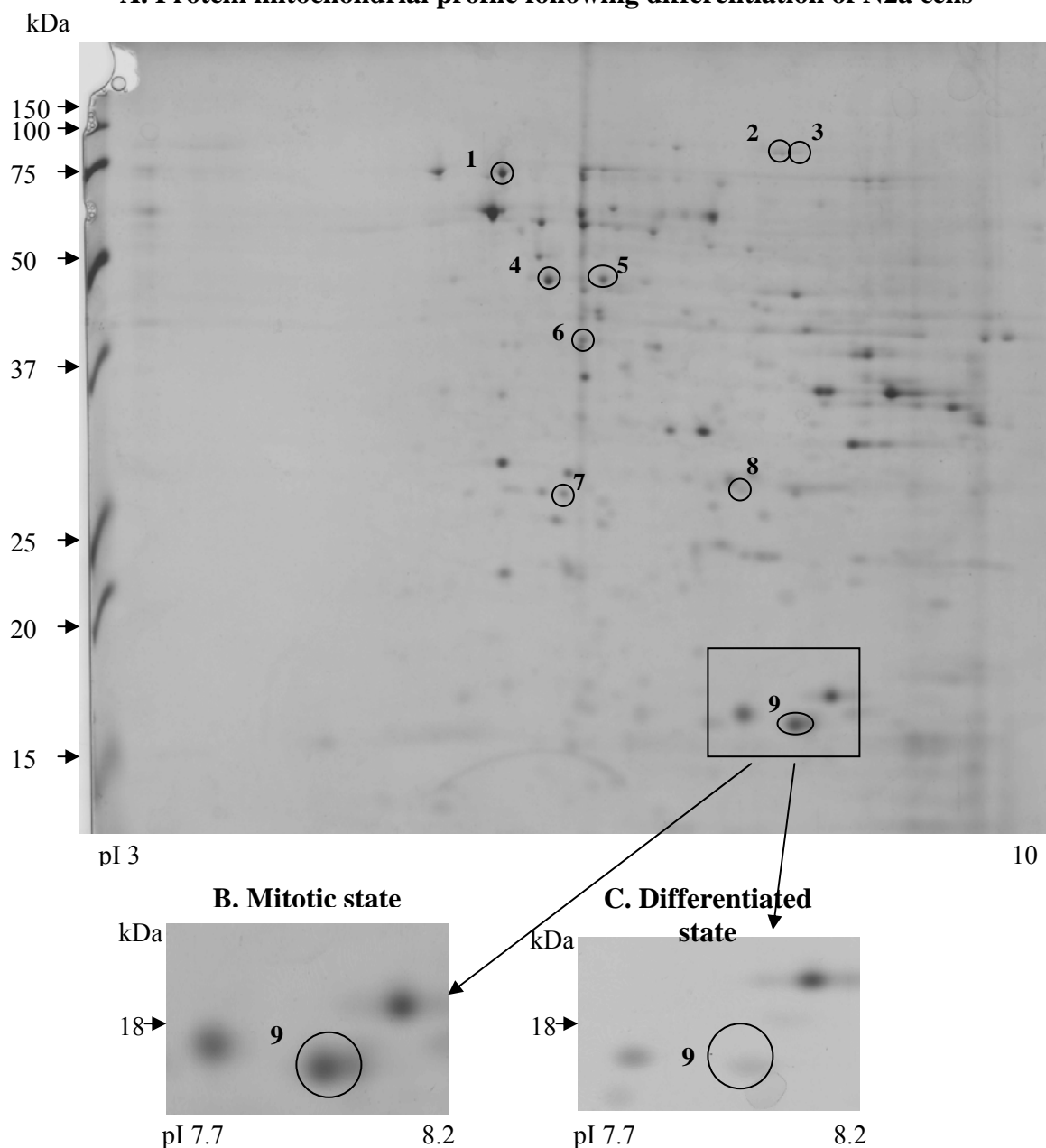


**Figure 3.15: Large-scale 2DE (pI 3-10) stained with silver stain showing spots changing in levels when cells are differentiated compared to mitotic cells**

Mouse N2a neuroblastoma cells were grown for 24 hours. Mitotic cells were left growing in growth medium while 0.3 mM dbcAMP in serum free medium was used to differentiate the cells. Mitochondria from mitotic samples and from differentiated samples were isolated using differential centrifugation. 200  $\mu$ g samples were run onto 12 % polyacrylamide resolving large-scale 2DE using pI 3-10 strips (17 cm) and silver stained gels were compared using Samespots Progenesis software. Circled spots represent spots that changed in intensity level between mitotic and differentiated samples using a paired t-test ( $n = 3$ ).

A. Full image of the gel from mitotic sample. B. Enlarged image of the squared area from mitotic sample. C. Enlarged image of the squared area from differentiated sample. MW: molecular weight markers.

Spot symbol <sup>1</sup>	Protein identification <sup>2</sup>	Average normalised volumes in differentiated samples <sup>3</sup>	Average normalised volumes in mitotic samples <sup>3</sup>	+/- % change compared to mitotic <sup>4</sup>
1	Stress-70 protein	5829 ± 489	4854 ± 500	+ 20 % *
2		1333 ± 1591	1902 ± 128	- 43 % **
3	Aconitate hydratase	1299 ± 104	2361 ± 151	- 82 % **
4		802 ± 132	1038 ± 119	- 29 % *
5		1687 ± 74	2464 ± 116	- 46 % *
6		2752 ± 534	4250 ± 212	- 54 % **
7		577 ± 29	1120 ± 386	- 94 % *
8		886 ± 187	1734 ± 386	- 96 % **
9		2271 ± 541	5386 ± 384	- 37 % *

**Table 3.9: Quantitative analysis of spots showing significant changes in differentiated cell profiles compared to mitotic cells**

Normalised density obtained using Samespot software (Progenesis) .

<sup>1</sup> Spot symbols confer to figure 3.15.

<sup>2</sup> Proteins identified by peptide mass fingerprinting. For accession numbers and more details on the Mascot database results refer to table 3.

<sup>3</sup> Average of normalised volumes (n = 3) ± Standard error of the mean

<sup>4</sup> Percentage increase = + Average of normalised volumes from differentiated samples / Average of normalised volumes from mitotic samples.

<sup>4</sup> Percentage decrease = - Average of normalised volumes from mitotic samples / Average of normalised volumes from differentiated treated samples.

\* Statistically significant increases p < 0.05 using a paired t-test.

\*\* Statistically significant increases p < 0.1 using a paired t-test.

### 3.3 DISCUSSION

#### 3.3.1 Purity of subcellular fractions

A comparative analysis revealed that mitochondrial protein recovery from mouse N2a cells was double that from human SH-SY5Y cells using the present protocol. As the amount of protein needed for further analysis, using a proteomic approach, was important, mouse N2a neuroblastoma cells were chosen for further analysis.

Even though protein recovery seemed higher in mitotic cells, the difference was not significant making both mitotic and differentiated states of N2a cells acceptable for the present study. Analysis of biochemical markers in each fraction showed that the level or activity of mitochondrial markers were higher in the mitochondrial fraction, which was not significantly different between mitotic and differentiated cells. Indeed, assessment of enrichment of mitochondria was around 5-fold using SDH activity and higher using cytochrome c as a marker. This enrichment was higher than observed in previously reported studies. For example, Almeida and Medina (1997) isolated mitochondria from primary neurons estimating a 3.7-fold enrichment in mitochondria based on citrate synthase activity. Scheffler *et al.* (2001) used the SH-SY5Y neuronal cell line and had no enrichment of a mitochondrial marker (cytochrome c oxidase activity) compared to the total extract. However, in their study, a purer mitochondrial extract was produced following a percoll / metrizamide two-step gradient, and mitochondrial activity may have been decreased due to further fractionation (damage due to extra steps).

In the present project, the presence of cytoplasmic, nuclear and microsomal markers was negligible compared to the high enrichment of mitochondrial markers. Only a low fraction of the cytoplasmic marker was found in the mitochondrial fraction compared to total extract in differentiated cells, which was slightly higher than in Scheffler *et al.* (2001), which was expected as they used a percoll / metrizamide gradient.

Lysosomal proteins were also enriched by 2-fold in the mitochondrial fraction from differentiated cells. To remove lysosomes, preliminary experiments were conducted involving pelleting the mitochondria through a sucrose cushion. Unfortunately, the yield of protein was too low for use in proteomics protocols (data not shown). This problem was also mentioned by Cox and Emili (2006) who suggested that gradient fractionation necessitated much more starting material with increased time and cost. In the present work,

it was decided to opt for high recovery of mitochondria despite the risk of lysosomal contamination. It was felt that because 2DE tends to resolve the high-abundance proteins, lysosomal proteins should be in the background of the gels. Moreover, it was observed that, although there was a 2-fold enrichment of lysosomal proteins in the mitochondrial fraction, the enrichment of lysosomal markers was higher in the cytoplasmic fraction compared to total extract (4.4-fold). This indicated a dominant presence of lysosomal proteins to the cytoplasmic fraction compared to the mitochondrial fraction.

Overall, the cytoplasmic fraction following differential centrifugation was negligibly contaminated with mitochondrial and nuclear fractions. Although the fraction was called “cytoplasmic fraction”, it is worth mentioning that it contained the majority of the endoplasmic reticulum and lysosomal proteins which was consistent with the crude fractionation in the study of Scheffler and colleagues (2001).

Although a high enrichment of lamin was observed in the nuclear fraction, this fraction was contaminated with cytoplasmic, microsomal, lysosomal and mitochondrial proteins. The presence of all the fractions in the nuclear fraction indicated possible presence of unbroken cells in the homogenate, estimated to be between 25 and 50 % (data not shown).

To conclude, it was felt that the mitochondrial fraction was adequate for further study. Even if the mitochondrial fraction was contaminated with lysosomes, it seemed unlikely to be a problem for 2DE analysis since low-abundance proteins are not always observed on 2DE and proteins were identified prior to further validation.

### **3.3.2 2DE: optimization and reproducibility**

Although 2DE has been widely used in many different studies, the technique is not used routinely in laboratories due to a lack of automation and low reproducibility (Govorun and Archakov, 2002). Moreover, different samples used have different ionic, hydrophobic and molecular weight compositions, which can be a source of variability, affecting how they behave when applied to an electric field, particularly in the IEF step. Consequently, it has been proposed that each laboratory should optimise 2DE methods to the best performance for each type of sample used (Rabilloud *et al.*, 2007). In the present project, each step was devised to obtain a mitochondrial profile that resolved as many spots as possible in a reproducible manner. A compromise between these two characteristics has sometimes been necessary.

It is well known that mitochondria are membrane rich organelles, with a majority of hydrophobic proteins (Reifschneider *et al.*, 2006). One limitation of the present study was sample preparation for the first dimension of 2DE. As the voltage is very high in IEF, any residual salts and ionic compounds had to be removed. Consequently, any solubilising agents and detergents used in the sample buffer could not be ionic, which generally are more efficient for the solubilisation of highly hydrophobic molecules (Rabilloud *et al.*, 2007). On the other hand, non ionic and zwitterionic detergents could be used and the most commonly used detergents in each category were tested: Triton-X-100 and CHAPS, respectively (Rabilloud *et al.*, 2007). With Triton-X-100, some low-abundance basic proteins seemed to be more intensely stained, but the staining of acidic proteins was weak. The latter was of great importance since acidic proteins included ATP synthase  $\beta$ -subunit (ATPase- $\beta$ ), which is an inner mitochondrial membrane protein. Chaotropic agents such as urea and thiourea solubilise proteins by breaking non-covalent interactions between various molecules in a system, causing protein unfolding (Rabilloud *et al.*, 2007). Although Triton-X-100 has been shown to be more efficient with thiourea (Rabilloud *et al.*, 2007 and in the present study; data not shown) and although acidic spots seemed to appear, they were not as intense or as well resolved as with CHAPS. Other zwitterionic detergents of the same family, for example ASB-14, are thought to be more efficient and their use has been increasing over the last few years, ASB-14 has been shown to solubilise membrane proteins more efficiently, if used in combination with thiourea (Luche *et al.*, 2003), but in the present study, although basic proteins seemed to be better resolved with ASB-14 combined with thiourea than with CHAPS, acidic proteins were barely detectable, similar to results shown with Triton-X-100. CHAPS remained, therefore, the detergent of choice for the analysis of mitochondrial proteome from mouse N2a neuroblastomas using pI 3-10 2DE. To remove residual lipids and salts that could interfere with IEF and mass spectrometry, acetone precipitation has widely been used prior to 2DE (Mastro and Hall, 1999). In the present study, precipitating samples with acetone prior to IEF did not improve resolution and the staining seemed to be less intense than without acetone precipitation. Moreover, it was thought that adding a step could increase variability to the procedure so it was decided that, for comparative studies, acetone precipitation would not be used.

When Merrill *et al.* (1979) used silver stain for the first time they introduced, at the time, the most sensitive non-radioactive protein stain for 2DE. It was a lot more sensitive than Coomassie brilliant blue stain with a detection limit of 1 ng compared to 10 ng, (Patton, 2002). Silver staining was also compatible with mass spectrometry; however, the gel to gel variability was high and the staining was not always uniform over the whole gel (Patton, 2002), which was also observed in the present study (discussed below). The stain can be semi-quantitative if glutaraldehyde is used in the sensitizing step of the staining protocol, showing a more uniform staining all over the gel, but not being compatible with mass spectrometry (Patton, 2002). Nevertheless, in the present project, although the staining seemed to improve when using glutaraldehyde, the variability between gels was still high (data not shown). Another limitation of silver stain, with or without aldehydes, is the low linear dynamic range for quantitation of spot intensities. Indeed, the linear range is only one order of magnitude (Lopez *et al.*, 2000) leading to saturation of the stain (with around 60 ng protein / spot) prior to the apparition of lower-abundance spots. An alternative to silver stain is the use of fluorescent dyes. SyproRuby has a similar detection limit to silver (0.5-1 ng) and a linear dynamic range of three orders of magnitude, saturating with spots containing over 2 µg protein (Lopez *et al.*, 2000).

In previous studies, one of the limitations of 2DE was described as the low reproducibility of the method (Dani and Dencher, 2008). Following optimization of the protocol, it was important to assess the reproducibility between gels for the same sample or replicate samples, initially using silver staining. Replicates of samples run in parallel showed that approximately the same number of spots was revealed and around 80 % of these spots varied in intensity by less than 2-fold, and around 95 % by less than 3-fold. Changes over the 3-fold threshold were then minimal. It was, however, interesting to note that changes were slightly more significant when the same sample was run on a different day compared to different samples electrophoresed in parallel. This showed that, although subcellular fractionation reproducibility was relatively low, as shown by high SEMs with the protein recovery and the markers data, the 2DE protocol was a greater source of variability for the mitochondrial proteome profile itself. On the other hand, when SyproRuby was used, 95 % of the spots showed a change in intensity by less than 2-fold change, improving the reproducibility.

To conclude, to reduce variability when comparing samples (treatments versus controls), it was deemed necessary to run samples in parallel for the IEF step and for the SDS-PAGE step and to stain with SyproRuby.

### 3.3.3 Integrity of mitochondrial fractions on 2DE

The 2DE profile of the mitochondrial proteome from mouse N2a neuroblastoma cells included proteins from all three compartments of the mitochondria (matrix and inner and outer mitochondrial membranes). This provides clear confirmation of enrichment of intact mitochondria in the mitochondrial fraction. It also agrees with the data showing enrichment of SDH and cytochrome c described earlier. On the other hand, there was some evidence for the presence of non-mitochondrial proteins such as GRP78,  $\beta$ -actin, STIP1 and protein disulfate isomerase A3, which could be indicative of contamination by the endoplasmic reticulum. Interestingly, GRP78 and STIP1 are proteins found in the contact sites between the mitochondria and the endoplasmic reticulum (Hayashi and Su, 2007). Moreover, proteins that are not specific to mitochondria were also present in 2DE profiles of mitochondria in other studies (Fukada *et al.*, 2004; Scheffler *et al.*, 2001). Thus, the N2a mitochondrial fraction was considered suitable for analysis of the mitochondrial proteome.

Up to 400 spots were visualised with the majority showing molecular weights between 20 and 60 kDa and pI values between 5 and 8. This is similar to previous studies of mitochondrial proteomes from different sources, even from plants. For examples, Krufft *et al.* (2001) visualised up to 600 spots in the mitochondrial proteome from Arabidopsis with the majority between 30 and 60 kDa and pI 4.5 and 8. Scheffler *et al.* (2001) analysed the mitochondrial proteome from human SH-SY5Y neuronal cells and observed the majority of spots between 20 and 80 kDa and pI 5 to 8. Moreover, Fukada *et al.* (2004) studied the mitochondrial proteome from NSC34 mouse spinal cord-neuronal cell line and observed up to 600 spots with a majority between 25 and 70 kDa and pI 4.5-8.

Only about two-third of the spots analysed (21 / 32) led to a positive identification of the protein, again in agreement with previous studies (Krufft *et al.*, 2001; Scheffler *et al.*, 2001 and Fukada *et al.*, 2004). This limitation could be due to the fact that most of the mitochondrial proteins are membrane proteins and extraction of peptides from the gel might be difficult due to the low solubility of some of these proteins. Moreover, many proteins were of basic pI. Such proteins, by their chemical composition, could be rich in lysine

residues and when cleaved by trypsin, the most widely used protease for mass spectrometry, produce many small peptide fragments, which would render their identification difficult. This problem would also be exacerbated when the basic proteins are of low molecular weight. Another limitation for mass spectrometry in the present study was that the limited amount of material loaded onto each gel might lead to spots with too low protein content to allow identification.

### 3.3.4 Changes in the mitochondrial proteome following cell differentiation

One of the characteristics of neurons in the brain is that they are in a post-mitotic state. One of the difficulties with using secondary neuroblastoma cultures is that, although they express some neuronal properties, they are mitotic and also express different characteristics compared to post-mitotic cells. Methods have been devised to differentiate cultured cells *in vitro*. For example, serum withdrawal supplemented with dbcAMP induces cell cycle arrest in mouse N2a neuroblastoma cells (Prashad and Rosenberg, 1976), resulting in elongation of axon-like processes due to changes in cytoskeletal protein arrangements.

In the present study, we investigated whether the differentiation process had direct effects on the mitochondrial proteome profile of N2a cells. Nine proteins showed significant changes in levels following differentiation, but, due to the variability of large-2DE, it is likely that these changes are not exclusive and that other changes may have been missed. Two of the nine spots were identified: stress-70 protein was observed to increase and aconitate hydratase was observed to decrease following cellular differentiation. Stress-70 protein is a mitochondrial heat shock protein and aconitase is a Krebs cycle enzyme. Several studies have shown that differentiation of cells leads to morphological changes in mitochondria. For example, Moyes and colleagues (1992) showed that differentiation of 3T3 fibroblasts led to changes in cristae structure formed by the inner mitochondrial membrane. They observed that the volume of cristae was decreasing in relation to an increase in enzyme activities, inferring a more efficient use of enzymes with less protein. Stress-70 protein has been implicated in apoptosis by protecting against cell death (Xu *et al.*, 2009). It was observed that the differentiation process in different cell lines shared similarities with the apoptotic process with a slight release of cytochrome c but no activation of caspase-3 combined with a rearrangement of Bcl<sub>2</sub> proteins and lower

mitochondrial potential (in keratinocyte differentiation, Von Ahsen *et al.*, 2000) linking mitochondria to the differentiation process.

In the present study, designed to choose the most suitable cellular state for study of the mitochondrial proteome, changes in expression levels of stress-70 protein and aconitase were not validated using an alternative detection method such as western blot analysis. Since differentiation led to distinct changes in proteome composition, it was decided that subsequent analyses would be conducted on differentiated cells.

## **CHAPTER IV:**

# **EFFECTS OF MPTP ON CELL VIABILITY OF DIFFERENTIATED MOUSE N2A NEUROBLASTOMA CELLS**

## 4.1 INTRODUCTION

### 4.1.1 Effects of MPTP on cell viability and mitochondrial activity in mouse N2a neuroblastoma cells

#### 4.1.1.1 MPTP-mediated sub-cytotoxic effects

An important step in studying the effects of MPTP on the mitochondrial proteome of mouse N2a neuroblastoma cells was to establish concentrations of the toxin that produced effects on the cell and the mitochondria prior to cell death. De Girolamo and colleagues (2000) previously used sub-cytotoxic concentrations of MPTP on mouse N2a neuroblastoma cells resulting in changes in cytoskeletal proteins. In particular, neurofilaments were modified in response to MPTP resulting in changes in axon outgrowth and cell morphology prior to cell death. Song and colleagues (1997) have also used sub-cytotoxic concentrations of MPTP on human SH-SY5Y neuroblastoma cells that did not affect cell viability but resulted in changes in cell morphology, cytoskeleton organisation and mitochondrial structure. The objective of these studies using sub-cytotoxic concentrations aimed to decipher the pathways involved in MPTP toxicity prior cell death as this may lead to a better understanding of the neurodegenerative process involved in PD.

#### 4.1.1.2 Monitoring cell viability following MPTP treatment in mouse N2a neuroblastoma cells

Several assays to study cell viability have been designed to monitor a wide range of essential cellular characteristics, such as membrane integrity (e.g. LDH release and trypan blue exclusion), metabolic activity (e.g. MTT reduction), protein content (e.g. Coomassie blue assay) or DNA synthesis (e.g. <sup>3</sup>H-thymidine assay).

De Girolamo *et al.* (2000) used one of the commonly used methods to monitor cell membrane integrity, the trypan blue exclusion assay, to establish whether the concentrations of MPTP used were sub-cytotoxic. The trypan blue dye is able to enter cells that had lost their membrane integrity and are then considered to be dying or dead, whilst healthy cells remain trypan blue dye-impermeable. This constitutes a rapid and relatively inexpensive way of checking cell permeability and cell membrane integrity.

Metabolic activity can also be an indicator of cell viability. For example, Amazzal *et al.* (2007) used both the trypan blue exclusion and MTT reduction assays for cell viability markers. The MTT assay was developed for cytotoxic assessment by Mosmann (1983). The tetrazolium salt MTT is cleaved by various dehydrogenase enzymes. The resulting coloured product concentration was proportional to the dehydrogenase enzyme activities present in each cell and can be measured spectrophotometrically.

Assessment of cellular ATP content could also be considered as a metabolic activity assay as it monitors cellular energy. De Girolamo and colleagues (2001) used the bio-luminescent ATP assay to monitor ATP presence in N2a neuroblastoma following MPTP treatment. In this bio-luminescent assay, ATP presence was monitored based on the capacity of the luciferase enzyme to catalyse the formation of a luminescent product in a proportional manner.

#### 4.1.1.3 Monitoring mitochondrial activity following MPTP treatment in mouse N2a neuroblastoma cells

Since the main objective of the present study was the analysis of the effects of MPTP on the mitochondrial proteome, it was necessary to establish whether the sub-cytotoxic concentrations used had an effect on mitochondrial activity.

Although not entirely specific to mitochondria, the ATP assay can be sometimes used as a measure of mitochondrial activity since these organelles are thought to produce most of the cellular ATP (Mootha *et al.*, 2003). Then, a change in extra-mitochondrial ATP production would not have a huge effect on mitochondrial ATP levels. Moreover, the major site of action of MPTP was observed to be the inhibition of the ETC via its metabolite, MPP<sup>+</sup> (Ramsay *et al.*, 1987) leading to mitochondrial ATP production reduction (Ramsay *et al.*, 1987). Consequently, the ATP assay could be considered as a measure of mitochondrial activity.

Another marker of mitochondrial activity is the assessment of mitochondrial membrane potential. As the ETC transfers protons through the IMM, it creates an electrical potential that polarises mitochondrial membranes. The fluorescent JC-1 assay was developed by Cossarizza and colleagues (1993). They used the JC-1 dye, a lipophilic cation that had the capacity to enter mitochondria. The dye was observed to aggregate in active polarised mitochondria and to form J-aggregates that emitted an orange-red signal at 590 nm when excited at 490 nm. Interestingly, when mitochondrial membrane potential collapsed, the dye could leave depolarised mitochondria as a monomeric form

that emitted a green signal at 530 nm when excited at 490 nm. The ratio of aggregated dye signal over monomeric dye signal can be measured and provide a relatively specific marker of mitochondrial activity.

#### 4.1.2 Investigation of cell death pathways

Whether neurodegeneration in PD has necrotic or apoptotic features has been the focus of a number of studies producing conflicting results involving both necrotic and apoptotic markers depending on models and toxin concentrations used (reviewed in Barzilai and Melamed, 2003). Two different studies by He and colleagues (2008) and Novikova *et al.*, (2006) have shown that in a mouse model, neurodegeneration due to acute MPTP treatment of mice did not show typical apoptotic markers, while injections of subacute or chronic treatments showed apoptotic markers (e.g. nuclear condensation, presence of apoptotic bodies).

It was therefore important in the present study to investigate whether early cell death markers were present following sub-cytotoxic MPTP treatment in mouse N2a neuroblastoma cells and the potential role of mitochondria if such markers were present.

##### 4.1.2.1 Cellular markers of necrosis

As previously described (section 1.3.2), necrosis was originally observed to be a passive, energy-independent type of cell death. One of the identified causes was calcium overload leading to its typical cellular characteristics: induction of mitochondrial permeability transition, osmotic swelling of mitochondria, rupture of the OMM, loss of energy, cell swelling, disruption of plasma membrane and release of cytoplasmic content into the extracellular environment (Kajta *et al.*, 2004).

However, studies have recently demonstrated that other types of necrosis could occur in different models of study. For example Niquet *et al.* (2006), studied a neuronal death pathway in primary cortical cultures, in which cells showed a necrotic morphology but with some features of the apoptotic pathway (caspase-3 activation, DNA fragmentation). Moreover, Boujrad *et al.* (2007) described a “programmed necrosis” that was mediated by apoptosis inducing factor found in the mitochondrial IMS and released in apoptotic cell death.

Typically, cell lysis is the most used characteristic for studying necrotic cells. Membrane exclusion assays (e.g. trypan blue) and cytoplasmic content release assays

(e.g. lactate dehydrogenase) are often used as necrotic markers. Moreover, mitochondrial membrane potential and cytochrome c release can be monitored as mitochondrial health markers but are not specific to necrotic cell death as they also occur in apoptosis (Halestrap *et al.*, 2000).

#### 4.1.2.2 Cellular markers of apoptosis

Apoptosis is a programmed and active process of the cell leading to death (also described in section 1.3.1). As opposed to necrotic cell death, typical characteristics are cell shrinkage leading to apoptotic body formation, nuclear and cytoplasmic condensation, chromatin fragmentation and intact cell membrane integrity (Orenius *et al.*, 2004).

Any protein involved in the apoptotic cascade can be used as markers of apoptotic cell death (e.g. Bcl<sub>2</sub> family proteins, caspases, mitochondrial proteins that can be released to the cytoplasm). Many have been used for the study of MPTP-induced cell death. The protein levels and mRNA levels of Bcl<sub>2</sub>-family proteins, particularly the anti-apoptotic Bcl<sub>2</sub> and pro-apoptotic Bax proteins, have been widely used as a marker of the cell death pathway (Yang *et al.*, 1998). Many cleaved caspases have been studied, depending on the pathway involved in the particular projects. Caspase-3, for example, has been widely used as it is activated in both extrinsic and intrinsic pathways and is the most central effector caspase along with its analog caspase-7 (Hartmann *et al.*, 2003; Bilslund *et al.*, 2002). To distinguish between the mitochondrial-dependent pathway with other apoptotic pathways, caspase-2 can be used as it is an initiator of the mitochondrial-dependent pathway (Orrenius *et al.*, 2004). Moreover, caspase-2 activity has been linked to MPP<sup>+</sup> toxicity (for example in Sanz *et al.*, 2008). Morphologically, DNA fragmentation and chromatin condensation have also widely been used as apoptotic markers (Novikova *et al.*, 2006), although they are not pathway specific.

### 4.1.3 Aims of the chapter

The pathways involved in MPTP-induced neurodegeneration have not been fully resolved. Investigating MPTP-induced cell death in mouse N2a neuroblastoma cells may add important insights into these pathways. It has previously been shown that morphological and biochemical changes occurred prior to cell death following sub-cytotoxic exposure to MPTP in differentiating mouse N2a neuroblastoma cells (De Girolamo *et al.*, 2000). Sub-cytotoxic concentrations of MPTP were used in this thesis to study early markers of neurodegeneration and more particularly of mitochondrial dysfunction. Consequently the primary objective of this chapter was to establish sub-cytotoxic MPTP concentrations using a variety of assays, namely monitoring cell lysis, metabolic activity and mitochondrial activity. This would establish the parameters for further studies to identify markers of neurodegeneration covered in subsequent chapters. Both necrosis and apoptosis have been observed in MPTP-induced neurodegeneration (Bilsland *et al.*, 2002; Lotharius *et al.*, 1991). Both pathways have common and different characteristics. A secondary objective of this chapter was to investigate whether early markers of cell death were observed using these sub-cytotoxic concentrations. Mitochondrial involvement was monitored by investigating mitochondrial potential, cytochrome c release and caspase-2 cleavage. Caspase-3 cleavage and activity were also used as an overall marker of apoptosis. These markers could give clues on which pathways are involved in MPTP-induced neuronal cell death and whether mitochondria are involved in this process.

## 4.2 RESULTS

### 4.2.1 Assessment of effects of MPTP on N2a neuroblastoma cell viability

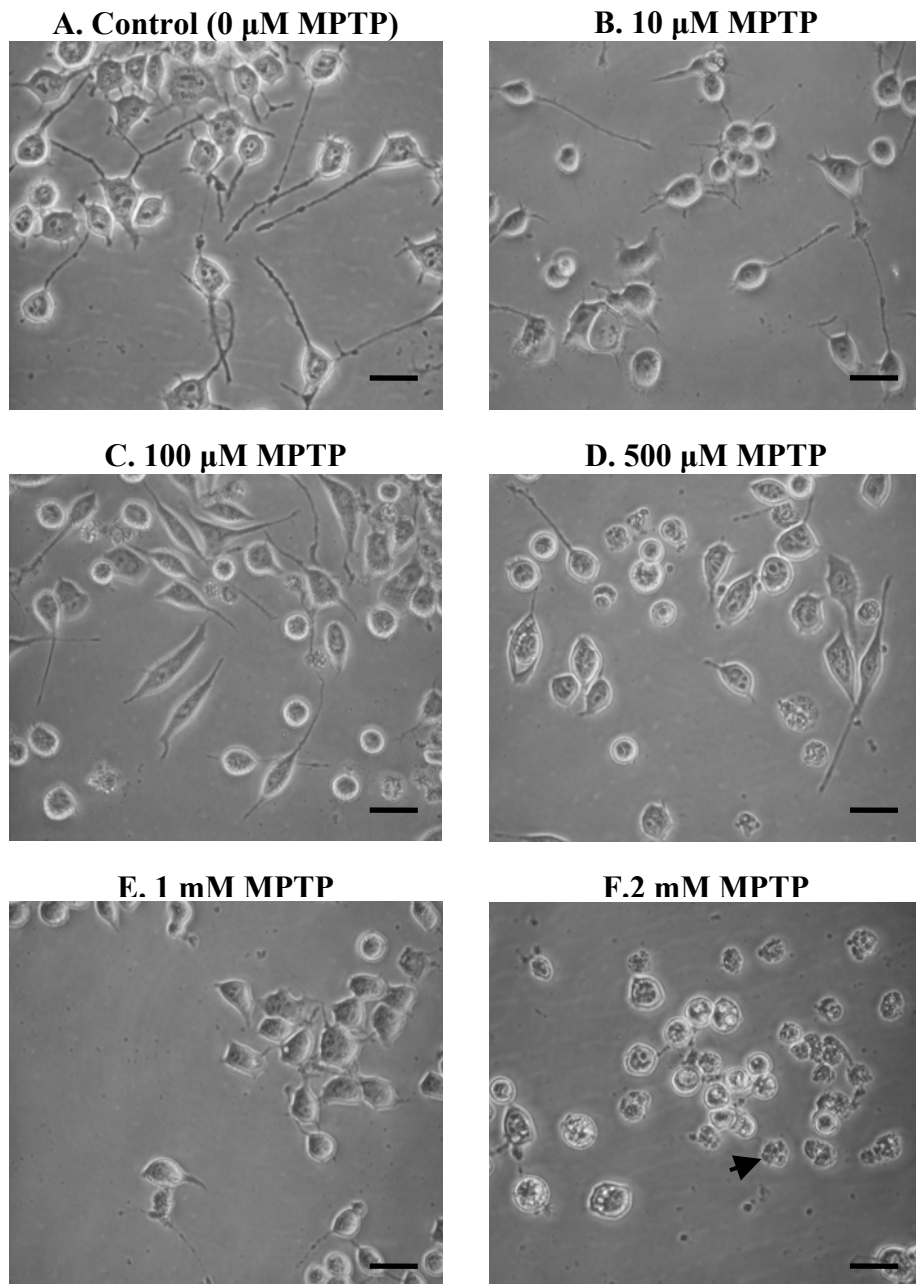
In order to establish cytotoxic and sub-cytotoxic MPTP concentrations in mouse N2a neuroblastoma cells, cellular morphology, cell membrane integrity, metabolic activity, cellular energy level and mitochondrial membrane potential were monitored following exposure of the toxin over time.

#### 4.2.1.1 Cellular morphology

Mouse N2a neuroblastoma cells were pre-differentiated in serum free medium supplemented with 0.3 mM dbcAMP for 16 hours prior to treatment with different MPTP concentrations (0 to 2 mM MPTP). The morphology of cells was then observed using an inverted microscope and pictures were taken following 24 (figure 4.1) and 48 hour (figure 4.2) treatments.

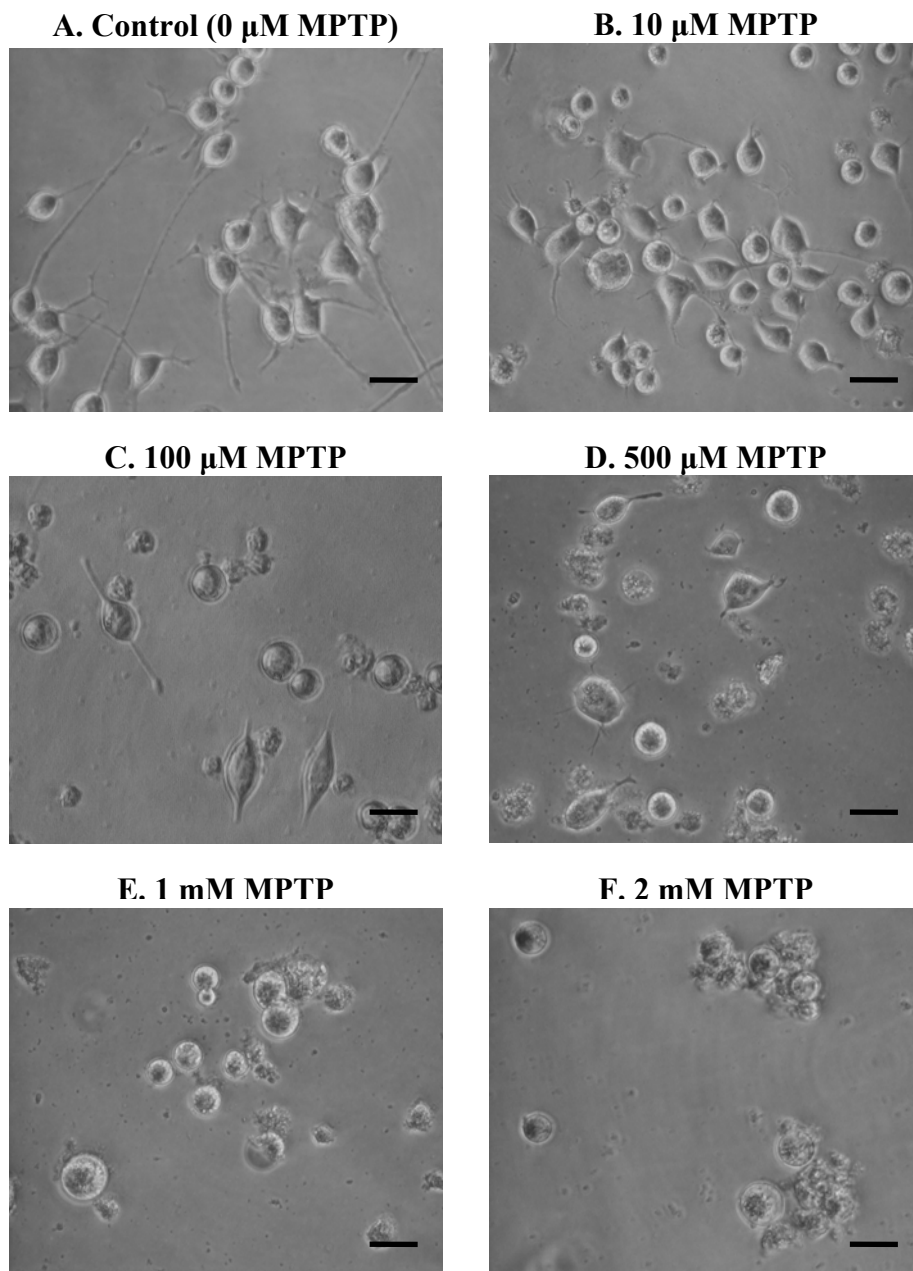
At 24 hours, control cells showed ovoid cell bodies with axon-like processes (figure 4.1A). Following 10  $\mu$ M MPTP treatment for 24 hours, cells looked similar to controls except that cells exhibited fewer axon-like processes (figure 4.1B). Morphological changes became more evident following 100  $\mu$ M MPTP for the same time-point compared to controls (figure 4.1C). Axon-like processes were generally shorter at this concentration and gradually deteriorated as the concentration of MPTP increased (figure 4.1C to 4.1E). Very short or no axon-like processes were observed following 24 hours exposure to 1 mM MPTP (figure 4.1E). However, with this treatment, cell bodies seemed to maintain membrane integrity when compared to cell bodies observed following 2 mM MPTP treatment (figure 4.1F). Indeed, 2 mM MPTP treatment exhibited cell death morphology characterised by reduction in cell volume, spherical cell shape and loss of membrane integrity.

Following 48 hours, control cells had similar morphology compared to controls for the 24 hour time-point (figures 4.1A and 4.2A). Morphological changes were highly apparent following 10  $\mu$ M MPTP treatment with virtually no axon-like processes and a few cell bodies with reduced volume (figure 4.2B). Following treatments with higher concentrations of MPTP, a mixture of morphologies could be observed. Some cells showed intact membrane while others exhibited loss of membrane integrity.

**24 hour time-point**

**Figure 4.1: Morphological changes of mouse N2a neuroblastoma cells following exposure to MPTP for 24 hours**

Cells were differentiated with 0.3 mM dbcAMP for 16 hours prior to treatment with a variety of MPTP concentrations for 24 hours: A. 0  $\mu$ M; B. 10  $\mu$ M; C. 100  $\mu$ M; D. 500  $\mu$ M; E. 1 mM; F. 2 mM MPTP ( $\times$  400 magnification). Scale bars represent 20  $\mu$ M. Arrow shows an example of a cell which has lost membrane integrity.

**48 hour time-point**

**Figure 4.2: Morphological changes of mouse N2a neuroblastoma cells following exposure to MPTP for 48 hours**

Cells were differentiated with 0.3 mM dbcAMP for 16 hours prior to treatment with a variety of MPTP concentrations for 48 hours: A. 0  $\mu$ M; B. 10  $\mu$ M; C. 100  $\mu$ M; D. 500  $\mu$ M; E. 1 mM; F. 2 mM MPTP ( $\times$  400 magnification). Scale bars represent 20  $\mu$ M.

This became more apparent as the concentration of MPTP increased from 100  $\mu\text{M}$  to 2 mM MPTP (figure 4.2C to F).

#### 4.2.1.2 Cell membrane integrity

To assess the extent of cell death caused by exposure to MPTP and establish sub-cytotoxic concentrations, cell membrane integrity was measured using the trypan blue exclusion assay as a marker of cell viability (refer to section 2.2.2.2).

Following 24 hours treatment, no decrease in cell viability was observed using the trypan blue exclusion assay with concentrations up to 1 mM compared to control (figure 4.3A). Concentrations greater than 1 mM showed a significant decrease in cell membrane integrity. Following 2 mM MPTP exposure for 24 hours, there was 60 % cell death. With 5 mM MPTP, no viable cells were observed. This showed that MPTP was cytotoxic at concentrations greater than 2 mM (figure 4.3A).

At a later time-point of 48 hours, cells were more sensitive to MPTP at lower concentrations. 10  $\mu\text{M}$  killed over 20 % of the cells which increased with increasing MPTP concentrations in a concentration-dependent manner (figure 4.3A).

#### 4.2.1.3 MTT reduction assay

As an alternative method of monitoring cell viability, the cellular metabolic activity was assayed using the MTT reduction assay (refer to section 2.2.2.3).

Following 24 hours treatment, no decrease in cell viability was observed using the MTT reduction assay with concentrations up to 1 mM compared to control (figure 4.3B). However, concentrations greater than 1 mM showed a significant decrease in MTT reduction. Following 2 mM and 5 mM MPTP exposure for 24 hours, there was a 40 % and 85 % decrease, respectively (figure 4.3B).

After 48 hours exposure, cells were more sensitive to MPTP with 10  $\mu\text{M}$  significantly decreasing cell viability by 35 %. Metabolic activity (as measured by MTT reduction) was reduced to 40 % by 100  $\mu\text{M}$  to 1 mM MPTP whilst concentrations of 2 and 5 mM MPTP resulted in viability being reduced to 20 % and 5 %, respectively (figure 4.3B).

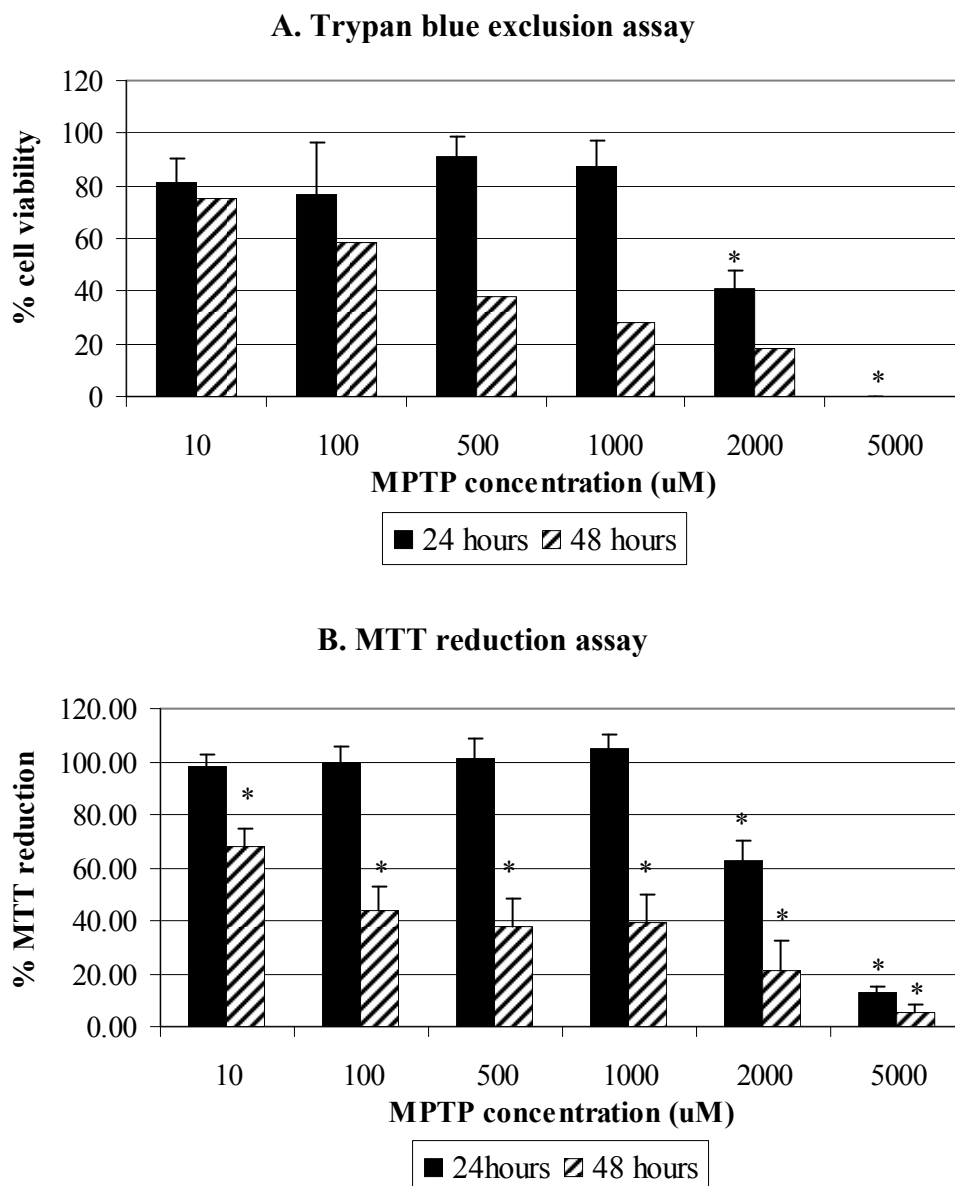


**Figure 4.3: Effects of different concentrations of MPTP on cell viability using two different assays in differentiated N2a cells following 24 hour and 48 hour treatments**

Cells were differentiated in serum free medium containing 0.3 mM dbcAMP for 16 hours. Different MPTP concentrations (0 to 5 mM) were then added to the medium for 24 hours (black) and 48 hours (striated) A. Trypan blue exclusion assay was measured. Control percentage of viable cell values were  $53.3 \pm 4.3$  at 24 hours ( $n = 4$ ) and  $50.6$  at 48 hours ( $n = 1$ ) and B. MTT reduction assay was also measured. Control mean absorbance values were  $A_{570nm} = 0.611 \pm 0.095$  at 24 hours and  $A_{570nm} = 0.610 \pm 0.081$  at 48 hours ( $n \geq 7$ ).

Results are expressed as mean % viability / reduction  $\pm$  SEM. Statistical analysis was carried out using the paired t-test with a two-tail distribution. All \* values  $p < 0.05$  when compared to respective controls.

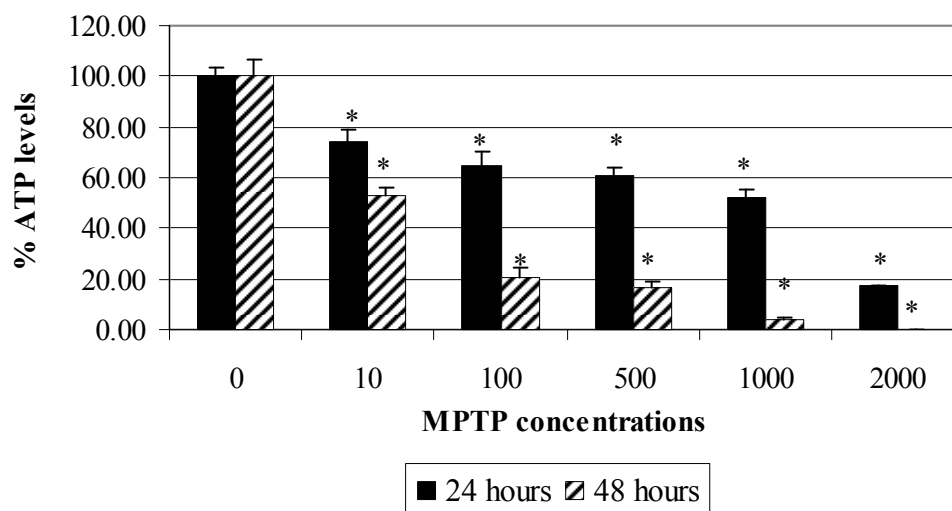
#### 4.2.1.4 Cellular ATP content

ATP levels were investigated as a complementary measure of metabolic activity (refer to section 2.2.2.5) and more particularly a measure of oxidative phosphorylation, as it accounts for most of the cellular ATP production.

MPTP caused a dose- and time-dependent decrease in ATP levels, with 1 mM MPTP producing 50 % depletion of ATP compared to control following 24 hours exposure and 10  $\mu$ M MPTP producing 50 % depletion following 48 hours exposure (figure 4.4). Following 24 hours exposure, ATP levels were reduced with concentrations as low as 10  $\mu$ M MPTP – which resulted in 25 % loss of ATP levels.

#### 4.2.1.5 Mitochondrial potential

Specific mitochondrial activity was measured by monitoring mitochondrial membrane integrity using the JC-1 fluorescent dye (refer to section 2.2.2.4). This dye fluoresces red within mitochondria when they are active and green within the cytoplasm when mitochondria depolarise and become inactive. Pictures were taken using a confocal laser microscope (figure 4.5A). Control cells showed a strong red signal evenly distributed in the cell body, in axon-like processes and corresponding to active, healthy and evenly distributed mitochondria (figure 4.5A a to c). Quantification of JC-1 signal using Leica confocal software and calculation of active / inactive mitochondria showed a ratio of around 1 (figure 4.5B). Following 1 mM MPTP treatment for 24 hours, no axonal mitochondria could be observed, consistent with previous morphological observations of axonal loss. JC-1 aggregates remained present in the cell body but not as evenly as the controls compared to the green signal (figure 4.5A d to f). Compared to controls, the green signal was more apparent in the overlay image (Figure 4.5A c and f). Individual red dots representing mitochondria looked bigger in a minority of the cells indicating mitochondrial swelling. Moreover, active / inactive mitochondria ratio decreased by 20 % but this drop was not significant indicating that some mitochondria became inactive but the majority were still active in each cell (figure 4.5B). Following 2 mM MPTP treatment, individual dots looked bigger, indicating mitochondrial swelling in most of the cells (figure 4.5A g to i). The active / inactive mitochondria ratio was significantly decreased by 40 % indicating a depolarisation of mitochondria at this concentration compared to controls (figure 4.5B).

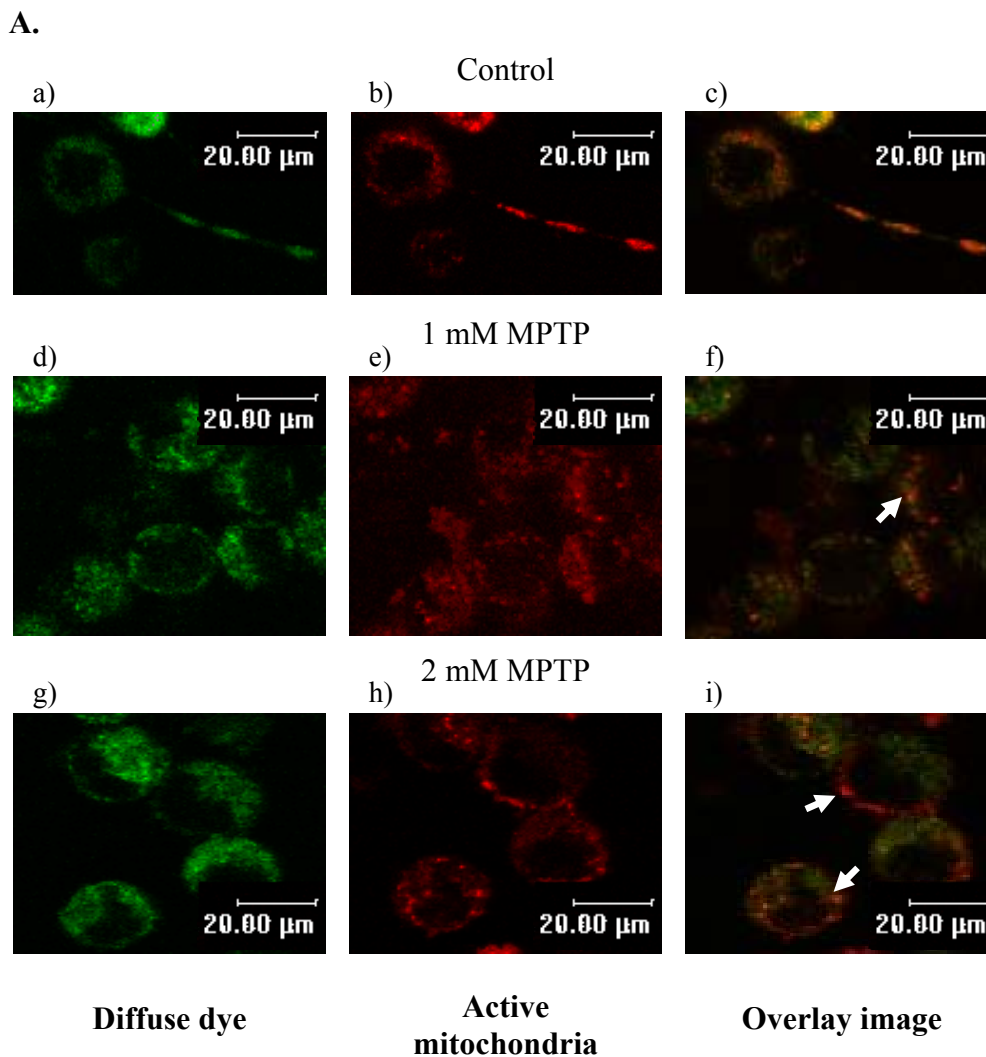


**Figure 4.4: Effects of different concentrations of MPTP on ATP levels in differentiated N2a cells following 24 hour and 48 hour treatments**

Cells were differentiated in serum free medium containing 0.3 mM dbcAMP for 16 hours. Different MPTP concentrations (0 to 2 mM) were then added to the medium for 24 hours (black) and 48 hours (striated) and cellular ATP levels were measured using the vialight bioluminescent assay.

Results are expressed as mean % ATP level  $\pm$  SEM. Statistical analysis was carried out using the paired t-test with a two-tail distribution. All \* values  $p < 0.05$  when compared to respective controls. ( $n \geq 6$  for 24 hours,  $n \geq 3$  for 48 hours).

## 24 hour time-point

**B.**

	control	1000 μM	2000 μM
Ratio of active / inactive mitochondria	1.00 ± 0.12	0.80 ± 0.18	0.60 ± 0.16 *

**Figure 4.5: Effects of different concentrations of MPTP on mitochondrial membrane potential in mouse N2a neuroblastoma cells following 24 hours treatment**

Cells were differentiated in serum free medium containing 0.3 mM dbcAMP for 16 hours. Different MPTP concentrations (0 to 2 mM) were then added to the medium for 24 hours and stained with 10 μM JC-1 fluorescent dye (refer to section 2.2.2.4). A. Cells were visualized by confocal laser microscopy (×630 magnification). Scale bars represent 20 μm. White arrows represent swollen mitochondria.

B. Red and green signal intensities were measured using Leica Confocal Software. Results are expressed as mean red / green (active / inactive) ratio ± SEM. Statistical analysis was carried out using the paired t-test with a two-tail distribution. All \* values  $p < 0.05$  when compared to respective controls.

a, d and g show diffused dye from inactive mitochondria; b, e and h show active mitochondria and c, f and I show overlay images.

## 4.2.2 Effects of MPTP on apoptosis markers

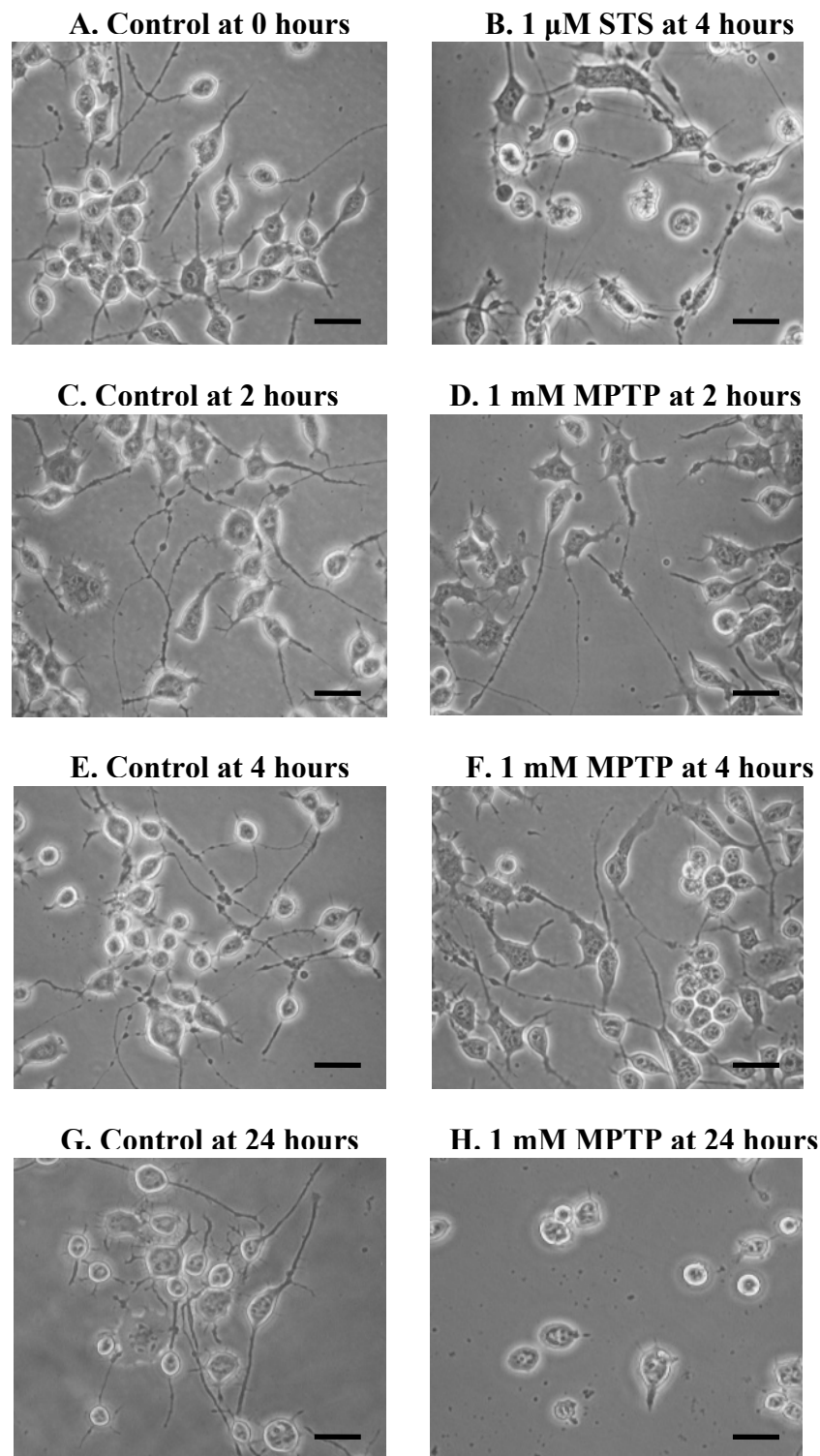
Apoptosis can be detected by assessing a variety of characteristics including typical cell morphology, cleavage of apoptotic markers and release of mitochondrial molecules to the cytoplasm. STS (staurosporine) has been observed to induce apoptosis in many models including mouse N2a neuroblastoma cells (Bronisz *et al.*, 2002). For the purpose of the present study, 1  $\mu$ M STS for 4 hours was used as a positive control of apoptosis.

### 4.2.2.1 Apoptotic morphology

Following pre-differentiation, cells treated with 1  $\mu$ M STS for 4 hours presented a mixture of morphological changes. Most of the cells exhibited swollen elongated cell bodies with longer axon-like processes compared to controls. The axon-like processes formed a connecting network between the cells. Accompanying these elongated shaped cells, some small detached cells with intact membranes were present in the medium indicating a minority of the cells had entered into late apoptosis (figure 4.6B).

Cells treated with 1 mM MPTP for 2 hours also showed elongated swollen cell bodies compared to controls (figure 4.6C and D).

Mouse N2a neuroblastomas treated with 1 mM MPTP for 4 and 8 hours resembled control cells (figure 4.6E and F; 8 hour data not shown). Following 24 hours exposure to 1 mM MPTP treatment, the cells had round intact cell bodies but short or virtually no axon-like processes (figure 4.6G and H).

**Treatments and time-points**

**Figure 4.6: Time-course of morphological changes of N2a neuroblastoma cells due to 1 mM MPTP treatment as compared to staurosporine, inducer of apoptosis.**

Cells were differentiated with 0.3 mM dbcAMP for 16 hours prior to treatment with either MPTP or STS. Pictures were taken over a time course of 24 hours: A. Control at time zero; B. 1  $\mu$ M STS for 4 hours; C. Control at 2 hours; D. 1mM MPTP at 2 hours E. Control at 4 hours; F. 1mM MPTP at 4 hours; G. Control at 24 hours; H. 1mM MPTP at 24 hours. Scale bars represent 20  $\mu$ m.

#### 4.2.2.2 Procaspase-2 cleavage

To further investigate whether apoptosis, and more particularly mitochondrial-dependent-apoptosis, was involved in MPTP-induced toxicity, caspase-2 cleavage was measured using a western blotting approach (refer to section 2.2.6 for protocol).

The anti-caspase-2 antibody recognised two different bands in the samples (figure 4.7A). The 48 kDa band represents the inactivated procaspase-2 whilst the 32 kDa band represents the active cleaved caspase-2. In controls, inactive caspase-2 predominated, although a basal level of caspase-2 was cleaved (active form). Following STS-induced apoptosis, caspase-2 was mainly cleaved showing a high activation of caspase-2. Following treatment with 1 mM MPTP, the procaspase-2 isoform was predominant at all the time-points studied, similar to controls (figure 4.7A). This showed that no significant activation of caspase-2 was occurring during a time-course using 1 mM MPTP treatment.

#### 4.2.2.3 Cytochrome c release

Cytochrome c is normally present in the mitochondrial fraction. Upon an apoptotic stimulus, e.g. which can be initiated by cleavage of caspase-2 in some models, cytochrome c is released into the cytoplasm (Garrido *et al.*, 2006). Figure 4.7B shows the levels of cytochrome c in the cytoplasm following different treatments. Compared to controls, cytochrome c release was significantly increased following STS-induced apoptosis. Following 1 mM MPTP treatments cytochrome c release was not significantly increased.

#### 4.2.2.4 Cleaved caspase-3

Caspase-3 is an effector caspase, which, upon a stimulus via other caspases, can be activated by cleavage and subsequently cleaves other targets (Katjta, 2004). The presence of active / cleaved form of caspase-3 was measured using an antibody that recognised only the cleaved caspase-3. Cleavage was only observed at a high level following treatment with STS. No detectable level of cleaved caspase-3 was seen with 1 mM MPTP using the western blot technique (figure 4.7C).

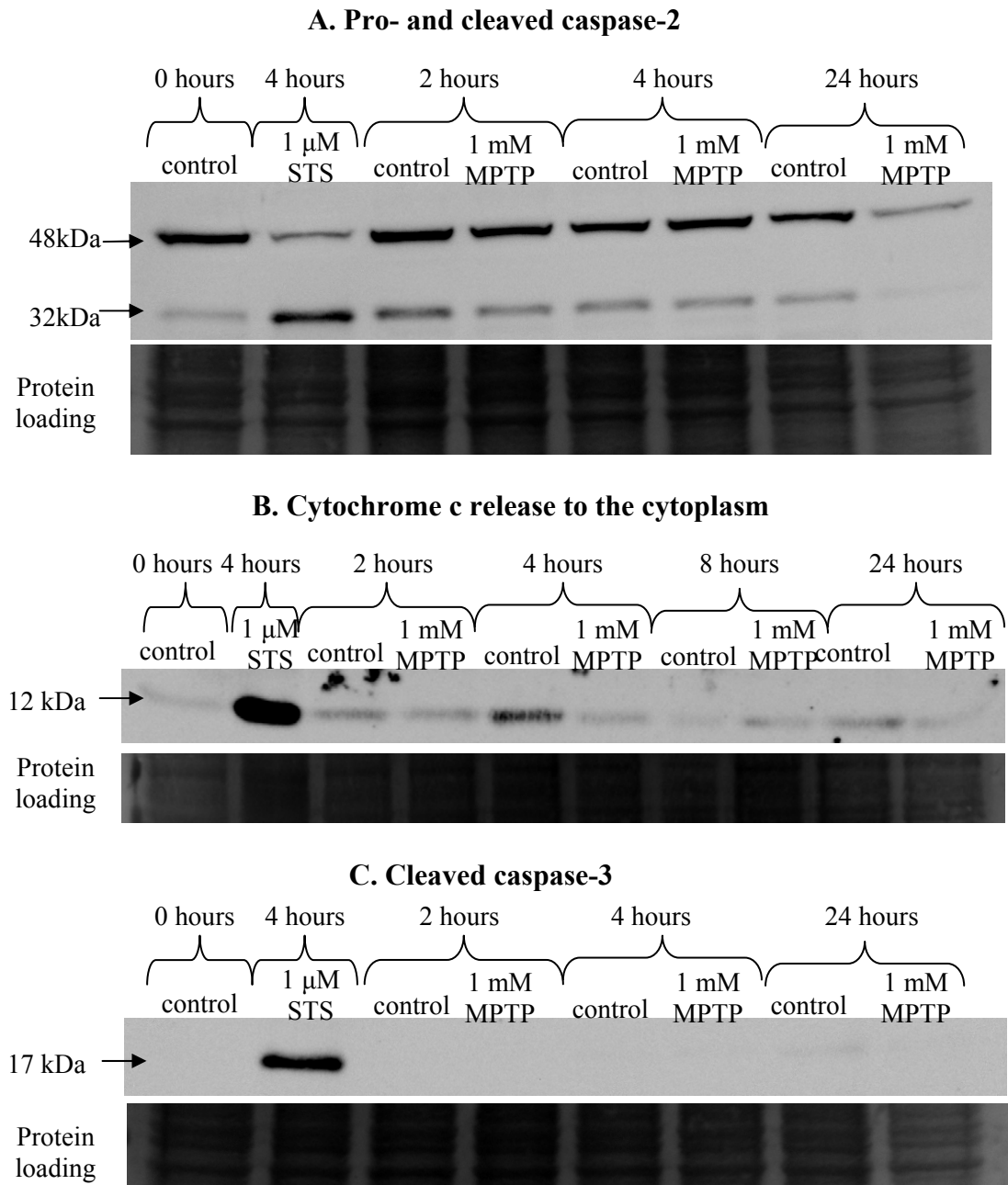


**Figure 4.7: Detection of apoptotic markers in differentiated N2a neuroblastoma cells by western blot analysis**

Differentiated mouse N2a neuroblastoma cells were fractionated using differential centrifugation (refer to methods section 2.2.4). Anti-pro- and cleaved caspase-2 (A), anti-cytochrome c (B) or anti-cleaved caspase-3 antibodies (C) were used to detect the presence of each respective protein in the cytoplasmic fractions; and detection by HRP-conjugated antibody with ECL substrates was carried out as described in section 2.2.6.2.

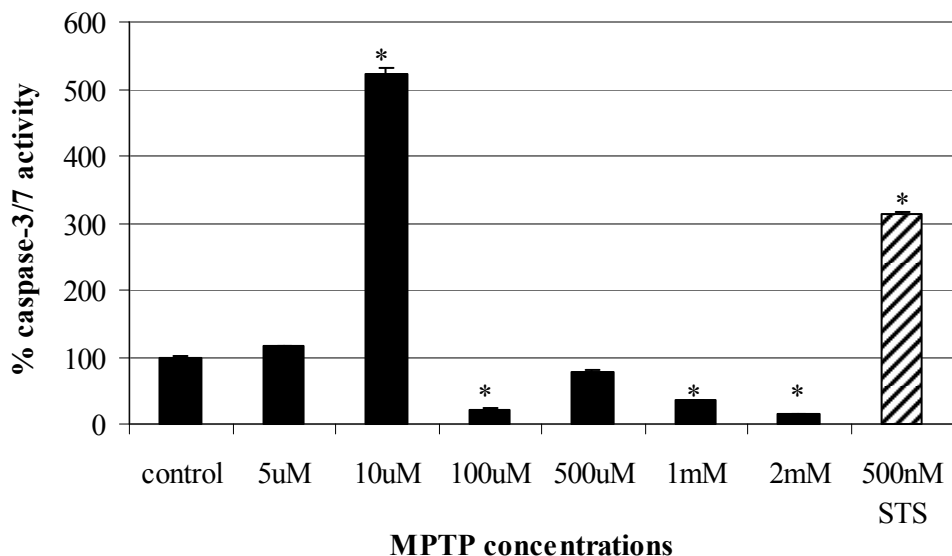
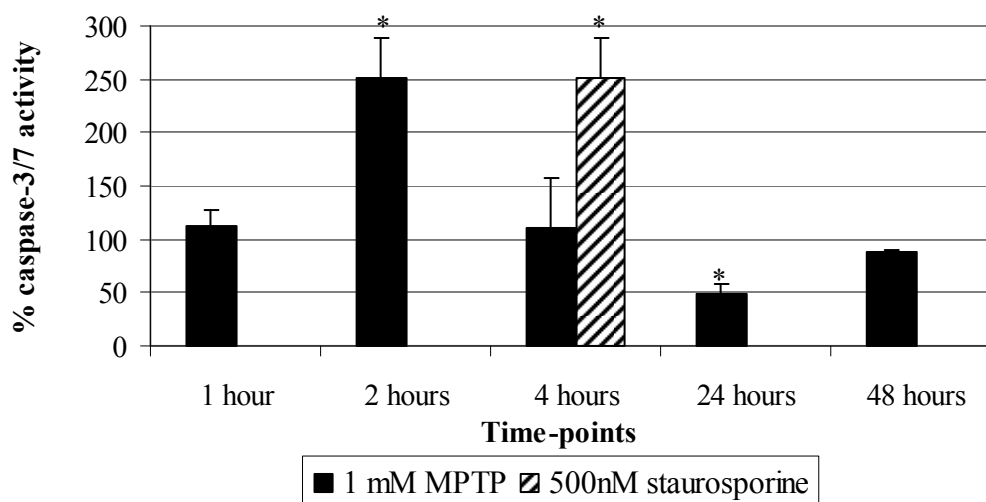
#### 4.2.2.5 Caspase-3/7 activation

Caspase-3/7 activation was also investigated using a fluorimetric assay (see section 2.2.12). This assay relies on the ability of active caspase-3-like proteases to cleave a fluorogenic substrate, DEVD-AMC, whose cleavage releases a fluorophore that can be measured using a fluorimeter (Garcia-Calvo *et al.*, 1998).

Caspase-3/7 activity was significantly increased following STS treatment compared to controls (figure 4.8A and B). This was in accordance with caspase-3 cleavage shown using western blotting in figure 4.7C.

Following treatment with different concentrations of MPTP for 24 hours, only 10  $\mu$ M MPTP showed a significant increase in caspase-3/7 activity, whilst higher MPTP concentrations had no activating effect (figure 4.8A). The use of 1 mM MPTP treatment over a 48 hour time-course, resulted in a transient increase of caspase-3/7 activity at 2 hours, not detected by cleaved capsase-3 western blot analysis (figure 4.7C).

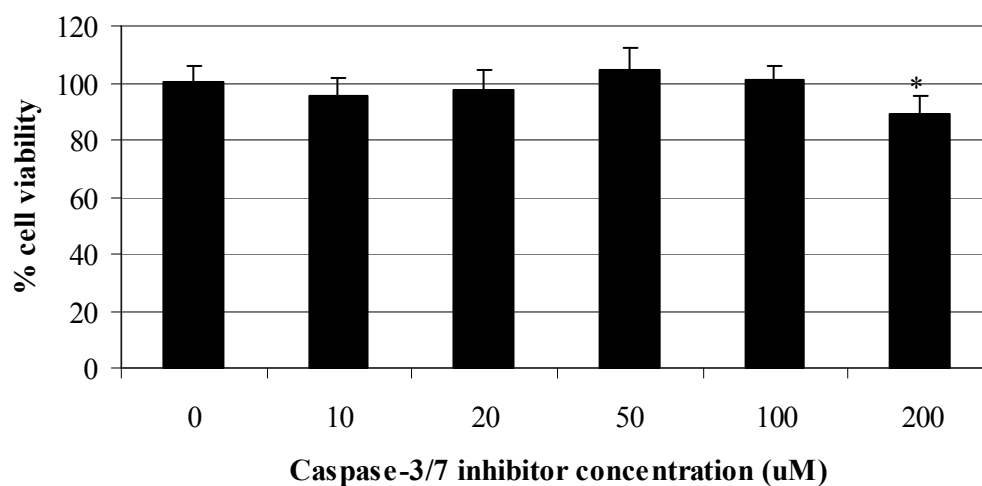
To further validate these increases in caspase-3/7 activity shown using the fluorimetric assay, a caspase inhibitor specific to caspase-3 and caspase-7 was used, DEVD-CHO. Figure 4.9 shows the *in vivo* effects of the caspase-inhibitor alone on cell viability using an MTT reduction assay. Only a high concentration of the inhibitor, 200  $\mu$ M significantly decreased cell viability. Concentrations lower than 200  $\mu$ M caused no significant cell death in N2a neuroblastoma. Figure 4.10A shows the effects of different concentrations of caspase-3/7 inhibitor (0 to 50  $\mu$ M) on control and STS-induced apoptotic samples. Indeed, even 5  $\mu$ M DEVD-CHO added one hour prior to STS treatment was sufficient to decrease the caspase-3/7 increase induced by STS. Following these results, 5  $\mu$ M DEVD-CHO were used for further analysis. Treatment with 1 mM MPTP for 2 hours, 10  $\mu$ M MPTP for 24 hours and 1  $\mu$ M STS for 4 hours led to increased levels of caspase-3/7 activity (figure 4.10B) similarly to previously seen (figure 8A and B). When 5  $\mu$ M specific caspase 3/7 inhibitor was added 1 hour prior to treatments, these increases in caspase-3/7 activity were completely inhibited in all three different treatments, further validating caspase-3/7 activity increases observed previously (Figure 4.10B).

**A. Effects of different MPTP concentrations on Caspase-3-like activity****B. Time dependent effects of MPTP on caspase-3-like activity**

**Figure 4.8: Effects of different concentrations and time-points of MPTP on caspase-3/7 activity in differentiated N2a cells**

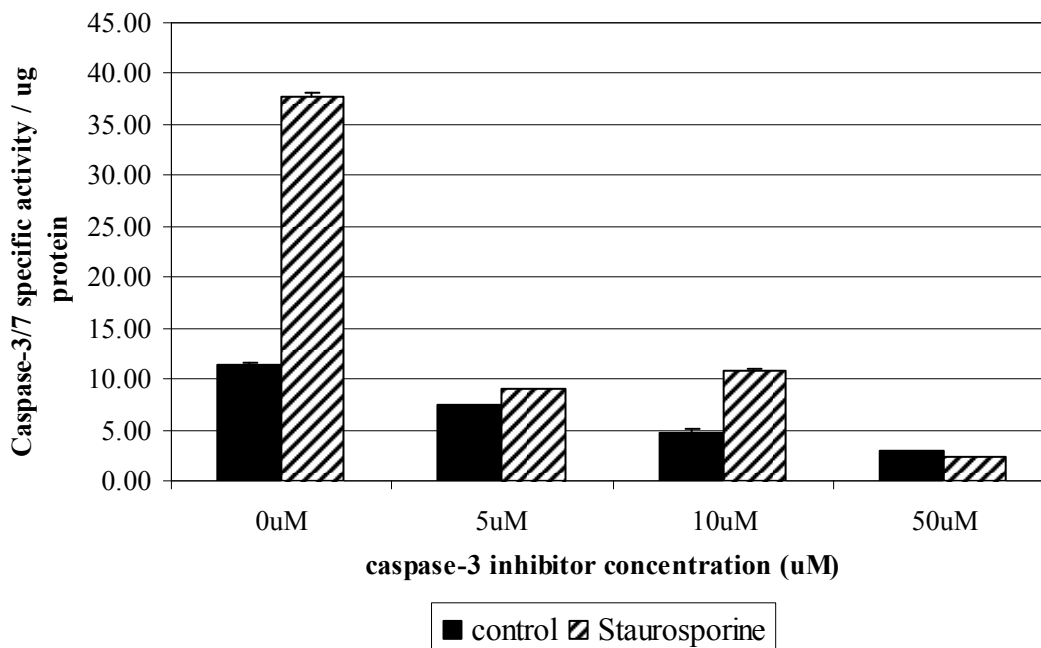
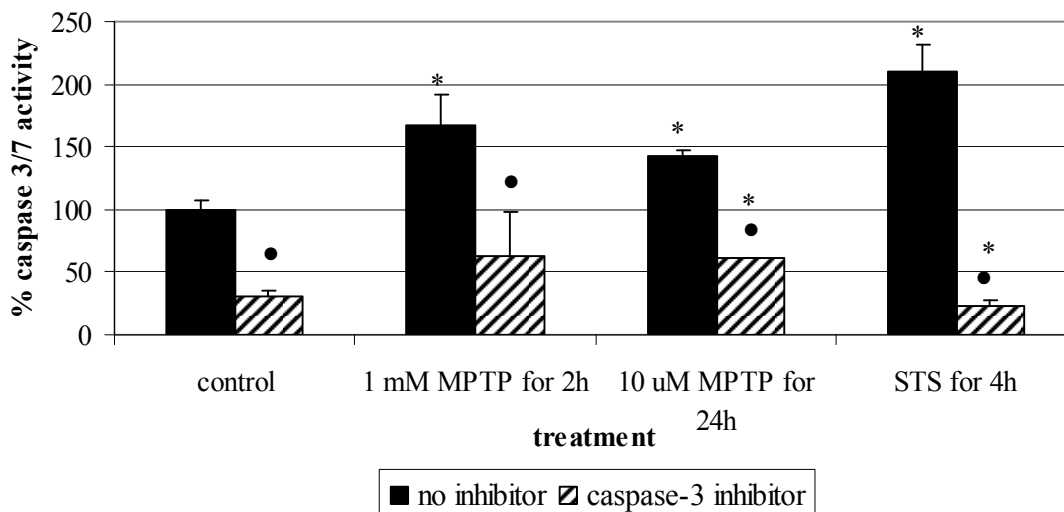
Cells were differentiated in serum free medium containing 0.3 mM dbcAMP for 16 hours. A. Different MPTP concentrations (0 to 2 mM) were then added to the medium for 24 hours (black). B. 1 mM MPTP was then added to the medium and cells extracted at different time-points. 1 mM STS for 4 hours was used as a positive control (stripes) (A and B). Caspase-3/7 activity was measured.

Results are expressed as mean % caspase activity  $\pm$  SEM. Statistical analysis was carried out using the paired t-test with a two-tail distribution. All \* values  $p < 0.05$  when compared to respective controls ( $n \geq 3$ ).



**Figure 4.9: Effects of different concentrations of caspase-3/7 inhibitor on cell viability in differentiated N2a cells following 25 hours exposure**

Cells were differentiated in serum free medium containing 0.3 mM dbcAMP for 16 hours. Different DEVD-CHO concentrations (0 to 200  $\mu$ M) were then added to the medium for 25 hours. The cells were assayed for MTT reduction ( $n = 8$ ) as a measure of cell viability. Results are expressed as mean % reduction  $\pm$  SEM. Statistical analysis was carried out using the paired t-test with a two-tail distribution. All \* values  $p < 0.05$  when compared to respective controls.

**A. Effects of Ac-DEVD-CHO on caspase-3-like activity in mouse N2a cells****B. Effects of Ac-DEVD-CHO on MPTP-induced caspase-3-like activity****Figure 4.10: Inhibition of caspase-3/7 activity due to MPTP neurotoxicity**

A. Mitotic cells were treated with different caspase-3/7 inhibitor (DEVD-CHO) concentrations (0 to 50  $\mu$ M) in duplicate one hour prior treating with or without 1  $\mu$ M STS for 4 hours ( $n = 2$ ).

B. Cells were differentiated in serum free medium containing 0.3 mM dbcAMP for 16 hours. 5  $\mu$ M caspase-3/7 inhibitor (DEVD-CHO) were added to the medium for 1 hour. MPTP (10  $\mu$ M for 24 hours and 1 mM for 2 hours) or STS (1  $\mu$ M for 4 hours) treatments were then added to the medium. Cells were then extracted and caspase-3/7 activity was measured (A and B).

Results are expressed as mean % caspase activity  $\pm$  SEM. Statistical analysis was carried out using the paired t-test with a two-tail distribution. All \* values  $p < 0.05$  when compared to respective controls. All • values  $p < 0.05$  when compared to respective treatment with no inhibitor ( $n \geq 3$ ).

### 4.3 DISCUSSION

#### 4.3.1 MPTP effects on cell viability and mitochondrial activity of N2a neuroblastoma

A variety of assays were used in order to establish the effects of different concentrations of MPTP on energy production, mitochondrial activity and cell viability. The results of these assays are summarised in table 4.1.

##### 4.3.1.1 Establishment of MPTP sub-cytotoxic concentrations

The trypan blue exclusion and MTT reduction assays measured two different cell characteristics to monitor cell viability. The former was based on cell integrity and the latter on cellular metabolic activity. Both assays showed similar results, suggesting that cell viability was not compromised by treatment for 24 hours with concentrations up to 1 mM MPTP and was significantly decreased following 2 mM MPTP treatment or higher (table 4.1). Cell viability was significantly decreased following 10  $\mu$ M MPTP exposure for 48 hours (table 4.1). Since cell death was observed with low concentrations of MPTP at this later time-point, the 48 hour time-point was not considered suitable for investigating sub-cytotoxic effects in this particular study.

Although cell viability was not affected by up to 1mM MPTP at 24 hours, cell morphological changes were evident with 10  $\mu$ M MPTP, and were increasing with 100  $\mu$ M and 1 mM MPTP treatments. Similar studies were carried out by De Girolamo *et al.* (2000), although they used co-differentiating cells while the present study used differentiated cells. Using a trypan blue assay, they observed that cell viability was not affected by MPTP concentrations up to 10  $\mu$ M following 24 hour treatments. Moreover, axons, defined as cell processes greater than two cell bodies in length, were significantly reduced at these sub-cytotoxic concentrations. In a subsequent study, De Girolamo *et al.* (2001) also measured cell viability using an MTT assay and found, contrary to the present study, a decrease in cell viability with concentrations from 50  $\mu$ M to 400  $\mu$ M MPTP following a 24-hour exposure. Although this was significant, the decrease was only small (10-15 % cell death).

<b>assay</b>	<b>24 hour time-point</b>	<b>48 hour time-point</b>
<b>Morphology</b>	Reduction in axonal processes from 10 $\mu$ M MPTP and cell death from 2 mM MPTP treatment	Change in cell body shape, reduction in axonal processes and cell death observed from 10 $\mu$ M MPTP treatment
<b>MTT reduction and trypan blue exclusion assays</b>	Cell viability reduced following treatment with concentrations greater than 1 mM MPTP	Cell viability reduced with concentrations as low as 10 $\mu$ M MPTP.
<b>ATP</b>	ATP levels reduced by 25 % with MPTP concentrations as low as 10 $\mu$ M, depletion of ATP increased as MPTP concentration increased	ATP levels reduce by 50 % with MPTP concentrations as low as 10 $\mu$ M. ATP levels depleted by 80 % following 2 mM treatment
<b>JC-1 stain</b>	Swollen mitochondria unevenly present in cell bodies starting with 1 mM MPTP and more obvious with 2 mM MPTP compared to controls. Mitochondrial membrane potential decreased with these concentrations.	

**Table 4.1: Summary of the toxicity assays used to assess MPTP effects on differentiated N2a neuroblastoma cells**

These disparities showed that the differentiated N2a neuroblastoma model used in the present study was slightly more resistant to MPTP than in the co-differentiating model used by De Girolamo *et al.* (2001). Indeed, de Araujo and Huber (2007) observed a rearrangement of cytoskeletal proteins in neuronal cells during the differentiation process. These observations may suggest a greater ATP demand during the early differentiation as opposed to the late differentiation process.

#### 4.3.1.2 Effects of MPTP on mitochondrial activity

ATP levels were also affected by sub-cytotoxic concentrations of MPTP, being reduced by 25 % and 50 % with 10  $\mu$ M and 1 mM MPTP, respectively, at 24 hours. Depletion of ATP by more than 50 % was needed to decrease cell viability, observed with 2 and 5 mM MPTP for 24 hours. This suggested that a reduction in ATP levels alone was not sufficient to lead to cell death unless it was reduced by more than 50 %. Consistent with this observation, following 48 hours MPTP treatment, 10  $\mu$ M MPTP was sufficient to reduce ATP levels to below 50 % and lead to cell death.

It has been well established that MPTP, via its metabolite MPP<sup>+</sup>, inhibits complex I of the ETC (Ramsay *et al.*, 1987; refer section 1.4 for a more detailed description). Singer and colleagues (1988) have shown that treatment with MPP<sup>+</sup> leads to ATP depletion in nigrostriatal neurons. Wu and colleagues (1990) found consistent results in hepatocytes showing that ATP levels were depleted only with MPP<sup>+</sup> and not MPTP when MAO inhibitors were used, signifying a main role for MPP<sup>+</sup> and its ability to inhibit complex I in ATP depletion. Moreover, it was shown that ATP depletion was happening prior to cell death and in a MPTP dose-dependent manner in hepatocytes (DiMonte *et al.*, 1986) and in rat brain synaptosomes (Scotcher *et al.*, 1990), consistent with the data retrieved in the present study.

Mitochondrial permeability transition leading to mitochondrial depolarisation has been observed to be regulated by membrane voltage. Calcium overload, increase in ROS, decrease of adenine nucleotides and increase in inorganic phosphates have all been shown to induce mitochondrial transition (Cassarino and Bennett, 1999). A direct consequence of mitochondrial transition is the opening of a transition pore which challenges the integrity of the mitochondrial double membrane.

The mitochondrial membrane potential was measured using the JC-1 dye and showed that mitochondria were depolarised with 2 mM MPTP. Whether depolarisation occurred

in mitochondria with lower concentrations, for example following 1 mM MPTP treatment for 24 hours was not obvious as the active / inactive mitochondria ratio decreased by only 20 % and was not significant compared to controls. A minority of the cells showed swollen mitochondria following 1 mM MPTP treatment while a majority exhibited this phenomenon when exposed to 2 mM MPTP. Mitochondrial swelling has previously been observed in  $MPP^+$  treated cortical neurons (Han *et al.*, 2003b) and can be a typical characteristic of mitochondrial calcium overload, also previously observed in PD study models (Chiueh *et al.*, 1993).

Cytochrome c release and release of other pro-death molecules to the cytoplasm has been observed to be one of the consequences of mitochondrial transition and depolarisation (Norenberg and Rao, 2007). In the present study, cytochrome c release was not obvious compared to controls using sub-cytotoxic concentrations, supporting the observation that mitochondria were not significantly depolarised using 1 mM MPTP treatment.

Cassarino and colleagues (1999) were the first to show that  $MPP^+$ -induced toxicity could occur via the opening of the transition pore using isolated mitochondria consistent with other studies relating a role of ETC inhibitors to mitochondrial transition pore opening (refer to section 1.3.4). More recently, Lee and colleagues (2006) have partially inhibited  $MPP^+$ -induced mitochondrial transition pore opening using cyclosporin A (a known inhibitor of the transition pore) in PC12 cells. In the present study, mitochondrial pore opening was observed in MPTP-induced toxicity in mouse N2a cells following a 24 hour exposure to a high concentration (2 mM) parallel to apparent cell death.

Following these data, it was accepted that treatment with 1 mM MPTP for 24 hours led to morphological changes, ATP depletion, minor non-significant mitochondrial changes but no decrease in cell viability. Consequently, further study of the mitochondrial proteome will be investigated mainly using 1 mM MPTP for 24 hours.

### 4.3.2 Markers of MPTP-induced cell death in mouse N2a neuroblastoma

Molecular pathways involved in neuronal cell death that occur in PD have been widely studied. Markers of necrosis and apoptosis, the main death pathways, have both been observed in PD mimetic models. Before the early 1990s, only necrotic markers, mainly morphologic, had been observed in models. Since then, different apoptotic markers have been observed in MPTP or MPP<sup>+</sup> treated *in vivo* and *in vitro* models (reviewed in Du *et al.*, 1997) including in human PD brains (Hartmann *et al.*, 2000). The question of whether neurodegeneration occurs via necrosis or apoptosis is still open although several studies tend to show that both can happen, depending on the model of study used. For example, He and colleagues (2008) have been using two different models of study in which they induced non apoptotic cell death by acute MPTP treatment in mice and induced apoptosis by sub-acute treatment of mice with MPTP. Chee and colleagues (2005) have observed both apoptotic and necrotic characteristics following treatment of mouse dopaminergic cells using MPP<sup>+</sup>.

In the present project, the MTT reduction assay showed that the overall cellular metabolic activity was maintained until exposure to 2 mM MPTP for 24 hours in mouse N2a neuroblastoma cells. The trypan blue exclusion assay, representing cell membrane integrity, as a measure of necrosis, showed similar results to the MTT assay. Two hypotheses could be drawn from these data: (a) there was no cell death with MPTP treatments with concentrations equal or lower than 1 mM for 24 hours and only necrosis occurred in the present model, (b) a minority of cells died of non-necrotic cell death, which was not detected by the MTT reduction assay due to compensatory metabolic activation of surviving neuronal cells. Since early apoptosis has been observed using sub-acute concentrations of MPTP (Du *et al.*, 1997), it was interesting to check whether apoptotic markers were present using the sub-cytotoxic concentrations previously established.

Western blot analysis showed that there was no significant increase of cleavage of caspase-2 and caspase-3 using different time-points of 1 mM MPTP treatment. Cytochrome c release was not increased using the same treatment. These results showed that there was no evidence of activation of the mitochondrial-dependent apoptotic pathway using sub-cytotoxic concentration of MPTP. These results were consistent with the JC-1 mitochondrial depolarisation assay which showed no significant depolarisation of mitochondria with concentrations of MPTP lower than 1 mM following 24 hour treatment, indicating that no opening of the transition pore occurred. This is in

agreement with a previous study that monitored J-aggregate formation in N2a cells following 10  $\mu\text{M}$   $\text{MPP}^+$  treatment and observed no significant effects (De Girolamo *et al.*, 2001).

Interestingly, using a specific fluorogenic substrate Ac-DEVD-AMC, caspase-3-like activity was transiently evident with either a low concentration MPTP (10  $\mu\text{M}$ ) for 24 hours (chronic exposure) or short acute exposures (2 hours) with 1 mM MPTP. This activity could be inhibited using an inhibitor of caspase-3 activity, Ac-DEVD-CHO demonstrating specificity of the assay for a caspase-3-like activity. Both substrates, Ac-DEVD-AMC, and inhibitor, Ac-DEVD-CHO, have shown specificity for both caspase-3 and caspase-7. Whether other caspases can interact with this substrate and inhibitor has not been described in the literature. Since caspase-3 was not cleaved and detected using the western blot approach, it could be postulated that caspases other than caspase-3 were transiently activated following low concentration MPTP treatment. Apoptotic markers in MPTP treated cell lines have already been documented (Chee *et al.*, 2005; Liu *et al.*, 2008). However no study showed the activation of caspase-3 protease or other apoptotic markers prior to cell death using sub-cytotoxic concentrations. Using cytotoxic concentrations, caspase-3-like activation has been found in PC12 following MPTP treatment (Shimoke *et al.*, 2003). In this particular study, the authors did not check which caspase was activated. Sanz *et al.* (2008) showed that  $\text{MPP}^+$  could induce caspase-2 activity via a p53-induced pathway in SH-SY5Y cells using cytotoxic concentrations. Another study confirmed the involvement of apoptosis in MPTP-induced cell death in rat PC12 cells via increased Bax/Bcl2 ratio mRNA expression (Liu *et al.*, 2008). Contradictory studies have been obtained showing that caspase-3 might not be involved in MPTP-induced apoptosis using different models. Indeed, using a mouse MN9D dopaminergic cell line, Chee and colleagues (2005) showed that caspase-3 and -9 were not activated in  $\text{MPP}^+$ -induced toxicity but caspase-2, -8, -6 and caspase-7 were cleaved in the same model. They also showed the involvement of mitochondria using cytotoxic concentrations since cytochrome c release occurred. In the present study, cytochrome c release following cytotoxic conditions (over 1 mM MPTP for 24 hours) has not been investigated; cytochrome c release could be expected in mouse N2a cells, since opening of the pores occurred at higher MPTP concentrations but this needs to be measured.

Activation of caspase-7 without caspase-3 cleavage has previously been observed in other pathological studies. For example, Lovastatin, an inducer of apoptosis, induced

caspase-7 activation but not caspase-3 in a cell line derived from prostate cancer (Marcelli *et al.*, 1998).

The transient activity of a caspase-3-like protease without caspase-2 cleavage or cytochrome c release to the cytoplasm coincides with the hypothesis that sub-cytotoxic concentrations of MPTP might trigger an extrinsic apoptotic pathway. As inferred by the MTT reduction and trypan blue exclusion assays, whether this activation of caspase-3-like protease was sufficient or not to lead to cell death prior to mitochondrial depolarisation has not been shown in the present study.

Other interesting observations have been made using the differentiated N2a cell model. Indeed, a basal level of cytochrome c release was observed in control cells. It has previously been observed that cytochrome c was released into the cytoplasm during cell differentiation of some types of cells (Garrido *et al.*, 2006). This is likely to be a consequence of serum withdrawal (a known activator of apoptosis; Martin *et al.*, 1988) which is required in the differentiation of cell. However, this is minimalised in this model by the addition of dbcAMP (Prashad and Rosenberg, 1978).

Additionally, following transient activation of caspase-3-like activity, levels of caspase activity were lower than controls. An explanation could be: the endogenous level of pro-caspase was limited and its activation led to depletion of the pro-form leading to a decrease in activity as the substrate levels were down.

Along with the establishment of a model to study mitochondrial proteome using sub-cytotoxic concentrations of MPTP, the data produced in the present chapter, accompanied with already established molecular events from previous studies, has given some new insights in MPTP-induced toxicity in mouse N2a neuroblastoma cells (Figure 4.11).

Interestingly, ATP depletion occurred prior to mitochondrial membrane depolarisation consistent with the study from Wu and colleagues (1990) in hepatocytes, showing that ATP depletion occurred prior to mitochondrial depolarisation and was a cause and not a consequence. The mitochondrial transition has been observed to occur with low adenine nucleotide concentrations (Cassarino and Bennet 1999). This ATP depletion occurred as morphological changes were observed as well as concomitant activation of a caspase-3 and/or caspase-7. It is worth mentioning that MPTP-induced toxicity has been shown to occur accompanied by ROS production and increased calcium levels (Chiueh *et al.*, 1993), although it was not investigated in the present model. However, the

mitochondrial swelling observed does suggest that calcium overload might be happening in these cells.

In addition to ATP depletion, usually accompanied by increased oxidative stress and calcium concentrations, this chapter showed that an early marker of apoptosis was activated following low concentrations of MPTP but did not directly lead to mitochondrial depolarisation or significant cell death. However, higher concentrations of MPTP led to significant cell death with necrotic features linked to mitochondrial potential loss. This two-step death pathway is in accordance with previous studies on MPTP-treated mice by He and co-workers (2008) and studies using rotenone, another complex I inhibitor, in dopaminergic cell cultures (Hartley *et al.*, 1994).

The apoptotic pathway has been observed to be an ATP-dependent process. An exacerbated depletion of ATP could be inhibiting the apoptotic process explaining why caspases were seen to be activated early in the MPTP treatment-course but not at later time-points when ATP levels were depleted by more than 30 % compared to controls. Eguchi *et al.* (1997) showed, using Jurkat and Hela cells, that the cellular ATP concentrations were important for cells to either undergo apoptosis or necrosis. Indeed, they proposed that apoptosis occurred only when enough ATP was present in the cells; following large depletion of ATP, cell underwent necrosis. However, a more recent study proposed that ATP depletion-induced by ETC inhibition did not lead to apoptosis in dopaminergic neurons but the ROS produced via ETC inhibition was the trigger of the cell death pathway (Watabe and Nakaki, 2007) being in disagreement with the former cited study.

To verify the two-step cell death hypothesis (ROS-dependent or not), it would be interesting to further characterise both steps. For example, western blot analysis using an anti-caspase-7 antibody and other caspases could be interesting to uncover which caspase is really activated using low concentrations of MPTP. Moreover, the protein and mRNA levels of Bcl<sub>2</sub>-family proteins could be monitored to assess whether apoptosis is happening or whether the transient caspase activation is part of another pathway.

Finally, cytochrome c release and other markers of cell death should be monitored at higher concentration than 1 mM MPTP for 24 hours to uncover which type of necrotic cell death pathway occurs following treatment with cytotoxic concentrations of MPTP.

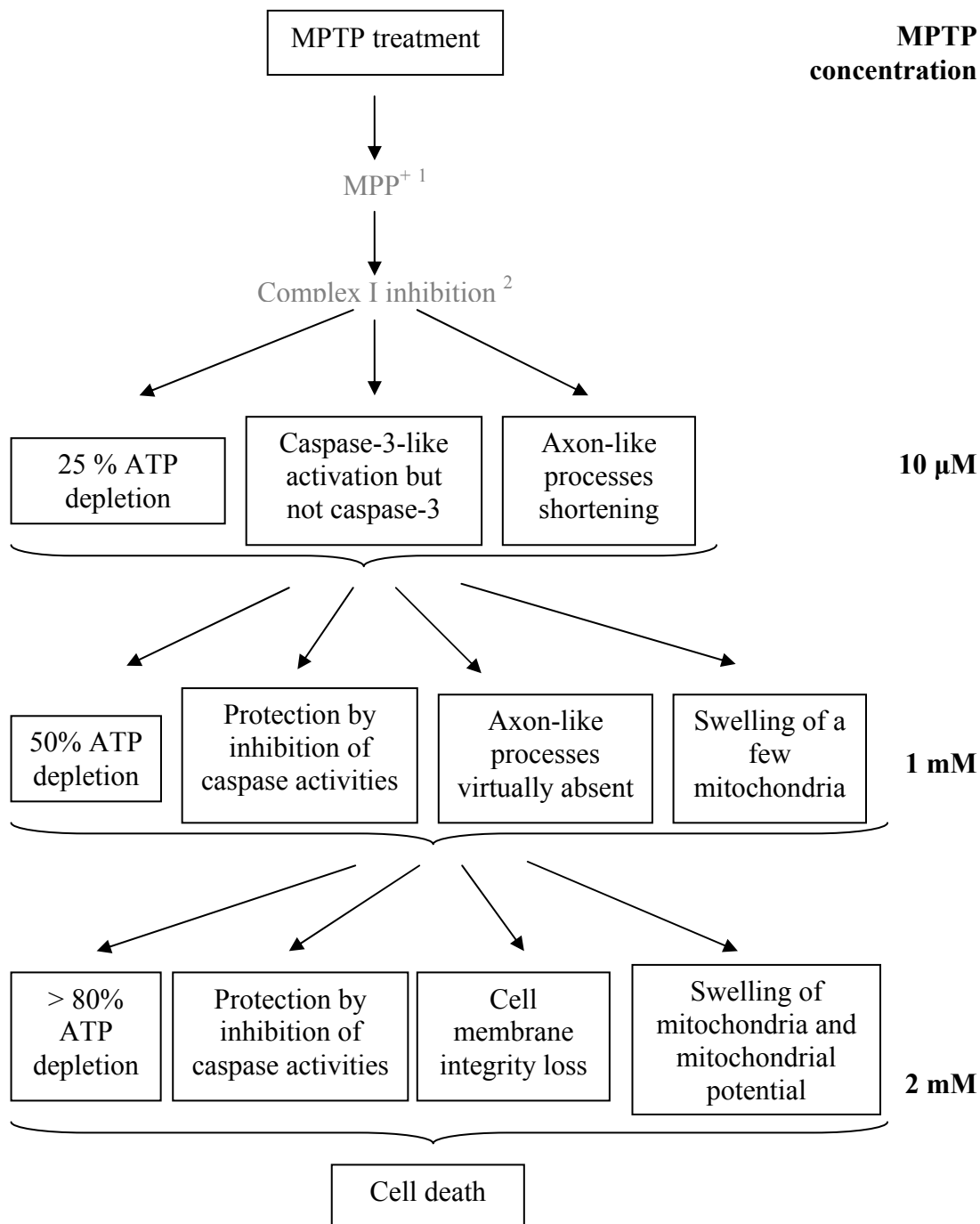


**Figure 4.11: Flow chart representing the molecular events induced by different concentrations of MPTP for 24 hours observed in the present study**

Grey writing: molecular events shown in previous studies

<sup>1</sup> Langston *et al.*, 1983; <sup>2</sup> Ramsay *et al.*, 1987

## **CHAPTER V:**

# **EFFECTS OF MPTP ON THE MITOCHONDRIAL PROTEOME**

## 5.1 INTRODUCTION

### 5.1.1 Proteomic approaches to a study of the mitochondrial proteome

The development of proteomic approaches has precipitated marker discovery research in the last few decades by allowing the study of complex mixtures at once (Anderson and Anderson, 1982). Proteomic approaches of relevance to PD have only emerged in the last half decade. Most of the studies have concentrated on total cell extracts from different models of neurodegeneration, including the use of toxins mimicking PD in cell lines (e.g. Jin *et al.*, 2006; Lee *et al.*, 2003) and in animals (De Iuliis *et al.*, 2005; Zhao *et al.*, 2007), the use of genetically modified animal models (Palacino *et al.*, 2004) and the use of post-mortem neurons from human patients (Basso *et al.*, 2004; Werner *et al.*, 2008). However, despite the evidence of mitochondrial dysfunction in PD (Gandhi and Wood, 2005), only a few studies have focused on the mitochondrial proteome.

As previously described elsewhere (section 3.1.3), it has been proposed that a reduction in complexity, such as fractionation of samples, was essential to increase efficiency of proteomic studies and observation of low-abundant proteins (Lopez and Melov, 2002) and that mitochondria were ideal organelles as the number of proteins they contain is estimated around 1,000, which is the limit of detection of gel-based and chromatography-based proteomic approaches (Taylor *et al.*, 2003b).

### 5.1.2 Molecular markers linking mitochondrial dysfunction and Parkinson's disease

The links between mitochondrial dysfunction and Parkinson's disease are numerous (as described in section 1.1.2). For example, abnormal mitochondrial morphology has been observed in MPTP treated SH-SY5Y cells (Song *et al.*, 1997) showing distorted cristae structure and a swollen appearance. In the present study, mouse N2a neuroblastoma cells also showed swollen mitochondria (refer to chapter IV section 4.2.1.5). Moreover, using a proteomic approach, Jin *et al.* (2005) studied the mitochondrial proteome following MPTP exposure to mice. Using a shotgun strategy followed by LC-MS/MS, they identified more than 300 mitochondrial proteins of which around 100 showed differences in abundance between MPTP treated samples compared to controls. This study showed that many proteins involved in most functions of mitochondria were

altered in MPTP-induced toxicity, consistent with the mitochondrial dysfunction hypothesis.

Additionally, the use of different models of study allowed the observation of other markers of mitochondrial protein dysfunction. For example, the levels of proteins and enzyme activities associated with *oxidative phosphorylation* have been linked to neurodegeneration. Complex I inhibition can lead to PD-like symptoms (Langston *et al.*, 1983). This led to the observation that ATP production was reduced linked with dysregulation of ATP synthase protein levels (Ferrer *et al.*, 2007).

PD has been linked to high mitochondrial *oxidative stress* and low *antioxidant defences* (Fukae *et al.*, 2007). The pathways involved in oxidative stress generation by mitochondria have previously been described in section 1.2.5.

*Chaperone proteins* have also been involved in mitochondrial dysfunction in PD. A particular example is the genetic link between chaperone DJ-1 and neurodegeneration. Loss of DJ-1 function reproduced PD features in human and animal models (Abou-Sleiman *et al.*, 2006). This was linked with increased oxidative stress and re-localisation of the protein to the mitochondria (Zhang *et al.*, 2005). Prohibitin, also thought to have a chaperone activity, has been observed to decrease in substantia nigra of PD patients (Ferrer *et al.*, 2007). Heat shock proteins have been considered to have a protective role in PD (Freyaldehyoven and Ali, 1996).

Another hallmark of PD was the modulation of phosphorylating kinases. In particular, two mitochondrial kinases have been linked with genetic cases of the neurodegeneration. PINK1, a threonine kinase found in the mitochondrial membrane, and leucine-rich-repeat kinase (LRRK)-2 have been found to partially interact with the OMM (Henchcliffe and Beal, 2008). Dysregulation of both kinases has been an important clue that phosphorylation pathways, including mitochondrial signalling pathways could be involved in PD.

### 5.1.3 Signaling pathways in Parkinson's disease

Modulations in kinase activity indicate that the cellular phosphoproteome can be altered. There have been several reports that phosphorylation pathways are involved in PD. A recent study showed that GSK3- $\beta$  was found in Lewy bodies in post-mortem samples of PD patients (Nagao and Hayashi, 2009). Focusing on the effects of MPTP on phosphorylation kinases, mitogen-activated protein kinases (MAPKs), have been

strongly linked to neurodegeneration. For examples, MPTP or its metabolite MPP<sup>+</sup> activated JNK in B65 cells (Saporito *et al.*, 2000) and mouse N2a neuroblastomas (De Girolamo and Billett, 2006) and p38 in mice (Karunakaran *et al.*, 2008). Moreover, inhibition of GSK3- $\beta$  was observed to be protective against MPTP in dopaminergic neurons (Wang *et al.*, 2007).

#### **5.1.4 Study of the mitochondrial phosphoproteome**

Although protein phosphorylation in mitochondria was observed a long time ago (Burnett and Kennedy, 1954), the significance of phospho-signaling in the organelle has been more widely studied in the past decade (reviewed in Horbinski and Chu, 2005). Over 60 mitochondrial proteins have been identified to be phosphorylated and 25 kinases and 8 phosphatases have been located in mitochondria (listed in Pagliarini and Dixon, 2008). Signalling kinases and phosphatases found in mitochondria include tyrosine kinases, serine / threonine kinases and protein tyrosine phosphatases. A few signaling molecules are specific to mitochondria, for example, the pyruvate dehydrogenase complex, PINK1, a dual-specific protein tyrosine phosphatase (called PTMT1) and the translocase of the inner mitochondrial membrane 50 (TIM50) (reviewed in Pagliarini and Dixon, 2008). Nevertheless, most of the signaling kinases and phosphatases have been found ubiquitously in the cell with specific function depending on subcellular localisation (Horbinski and Chu, 2005). These include PKA, found in the IMM and thought to promote complex I activity and cell survival; Akt, generally linked to cell survival and found in mitochondrial membranes mostly and also in the matrix, has a role in the phosphorylation of ATP synthase- $\beta$  subunit; GSK3- $\beta$ , also found in mitochondria with a pro-apoptotic role; protein kinase C (pKC) found in the IMM and cristae and thought to have a pro-apoptotic role and to inhibit mitochondrial function; and a variety of MAPKs including the MAPK kinase 1 (MEK1), the extracellular-signal regulated protein kinase (ERK) 1/2, p38 and JNK (reviewed in Horbinski and Chu, 2005). Although most of the phosphorylated proteins observed in the mitochondria are phosphorylated via serine / threonine residues, tyrosine phosphorylation has also been observed in mitochondria and has been increased with oxidative stress stimuli (reviewed in Salvi *et al.*, 2005).

### 5.1.5 Approaches to the study of the phosphoproteome

Although over 50 % of proteins can undergo phosphorylation, accounting for up to 100,000 phosphorylation sites in mammalian cells, phosphoproteins normally account for 1-2 % of total proteins (Reviewed in Reinders and Sickmann, 2005). So, despite a growing research interest in phosphorylation, there is a need for highly sensitive and high-throughput methods. Different methods for the study of the phosphoproteome have been developed (reviewed in Delom and Chevet, 2006). Gel-based methods remain the simplest approaches, often combined with different detection methods such as western blotting. The most sensitive approach is the use of  $^{32}\text{P}$  or  $^{33}\text{P}$  radioactive labelling. However, it tends to be replaced with safer and more convenient methods (Reinders and Sickmann, 2005). Dyes specific to phosphoproteins have recently been developed. An example is the fluorescent ProQ Diamond dye (Molecular Probes) which has a sensitivity in the order of nanogram and it has a broad linear spectrum allowing quantitative proteomics. This dye can be used to compare two samples, as experimented by Hoper *et al.* (2006), studying the effects of calcium on mitochondrial matrix phosphoproteome. Other advantages are the fact that it is compatible with other stains (e.g. total protein stains) and also with mass spectrometry (Reinders and Sickmann, 2005). Western blotting approaches are also possible using antibodies specific to phospho-amino acids such as anti-phospho-tyrosine, -threonine and -serine antibodies. However, such approaches depend on the sensitivity of the antibody used and availability of the phosphorylated sites on the protein (Reinders and Sickmann, 2005). Other methods exist, including the enrichment of phosphoproteins or peptides using fractionation techniques. Although these methods are more difficult to optimise than gel-based methods, they can be more sensitive and quantitative (Baumann and Meri, 2004). A disadvantage of these approaches is the need for more starting material, which is restricted when using cell culture models.

### 5.1.6 Aims of the chapter

In order to contribute to uncovering molecular events involved in PD-induced mitochondrial dysfunction, methods for study of the mitochondrial proteome, including the optimisation of 2DE (refer to chapter III) and establishment of sub-cytotoxic concentrations of MPTP on mouse N2a neuroblastoma cells (refer to chapter IV) have been developed.

The main aim of the present study was to investigate the effects of MPTP on the mitochondrial proteome of mouse N2a cells, using 2DE. Attempts were made to identify proteins whose levels were altered using peptide mass fingerprinting, and validation included the use of western blotting.

In addition to the changes in protein levels, post-translational modifications have been implicated in PD, supported by the observation of increased oxidative stress inducing increase in protein, lipid and nucleotide oxidation but also contributing to modulations in kinases and phosphatases (Jenner *et al.*, 1992; Nagao and Hayashi, 2009). As previously reviewed, many kinase activities have been targeted by MPTP toxicity, some of which have been localised in mitochondria (section 5.1.3-4). A further aim was to study the effects of MPTP on the mitochondrial phosphoproteome using different approaches including antibody-based methods and gel-electrophoresis followed by specific staining of phosphoproteins. Modulations in the phosphoproteome would complement the discovery of potential markers of mitochondrial dysfunction and molecular pathways involved in the process.

## 5.2 RESULTS

### 5.2.1 MPTP effects on the mitochondrial proteome from differentiated mouse N2a neuroblastoma cells

The effects of sub-cytotoxic concentrations of MPTP on the mitochondrial proteome were studied using 2DE. Isolated mitochondria were further analysed by separating mitochondrial proteins via their charge and their molecular mass, consecutively. Triplicates of paired samples, one control paired to one treatment (cells treated with 1 mM MPTP for 24 hours), were run in parallel and images were taken (as described in section 2.2.8.5) and analysed using the Samespots software (Progenesis). Each gel image was aligned to one control chosen gel (called reference). The statistical package allowed choosing the best alignment features. Each treatment gel was paired with its corresponding control gel. Spots showing a change in level between control and treatment with a  $p < 0.1$  using a paired student t-test were selected. Such spots are circled in figures 5.1 and 5.2.

#### 5.2.1.1 pI 3-10 analysis

Using pI 3-10 strips for the first dimension of 2DE, a total of 19 spots were observed to vary in levels following treatment with sub-cytotoxic concentrations of MPTP, of which 10 had a  $p < 0.05$ . These 19 spots are highlighted in figure 5.1 and are labelled with a letter for non-identified proteins and with a number for identified proteins according to previous designation used in section 3.2.8 (figure 3.12). Quantitative analysis is shown in table 5.1. The fold changes were quite low varying between 17 % and 115 % (table 5.1). Most of these proteins showed an increase in level following treatment and five showed a decrease.

Out of the 19 proteins, 6 were identified by peptide mass fingerprinting (refer to section 3.2.8 and figures 3.12-13 and table 3.8). The six identified proteins all showed an increase in level (table 5.1). These were ATP synthase F1 complex  $\alpha$ -subunit isoform 1 (spots 9), electron transfer flavoprotein subunit alpha (spot 18), fumarate hydratase (spots 10), malate dehydrogenase (spot 15), glutamate oxaloacetate transaminase 2, (GOT2) (spot 13) and voltage-dependent-anion channel 1 (VDAC1) (spot 19).

Interestingly, most of the proteins changing in levels using pI 3-10 strips were relatively high abundance proteins with basic isoelectric points (pI) (around pI 8.5 to 9.5). It can

be hypothesised that changes in levels of low-abundance proteins were not detected using these broad range pI strips.

Spots B and E were both in the smear of high abundance proteins indicating that they could be isoforms or post-translationally modified proteins of these high abundance proteins. Spot B was in the proximity of a spot previously identified as 60 kDa heat shock protein (spot 6 from figure 3.12) but slightly more basic. Similarly, spot E was at proximity of a spot previously identified as  $\beta$ -actin (spot 11 from figure 3.12).

#### 5.2.1.2 pI 5-8 analysis

In order to observe changes in low-abundance proteins, the use of narrower pI strips was the next step. Moreover, the use of such strips could be useful for observing different isoforms of the same protein (e.g. the observation of isoforms around spots B and E, both between pI 5.7 to 6).

Using a similar approach to section 5.2.1.1, mitochondrial proteins were separated using 2DE using pI 5-8 strips and treatments were compared to controls using the SameSpots software.

Up to 13 spots showed changes in levels (figure 5.2), all but one increasing. The percentage changes were similar to those observed with the broad range pI 3-10 strips, varying from 27 to 74 % change (table 5.2).

Three of the proteins, whose levels were increased were identified as 60 kDa heat shock protein (Hsp60), Stress-induced phosphoprotein 1 (STIP1) and ATP synthase F0 complex subunit- $\delta$  (refer to figure 3.12). Moreover, spot N, an acidic spot in the proximity of the spot previously identified as heat shock cognate 71 kDa protein (Hsc70, spot 1 in figure 3.12-13 and table 3.8) was observed to increase in levels indicating a possible involvement of Hsc70 in MPTP toxicity.

None of the spots observed to change in levels using the pI 3-10 strips were observed using pI 5-8 strips. In the pI 5-8 region, more spots were observed to change; some were of lower abundance than observed using pI 3-10 strips.

The basic form of Hsp60 shown to significantly increase in section 5.2.1.1 did not show significant changes in levels despite being well focused compared to gels resolved using pI 3-10 strips. The spot previously identified as  $\beta$ -actin was not focussing well using pI 5-8 strips, making the quantitative analysis difficult for this protein.

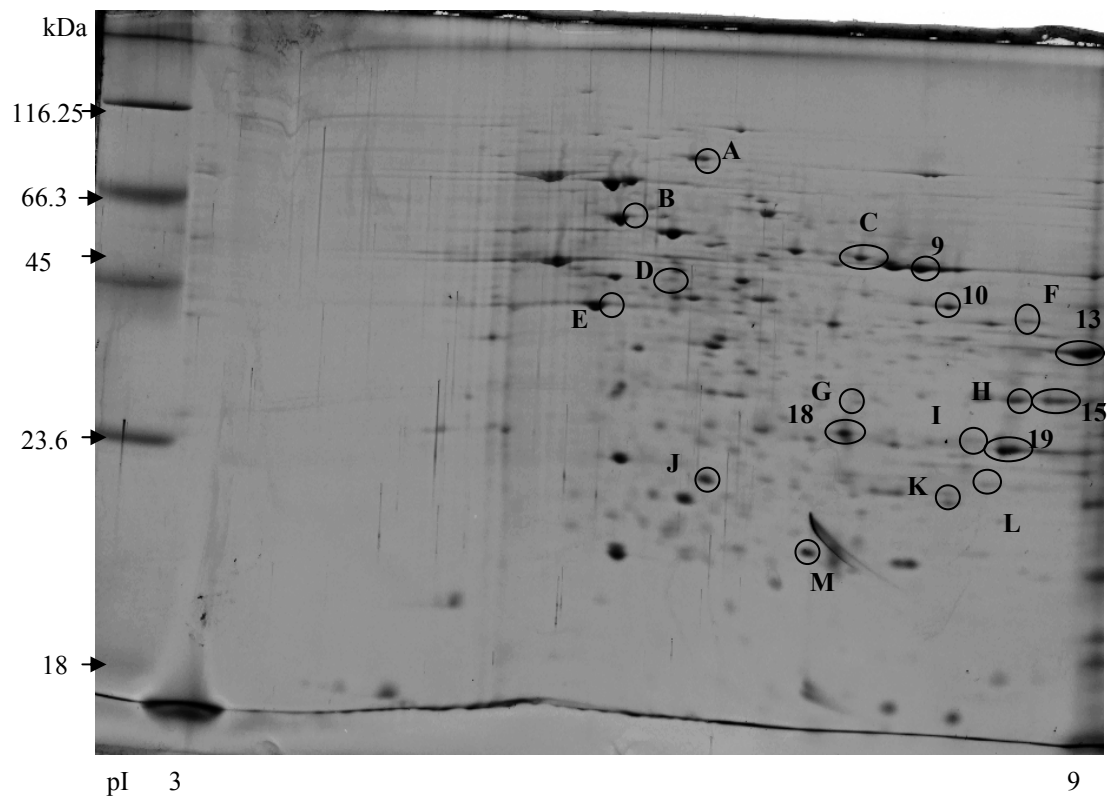


**Figure 5.1: Mini 2D-electrophoretogram (pI 3-10) stained with SyproRuby showing spots changing in levels in MPTP treated differentiated N2a cells**

Mouse N2a neuroblastomas were differentiated for 16 hours in serum free medium supplemented with 0.3 mM dbcAMP. Following incubation, cells were treated with 1 mM MPTP or not (controls) for 24 hours. Subcellular fractionation was then carried out. 50  $\mu$ g proteins from mitochondrial fractions for each treatment were fractionated by 2DE (pI 3-10 strips and 12 % resolving gel) and visualized using SyproRuby. Pictures of gels were compared using SameSpots Progenesis software. Circled spots represent spots that significantly ( $p < 0.1$ ) changed in density level between 1 mM MPTP and control samples following a student paired t-test ( $n = 3$ ). Numerical data are represented in table 5.1.

Letters represent spots showing significant changes between treatments and controls but that have not been identified.

Digits represent spots showing significant changes between treatments and controls that have been identified using MALDI-TOF mass spectrometry (refer to figure 3.12 for example and table 3.8).

Spot symbol <sup>1</sup>	Protein identification <sup>2</sup>	Average normalised volumes in control samples <sup>3</sup>	Average normalised volumes in treated samples <sup>3</sup>	+/- % change compared to controls <sup>4</sup>
A		583.81 ± 66.68	438.42 ± 24.30	- 33 % †
B	In the smear of Hsp60	576.48 ± 87.29	413.31 ± 50.62	- 40 % †
C		1428.41 ± 148.13	1709.37 ± 136.06	+ 20 % †
9	ATP synthase, F1 complex $\alpha$ -subunit isoform 1	5381.89 ± 756.76	4595.48 ± 696.56	- 17 % †
D		212.38 ± 12.98	250.05 ± 11.20	+ 18 % *
E	In the smear of putative $\beta$ -actin	473.30 ± 19.98	713.80 ± 42.51	+ 51 % *
10	Fumarate hydratase	1123.07 ± 70.35	1437.70 ± 128.52	+ 28 % †
F		205.69 ± 39.53	407.11 ± 51.45	+ 98 % *
13	Glutamate oxaloacetate transaminase 2	5559.19 ± 915.92	6899.94 ± 628.47	+ 24 % *
G		442.34 ± 42.46	277.48 ± 33.27	- 59 % *
H		1077.13 ± 248.56	1589.04 ± 178.86	+ 48 % *
15	Malate dehydrogenase	2416.24 ± 210.98	3757.51 ± 70.02	+ 56 % *
18	Electron transfer flavoprotein subunit $\alpha$	802.37 ± 27.45	1193.65 ± 37.60	+ 49 % *
I		509.11 ± 43.11	756.48 ± 72.92	+ 49 % †
19	Voltage-dependent-anion channel 1	3954.00 ± 453.73	5122.56 ± 766.40	+ 30 % †
J		520.65 ± 40.80	336.60 ± 41.10	- 55 % *
K		385.77 ± 76.98	828.86 ± 134.53	+115 % *
L		603.25 ± 82.27	710.00 ± 108.54	+ 18 % †
M		487.09 ± 89.22	606.93 ± 63.36	+25 % †

**Table 5.1: Quantitative analysis of spots showing significant changes in MPTP treated profiles compared to controls (pI 3-10 analysis)**

Normalised density obtained using Samespot software (Progenesis) .

<sup>1</sup> Spot symbols confer to figure 5.1.

<sup>2</sup> Proteins identified by peptide mass fingerprinting. For accession numbers and more details on the Mascot database results refer to table 3.2.

<sup>3</sup> Average of normalised volumes (n = 3) ± Standard error of the mean

<sup>4</sup> Percentage increase = + Average of normalised volumes from MPTP samples / Average of normalised volumes from control samples

<sup>4</sup> Percentage decrease = - Average of normalised volumes from control samples / Average of normalised volumes from MPTP treated samples

\* Statistically significant changes p < 0.05 using a paired t-test

† Statistically significant changes p < 0.1 using a paired t-test

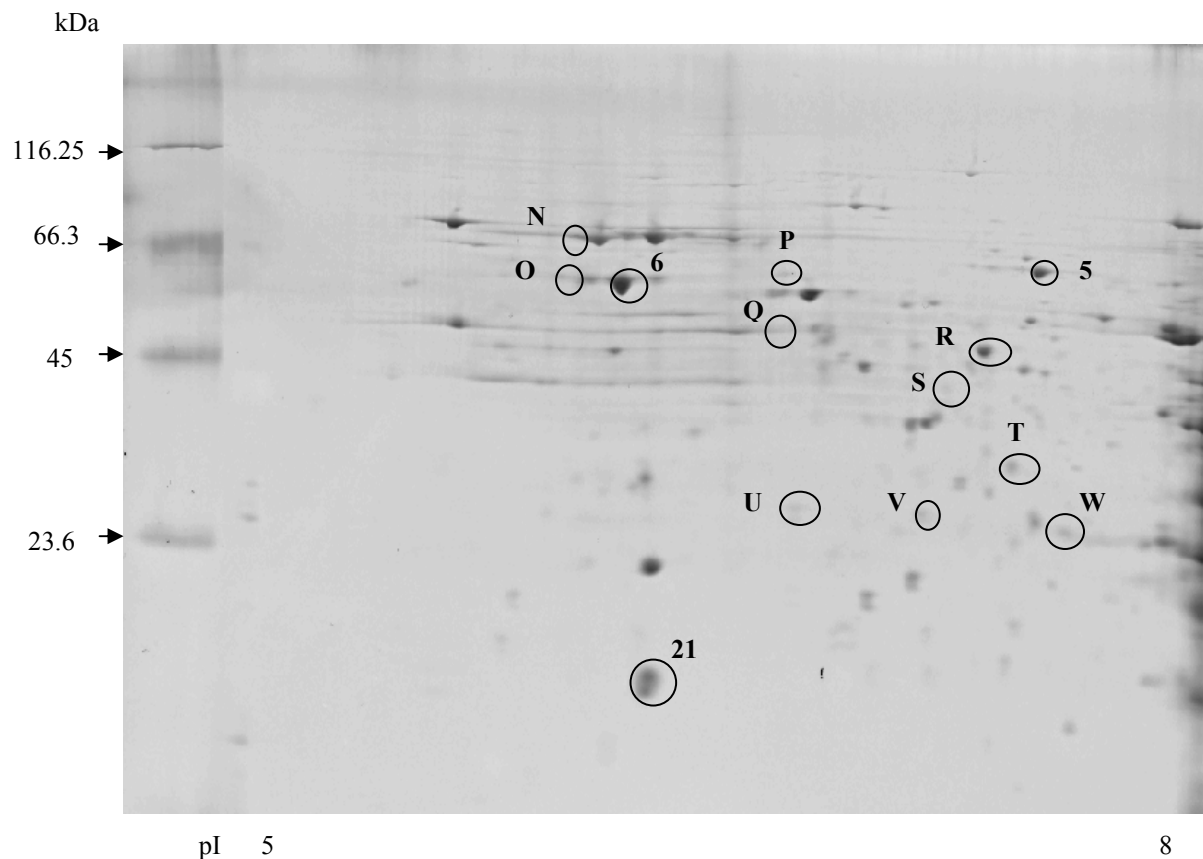


**Figure 5.2: Mini 2D-electrophoretogram (pI 5-8) stained with SyproRuby showing spots changing in levels in MPTP treated differentiated N2a cells**

Mouse N2a neuroblastomas were differentiated for 16 hours in serum free medium supplemented with 0.3 mM dbcAMP. Following incubation, cells were treated with 1 mM MPTP or not (controls) for 24 hours. Subcellular fractionation was then carried out. 50  $\mu$ g proteins from mitochondrial fractions for each treatment were fractionated by 2DE (pI 5-8 strips and 12 % resolving gel) and visualized using SyproRuby. Pictures of gels were compared using Samespots Progenesis software. Circled spots represent spots that significantly ( $p < 0.1$ ) changed in density level between 1 mM MPTP and control samples following a student paired t-test ( $n = 3$ ). Numerical data are represented in table 5.2.

Letters represent spots showing significant changes between treatments and controls but that have not been identified.

Digits represent spots showing significant changes between treatments and controls that have been identified using MALDI-TOF mass spectrometry (refer to figure 3.12 for example and table 3.8).

Spot symbol <sup>1</sup>	Protein identification <sup>2</sup>	Average normalised volumes in control samples <sup>3</sup>	Average normalised volumes in treated samples <sup>3</sup>	+/- % change compared to controls <sup>4</sup>
N	In the smear of Hsc70	453.62 ± 60.89	761.21 ± 90.71	+ 68 % <sup>†</sup>
O		393.98 ± 28.92	510.64 ± 33.67	+ 30 % <sup>†</sup>
5	Stress-induced-phosphoprotein 1	1564.27 ± 385.70	2094.72 ± 375.71	+ 34 % <sup>†</sup>
6	60 kDa Heat shock protein	3040.35 ± 150.44	3863.02 ± 160.79	+ 27 % <sup>†</sup>
P		301.93 ± 44.39	389.34 ± 36.70	+ 29 % <sup>*</sup>
Q		426.15 ± 63.48	555.41 ± 49.78	+ 30 % <sup>*</sup>
R		1121.52 ± 103.41	1648.35 ± 103.75	+ 47 % <sup>†</sup>
S		135.76 ± 9.22	82.26 ± 14.02	- 65 % <sup>*</sup>
T		849.65 ± 142.41	1163.51 ± 137.07	+ 37 % <sup>*</sup>
U		413.47 ± 34.24	572.04 ± 47.89	+ 38 % <sup>*</sup>
V		425.64 ± 58.80	540.28 ± 31.39	+ 27 % <sup>*</sup>
W		788.81 ± 124.67	1374.59 ± 189.30	+ 74 % <sup>*</sup>
21	ATP synthase, F0 complex subunit d	3871.90 ± 447.06	5530.40 ± 613.96	+ 43 % <sup>*</sup>

**Table 5.2: Quantitative analysis of spots showing significant changes in MPTP treated profiles compared to controls (pI 5-8 analysis)**

Normalised density obtained using Samespot software (Progenesis)

<sup>1</sup> Spot symbols confer to figure 5.2.

<sup>2</sup> Proteins identified by peptide mass fingerprinting

<sup>3</sup> Average of normalised volumes (n = 3) ± Standard error of the mean

<sup>4</sup> Percentage increase = + Average of normalised volumes from MPTP samples / Average of normalised volumes from control samples

<sup>4</sup> Percentage decrease = - Average of normalised volumes from control samples / Average of normalised volumes from MPTP treated samples

\* Statistically significant changes p < 0.05 using a paired t-test

† Statistically significant changes p < 0.1 using a paired t-test

## 5.2.1.3 pI 7-10

A similar 2DE approach with pI 7-10 focusing strips was used. Due to a high variability between replicates, no change could be observed using the SameSpots software. Nevertheless, since the alignment between the gel images was poor, changes were probably occurring but could not be detected. A typical gel image using pI 7-10 strips is shown in figure 5.3.

## 5.2.1.4 Validation of markers

A few proteins that showed changes in levels following MPTP treatment and that were identified using peptide mass fingerprinting were further investigated using a western blot approach. The four selected proteins were 60 kDa heat shock protein (Hsp60), heat shock cognate 71 kDa protein (Hsc70), glutamate oxaloacetate transaminase 2 (GOT2) and voltage-dependent anion channel 1 (VDAC1).

- Heat shock proteins

a) Hsp60: 60 kDa heat shock protein

Figure 5.4 shows the western blot probed using an anti-Hsp60 antibody. The levels of Hsp60 were high in the mitochondrial and nuclear fractions (probably due to mitochondrial contamination) and low in the cytoplasmic fraction (figure 5.4A).

An upregulation was observed in all fractions but significant only in the mitochondrial fraction (Figure 5.4B). A small increase was observed in the total extract probably because there was no enrichment of the protein compared to total proteins.

The use of 2-dimensional western blot analysis showed that the anti-Hsp60 antibody recognised at least three distinct forms of Hsp60 (figure 5.4C). The main form is the middle one, showing a net increase in intensity compared to the two other ones following MPTP treatment.

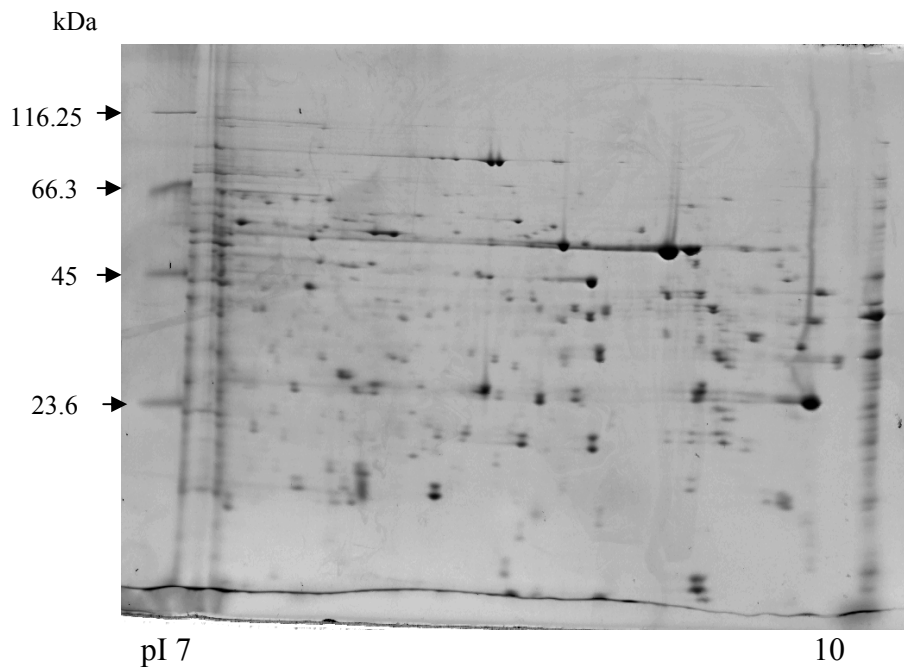
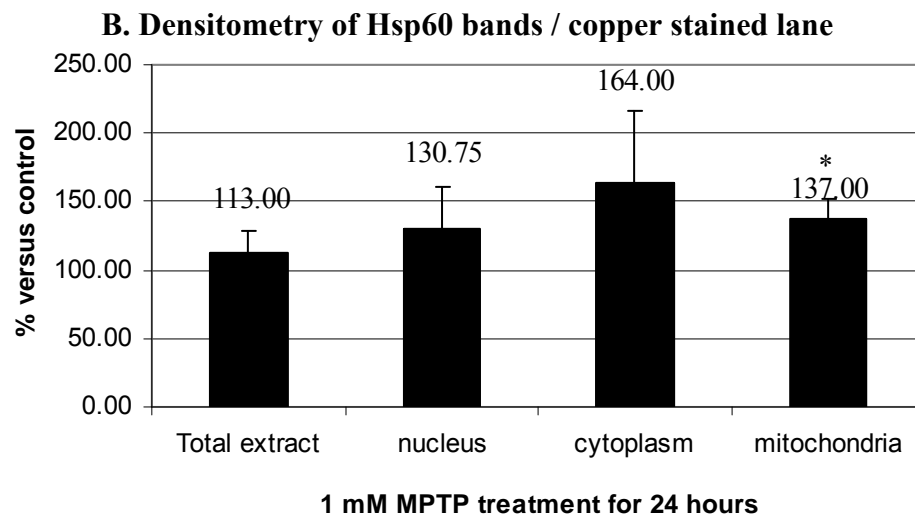
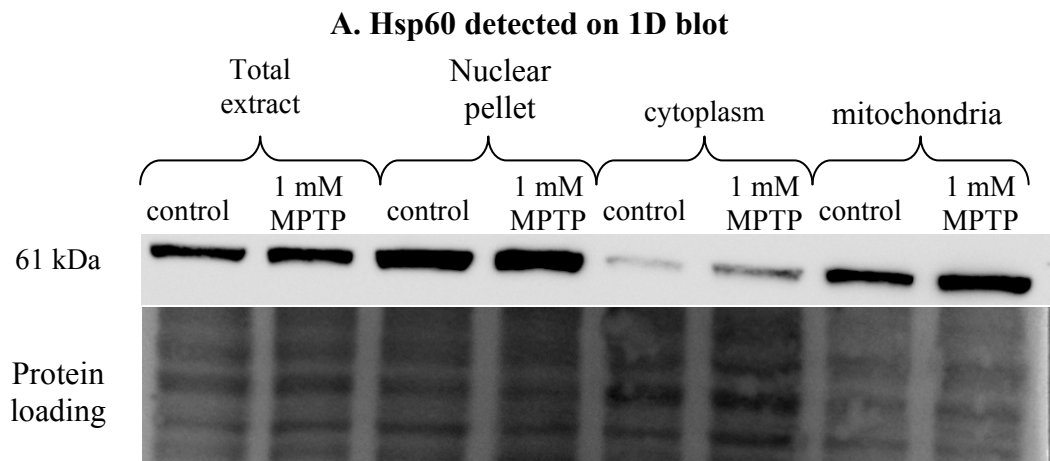


**Figure 5.3: Mini 2D-electrophoretogram (pI 7-10) stained with SyproRuby showing spots changing in levels in MPTP treated differentiated N2a cells**

Mouse N2a neuroblastomas were differentiated for 16 hours in serum free medium supplemented with 0.3 mM dbcAMP. Following incubation, cells were treated with 1 mM MPTP or not (controls) for 24 hours. Subcellular fractionation was then carried out. 50  $\mu$ g proteins from mitochondrial fractions for each treatment were fractionated by 2DE (pI 7-10 strips and 12 % resolving gel) and visualized using SyproRuby. Gel profiles were too variable to observe significant changes. Representative electrophoretogram from a 1 mM MPTP treated sample.



**C. Hsp60 detected on 2D-blots in mitochondrial fractions**

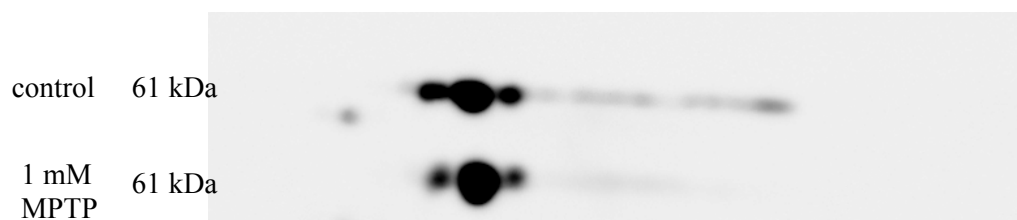


**Figure 5.4: Changes in 60 kDa heat shock protein (Hsp60) levels in various subcellular fractions following 1 mM MPTP treatment for 24 hours**

Mouse N2a neuroblastomas were differentiated for 16 hours in serum free medium supplemented with 0.3 mM dbcAMP. Following incubation, cells were treated with 1 mM MPTP for 24 hours or not (controls). Subcellular fractionation was then carried out.

A. 20  $\mu$ g protein from each fraction for each treatment were fractionated by 1D-SDS-PAGE (12 % resolving gel) and then transferred onto a nitrocellulose membrane. Blots were stained with copper (refer to section 2.2.6.1) to check for protein loading before probing with anti-Hsp60 antibody (1 in 5,000 dilution) followed by the ECL detection procedure (refer to section 2.2.6.2)

B. Densitometry of each band was quantified using Aida software. Each band was compared to total protein. The histogram bars represents % Hsp60 / total protein ratio versus controls.

\*  $p < 0.05$  against control using a paired t-test with a two-tailed distribution ( $n = 4$ ).

C. 2D-blots of 50  $\mu$ g protein from mitochondrial fractions labeled with the same anti-Hsp60 antibody as used in A.

## b) Hsc70: Heat shock cognate 71 kDa protein

Figure 5.5 shows the western blot analysis using anti-Hsc70 antibody. Hsc70 protein was present in all fractions (figure 5.5A). A significant increase in level was observed in the mitochondrial fraction only (Figure 5.5A and B). No change was observed in the total extract, the nuclear fraction and the cytoplasmic fraction.

The use of 2-dimensional western blot analysis showed that the anti-Hsc70 antibody recognised two forms of Hsc70 (figure 5.5C). The acidic form was almost absent in the control and its detection was greatly increased following 1 mM MPTP treatment for 24 hours.

- GOT2: Glutamate oxaloacetate transaminase 2

Figure 5.6 shows the western blot analysis using anti-GOT2 antibody. The levels of GOT2 were high in the mitochondrial and nuclear fractions (probably due to mitochondrial contamination) and low in the cytoplasmic fraction (figure 5.6A). An increase in level was observed in all fractions, as well as in the total extract, but significant only in the mitochondrial and nuclear fractions (Figure 5.6B).

The use of 2-dimensional western blot analysis showed that the anti-GOT2 antibody recognised one spot with increased intensity following 1 mM MPTP treatment for 24 hours but no changes were observed on the shape of the spot (figure 5.6C).

- VDAC1: Voltage-dependent anion channel 1

Figure 5.7 shows the western blot analysis using anti-VDAC1 antibody. The levels of VDAC1 were high in the mitochondrial and nuclear fractions (probably due to mitochondrial contamination) and low in the cytoplasmic fraction (figure 5.7A). An increase in level was observed in cytoplasmic and mitochondrial fractions as well as in the total extract but significant only in the mitochondrial fraction probably due to a high variability in the cytoplasmic fraction (Figure 5.7B). Interestingly, a significant decrease in intensity was observed in the nuclear fraction.

The use of 2-dimensional western blot analysis showed that the anti-VDAC1 antibody recognised up to 7 distinct spots. The two spots observed at the far right end of the blot probably corresponded to non focused VDAC1 protein, leaving up to 5 well focused spots. The overall intensity seemed to be increased following treatment with 1 mM MPTP for 24 hours.

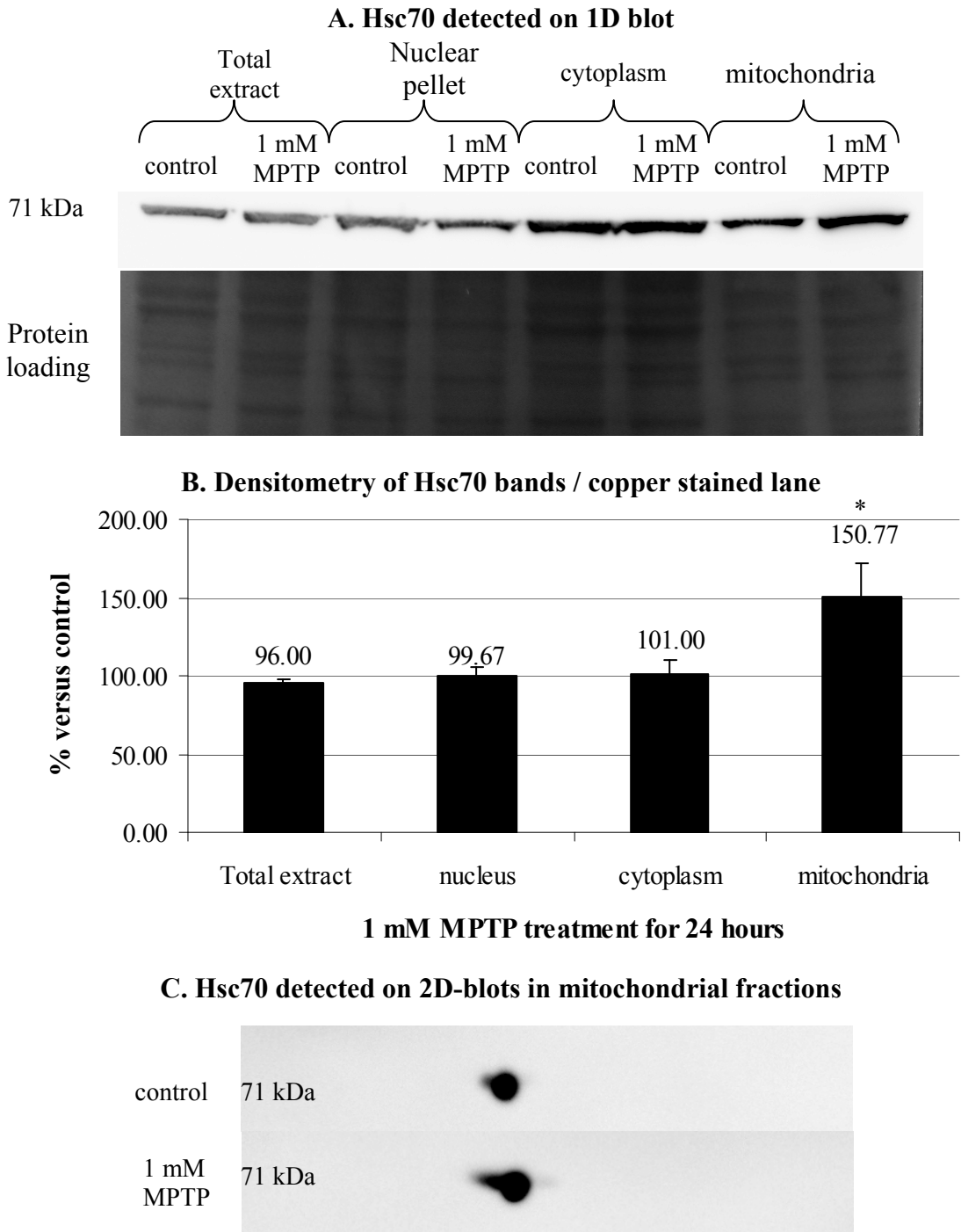


**Figure 5.5: Changes in heat shock cognate 71 kDa protein (Hsc70) in various subcellular fractions following 1 mM MPTP treatment for 24 hours**

Mouse N2a neuroblastoma were differentiated for 16 hours in serum free medium supplemented with 0.3 mM dbcAMP. Following incubation, cells were treated with 1 mM MPTP for 24 hours or not (controls). Subcellular fractionation was then carried out.

A. 20 µg protein from each fraction for each treatment were fractionated by 1D-SDS-PAGE (12 % resolving gel) and then transferred onto a nitrocellulose membrane. Blots were stained with copper (refer to section 2.2.6.1) to check for protein loading before probing with anti-Hsc70 antibody (1 in 10,000 dilution) followed by the ECL detection procedure (refer to section 2.2.6.2) B. Densitometry of each band was quantified using Aida software. Each band was compared to total protein. The histogram bars represents % hsc70 / total protein ratio versus controls. \*  $p < 0.05$  against control using a paired t-test with a two-tailed distribution ( $n = 3$ ).

C. 2D-blot of 50 µg protein from mitochondrial fractions labeled with the same anti-Hsc70 antibody as used in A.

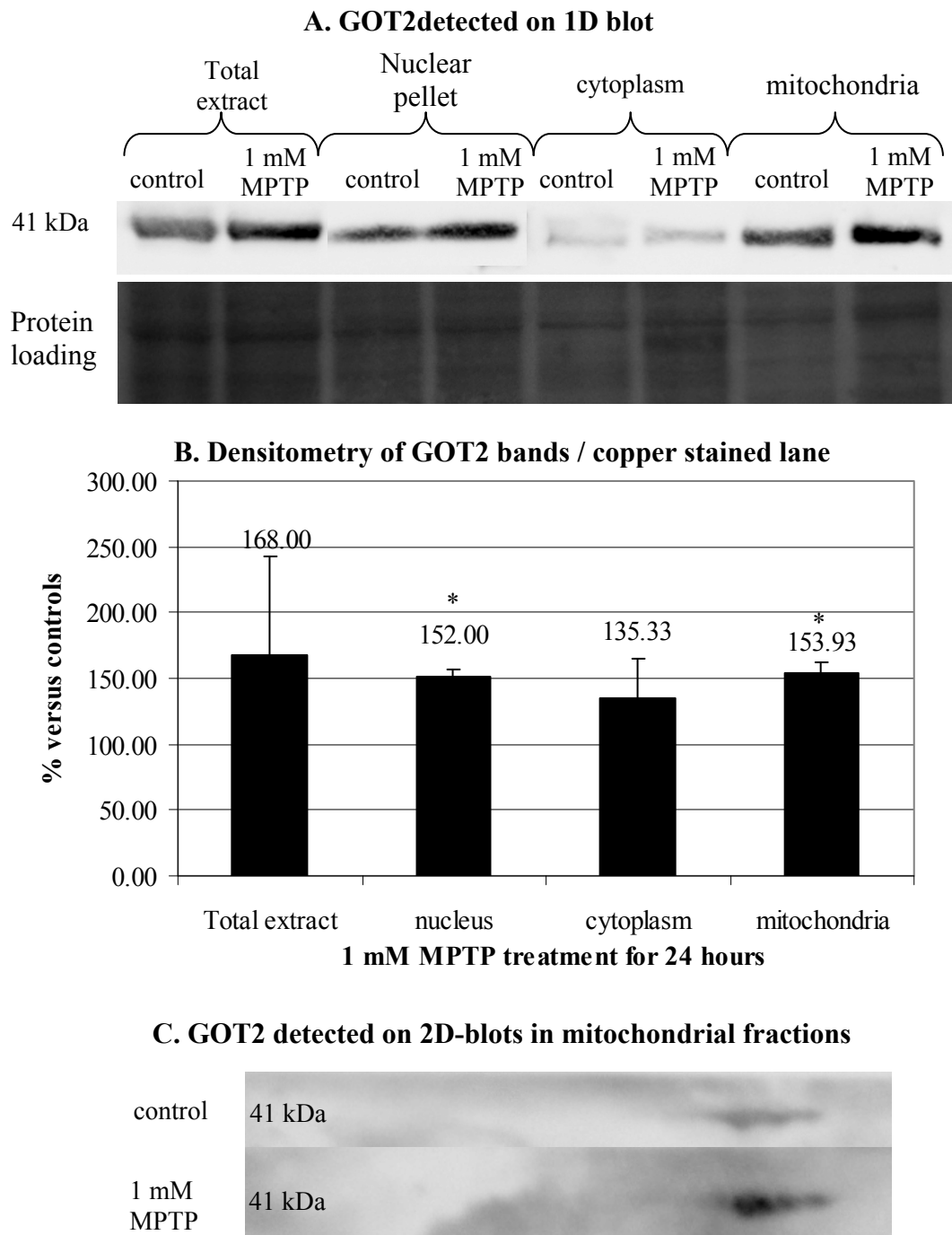


**Figure 5.6: Changes in glutamate oxaloacetate transaminase 2 (GOT2) in various subcellular fractions following 1 mM MPTP treatment for 24 hours**

Mouse N2a neuroblastoma were differentiated for 16 hours in serum free medium supplemented with 0.3 mM dbcAMP. Following incubation, cells were treated with 1 mM MPTP for 24 hours or not (controls). Subcellular fractionation was then carried out.

A. 20 µg protein from each fraction for each treatment were fractionated by 1D-SDS-PAGE (12 % resolving gel) and then transferred onto a nitrocellulose membrane. Blots were stained with copper (refer to section 2.2.6.1) to check for protein loading before probing with anti-GOT2 antibody (1 in 500 dilution) followed by the ECL detection procedure (refer to section 2.2.6.2)

B. Densitometry of each band was quantified using Aida software. Each band was compared to total protein. The histogram bars represents % GOT2 / total protein ratio versus controls.

\*  $p < 0.05$  against control using a paired t-test with a two-tailed distribution ( $n = 7$  for mitochondrial fractions,  $n = 3$  for other fractions ). C. 2D-blot of 50 µg protein from mitochondrial fractions labeled with the same anti-GOT2 antibody as used in A.

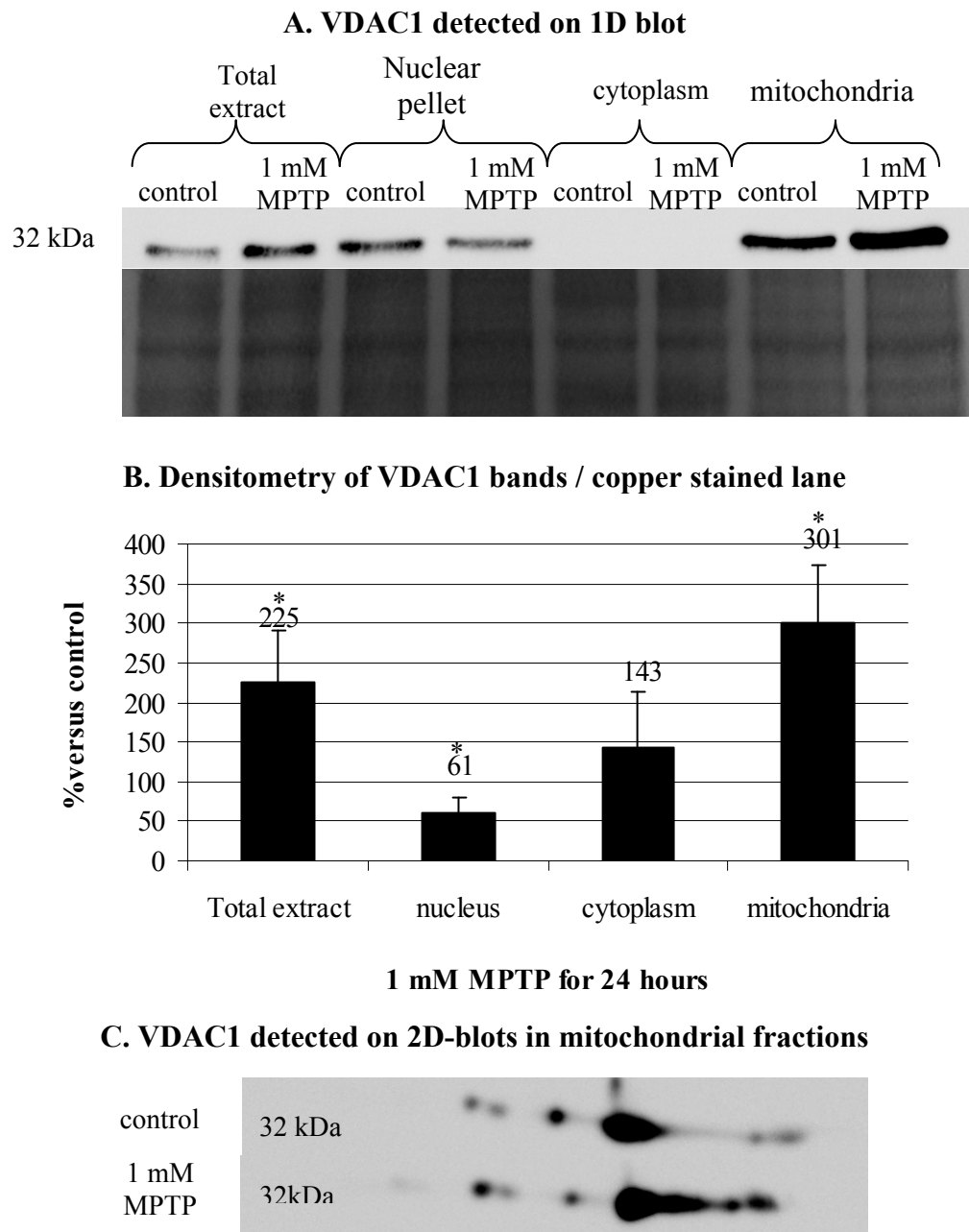


**Figure 5.7: Changes in voltage-dependent anion channel 1 (VDAC1) levels in various subcellular fractions following 1 mM MPTP treatment for 24 hours**

Mouse N2a neuroblastomas were differentiated for 16 hours in serum free medium supplemented with 0.3 mM dbcAMP. Following incubation, cells were treated with 1 mM MPTP for 24 hours or not (controls). Subcellular fractionation was then carried out.

A. 20  $\mu$ g protein from each fraction for each treatment were fractionated by 1D-SDS-PAGE (12 % resolving gel) and then transferred onto a nitrocellulose membrane. Blots were stained with copper (refer to section 2.2.6.1) to check for protein loading before probing with anti-VDAC1 antibody (1 in 1,000 dilution) followed by the ECL detection procedure (refer to section 2.2.6.2)

B. Densitometry of each band was quantified using Aida software. Each band was compared to total protein. The histogram bars represents % VDAC1 / total protein ratio versus controls.

$p < 0.05$  against control using a paired t-test with a two-tailed distribution ( $n = 8$  for mitochondrial fractions,  $n = 5$  for other fractions ). C. 2D-blot of 50  $\mu$ g protein from mitochondrial fractions labeled with the same anti-VDAC1 antibody as used in A.

## 5.2.2 Effects of MPTP on the phosphoproteome

The phosphoproteome can be studied using a range of methods. In the present study, two different approaches were used to investigate whether MPTP had an effect on the phosphorylation state of the cell and, more particularly, of the mitochondrial proteins.

### 5.2.2.1 Study of the phosphoproteome using western blot analysis

The first approach used to investigate the effects of MPTP on the phosphoproteome was a western blot-based analysis using a range of antibodies directed against phosphorylated residues.

#### - Phosphoserine antibody

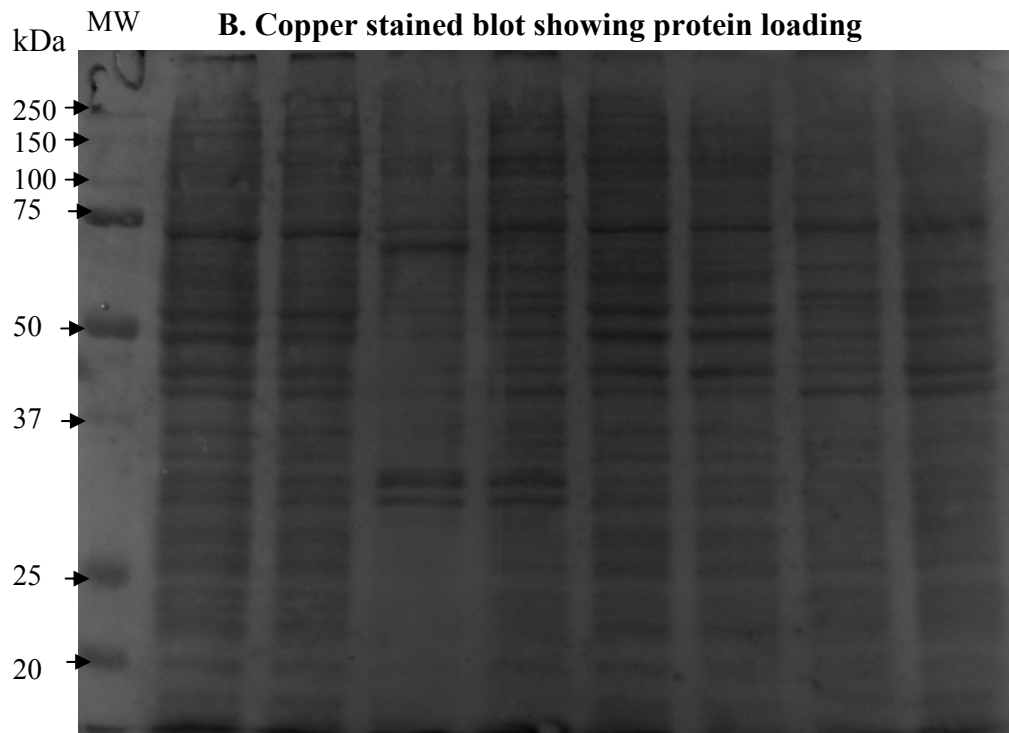
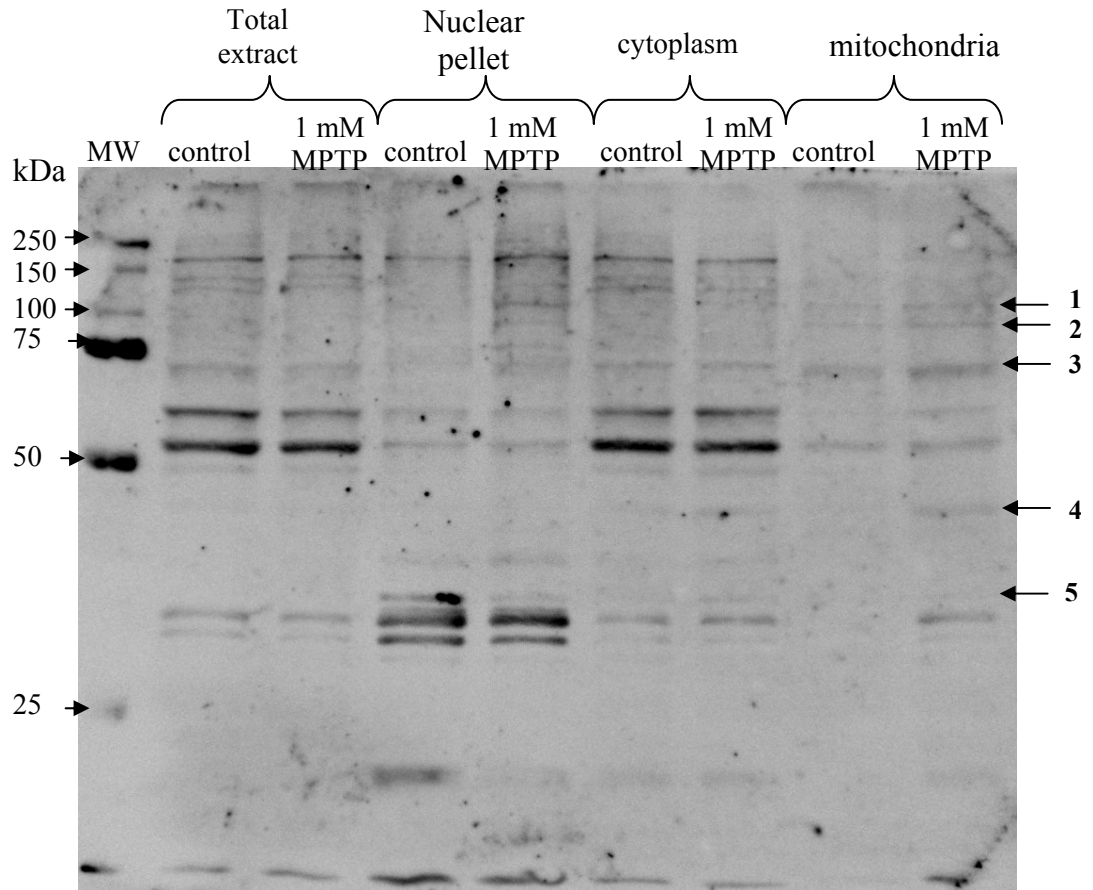
Figure 5.8A shows serine phosphorylation in various subcellular fractions from control and MPTP treated cells. The three fractions showed different profiles to one other: overall, the level of serine phosphorylation was lower in the mitochondrial proteins compared to other fractions. The total extract profile was similar to the profile from the cytoplasmic fraction indicating that most serine phosphorylation involved cytoplasmic proteins.

Changes in serine phosphorylation following treatment with MPTP were present in all subfractions. Nevertheless, only changes observed in the mitochondrial fraction were quantified using Aida Analyser software by measuring the intensity of each band normalised to protein loading represented by copper stain (figure 5.8B) and comparing MPTP treatments with respective controls. As shown by the table in figure 5.8C, 4 bands showed changes in intensity. Serine phosphorylation was increased following treatment with sub-cytotoxic concentrations of MPTP.

Bands 1, 2 and 3 appeared to be specific to mitochondria, whereas band 4 seemed to be also found in the cytoplasm.

Interestingly, the major change in serine phosphorylation following MPTP treatment was observed in the nuclear fraction with a large decrease in serine phosphorylation of band 5 which corresponded to an increase in serine phosphorylation of a protein with the same molecular weight in the cytoplasmic fraction (figure 5.8A). Although changes in phosphorylation were observed following MPTP treatment, no protein identification of these proteins was carried out.

**A. Phosphoserine detection**



### C. Quantitative changes in serine phosphorylation in mitochondrial proteins

Band no.	+/- % change compared to controls
1	+ 77 % <sup>†</sup>
2	+ 66 % <sup>*</sup>
3	+ 90 %
4	+ 107% <sup>*</sup>

**Figure 5.8: Detection of proteins phosphorylated via a serine amino acid in various subcellular fractions in cells treated with 1 mM MPTP for 24 hours compared to controls**

Mouse N2a neuroblastomas were differentiated for 16 hours in serum free medium supplemented with 0.3 mM dbcAMP. Following incubation, cells were treated with 1 mM MPTP for 24 hours or not (controls). Subcellular fractionation was then carried out. 20  $\mu$ g protein from each fraction for each treatment were fractionated by 1D-SDS-PAGE (12 % resolving gel) and then transferred onto a nitrocellulose membrane. Blots were stained with copper (refer to section 2.2.6.1) to check for protein loading (B). This was followed by probing with anti-phosphoserine antibody (1 in 500 dilution) followed by the ECL detection procedure (refer to section 2.2.6.2) (A). Densitometry of each band was quantified using Aida software. Each band was compared to total protein and expressed as % phosphoserine / total protein ratio versus controls (C). <sup>\*</sup>  $p < 0.05$  and <sup>†</sup>  $< 0.1$  against control using a paired t-test with a two-tailed distribution (n =3).

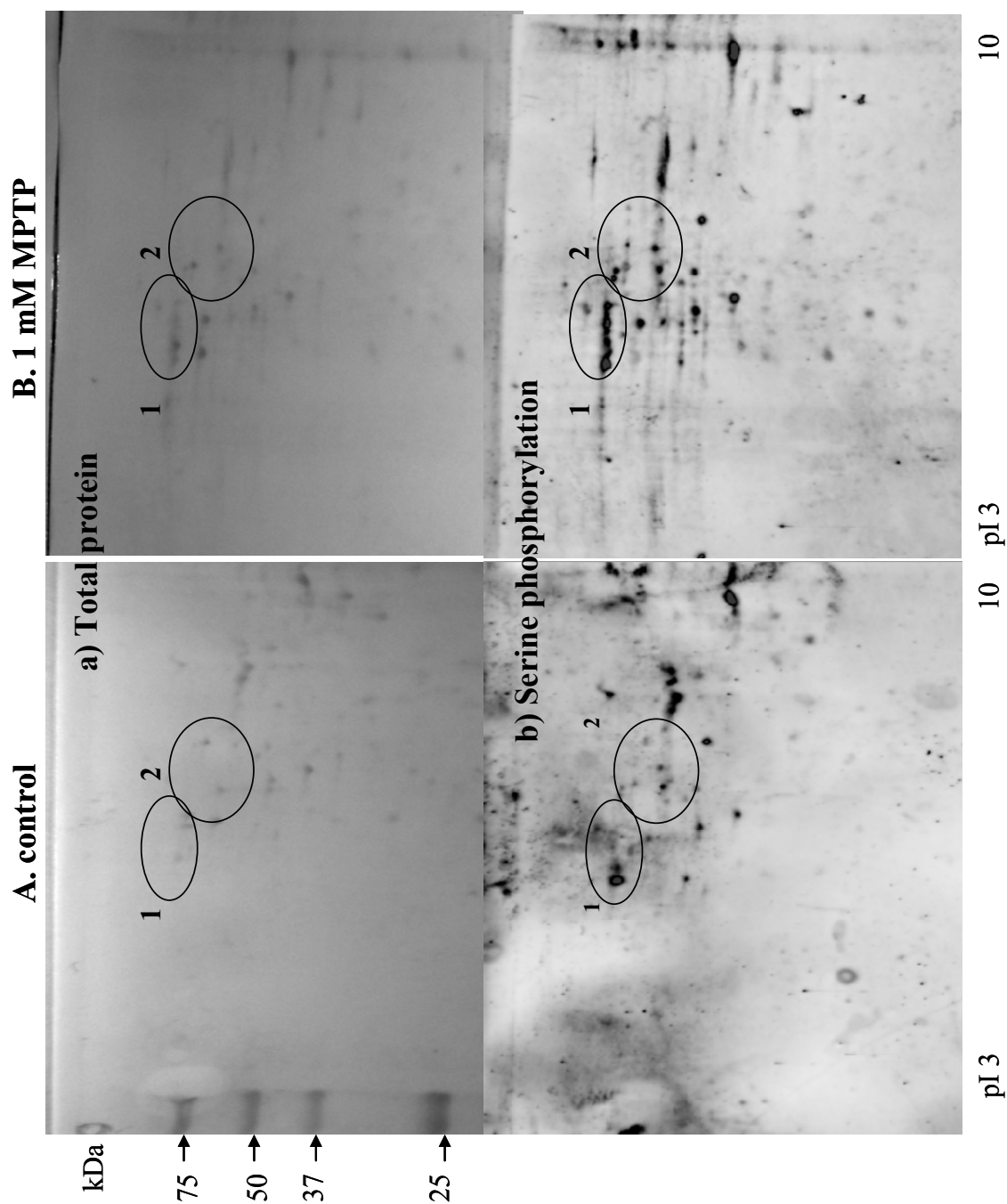
In order to observe more changes in the mitochondrial proteome and assist in the identification of proteins, mitochondrial fractions were electrophoresed using 2DE, transferred onto a nitrocellulose membrane and probed with the same anti-phosphoserine antibody as used for 1D-western blot analysis. The resultant mitochondrial serine phosphoproteomes are shown in figure 5.9. As already mentioned, following the 1-dimensional study, serine phosphorylation was, in general, increased in the mitochondrial fractions following MPTP treatment. More particularly, two main areas showed changes in serine phosphorylation with one around 75 kDa (annotated as circle 1) and one around 50 kDa (circle 2) (Figure 5.9b). Interestingly, circle 1 corresponds to the area where Hsp70 family proteins are focused indicating a potential role of serine phosphorylation in Hsp70 family protein function following MPTP treatment, notably GRP75 protein and Hsc70.

- Phosphothreonine phosphorylation

Figure 5.10A shows the effects of treatment with 1 mM MPTP for 24 hours on threonine phosphorylation in subcellular fractions from mouse N2a cells. The three sub-fractions showed different profiles. Strongly stained bands are observed in all three fractions and all contribute to the profile in the total extract; in this case, the total extract profile does not match the profile of the cytoplasm.

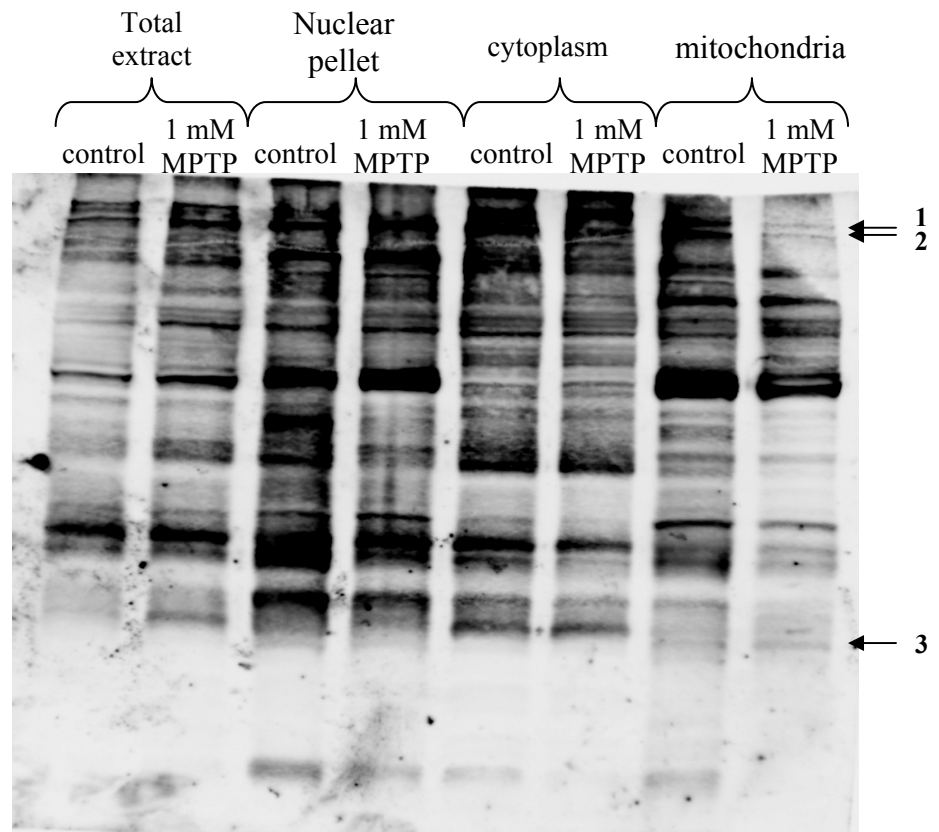
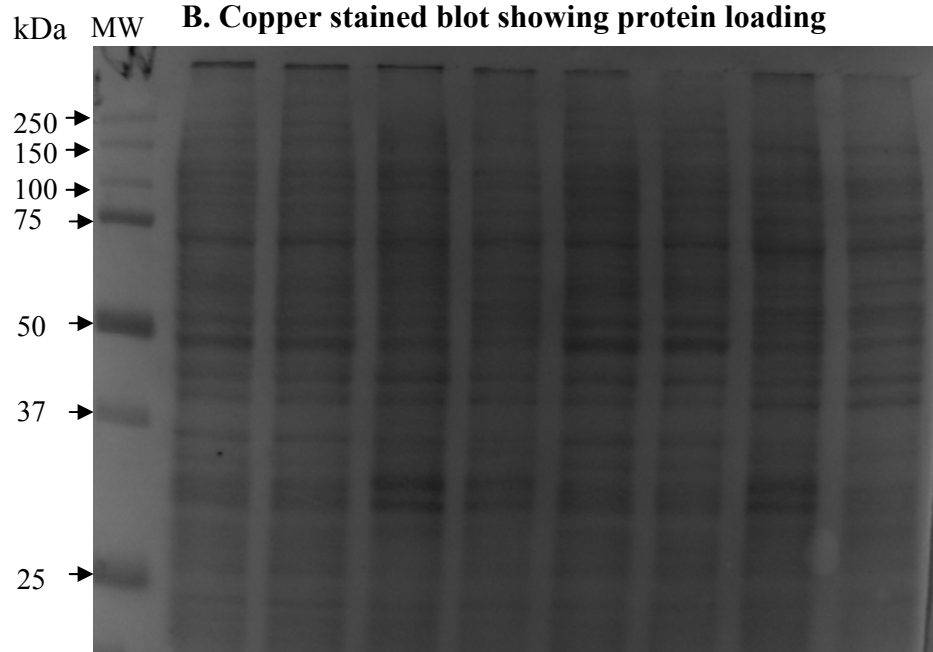
As before, only changes observed in the mitochondrial fraction were quantified using the Aida Analyser software by measuring the intensity of each band normalised to protein loading represented by copper stain (figure 5.10B) and comparing MPTP treatments with respective controls. Bands 1 and 2 showed a decrease in threonine phosphorylation, while band 3 showed an increased level (figure 5.11C). Band 1 and 2 appeared to also be present in the cytoplasmic fraction, while band 3 seemed to be specific to mitochondria (figure 5.10A).

Although changes in phosphorylation were observed following MPTP treatment, no protein identification of these proteins was carried out. 2D-western blot analysis was not possible due to the low sensitivity of the antibody using this approach, despite the strong staining obtained on the 1D-blot.



**Figure 5.9: 2D-blot detection of proteins phosphorylated via a phosphoserine amino acid in mitochondrial fractions from cells treated with 1 mM MPTP for 24 hours compared to controls**

Mouse N2a neuroblastomas were differentiated for 16 hours in serum free medium supplemented with 0.3 mM dbcAMP. Following incubation, cells were treated with 1 mM MPTP for 24 hours (B) or not (controls) (A). Subcellular fractionation was then carried out. 50  $\mu$ g protein from each fraction for each treatment were fractionated by 2DE (pI 3-10; 12 % resolving gel) and then transferred onto a nitrocellulose membrane. Blots were stained with copper (refer to section 2.2.6.1) to check for protein loading (a) before probing with anti-phosphoserine antibody (1 in 200 dilution) (b) followed by the ECL detection procedure (refer to section 2.2.6.2). Circles show area of potential changes between treated and untreated samples.

**A. Phosphothreonine detection****B. Copper stained blot showing protein loading**

**C. Quantitative changes in threonine phosphorylation in mitochondrial proteins**

<b>Band no.</b>	<b>+/- % change compared to controls</b>
1	- 27 % <sup>†</sup>
2	-51 % <sup>†</sup>
3	+ 47 % <sup>*</sup>

**Figure 5.10: Detection of proteins phosphorylated via a threonine amino acid in various subcellular fractions in cells treated with 1 mM MPTP for 24 hours compared to controls**

Mouse N2a neuroblastomas were differentiated for 16 hours in serum free medium supplemented with 0.3 mM dbcAMP. Following incubation, cells were treated with 1 mM MPTP for 24 hours or not (controls). Subcellular fractionation was then carried out. 20 µg protein from each fraction for each treatment were fractionated by 1D-SDS-PAGE (12 % resolving gel) and then transferred onto a nitrocellulose membrane. Blots were stained with copper (refer to section 2.2.6.1) to check for protein loading (B). This was followed by probing with anti-phosphothreonine antibody (1 in 500 dilution) followed by the ECL detection procedure (refer to section 2.2.6.2) (A). Densitometry of each band was quantified using Aida software. Each band was compared to total protein and expressed as % phosphothreonine / total protein ratio versus controls (C). \*  $p < 0.05$  and <sup>†</sup>  $< 0.1$  against control using a paired t-test with a two-tailed distribution (n =3).

- Tyrosine phosphorylation

Figure 5.11A shows the effects of treatment with 1 mM MPTP for 24 hours on tyrosine phosphorylation in subcellular fractions from mouse N2a cells. The three subfractions showed similar levels of tyrosine phosphorylation but different profiles, although the nuclear fraction was similar to the mitochondrial fraction. This might be due to the mitochondrial contamination in the nuclear fraction, also indicating that tyrosine phosphorylation might be low in the nucleus compared to the mitochondria.

Changes in tyrosine phosphorylation following treatment with MPTP were present in all subfractions. Nevertheless, only changes observed in the mitochondrial fraction were quantified (figure 5.11C). The levels of three bands were altered following MPTP treatment; bands 1 and 2 showed an increase in tyrosine phosphorylation, while band 3 showed a decreased level. Band 1 appeared to be also present in the cytoplasmic fraction, while bands 2 and 3 seemed to be specific to mitochondria.

Although changes in phosphorylation were observed following MPTP treatment, no protein identification of these proteins was carried out. 2D-western blot analysis was not possible due to the low sensitivity of the antibody using this approach.

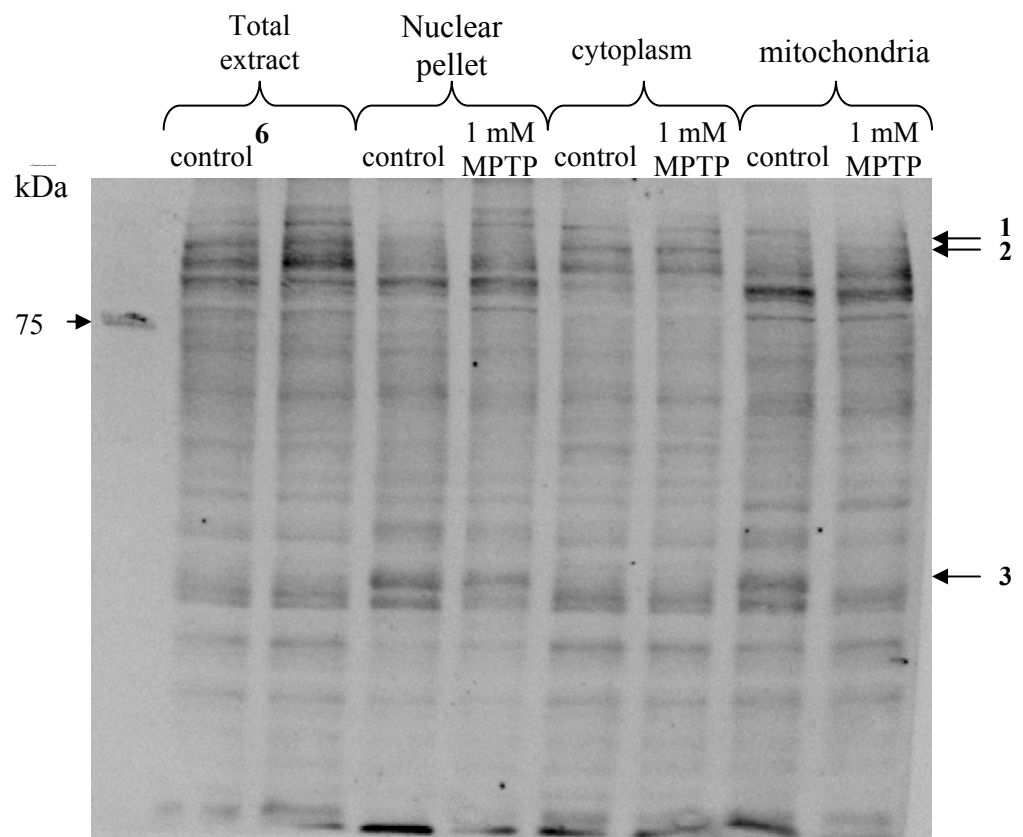
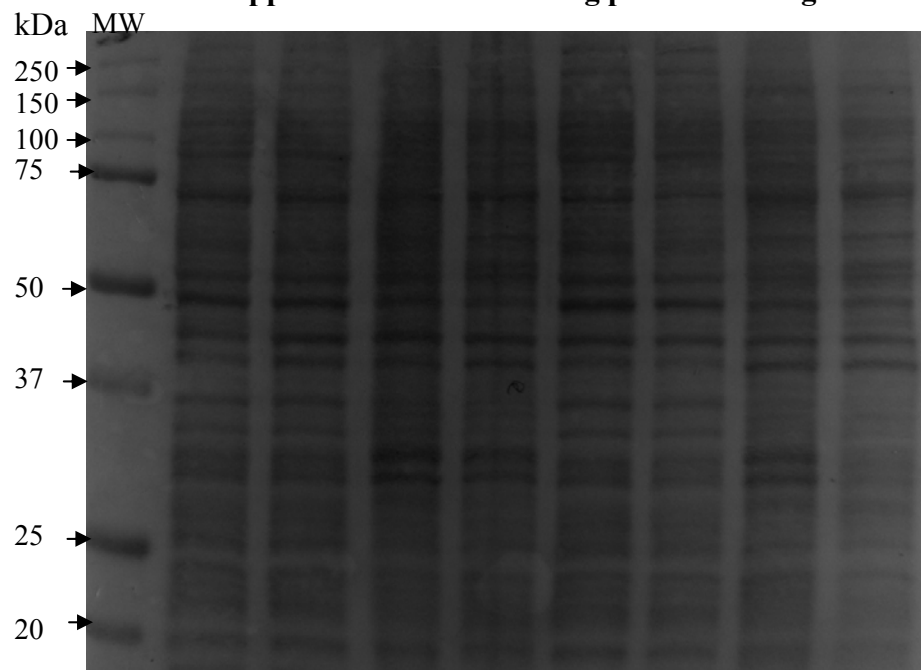
5.2.2.2 Study of the phosphoproteome using SDS-PAGE analysis

The second approach for the study of the mitochondrial proteome was using a fluorescent dye reactive with all phosphorylated proteins called ProQ Diamond phosphoprotein stain (Molecular Probes).

- 1D-SDS-PAGE

Figure 5.12 shows triplicate pairs of mitochondrial samples, MPTP treatment versus control, stained with ProQ Diamond for phosphorylated proteins (figure 5.12A) followed by SyproRuby stain (Molecular probes) for all proteins (Figure 5.12.B).

The phosphoprotein profile was different to the total protein profile showing the specificity of each stain, whilst different replicates were very similar to each other.

**A. Phosphotyrosine detection****B. Copper stained blot showing protein loading**

### C. Quantitative changes in tyrosine phosphorylation in mitochondrial proteins

Band no.	Change fold (n ≥ 2)
1	+ 47 %
2	+ 24 % *
3	- 15 %

**Figure 5.11: Detection of proteins phosphorylated via a tyrosine amino acid in various subcellular fractions in cells treated with 1 mM MPTP for 24 hours compared to controls**

Mouse N2a neuroblastomas were differentiated for 16 hours in serum free medium supplemented with 0.3 mM dbcAMP. Following incubation, cells were treated with 1 mM MPTP for 24 hours or not (controls). Subcellular fractionation was then carried out. 20 µg protein from each fraction for each treatment were fractionated by 1D-SDS-PAGE (12 % resolving gel) and then transferred onto a nitrocellulose membrane. Blots were stained with copper (refer to section 2.2.6.1) to check for protein loading (B). This was followed by probing with anti-phosphotyrosine antibody (1 in 500 dilution) followed by the ECL detection procedure (refer to section 2.2.6.2) (A). Densitometry of each band was quantified using Aida software. Each band was compared to total protein and expressed as % phosphotyrosine / total protein ratio versus controls (C). \* p < 0.05 and † < 0.1 against control using a paired t-test with a two-tailed distribution (n =3).

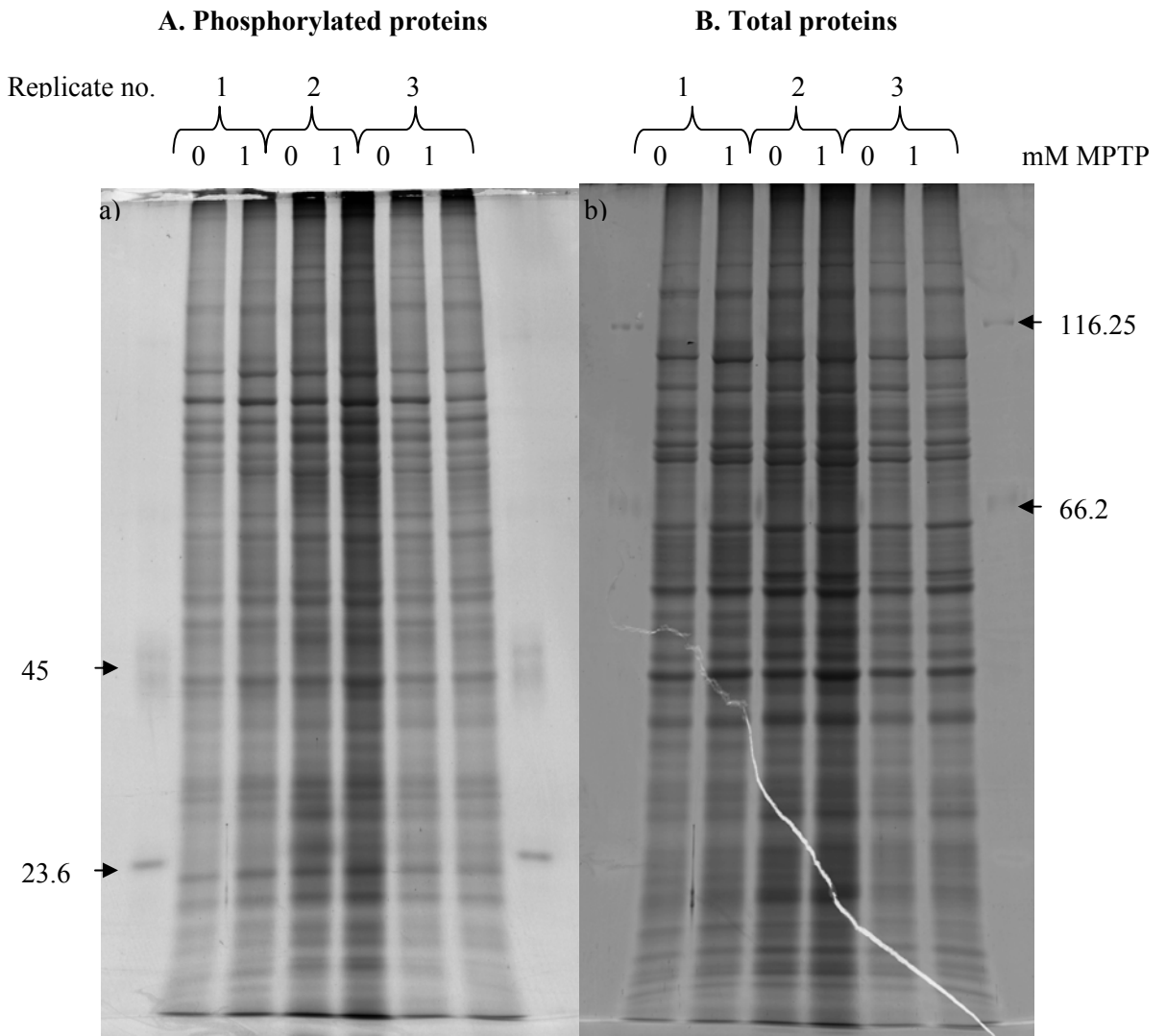


**Figure 5.12: Detection of phosphorylated proteins in mitochondrial fractions following 1 mM MPTP treatment for 24 hours using 1D-SDS-PAGE**

Mouse N2a neuroblastomas were differentiated for 16 hours in serum free medium supplemented with 0.3 mM dbcAMP. Following incubation, cells were treated with 1 mM MPTP for 24 hours or not (controls). Subcellular fractionation was then carried out. 50  $\mu$ g protein from triplicate mitochondrial fractions for each treatment were fractionated by 1D-SDS-PAGE (12 % resolving gel) followed by staining with A. ProQ Diamond for the detection of total phosphorylated proteins, B. Sypro Ruby for the detection of total proteins.

No obvious reproducible changes were observed in the three replicates using ProQ Diamond (figure 5.12A) following 1 mM MPTP treatment. This was contrary to the western blot analysis using a series of phospho-antibodies. However, there were so many phosphorylated proteins using the fluorescent dye, that changes in levels of one protein was more difficult to observe than when using phospho-specific antibodies with their restricted activities.

-    2D-SDS-PAGE

In order to observe more effects of MPTP on the mitochondrial phosphoproteome, 2DE from treated and untreated samples were stained using ProQ Diamond prior to being stained with Sypro Ruby.

a) pI 3-10

Figure 5.13 shows a typical 2D-electrophoretogram following ProQ Diamond stain. The picture showed that, in general, phosphorylated proteins were represented as trails of spots. This is probably due to the property of phosphorylated proteins to shift slightly to the acidic end, and the more a protein is phosphorylated, the more acidic is its pI. So while Sypro Ruby stain revealed the main isoform as a well focused spot (figure 5.13B), ProQ Diamond showed a trail of spots for highly phosphorylated proteins (figure 5.13A). The overlay image (figure 5.13C) shows the phosphorylated proteins (in green) compared total proteins (in pink). Most of the spots revealed by Sypro Ruby represented non-phosphorylated isoforms of proteins as both stained pictures did not align well.

Because there were so many phosphorylated proteins, they did not focus very well using pI 3-10 strips and differences between MPTP treatment and control were not obvious.

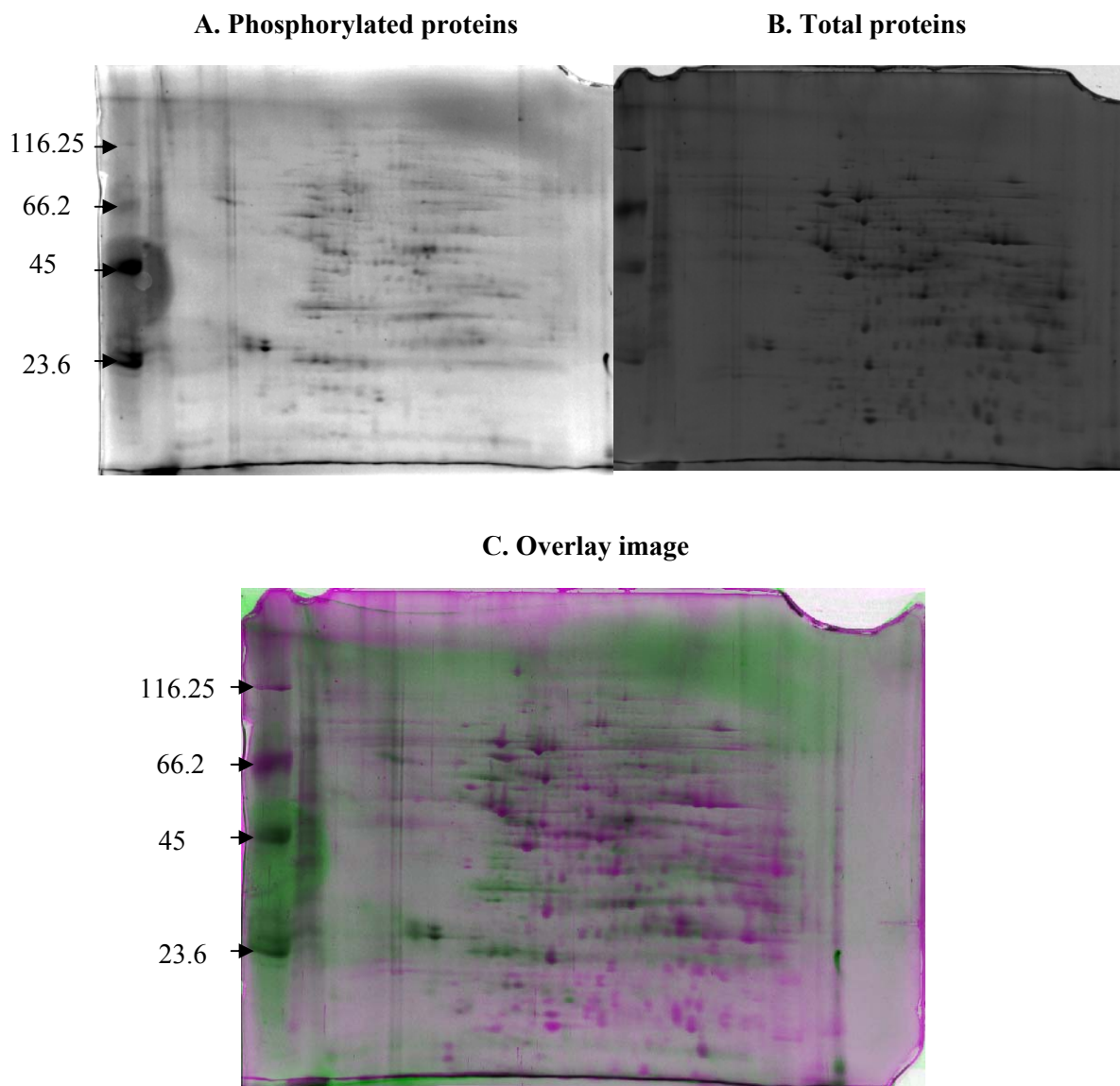


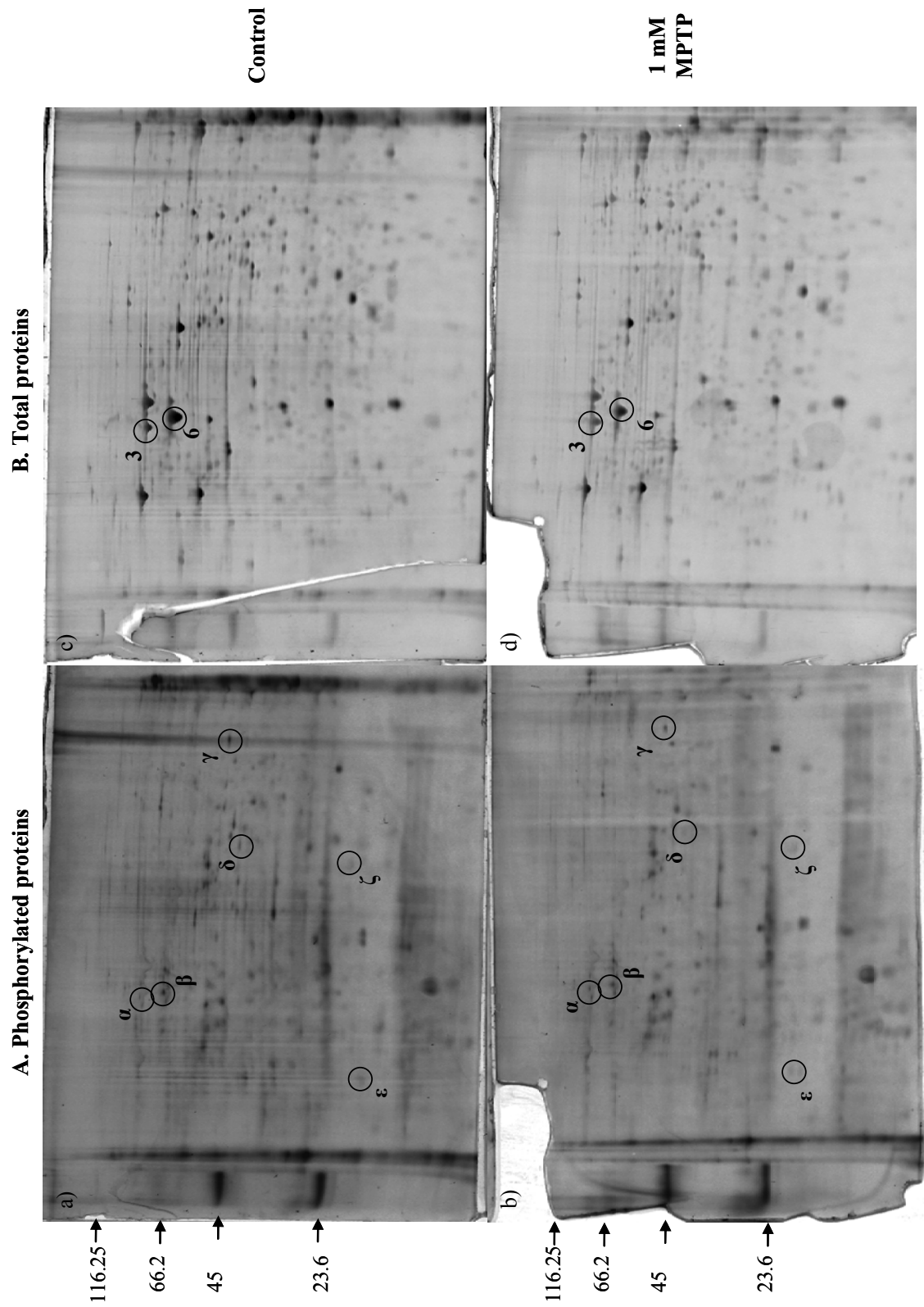
**Figure 5.13: Detection of phosphorylated proteins in mitochondrial fractions using 2DE (pI 3-10)**

Mouse N2a neuroblastomas were differentiated for 16 hours in serum free medium supplemented with 0.3 mM dbcAMP. Following incubation, cells were treated with 1 mM MPTP for 24 hours or not (controls). Subcellular fractionation was then carried out. 50  $\mu$ g protein from mitochondrial fractions for each treatment were fractionated by 2DE (pI 3-10, 12 % resolving gel) followed by staining with: A. ProQ Diamond for the detection of total phosphorylated proteins, and B. Sypro Ruby for the detection of total proteins. C. Both images were overlaid using the Samespots software. Pink: total proteins; Green: phosphorylated proteins. This representative gel shows a profile from a MPTP treated sample.

## b) pI 5-8

Following the sensitivity limitation of broad range pI 3-10 strips, the analysis of phosphorylated proteins was carried out using pI 5-8 strips for the first dimension of 2DE. Figure 5.14 shows the effects of MPTP on the mitochondrial phosphoproteome as compared to the total proteome. Gels were analysed using the SameSpots software and differences between the two treatments were observed. The major changes in phosphorylation levels are shown in figure 5.14C. Following MPTP treatment, spots  $\alpha$  to  $\gamma$  showed an increase in phosphorylation levels while spots  $\delta$  to  $\zeta$  showed a decrease in phosphorylation levels.

Interestingly spot  $\alpha$  co-localised with a spot that was previously observed to be increasing following MPTP toxicity in the total proteome analysis using pI 5-8 (section 5.2.1.2). The spot was annotated as spot N in figure 5.2 and hypothesised to be an isoform of heat shock cognate 71 kDa protein (spot 3 in figure 5.15 and 6.14B). A phosphorylated spot (spot  $\beta$ ), in the proximity of Hsp 60 (spot 6) also showed an increase in phosphorylation following MPTP treatment.



**C. Quantitative analysis of changes in phosphorylation**

<b>Spot number</b>	<b>+/- % change compared to controls</b>
$\alpha$	+ 57 % *
$\beta$	+ 17 % *
$\gamma$	+ 59 %
$\delta$	- 70 %
$\varepsilon$	- 20 % *
$\zeta$	- 22 % *

**Figure 5.14: Detection of phosphorylated proteins in mitochondrial fractions using 2DE (pI 5-8 range strips)**

Mouse N2a neuroblastomas were differentiated for 16 hours in serum free medium supplemented with 0.3 mM dbcAMP. Following incubation, cells were treated with 1 mM MPTP for 24 hours or not (controls). Subcellular fractionation was then carried out.

50  $\mu$ g protein from mitochondrial fractions for each treatment were fractionated by 2DE (pI 5-8, 12 % resolving gel) followed by staining with: A. ProQ Diamond for the detection of phosphorylated proteins, a) with control sample and b) with MPTP treated sample, spots  $\alpha$  to  $\zeta$  showed variations in levels between treatments; B. Sypro Ruby for the detection of total proteins c) with control sample and d) with MPTP treated sample. Spot 3 identified by peptide mass fingerprinting as Hsc70; Spot 6 identified as Hsp60. (refer to figure 3.12 for spot identification map).

C. Densitometry of spots circled was quantified using Samespots software. \*  $p < 0.05$  against control using a paired t-test with a two-tailed distribution ( $n = 3$ ).

$\alpha$  and  $\beta$  are in the vicinity and thought to be post-translationally modified forms of spots 3 and 6, respectively.

### 5.3 DISCUSSION

#### 5.3.1 Effects of MPTP on N2a neuroblastoma mitochondrial proteome

Using a proteomic approach consisting of 2DE followed by image analysis and peptide mass fingerprinting, around 32 proteins from the mitochondrial proteome were observed to vary in levels following sub-cytotoxic treatment with MPTP. Out of these proteins, nine were identified and the identities of three more were hypothesised as they were in close proximity with identified proteins. The identities of these proteins are shown in table 5.3. They are related to different functions in the cell including chaperone and co-chaperone family proteins, metabolic enzymes, enzymes linked to oxidative phosphorylation and an outer mitochondrial membrane channel. A potential role for these proteins in MPTP-induced toxicity will be discussed later (see section 5.3.3).

Changes observed using both pI 3-10 and pI 5-8 strips were between 17 and 115 %. Although these changes occurred for each replicate between the two treatments (MPTP versus control), the use of a validation process was necessary to confirm these changes and the validation of the 8 non-validated identified proteins would be required to confirm their involvement in MPTP-induced toxicity.

Fukada and colleagues (2004) used a similar approach to study the mitochondrial proteome using a cellular model of familial amyotrophic lateral sclerosis (ALS). They identified up to 45 proteins changing in expression levels using pI 3-10 broad range IPG strips (using triplicates). Similarly, Van Laar *et al.* (2008) identified 17 proteins varying in expression in the mitochondrial proteome of a rat model exposed to dopamine quinone (using 5-6 replicates). These two analyses demonstrated that 2D-PAGE using broad range pI 3-10 analysis was acceptable and efficient. In the former study, no validation of observed changes in expression was undertaken. In the latter analysis, 2 out of the 17 proteins were validated using western blot analysis. Although several studies have been carried out using 2DE using narrower pI ranges (De Iuliis *et al.*, 2005), none were carried out using mitochondrial proteomes.

Spot symbol <sup>1</sup>	pI spectrum analysis	Protein identification <sup>2</sup>	+/- % change in 2DE analysis <sup>3</sup>	+/- % change in western blot analysis <sup>4</sup>
6	pI 5-8	60 kDa heat shock protein	+ 27 % †	+ 37 % *
13	pI 3-10	Glutamate oxaloacetate transaminase 2	+ 24 % *	+ 54 % *
19	pI 3-10	Voltage-dependent-anion channel 1	+ 30 % †	+ 201 % †
5	pI 5-8	Stress-induced-phosphoprotein 1	+ 34 % †	
9	pI 3-10	ATP synthase, F1 complex $\alpha$ -subunit isoform 1	- 17 % †	
10	pI 3-10	Fumarate hydratase	+ 28 % †	
15	pI 3-10	Malate dehydrogenase	+ 56 % *	
18	pI 3-10	Electron transfer flavoprotein subunit $\alpha$	+ 49 % *	
21	pI 5-8	ATP synthase, F0 complex subunit d	+ 43 % *	
B	pI 3-10	In the smear of Hsp60	- 40 % †	
E	pI 3-10	In the smear of putative $\beta$ -actin	+ 51 % *	
N	pI 5-8	In the smear of Hsc70	+ 68 % †	+ 51 % * (total protein)

**Table 5.3: Identified proteins showing changes in levels following sub-cytotoxic MPTP treatment**

Normalised density obtained using Samespot software (Progenesis) .

<sup>1</sup> Spot symbols confer to figures 5.1 and 5.2

<sup>2</sup> Proteins identified by peptide mass fingerprinting. For accession numbers and more details on the Mascot database results refer to table 3.8.

<sup>3</sup> Change fold as shown in tables 5.1 and 5.2 using 2DE analysis

<sup>4</sup> Change fold as shown in figures 5.4 to 5.7 using western blot analysis

\* Statistically significant increases  $p < 0.05$  using a paired t-test

† Statistically significant increases  $p < 0.1$  using a paired t-test

### 5.3.2 Effects of MPTP toxicity on phosphorylating pathways

The present study shows that mouse N2a neuroblastoma cells have a complex mitochondrial phosphoproteome. Based on 1D-western blots, a higher number of proteins were shown to be phosphorylated via threonine residues than via serine and tyrosine residues. In broad terms this mitochondrial proteome followed the total cell consensus where threonine phosphorylation ratio is 1000 to 100 serine phosphorylation to 1 tyrosine phosphorylation (Raggiaschi *et al.*, 2006). Several mitochondrial proteins have been observed to vary in phosphorylation status following MPTP-induced toxicity, 6 of which were shown to vary using the ProQ Diamond dye. Consistently, heat shock family proteins seemed to be targets of phosphorylation modulated by MPTP treatment. Increase in serine phosphorylation was observed for GRP75, and overall phosphorylation was increased in what was thought to be forms of Hsc70 and Hsp60.

Nakamura *et al.*, (2006) used 2-DE followed by ProQ Diamond staining to look at the effects of 6-OHDA, another toxin mimicking PD's biochemical features, on the whole phosphoproteome of SH-SY5Y cells. Using pI 3-10 strips they observed changes in phosphorylation patterns of 4 different proteins. None of them were mitochondrial.

All three most commonly phosphorylated residues (threonine, serine and tyrosine) were sensitive to MPTP-induced toxicity showing that several kinases must have been involved. Recently, many kinases and phosphatases have been found in the mitochondria. Some of them have been linked to PD. First of all PINK1 and LRRK2, both kinases, have been linked with genetic cases of the disease and have been found within or interacting with the mitochondria (Henchcliffe and Beal, 2008). Moreover, several signaling kinases are known to be modulated in PD and have been co-localised with the mitochondria. For example, activated ERK 1/2 was found to translocate to mitochondria following 6-OHDA treatment (Kulich *et al.*, 2007), indicating that ERK 1/2 specifically localised in the mitochondria could be a marker of mitochondrial dysfunction. Similarly, in mice GSK3- $\beta$  was shown to be increased following MPTP toxicity in both mitochondria and cytosol (Petit-Paitel *et al.*, 2009). Moreover, the mitochondrial form of GSK3- $\beta$  was found to inhibit complex I when constitutively active in SH-SY5Y cells, leading to ATP depletion and ROS production (King *et al.*, 2008). These two kinases as well as other mitochondrial kinases could be causing the modulations in phosphorylation found in the mitochondrial phosphoproteome of mouse N2a cells following MPTP treatment.

Both quantitative and phosphorylation analyses of the mitochondrial proteome have been shown to be more sensitive with narrower pI ranges. Further work could be undertaken focusing in even narrower pI ranges to observe more subtle shifts of spots. Moreover, a further optimisation of basic narrow pI range analyses could be highly useful for both the total proteome and phosphoproteome as many changes were observed in the basic end of broad range pI analyses.

### **5.3.3 Mitochondrial markers of MPTP-induced toxicity**

#### **5.3.3.1 Chaperone and co-chaperone proteins sensitive to MPTP-induced toxicity**

2DE analysis of the mitochondrial proteome of N2a cells revealed an increase of 30 % in Hsp60 levels following MPTP treatment compared to controls. This increase was validated using western blot analysis showing an increase in levels of 37 % in the mitochondrial fraction. Increased levels in the other subcellular fractions and total extract were also observed although these were smaller and not statistically significant.

Although identification has not been confirmed, another spot close to and on the basic side of Hsp60 also increased following MPTP treatment. This spot was shown to change using the broad range pI but was not repeated in the pI 5-8 analysis, where spots were better focused. Consequently, there were concerns that it was an artefact due to pot smearing. A 2D-western blot analysis of Hsp60 showed that there were spots on each side of the main Hsp60 spot, probably post-translationally modified forms. However, this analysis did not conclusively reveal whether these isoforms were changing in levels. Later analysis involving ProQ Diamond staining showed that the acidic form (spot  $\beta$  in figure 5.14) of the protein (spot 6 in figure 5.14) aligned with a phosphorylated spot that was slightly (17%) increased following MPTP treatment. Since Hsp60 (spot 6 in figure 5.14) has been observed to have ATPase activity (Weissman *et al.*, 1995), it was not surprising to observe that it could be phosphorylated. It is also worth noting that Hsp60 expression has been linked to the activation of ERK1/2 (Zhang *et al.*, 2004).

Hsp60, also called chaperonin, is mostly found in mitochondria, although there has been evidence of Hsp60 in the cytoplasm in recent studies (Chandra *et al.*, 2007). Hsp60 has mainly been found in the mitochondrial matrix where it plays an important role in the folding of mitochondrial proteins following their entry to the organelle. It also has a role

in preventing misfolding that can occur in stress conditions (reviewed in Deocaris *et al.*, 2006). Other extra-mitochondrial roles include intracellular trafficking of proteins, interaction with survival proteins such as p53 and survivin along with a pro-death role in its ability to activate caspase-3 when released from mitochondria in response to specific stimuli (Cappello *et al.*, 2008).

Dysregulation of Hsp60 has previously been observed in a variety of neurodegenerations. Indeed, it has been observed that a missense mutation could cause a brain hypomyelinating leukodystrophy in certain individuals (Magen *et al.*, 2008). The mutated form was observed to have lost its chaperone activity. Hsp60 expression was also observed to be decreased in models of Alzheimer disease (Tsuji *et al.*, 2002). Interestingly, Hsp60 was upregulated in a rat model of schizophrenia (Paulson *et al.*, 2005). More particularly, using models mimicking PD, Jin and colleagues (2006) used a proteomic approach to measure protein expression levels in the substantia nigra of patients using post-mortem samples and, amongst many other proteins, found that Hsp60 protein levels were increased. Moreover, Barzilai and colleagues (2000) observed an upregulation in Hsp60 mRNA expression in response to dopamine toxicity in dopaminergic neurons as a model mimicking PD. Upregulation and downregulation of Hsp60 expression observed in different models of neurodegeneration demonstrates its antagonistic dual role in survival and death pathways. However, consistent with our findings, Hsp60 mRNA and protein levels have been observed to be upregulated using different PD-models (Jin *et al.*, 2006; Barzilai *et al.*, 2000).

Following MPTP treatment, the pI-5-8 2-DE analysis of mitochondrial fractions showed an increase in the level of a spot in the proximity of a spot identified as heat shock cognate 71 kDa protein (also called Hsc70, HspA8 and Hsc73). 1D-blot analysis confirmed a 50% increase in Hsc70 in the mitochondrial fraction, and no change in levels of the protein in other subcellular fractions. The 2D-blot analysis showed that there was an acidic isoform of the protein, highly increased in intensity following MPTP treatment. This increase, in the gel analysis, was quantified as 70 %, which was underestimated in the 1D-blot analysis because the total level of Hsc70 included two forms: the main spot and the acidic spot. This represented an acidic shift of the Hsc70 protein probably due to post-translational modifications. Further analysis using ProQ Diamond staining showed that the acidic form of the protein aligned with a phosphorylated spot that increased in levels following MPTP treatment.

Hsc70 is a constitutively expressed protein of the Hsp70 family. It is found ubiquitously in the cell. Meimaridou and colleagues (2009) recently reviewed the different roles of Hsc70 and some of its modes of action. They related that one of its main roles as a chaperone was to bind nascent peptides and facilitate their folding as they exited the ribosomes. Hsc70 has been reported to have a role in endocytosis acting as an ATPase in the disassembly of clathrin vesicle during transport of membrane components, for example, and in exocytosis by interacting with a protein essential for exocytosis (Meimaridou *et al.*, 2009). Hsc70 has also been attributed to have a role in protein degradation by targeting proteins (including membrane proteins) to the ubiquitin proteasome system (UPS) or the lysosomes, depending on the protein to be degraded (Meimaridou *et al.*, 2009). While Hsp60 was observed to have a role both in pro- and anti-apoptotic pathways (Capello *et al.*, 2008), Hsc70 has been observed to have anti-apoptotic activity by inhibiting p53, inhibiting stress-activated kinases (such as JNK) and permeabilising lysosomal membranes (Guarrido *et al.*, 2006).

The role of both Hsc70 and Hsp60 in folding proteins in the cytoplasm or mitochondria, respectively, is ATP-dependent (Hartl and Hayer Hartl, 2009). The cycle by which Hsc70 is folding nascent pre-proteins is also dependent on other co-chaperones. Interestingly, one of these co-chaperones was observed to be stress-induced phosphoprotein 1 (STIP1), also called Hop (Meimaridou *et al.*, 2009), which was increased by 34% following MPTP treatment in the present study. Although the increase in STIP1 was not validated, it could be linked to the increased levels of Hsc70.

In disagreement with our findings, the proteomic analysis conducted by Jin and colleagues (2005) showed decreased levels of Hsc70 in the mitochondria of MPTP treated mice. Heat shock has long been observed to be protective of MPTP toxicity in a variety of models (Freyalدهoven and Ali, 1996; Quigney *et al.*, 2003; Donaire *et al.*, 2005) by inducing the expression of a variety of heat shock proteins. Moreover, the substrate of dopamine, L-DOPA, used as a treatment of PD, was shown to increase Hsc70 expression (Calabrese *et al.*, 2007). All these studies related the protective effects of Hsc70 in PD and in MPTP-induced toxicity. Thus in the present study, the upregulation of phosphorylated Hsc70 protein in the mitochondria following treatment with sub-cytotoxic concentrations of MPTP probably has a protective role. It would be interesting to check levels of Hsc70 following treatment with cytotoxic concentrations of MPTP.

Other previous studies using models mimicking PD have shown changes in expression of different members of the Hsp70 family (Freyaldenhoven and Ali, 1996; Fan *et al.*, 2006) and more precisely mitochondrially expressed members such as Heat shock-related 70 kDa protein2 (Hsp72) and glucose-regulated protein 75 (Grp75) (Fan *et al.*, 2005; Van Laar *et al.*, 2008). However, in the present study, no changes in the levels of Grp75 was detected (refer to figure 3.12 spot 4 for location of GRP75 on profile map).

Overall, the upregulation of chaperones and co-chaperones following exposure of N2a cells to sub-cytotoxic concentrations of MPTP could be due to their pro-survival and anti-apoptotic roles. It could also be due to their ability to reshape misfolded proteins and participate in the degradation of misfolding and aggregating proteins due to oxidative stress observed in Parkinson's disease (Jin *et al.*, 2005).

#### 5.3.3.2 Metabolic enzyme protein levels

The levels of several metabolic enzymes increased following treatment with sub-cytotoxic concentrations of MPTP.

Glutamate oxaloacetate 2 transaminase (GOT2), also called mitochondrial aspartate amino transferase, increased by 24 % according to 2DE analysis and 54% according to 1D-western blot analysis. Using western blot analysis, non-significant increased levels were also observed in nuclear and cytoplasmic fractions.

GOT catalyses the transfer of amine groups between aspartate and glutamate following the reaction below.



It is a reversible enzyme from the amino acid synthesis pathway, including the neurotransmitter glutamate and the urea cycle. Two isoforms have been found: GOT1 in the cytoplasm and GOT2 in the mitochondria. GOT2 is found in the matrix but can interact with the IMM close to complex I (McKenna *et al.*, 2000).

Although their expression levels have not been validated, two other metabolic enzymes increased following MPTP-induced treatment. Indeed, malate dehydrogenase (MDH) protein levels increased by 56 % and fumarate hydratase (FMH) by 28 %. Both enzymes are subsequent enzymes of the Krebs cycle as shown in figure 5.15.

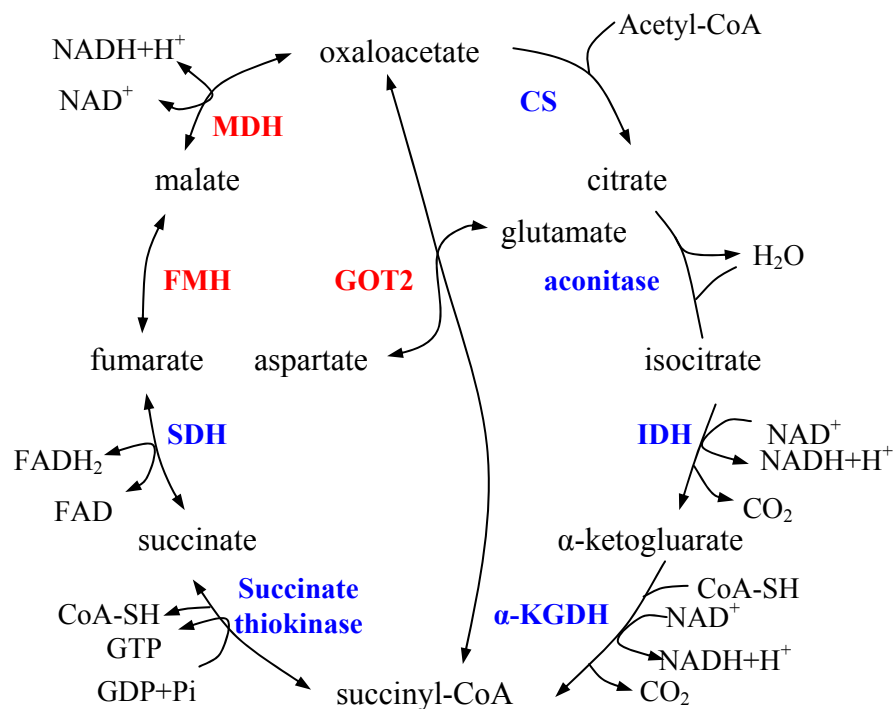


**Figure 5.15: Biochemical reactions involved in the TCA cycle and the link with the first enzyme of amino acid synthesis, GOT2**

**Blue print:** metabolic enzymes involved in the TCA cycle that did not show significant changes or were not identified in mouse N2a neuroblastoma following 1 mM MPTP treatment for 24 hours

**Red print:** metabolic enzymes involved in the TCA cycle that showed significant upregulated protein levels in mouse N2a neuroblastoma following 1 mM MPTP treatment for 24 hours

CS: citrate synthase; IDH: isocitrate dehydrogenase;  $\alpha$ -KGDH:  $\alpha$ -ketoglutarate; SDH: succinate dehydrogenase; FMH: fumarase; MDH: malate dehydrogenase; GOT2: glutamate oxaloacetate transaminase 2.

Increased protein levels are not always linked to increased enzyme activity. There are several hypotheses that can be drawn from an increased protein level. The three main causes could be an upregulation of protein levels independent of protein function due to upregulation of transcription factors, for example, or increased protein translation. Another cause could be a decreased proteolysis of the protein. The enzyme protein could also have an increased level for a role other than enzymatic activity.

Interestingly, these three upregulated enzymes were consecutive enzymes sharing substrates and products (figure 5.15). Moreover, all three were reversible, which made difficult the interpretation as no substrate or product was analyzed and thus the direction the enzyme was driven is not known. Following inhibition of complex I by MPTP via  $MPP^+$  (Langston *et al.*, 1983), the metabolites of the Krebs cycle ( $NADH + FADH_2$ )

cannot be re-oxidised via the ETC. A study of the effects of MPTP on monkeys showed that MDH and GOT2 activities were increased following the treatment in the cerebellum (Villa *et al.*, 1994). In another study, the overall rate of the Krebs cycle was shown to decrease in MPTP treated monkeys (Kanamatsu *et al.*, 2007). Consequently the Krebs cycle was expected to show dysregulation and other pathways capable of re-oxidising co-factors are expected to be activated. For example, instead of using oxaloacetate to initiate the Krebs cycle and produce citrate via citrate synthase, MDH might be reversed and use oxaloacetate to form malate which can be shuttled out of the mitochondria and used as substrate for other metabolic processes (Mazzio and Soliman, 2003). Mazzio and Soliman (2003) proposed this hypothesis, following their work using different carbohydrate and amino acid substrates to try and protect mouse N2a cells against MPP<sup>+</sup> toxicity. They found that glucose, phosphoenolpyruvate, pyruvate, as well as malate all increased ATP production but not oxygen consumption showing that energy production was from a pathway other than the oxidative phosphorylation. They hypothesized that MPP<sup>+</sup> led to the reversion of the Krebs cycle to produce phosphoenolpyruvate and to the use of anaerobic pathways such as lactate production in mouse N2a neurons.

Alternatively, malate can be metabolized to fumarate via fumarase and the product could be used to increase complex II activity by re-oxidising FADH<sub>2</sub>. However, this pathway would require intact ETC components, excluding complex I activity.

Extracellular glutamate levels have been previously described in PD (Lange *et al.*, 1997) and a role for glutamate excitotoxicity in cell death following MPTP-induced toxicity have also been observed more recently in a mouse model (Meredith *et al.*, 2009). Whether GOT2 upregulation would favour glutamate synthesis as well as oxaloacetate synthesis for it to be used to produce phosphoenolpyruvate as described previously or favours glutamate scavenging and amino acid synthesis, has not been resolved here.

Although only GOT2 upregulation was validated, over-expression of MDH and FMH both made sense when compared to GOT2 over-expression in the context of using Krebs cycle products as substrates to produce energy via anaerobic means in the cytoplasm. Whether this would lead to glutamate excitotoxicity or would be a protective consequence still remains to be resolved.

## 5.3.3.3 Proteins linked to oxidative phosphorylation

Three proteins related to the oxidative phosphorylation system were showing altered levels. Of the three, two of them were subunits of ATP synthase, also called complex V. Indeed, a spot identified as ATP synthase F1 complex  $\alpha$ -subunit isoform 1 showed a significant decrease in level by 17 %. Interestingly, another spot identified as ATP synthase, F0 complex subunit  $\delta$  showed an increase by 43 % in level following MPTP-induced toxicity. ATP synthase F1 complex  $\beta$ -subunit was also identified but did not show any significant changes in levels following MPTP treatment. Whether the latter subunit was not affected by sub-cytotoxic MPTP treatment or the proteomic approach used in the study was not sensitive enough to observe a change has not been investigated. However, a western blot analysis using human post-mortem substantia nigra by Ferrer and colleagues (2007) showed a decreased level of ATP synthase  $\beta$ -subunit while the levels were increased in frontal cortex of the same patients. Dysregulation of complex V following MPTP treatment could be a direct consequence of complex I inhibition as less electrons are transferred through the ETC and the proton-motric force would be weaker as a direct consequence.

Inconsistency in the different subunits of mitochondrial ATP synthase has already been observed in the literature. In a proteomic study of post-mortem neurons of the substantia nigra, Basso and colleagues (2004) had already observed a significant increase in ATP synthase  $\delta$ -subunit while a non-significant decrease in ATP synthase  $\alpha$ -subunit was observed, consistent with the present findings. Due to the complexity of mitochondrial ATP synthase structure and the different roles of each subunit, inconsistency of the different subunits following MPTP-induced toxicity could be possible. Both  $\alpha$  and  $\beta$ -subunits were observed to bind nucleotides such as ADP while only the  $\beta$ -subunit had the catalytic activity of synthesising ATP (Grover *et al.*, 2008). The decrease in  $\alpha$ -subunit might be linked to a decrease in nucleotide binding probably due to a drop in ADP substrate in mitochondria since it was previously hypothesised that ATP production might be increased in the cytoplasm via lactate formation. On the contrary, an increase in  $\delta$ -subunit was observed. This subunit was observed to participate in holding both F1 and F0 subunits of complex V. Because the catalytic unit seemed to decrease in levels, there might have been a compensatory mechanism that increased structural subunit levels in order to try and maintain complex V integrity.

Another oxidative phosphorylation-related protein showed a change in level following MPTP-induced toxicity. Electron transfer flavoprotein subunit  $\alpha$  (ETF  $\alpha$ ) was up-

regulated by 49 % compared to controls. ETF was observed to participate in the transfer of electrons from reduced acyl CoA via the acyl CoA dehydrogenase in the fatty acid  $\beta$ -oxidation pathway to FADH<sub>2</sub>. Electron transfer flavoprotein (ETF) transfers the electrons from FADH<sub>2</sub> to electron transfer-ubiquinone reductase on the ETC. This reaction occurred between complex II and complex III of the ETC (Schapira *et al.*, 2006). Although it has not been observed in previous studies, increased levels seemed coherent as a decrease in complex I activity could lead to an increase of complex II activity to try and increase ATP synthesis as a compensatory effect.

Although such observations seemed to be in accordance with the literature, it would be important to validate these changes in expression using western blot analysis. This validation would be important for supporting the hypotheses stated but also to check the overall level of each subunit as only one spot was identified for each subunit not taking in account any post-translational modifications that could occur following MPTP treatment.

#### 5.3.3.4 Voltage-dependent-anion channel 1

The last spot identified to show changes in levels following MPTP treatment was VDAC1. Two-dimensional gel electrophoresis analysis showed an increase of 30 % compared to controls. One-dimensional western blot analysis showed an increase of 200 %. This difference between the two methods might be due to an underestimation of the level of change in the proteomic approach due to variability issues. Moreover 2DE was measuring the level of one spot while the antibody based method was measuring the total VDAC1 level corresponding to 5 different spots as shown by 2D-blot analysis. This observation led to the thought that more than one VDAC1 spot might have increased levels following MPTP-induced toxicity.

VDAC is an outer mitochondrial membrane gated channel (Lemasters and Holmuhamedov, 2006) with many important roles in the cell. It can channel small molecular weight molecules including cations, nucleotides, creatine and NADH (Lemasters and Holmuhamedov, 2006) and has been linked with apoptosis (Shoshan-Barmatz *et al.*, 2006; Tsujimodo and Shimizu, 2002) and energy storage (Vyssokikh and Brdiczka, 2003).

MPTP-induced toxicity has not previously been linked to VDAC protein levels. Nevertheless, VDAC protein and mRNA levels were observed to be elevated following

rotenone-induced toxicity in Human SH-SY5Y neuronal cells. This upregulation could be inhibited by pre-treatment with an antioxidant (Xiong *et al.*, 2009). Another group, Premkumar and Simankov (2002), linked VDAC level dysregulation with dopamine toxicity in neuronal cells. In their study, they discovered that VDAC isoforms 1, 2 and 3 were down-regulated and that overexpression of VDAC was protective of the cells. Even though the results were not correlated, dopamine toxicity acted differently to rotenone and MPTP, both complex I inhibitors. The role of VDAC in complex I inhibition-induced toxicity is not yet fully resolved.

## **CHAPTER VI:**

# **MODIFIED EXPRESSION OF VOLTAGE-DEPENDENT ANION CHANNEL FOLLOWING MPTP TREATMENT**

## 6.1 INTRODUCTION

### 6.1.1 The voltage-dependent anion channel

#### 6.1.1.1 Structure and general functions

The voltage-dependent-anion channel (VDAC), also called the mitochondrial porin, was first described by Schein and colleagues in 1976 (reviewed in Lawen *et al.*, 2005). It is the most abundant protein of the OMM (Vyssokikh and Brdiczka, 2003) and composes a channel that is permeable to molecules up to 5 kDa depending on the gating voltage (Lemasters *et al.*, 2006). Its structure, as deduced from biochemical and function studies, is composed of a transmembrane  $\alpha$ -helix and 13 transmembrane  $\beta$ -strands enclosing an aqueous channel of 2.5 to 3 nm of internal diameter (Colombini *et al.*, 2009) (Figure 6.1).

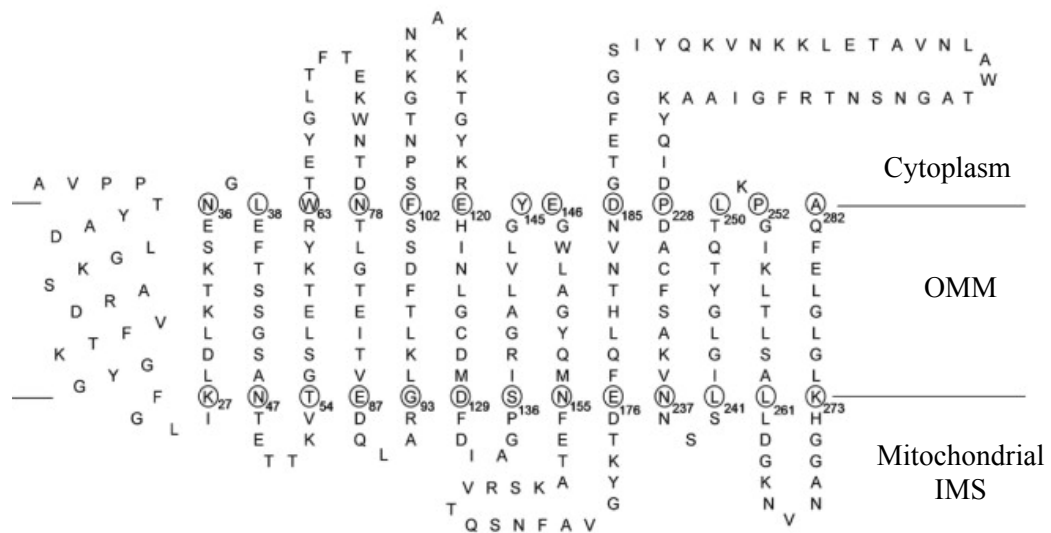


**Figure 6.1: VDAC folding pattern in the OMM as deduced by functional studies**

Taken from Colombini *et al.*, 2009

Three isoforms exist in humans and mice with between 67 % and 71 % homology in amino acid sequence (Lawen *et al.*, 2005). VDAC1, the most abundant isoform, has no targeting segment in its amino acid sequence and has been found to a lesser extent in other cellular membranes, for example the plasma membrane (Lawen *et al.*, 2005). Interestingly, two splice-variants of VDAC1 have been found. The VDAC1 isoform found in the plasma membrane has 13 more amino acids on the N-terminal end of the sequence than the variant found in the OMM (Buettner *et al.*, 2000).

Knockdown and overexpression analyses have helped to understand the roles of each VDAC isoform. VDAC1 has been found to have a role in foetal survival, which was enhanced with VDAC3 expression knockdown (Anflous-Pharaya *et al.*, 2007). Moreover, single knockdown of VDAC1 and double knockdowns of VDAC1 and 3 showed a decrease in glycolysis, due to an inhibition of hexokinase interaction to the mitochondria (Anflous-Pharayay *et al.*, 2007). VDAC2, the less prevalent isoform, has been associated with anti-apoptotic activity (Shoshan-Barmatz *et al.*, 2006).

Interestingly, VDAC has been observed to be enriched in contact sites between mitochondria and between mitochondria and endoplasmic reticulum (ER), indicating a role for the channel in the interactions between mitochondria and ER, in addition to between mitochondria and the cytoplasm (Shoshan-Barmatz *et al.*, 2006). The list of molecules which can pass through the channel includes creatine phosphate, adenine nucleotides (e.g. ATP and ADP), inorganic phosphates, succinate, citrate, glutamate, cations (e.g.  $\text{Ca}^{2+}$ ,  $\text{Na}^+$ ,  $\text{K}^+$ , ...) (Lemasters and Holmuhamedov, 2006) and superoxide anion (Han *et al.*, 2003a).

Permeabilisation of the OMM is thought to be mainly regulated by the permeabilisation of VDAC, depending on the voltage state of the channel and on the action of several modulators. The channel is known to have different states: the “open state” with high conductance, allowing the passage of a range of metabolites, preferentially anions; and the “closed state”, with low conductance and, despite the name, allowing cations, such as  $\text{Ca}^{2+}$ ,  $\text{Na}^+$  and  $\text{K}^+$  to travel through (Rostovtseva and Berzrukov, 2008). Many molecules have been observed to interact with VDAC including NADH (tends to a closed state and reduce ADP permeability), glutamate, cytoskeletal proteins (e.g. MAP2, actin, gelsolin, dynein light chain), GRP75 (decrease channel voltage), the superoxide anion (increases the permeability of the channel), ROS and RNS (Hajnoczsky *et al.*, 2002; Lemasters *et al.*, 2006; Shoshan-Barmatz *et al.*, 2006). Additionally, VDAC has been found to be a target for phosphorylation, more particularly for signaling kinases. Kinases able to modulate VDAC function include C-Raf, pKA, pKC, GSK-3 $\beta$ , p38 and tyrosine phosphorylating kinases; thought to have different effects on the protein state (Lemasters *et al.*, 2006; Hajnoczsky *et al.*, 2002, Das *et al.*, 2008; Schwertz *et al.*, 2007).

Moreover, VDAC has been found to bind a number of proteins. For example, Bcl<sub>2</sub>-family proteins have been found to bind VDAC, resulting in modulation of apoptotic cell death (Hajnoczsky *et al.*, 2002). Moreover, VDAC has been also linked to the mitochondrial transition pore by interacting with the adenine nucleotide translocator (ANT) and

benzodiazepine receptor, increasing the possible involvement of the protein in cell death (Tsujimoto and Shimizu, 2002). Other proteins binding and modulating VDAC in a metabolic context are hexokinase (HK, specific to VDAC1), creatine kinase (CK) and glycerol kinase (Shoshan-Barmatz *et al.*, 2006; Vyssokikh and Brdiczka, 2003). In this context, VDAC is proposed to be a link between ATP levels and glycolysis rate, as a modulator between the mitochondrial and cytoplasmic metabolic pathways.

#### 6.1.1.2 The role of VDAC in cell death

Whether or not VDAC plays a role in cell death has become a controversial topic. Many molecular events described in the last decade tend to show an interaction of VDAC isoforms with anti- and pro-apoptotic molecules, implying a role of VDAC in apoptotic cell death. Several proteins from the Bcl<sub>2</sub> family have been co-immunoprecipitated with VDAC isoforms, such as Bax, Bak, Bcl<sub>2</sub>, Bcl-x<sub>L</sub> and Bim (Lawnen *et al.*, 2003; Shoshan-Barmatz *et al.*, 2006). More particularly, anti-apoptotic molecules have been linked to an “open state” (high conductance) of VDAC, while pro-apoptotic molecules have been linked to a “closed state” (low conductance). For example, the anti-apoptotic molecule Bcl-x<sub>L</sub> was shown to promote the VDAC “open state” configuration and prevent the low conductance configuration, allowing passage of metabolites between both the cytoplasm and the mitochondrial intermembrane space, as observed in the normal, healthy cellular state (Vander-Heinden *et al.*, 2001). Pro-apoptotic molecules, such as Bax, Bak and truncated Bid (tBid) have been shown to interact with VDAC (reviewed in Shoshan-Barmatz *et al.*, 2006). For example, Bax is thought to oligomerise with tBid molecules to form a pore on the OMM, mediating cytochrome c release. The interaction between VDAC and Bax is thought to be a trigger for this pore formation, although whether VDAC is physically part of this pore still remains to be elucidated (Tsujimoto and Shimizu, 2002; Shoshan-Barmatz *et al.*, 2006). Baines and colleagues (2007), using multiple VDAC knockdowns, have postulated that these channels were dispensable for apoptosis to happen. Indeed, using a double knockdown (VDAC1/3<sup>(-/-)</sup>) and VDAC2 siRNA (silenced gene), they showed that STS-induced apoptosis still occurred, denying the role of VDAC in the apoptotic process. Nevertheless, the VDAC1/3<sup>(-/-)</sup> knockdown, with or without VDAC2 siRNA, seemed to be more sensitive to STS-induced toxicity than controls; showing that VDAC isoforms may have more an anti-apoptotic role than a pro-apoptotic role in their model. More recently,

Tomasello *et al.* (2009) have concentrated on the VDAC1 isoform in a combination of knockdown and overexpression studies. Overexpression of VDAC1 led to mitochondrial potential collapse, which could be inhibited by specific inhibitors of (a) the potential transition pore (cyclosporine A), (b) ROS production (N-acetyl-cysteine, NAC) and (c) apoptosis (Bcl<sub>2</sub>); however, a broad caspase inhibitor had no effects. Down-regulation of VDAC1 slowed cell growth and decreased ATP production but it was evident that VDAC1 was a dispensable element for cell survival. They also showed that both knock down and overexpression of VDAC1 had no effect on STS-induced toxicity. ROS-induced toxicity, using selenium as an inducer of oxidative stress, was increased by overexpression of VDAC1 but cell death was unaffected by knocking down VDAC. Although there are still discrepancies on the specific molecular events involving VDAC, and more particularly VDAC1, in apoptosis, it seems clear that the porin has a role in at least some models of induced apoptotic cell death.

As noted by Tomasello *et al.* (2009), the mitochondrial transition pore has been linked to cell death-induced by VDAC overexpression. Indeed, whether or not VDAC is part of the transition pore has been debated over the past few years. One of the reasons VDAC was originally thought to be part of the transition pore was the characteristics they shared (reviewed in Shoshan-Barmatz *et al.*, 2006). They were enriched at contact sites between the IMM and OMM; they immunoprecipitated with ANT and cyclophylin D (also thought to be part of the transition pore); their voltage dependence, conductance and pore size were similar; they both had a role in apoptosis, were inhibited by NADH and were dependent on calcium concentrations. Moreover, anti-human VDAC1 antibodies have been shown to block the mitochondrial potential collapse and pore opening (Shimizu *et al.*, 2001). Nevertheless, Baines *et al.*'s work (2007) has opened new questions about the potential role of VDAC in the transition pore and, although VDAC is thought to have a role in some death models in pore forming, it might not form the pore itself (reviewed in Halestrap, 2009). Interestingly, it has recently been shown that Bax interacts with not only VDAC but also with the translocase of the OMM (TOM complex) (Ott *et al.*, 2009). This re-enforced the observation that VDAC knock down cells express higher levels of the TOM complex protein TOM40; suggesting that the TOM complex can have some roles that are similar to VDAC (Antos *et al.*, 2001; Kmita *et al.*, 2004).

### 6.1.1.3 The role of VDAC in glycolysis

The mitochondrial porin has been shown to also have a role in cell survival via its role in glucose metabolism. Indeed, HK has been found to bind VDAC1 and this interaction is thought to occur to facilitate the access of the enzyme to ATP being produced via the ETC, and this would lead to increased glycolysis and oxidative phosphorylation (Golshani-Hebroni and Bessman, 1997). Binding of HK to VDAC is inhibited by changing glutamate 72 of the VDAC1 sequence to glutamine (Zaid *et al.*, 2005). Phosphorylation of VDAC1 by GSK-3 $\beta$  potentiates cell death accompanied with mitochondrial swelling, cytochrome c release and mitochondrial permeability transition (Rostovtseva and Berzrukov, 2008) with evidence of pro-apoptotic molecules (e.g. Bax) binding to VDAC1 instead of HK, at the same binding site (Anflous-Pharayas *et al.*, 2007).

## 6.1.2 Electron transfer chain inhibitors

As noted earlier (refer to section 1.1), complex I of the ETC was observed to be decreased in PD patients (Brazilai and Mehamed, 2003). Moreover, the ETC was also observed to be impaired in other neurodegenerative conditions; for example, impairment of complex II was observed in Huntington's disease (HD) patients (Perez de la Cruz and Santamaria, 2007) and impairment of complex IV was observed in some models of Alzheimer's disease (AD) (Atamna and Frey, 2007). Whether impairment of the electron transfer chain complexes are causes or consequences of neurodegenerative diseases has not yet been resolved; however, they are common biochemical characteristics that might lead to other features which are common in neurodegenerative conditions. This could be related to the fact that all complex inhibition lead to ATP depletion and ROS production (Casarino and Bennett, 1999; Coles *et al.*, 1979; Han *et al.*, 2008a; Szabados *et al.*, 2004).

### 6.1.2.1 Rotenone: a complex I inhibitor

Similarly to MPP<sup>+</sup>, rotenone has been widely used in research to study the molecular events in PD (Zhou *et al.*, 2004). Rotenone is a well known selective inhibitor of complex I that was shown to induce progressive degeneration of nigrostriatal neurons and glial cells in rats (Bové *et al.*, 2005). Different experimental models showed that it produced Lewy body-like

cytoplasmic inclusions in the remaining dopaminergic neurons and rotenone-induced toxicity led to aggregation of ubiquitin and  $\alpha$ -synuclein in dopaminergic neuroblastoma cells (Zhou *et al.*, 2004; Diaz-corrales *et al.*, 2005).

#### 6.1.2.2 3-nitropropionic acid: a complex II inhibitor

3-nitropropionic acid (3-NP) was originally found to cause degeneration of the putamen and caudate nucleus associated with severe neurological symptoms in humans. Moreover, 3-NP has been widely used in the study of HD as its effects on animals showed similar biochemical and behavioural features to the disease (reviewed in Brouillet *et al.*, 2005). 3-NP toxicity was shown to occur via irreversible inhibition of SDH, also known as complex II (Coles *et al.*, 1979), which causes the inhibition of the Krebs cycle in addition to inhibition of the electron transfer.

#### 6.1.2.3 Antimycin A: a complex III inhibitor

Antimycin A is a complex III inhibitor, more specifically the electron transfer between cytochrome b and cytochrome  $c_1$  (Izzo *et al.*, 1978). The direct consequences of antimycin A toxicity in cultured cells were the usual effects due to ETC inhibition (increase in ROS production and ATP depletion) accompanied with collapse of mitochondrial potential, leading to apoptotic cell death (Han *et al.*, 2008a).

#### 6.1.2.4 Sodium azide: a complex IV inhibitor

Sodium azide has been shown to cause degeneration of cortical and hippocampal areas in rats (Cada *et al.*, 1995); moreover, Bennet *et al.* (1992) showed that it led to learning memory deficit in rats. Sodium azide is a widely used complex IV inhibitor for the study of AD (Szabados *et al.*, 2004). The specific molecular events consequent to sodium azide treatment in animal models are chemical hypoxia (Reviewed in Szabados *et al.*, 2004).

### 6.1.3 Aims of the chapter

VDAC1 protein level was previously observed to increase by 3-fold following treatment with sub-cytotoxic concentrations of MPTP (1 mM for 24 hours, refer to section 5.2.1). VDAC1 has been found to have various roles in energy consumption, cell metabolism and cell survival (reviewed in Vyssokikh and Brdiczka, 2003), regulated mainly by phosphorylation (Hajnoczsky *et al.*, 2002, Das *et al.*, 2008; Schwertz *et al.*, 2007); and a variation in protein levels may underline an important process involved in the molecular events preceding cell death observed in PD.

The overall objective of this chapter was to further characterise VDAC1 upregulation occurring prior to cell death following inhibition of the ETC.

The first aim was to check whether other sub-cytotoxic concentrations of MPTP led to changes in VDAC levels. Secondly, since MPTP causes inhibition of complex I, via its metabolite MPP<sup>+</sup>, the effects of another complex I inhibitor (rotenone) and inhibitors of other complexes (3-NP, antimycin A and sodium azide) on VDAC1 levels were also investigated.

In an attempt to explain how VDAC1 protein levels were upregulated, and more particularly, whether it was due to increased gene expression, another aim was to measure levels of VDAC1 mRNA following a range of sub-cytotoxic treatments with various complex inhibitors.

A final aim was to investigate the phosphorylation status of VDAC1 following treatment with 1 mM MPTP. This hopefully would give some insights into the signaling status of the cells and VDAC1 upregulation, whether in favour of cell death or cell survival.

## 6.2 RESULTS

### 6.2.1 Effects of neurotoxins on VDAC expression

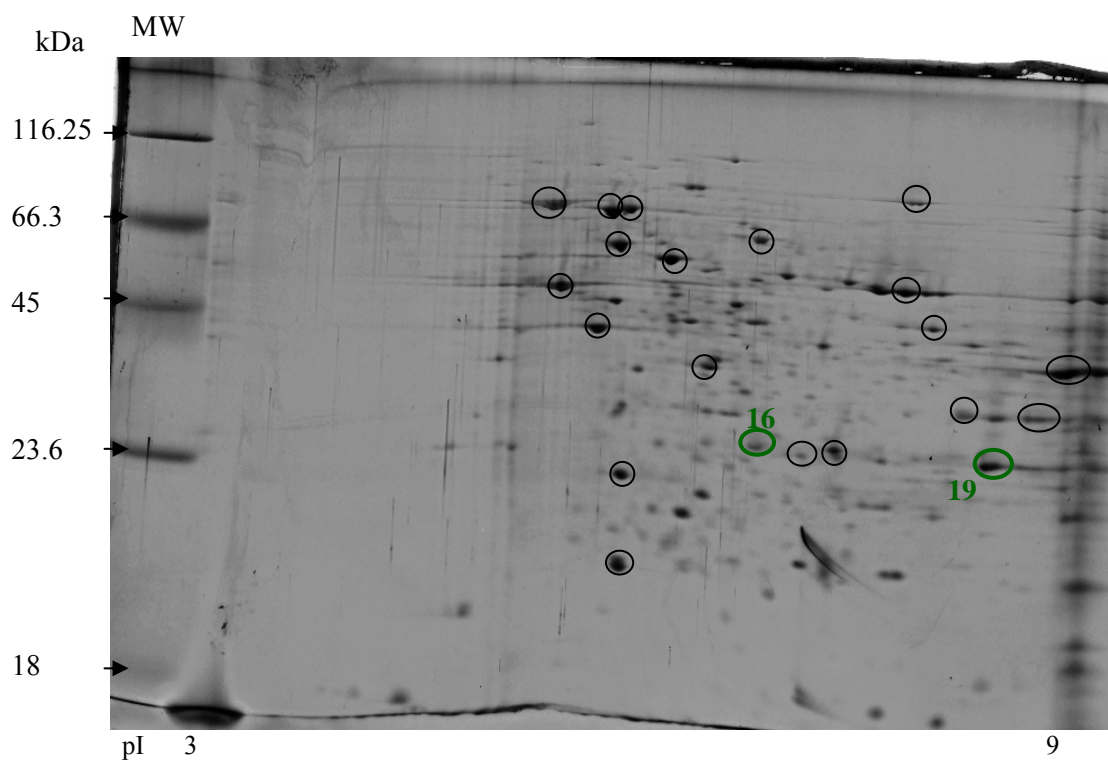
#### 6.2.1.1 Identification of VDAC1 from 2DE using MALDI-TOF mass spectrometry

Figure 6.2 shows a typical 2DE profile and the location of two identified isoforms of VDAC (spots 16 and 19). Figure 6.3A shows a typical mass spectrum obtained using MALDI-TOF analysis of tryptic fragments of spot 19. The mass list from the spectrum was transferred to the Mascot database and a significant positive identification was obtained as VDAC1 (figure 6.3B). The peptides covered 81 % of the sequence matched (compared to VDAC1\_MOUSE sequence from SwissProt database in <http://www.uniprot.org>), which is a large coverage and the score of 215 was highly significant (score > 54). Moreover, this spot was identified 12 times using peptide mass fingerprinting using different 2DE, confirming the identification. It is worth noting that the Mascot database sequence to which the peptide list was compared corresponded to the splice-variant containing 13 extra amino acids. The VDAC1 protein found *in vivo* in the OMM was found to lack these 13 amino acids as previously explained.

#### 6.2.1.2 Concentration and time-dependent MPTP effects on VDAC levels

Figure 6.4 shows that VDAC1 levels, monitored using an anti-VDAC1-specific antibody, increased following 24 hours exposure to MPTP in a dose-dependent manner. Because only one replicate is shown here, no statistical analysis could be undertaken, but VDAC1 levels increased with the lowest MPTP concentration used (10  $\mu$ M).

Increases in VDAC1 levels were also time-dependent, with some increase evident following 8 hours exposure to 1 mM MPTP, becoming significant at 24 hours (figure 6.5). Overall, the increase in VDAC1 levels following 1 mM MPTP treatment, normalised for total protein loading, was around 3-fold (300 %), in agreement with data shown previously (section 5.2.1.4 figure 5.7; n=7).

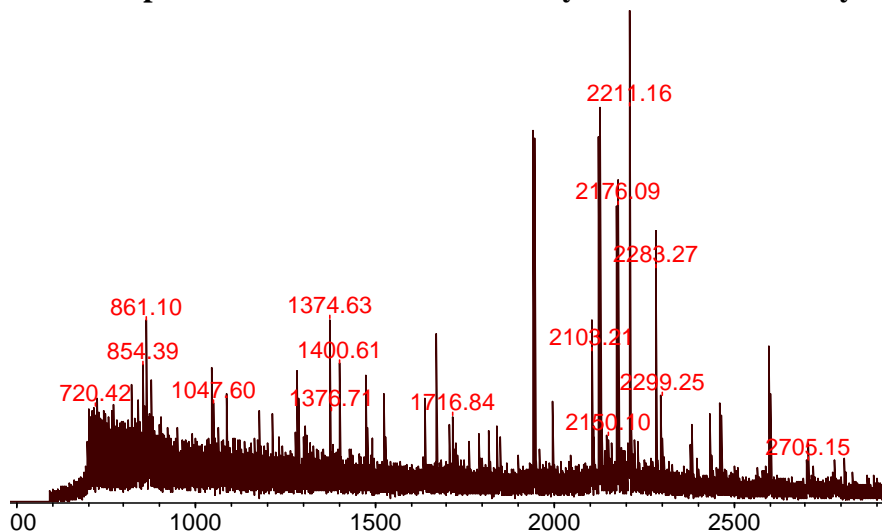


**Figure 6.2: 2D-gel electrophoretogram (pI 3-10) stained with SyproRuby showing spots identified as VDAC isoforms following peptide mass fingerprinting**

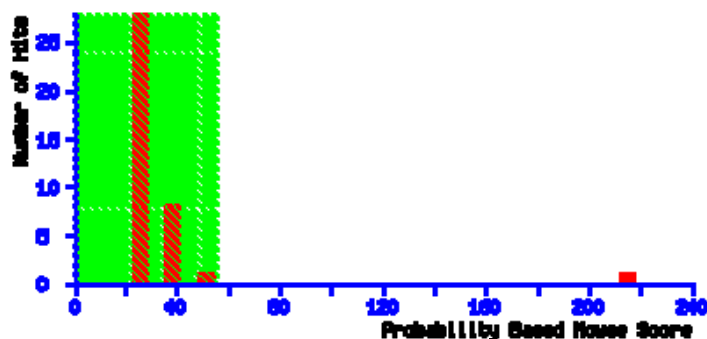
Mouse N2a neuroblastomas were differentiated for 16 hours in serum free medium supplemented with 0.3 mM dbcAMP. Following incubation, cells were treated with 1 mM MPTP or not (controls) for 24 hours. Subcellular fractionation was then carried out. 50  $\mu$ g proteins from mitochondrial fraction for each treatment were fractionated by 2DE (pI 3-10 strips and 12 % resolving gel) and visualized using SyproRuby. Spots were picked, trypsinised, followed by MALDI-TOF mass spectrometry and attempts made to identify spots using Mascot database (<http://www.matrixscience.com>). Circled spots were previously identified (refer to chapter III figure 3.12 and table 3.2).

**Green circled spots:** 16. Voltage-dependent-anion channel protein 2 (VDAC2); 32 kDa, pI 7.44  
19. Voltage-dependent-anion channel 1 (VDAC1); 30 kDa, pI 8.62

### A. Mass spectrum of VDAC1 obtained by MALDI-TOF analysis



### B. Mascot database results for VDAC identification



VDAC1\_MOUSE Score: **215** Expect:  $5.1e-18$

Voltage-dependent anion-selective channel protein 1 OS=Mus musculus

Nominal mass ( $M_r$ ): 32502; Calculated pI value: 8.55

### C. Sequence coverage of peptide mass list for VDAC1 identification

Number of mass values matched: **19**

Sequence Coverage: **81%**

```

1  MCSFFLVLLL WQNMAVPPTY ADLGKSARDV FTKGYGFGLI KLDLTKSEN
51 GLEFTSSGSA NTETTKVNGS LETKYRWTEY GLTFTEKWNT DNTLGTEITV
101 EDQLARGLKL TFDSSFSPNT GKKNAKIKTG YKREHINLGC DVDFDIAGPS
151 IRGALVLGYE GWLAGYQMNF ETSKSRVTQS NFAVGKYTDE FQLHTNVNDG
201 TEFGGSIYQK VNKKLETAVN LAWTAGNSNT RFGIAAKYQV DPDACFSAKV
251 NNSSLIGLGY TQTLKPGIKL TLSALLDGKN VNAGGHKLGL GLEFQA

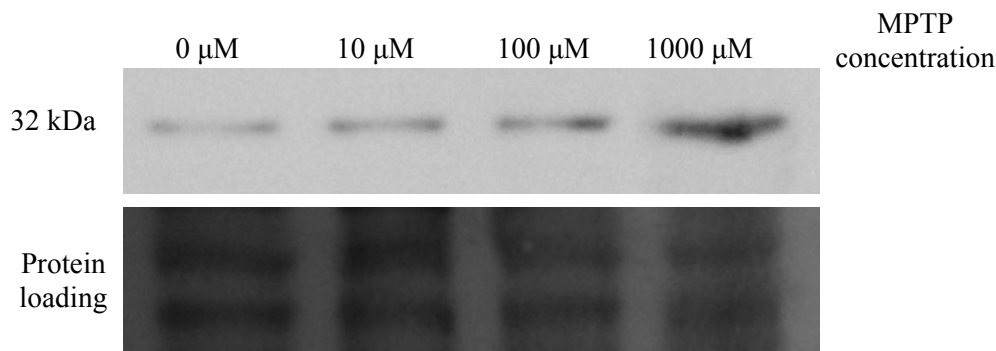
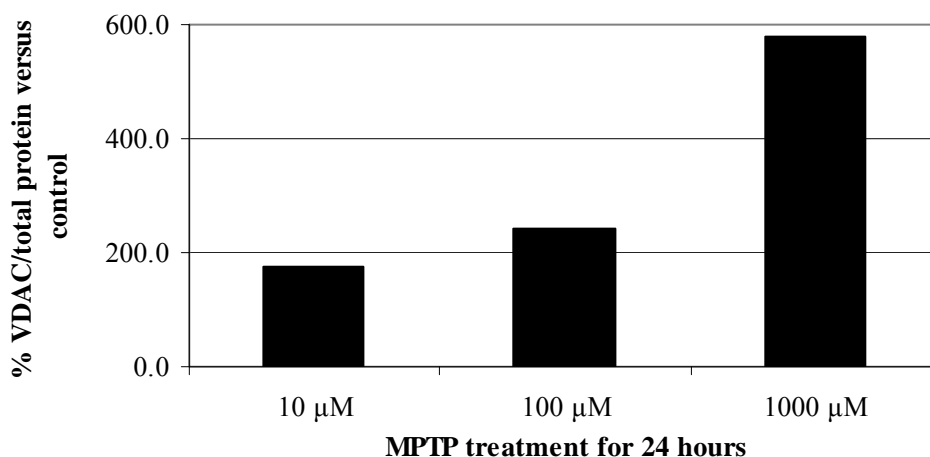
```

### Figure 6.3: MALDI-TOF analysis and protein identification of VDAC1 spot

Spot 19 (figure 6.2) from a silver stained 2DE of mitochondrial samples was picked, trypsinised and processed via MALDI-TOF mass spectrometry. The peptide mass list obtained was transferred to the Mascot database and one spot was identified as VDAC1.

A. Mass spectrum obtained by MALDI-TOF.

B. Identity probability of VDAC1. C. VDAC1 sequence and coverage of peptides from the spectrum. *Italic amino acid sequence*: 13 amino acids thought to be absent in the mitochondrial VDAC1 found *in vivo*.

**A. Concentration-dependent MPTP effects on VDAC1 levels detected on 1D blots****B. Quantification of concentration-dependent MPTP effects on VDAC1 levels****Figure 6.4: VDAC1 protein expression following exposure to different MPTP concentrations for 24 hours**

Mouse N2a neuroblastomas were differentiated for 16 hours in serum free medium supplemented with 0.3 mM dbcAMP. Following incubation, cells were treated with different concentrations (0 to 1 mM) MPTP for 24 hours. Subcellular fractionation was then carried out.

A. 20  $\mu\text{g}$  protein from mitochondrial fractions for each treatment were fractionated by 1D-SDS-PAGE (12 % resolving gel) and then transferred onto a nitrocellulose membrane. Blots were stained with copper (refer to section 2.2.6.1) to check for protein loading before probing with anti-VDAC antibody (1 in 1,000 dilution) followed by the ECL detection procedure (refer to section 2.2.6.2).

B. Densitometry of each band was quantified using Aida software. Each band was compared to total protein. The histogram bars represents % VDAC / total protein ratio versus controls ( $n = 1$ ).

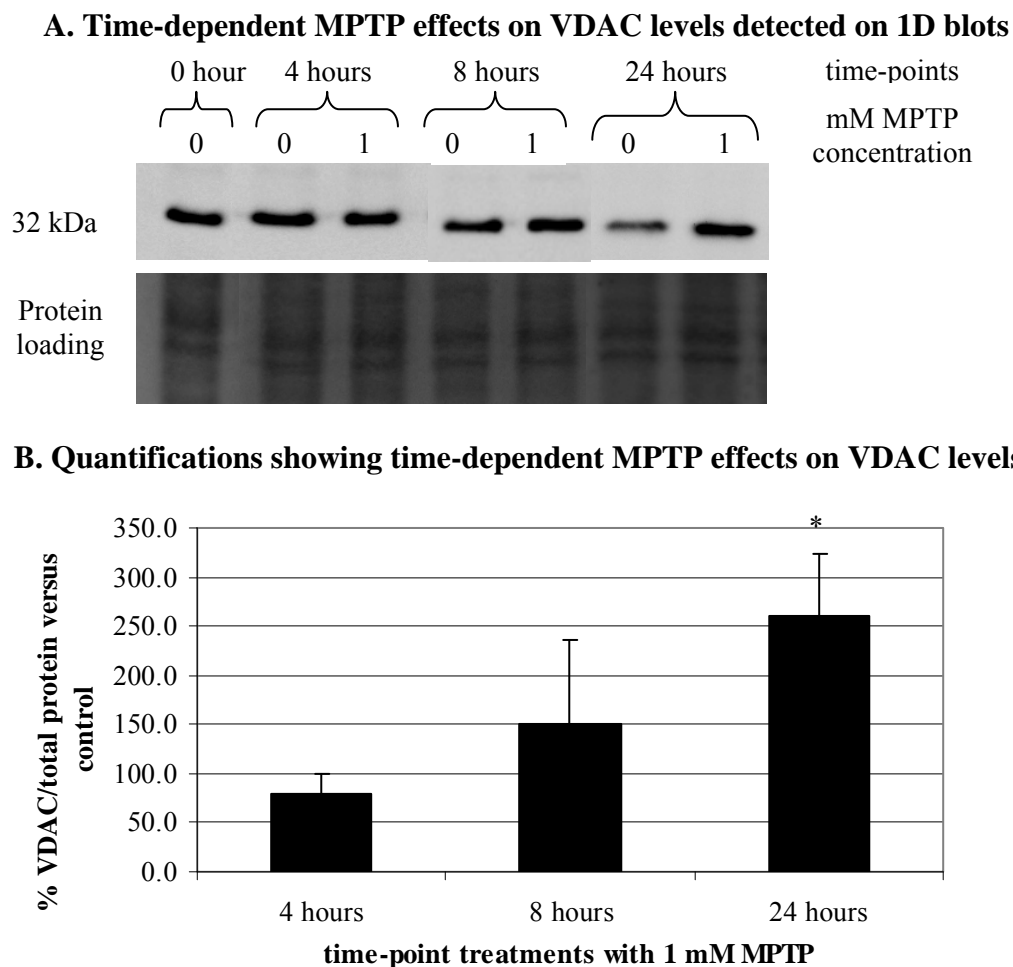


**Figure 6.5: VDAC protein expression following exposure to 1 mM MPTP treatment over 24 hour time-course**

Mouse N2a neuroblastoma cells were differentiated for 16 hours in serum free medium supplemented with 0.3 mM dbcAMP. Following incubation, cells were treated with 1 mM MPTP over a 24 hour time-course. Subcellular fractionation was then carried out.

A. 20  $\mu$ g protein from mitochondrial fractions for each treatment were fractionated by 1D-SDS-PAGE (12 % resolving gel) and then transferred onto a nitrocellulose membrane. Blots were stained with copper (refer to section 2.2.6.1) to check for protein loading before probing with anti-VDAC1 antibody (1 in 1,000 dilution) followed by the ECL detection procedure (refer to section 2.2.6.2).

B. Densitometry of each band was quantified using Aida software. Each band was compared to total protein. The histogram bars represents % VDAC / total protein ratio versus controls  $\pm$  SEM. All \* values  $p < 0.05$  when compared to respective controls. (n = 3).

### 6.2.1.3 Effects of other complex inhibitors on VDAC protein levels

In order to investigate whether or not the effect of MPTP on VDAC1 levels was specific to complex I inhibition, the effects of other complex inhibitors were analysed.

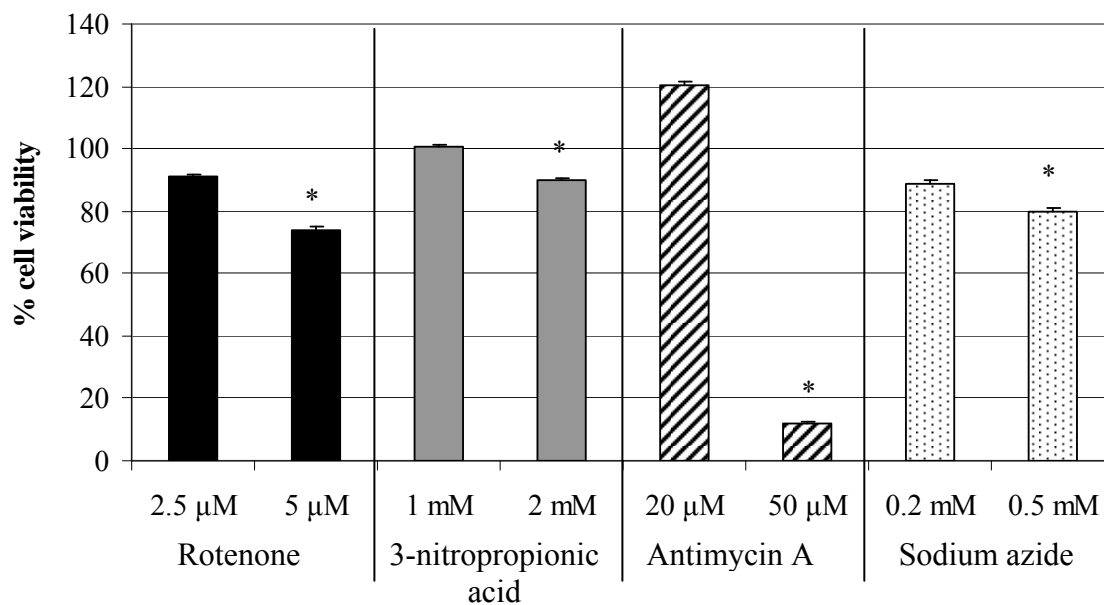
Sub-cytotoxic concentrations of different complex inhibitors were first established by analysing cell viability using a range of inhibitor concentrations. Figure 6.6 shows the highest concentration tolerated without cell death (sub-cytotoxic) and the minimum concentration leading to cell death (cytotoxic). The sub-cytotoxic concentrations, following 24 hour exposure, used for further analyses were 2.5  $\mu$ M for rotenone, 1 mM for 3-NP, 20  $\mu$ M for antimycin A and 0.2 mM for sodium azide; inhibiting complexes I, II, III and IV of the electron transfer chain, respectively.

Using these sub-cytotoxic concentrations, the effects of each complex inhibitor on VDAC1 protein levels were investigated using a western blot approach (figure 6.7). All inhibitors resulted in a mean increase in VDAC1 protein levels, statistically significant with MPTP, in agreement with previous data, and with rotenone. 3-NP and sodium azide did not show significant effects on VDAC1 levels following MPTP treatment since only duplicates were analysed, although both replicates showed an increase. With antimycin A, one of the duplicates showed upregulation of VDAC1 protein levels, while the second showed no effect (figure 6.7B).

### 6.2.1.4 VDAC1 mRNA expression

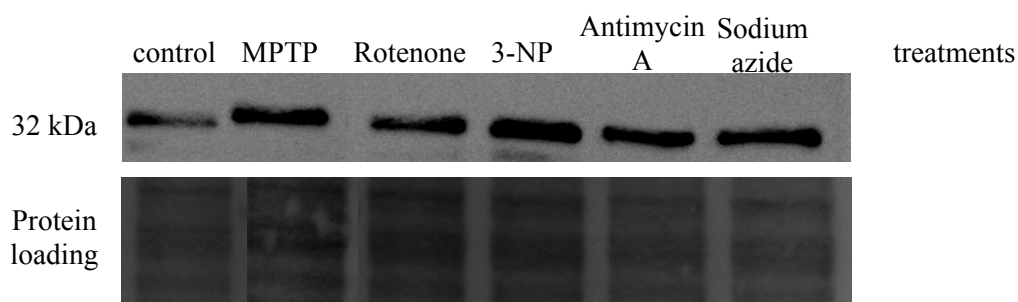
As VDAC1 protein levels were shown to be increased, it was interesting to investigate whether this was due to increased transcription.

First, semi-quantitative RT-PCR was carried out, using GAPDH as a housekeeping gene. Mouse VDAC1- and GAPDH-specific primers were used to amplify gene transcripts in control and MPTP treated mouse N2a neuroblastoma cells (Figure 6.8A). Quantification of PCR products using the AIDA software (figure 6.8B) revealed a 30 % increase in VDAC1 mRNA levels following MPTP treatment; however this was not significant using a paired t-test. Nevertheless, the probability was approaching significance ( $p = 0.06$ ;  $n = 5$ ).



**Figure 6.6: Sub-cytotoxic and cytotoxic concentrations of various complex inhibitors measured by MTT reduction assay**

Mouse N2a neuroblastoma cells were differentiated for 16 hours in serum-free medium supplemented with 0.3 mM dbcAMP. Following incubation, cells were treated with different concentrations (0 to 5 mM) of complex inhibitors for 24 hours. MTT reduction assay was then performed. Sub-cytotoxic and cytotoxic concentrations are shown. All \* values  $p < 0.05$  when compared to respective controls using a paired t-test. ( $n = 7$ ).

**A. Effects of complex inhibitors on VDAC1 protein levels****B. VDAC1 protein levels following treatments with complex inhibitors**

Inhibitors	Sample 1	Sample 2	Sample 3	Average	Range of variation
1 mM MPTP	245	159	154	186 *	+ 59; - 32
2.5 $\mu$ M rotenone	179	117	187	161 *	+ 26; - 44
1 mM 3-NP	363	201		282	+/- 81
20 $\mu$ M antimycin A	216	100		158	+/- 58
0.2 mM sodium azide	260	128		194	+/- 66

**Figure 6.7: Effects of subcytotoxic concentrations of complex inhibitors on VDAC1 protein levels using western blot analysis**

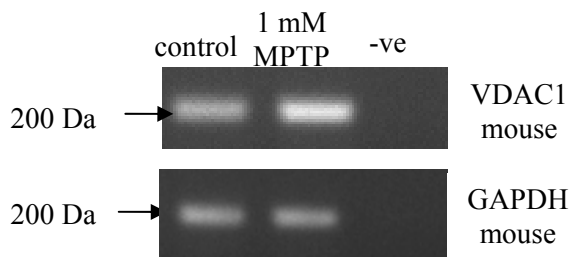
Mouse N2a neuroblastoma cells were differentiated for 16 hours in serum-free medium supplemented with 0.3 mM dbcAMP prior to treatment with sub-cytotoxic concentrations of various electron transfer inhibitors for 24 hours. Subcellular fractionation was then carried out to isolate mitochondria.

A. 20  $\mu$ g protein from mitochondrial fractions for each treatment were fractionated by 1D-SDS-PAGE (12 % resolving gel) and then transferred onto a nitrocellulose membrane. Blots were stained with copper (refer to section 2.2.6.1) to check for protein loading before probing with anti-VDAC1 antibody (1 in 1,000 dilution) followed by the ECL detection procedure (refer to section 2.2.6.2).

B. Table representing densitometry data showing the % VDAC1 / total protein ratio compared to controls. All \* values  $p \leq 0.05$  when compared to respective controls using a paired t-test. (n = 3).

3-NP: 3-nitropropionic acid.

### A. Effects of MPTP on VDAC1 mRNA expression using semi-quantitative RT-PCR



### B. Quantification of VDAC1 mRNA expression using semi-quantitative RT-PCR

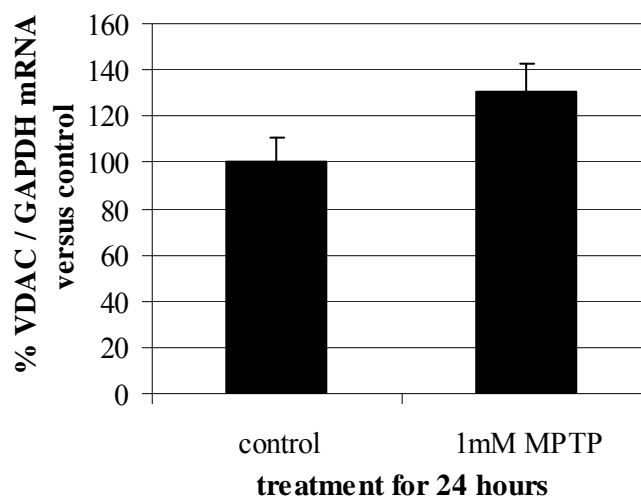


**Figure 6.8: Effects of 1 mM MPTP for 24 hours VDAC1 mRNA expression as measured by semi-quantitative RT-PCR**

Mouse N2a neuroblastoma cells were differentiated for 16 hours in serum-free medium supplemented with 0.3 mM dbcAMP. Following incubation, cells were treated with 1 mM MPTP for 24 hours. mRNA was then extracted and reverse transcribed to cDNA. Using VDAC and GAPDH specific primers, cDNA amplicons were amplified. PCR products were electrophoresed onto an agarose gel and visualized with U.V. light. A. Pictures were taken and B. bands were quantified using the AIDA software. % VDAC / GAPDH intensities ratios were calculated, compared to controls. All \* values  $p < 0.05$  when compared to respective controls. (n = 5).  
 -ve: negative control (primer mix with no DNA in the PCR mixture).

Thus, real-time PCR was used to provide more accurate estimates of mRNA levels (see section 2.2.14 for detailed information). Standards for each gene were used in order to quantify the exact number of mRNA copies in each sample, normalised against numbers of GAPDH mRNA copies. VDAC1 and GAPDH cDNA inserts were prepared, cloned, amplified, purified and serial dilutions were prepared to give standards with known copy number. Figure 6.9 shows an example of the results for VDAC1 standards.

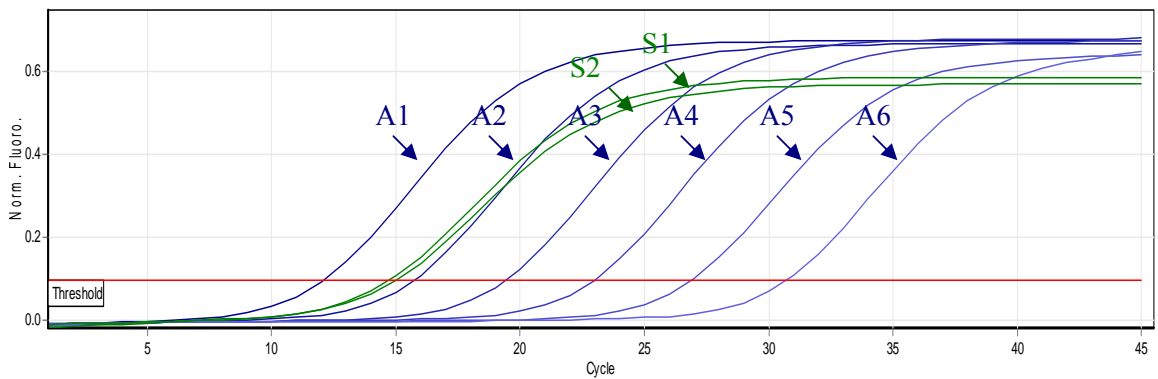
From the real-time PCR profile (figure 6.9A), the cycle number for the threshold value (Ct) was provided and used to compile a standard calibration of Ct versus concentration (figure 6.9B), used to then calculate copy numbers in unknown samples (figure 6.9C). VDAC1 mRNA was expressed as ratio of molecules VDAC1 mRNA per 1,000 molecules GAPDH mRNA. Figure 6.10 shows the average ratios for each sample. No significant differences were observed following 1 mM MPTP treatment over a 24 hour time-course compared to respective controls (figure 6.10A). Similarly, no significant differences were observed in samples treated with sub-cytotoxic concentrations of the other complex inhibitors following 24 hour treatments (rotenone, 3-NP, antimycin A and sodium azide) (figure 6.10B).

## **6.2.2 VDAC post-translational modifications**

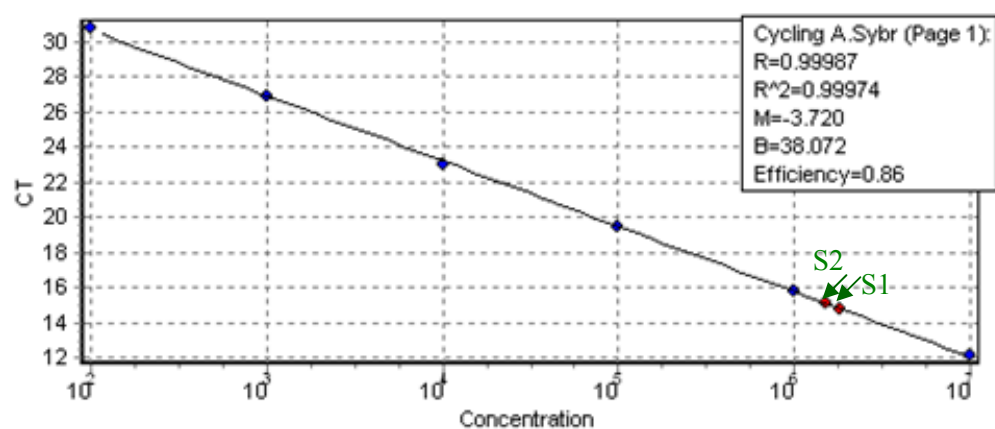
### **6.2.2.1 Multiple forms of VDAC1 identified on 2D-western blot analysis**

Using 2D-blot analysis, multiple forms were detected by the anti-VDAC1 antibody (refer to figure 5.7). Figure 6.11 shows different replicates of pairs of MPTP treated and respective control samples electrophoresed, transferred to membrane and immunoprobed in parallel. In the pI 3-10 analysis, detection of VDAC1 forms was variable between replicates (figure 6.11A). Despite the variability, the overall intensity increased following 1 mM MPTP treatment for 24 hours. Moreover, two to three small spots seemed to appear with an acidic shift and the intensity of the trail on the basic side of the main spot also increased consistently following MPTP exposure.

### A. Real-time PCR graph results for VDAC1 mRNA standard quantitation



### B. Standard calibration for VDAC1 mRNA expression analysis



### C. Raw data from the standard calibration for VDAC1 mRNA expression analysis

No.	Type	Ct	Given Conc (copies/reaction)	Calc Conc (copies/reaction)	% Var
A1	Standard	12.13	10,000,000.00	9,429,756	5.70%
A2	Standard	15.76	1,000,000.00	996,254	0.40%
A3	Standard	19.43	100,000.00	102,470	2.50%
A4	Standard	23.00	10,000.00	11,261	12.60%
A5	Standard	26.92	1,000.00	998	0.20%
A6	Standard	31.76	100	92	7.60%
S1	24h control	15.07		1,531,103	
S2	24h MPTP	14.79		1,818,193	

**Figure 6.9: Example of quantitative analysis of VDAC1 mRNA expression using real-time PCR**

VDAC1 PCR products were cloned into the pCR2.1 vector followed by transformation into TOP10 *E.coli*. Following amplification of the plasmid, the DNA fragment was extracted, purified and linearised. Different dilutions were prepared prior to analysis by real-time PCR (refer to sections 2.2.14.2-4).

A. real-time PCR results using the Rotor-gene 6000 series software. Red line: threshold automatically calculated by the software. The no. cycles of each standard at the threshold are called Ct values for each sample.

B. Standard calibration for VDAC1 standards of Ct values against dilutions (copies / reaction).

C. Table showing the raw data for each standard value and two examples of samples.

Conc: concentration; Var: variation

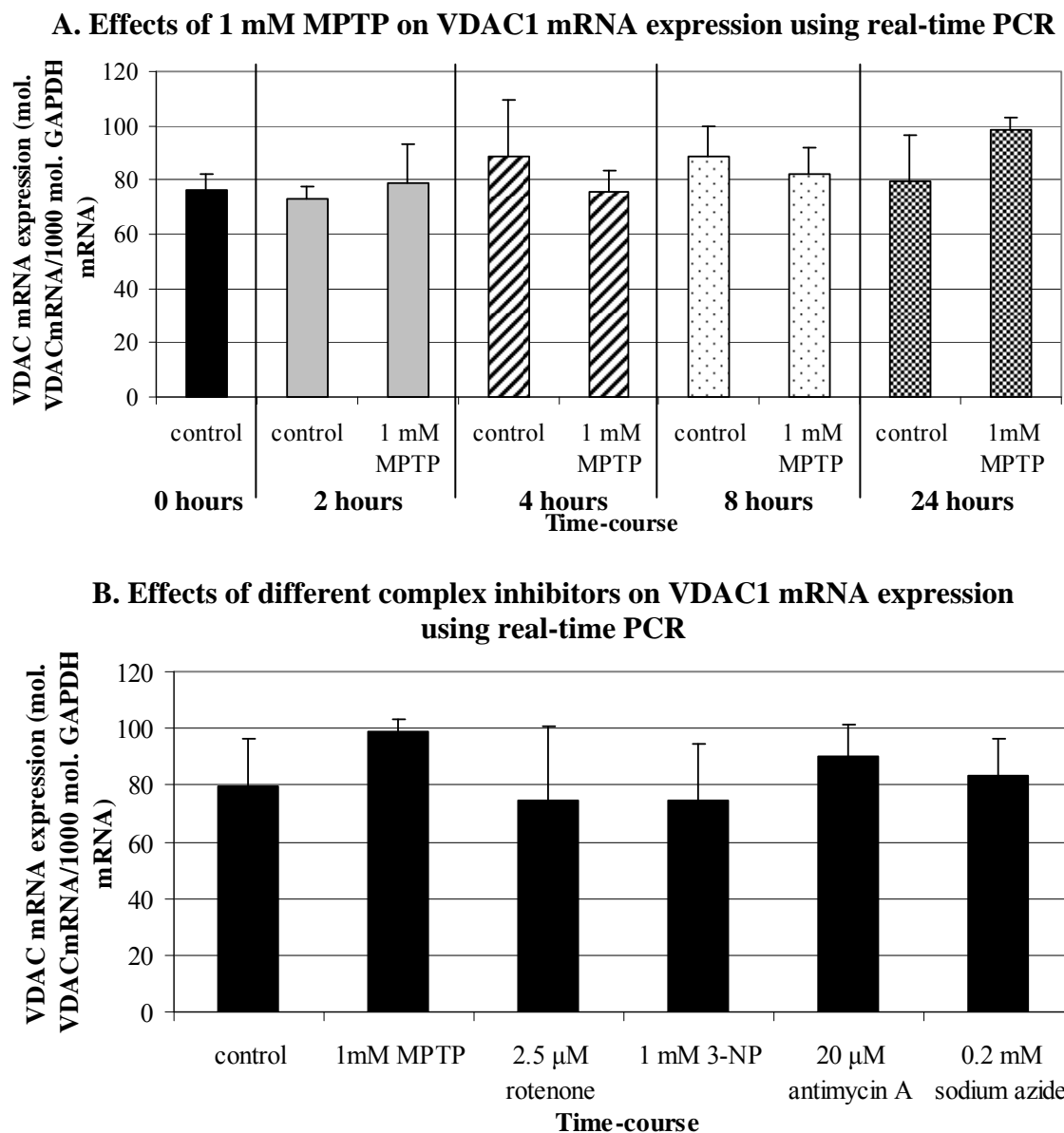


**Figure 6.10: Effects of electron transfer inhibitors on VDAC1 mRNA expression as measured by real-time PCR**

Mouse N2a neuroblastomas were differentiated for 16 hours in serum-free medium supplemented with 0.3 mM dbcAMP. Following incubation, cells were treated with 1 mM MPTP for up to 24 hours (A) or with other complex inhibitors for 24 hours (B). mRNA were then extracted and reverse transcribed to cDNA. Using VDAC1 and GAPDH specific primers, cDNA amplicons were amplified using real-time PCR. Relative amount of VDAC1 and GAPDH amplicons could be calculated by comparing to a standard calibration for each gene (figure 6.8). The data are expressed as molecules VDAC1 mRNA / 1,000 molecules GAPDH mRNA ratios  $\pm$  SEM and each was compared to respective control. All \* values  $p < 0.05$  when compared to respective controls. (n = 3 each run twice independently). 3-NP: 3-nitropropionic acid.

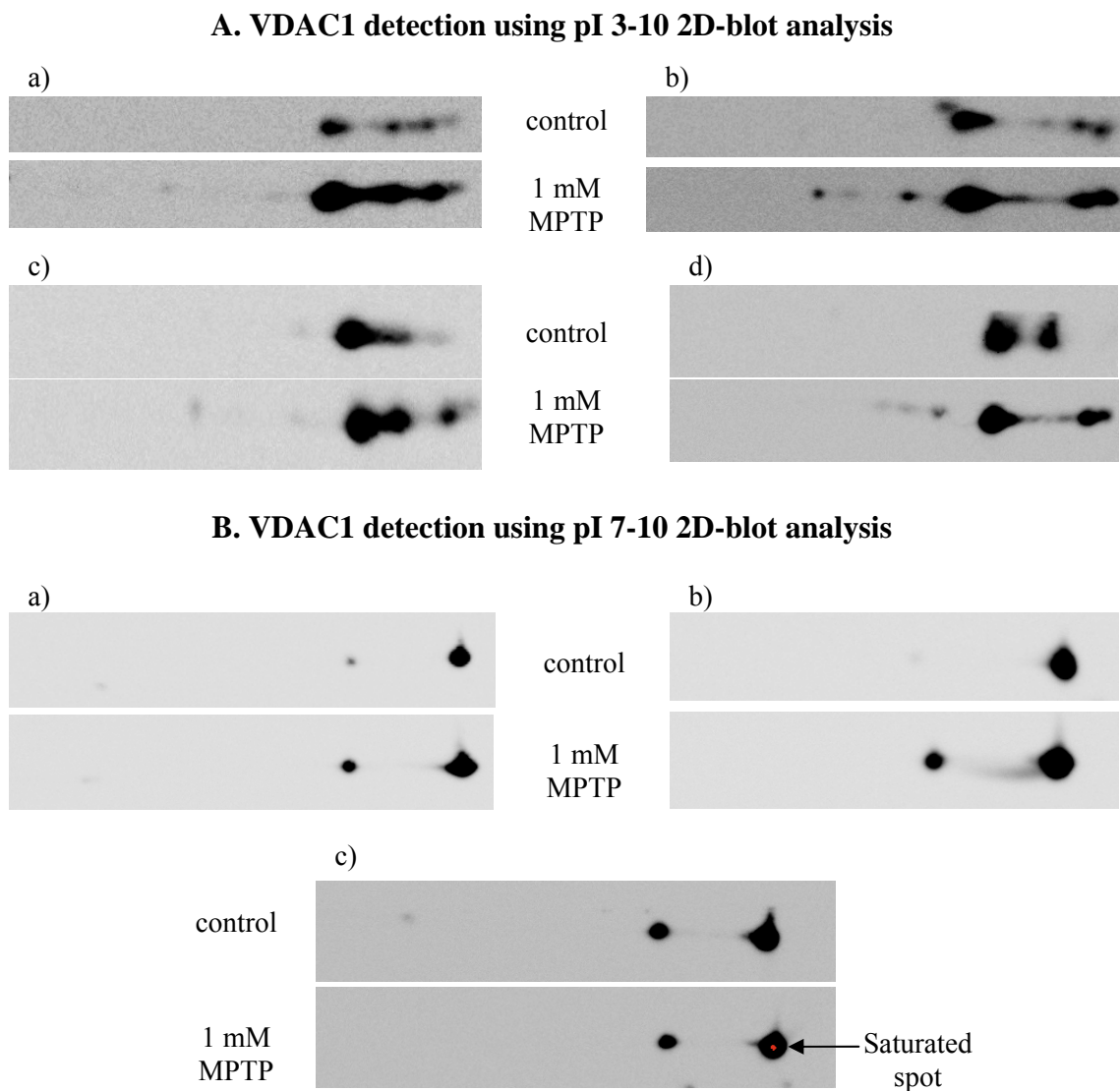


**Figure 6.11: Detection of VDAC1 isoforms on 2D-blot analysis using pI 3-10 and pI 7-10 strips**

Mouse N2a neuroblastomas were differentiated for 16 hours in serum free medium supplemented with 0.3 mM dbcAMP. Following incubation, cells were treated with 1 mM MPTP for 24 hours. Subcellular fractionation was then carried out. 50  $\mu$ g protein from mitochondrial fractions for each treatment were fractionated by 2DE (12 % resolving gel) with A. pI 3-10 IPG strips (n = 4) and B. pI 7-10 IPG strips (n = 3) and then transferred onto a nitrocellulose membrane. Blots were stained with copper (refer to section 2.2.6.1) to check for protein loading before probing with anti-VDAC antibody (1 in 1,000 dilution) followed by the ECL detection procedure (refer to section 2.2.6.2).

Further analysis of these different spots was attempted using a more focused pI range (pI 7-10) for 2D blot analysis. Figure 6.11B shows that only 2 forms were observed compared to the multiple spots detected with the same antibody using pI 3-10 IPG strips. Total VDAC detection using pI 7-10 strips consistently increased following 1 mM MPTP treatment.

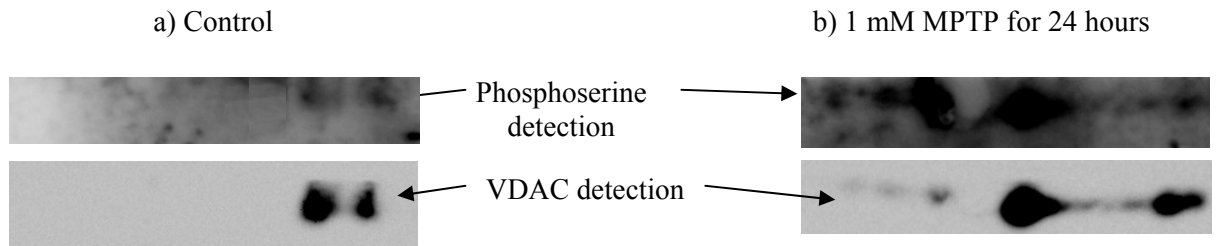
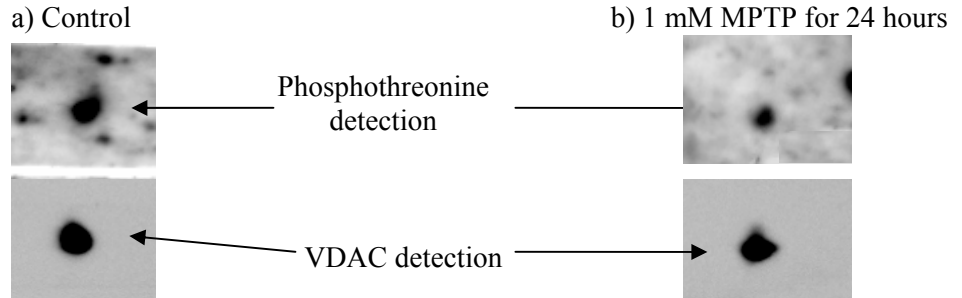
#### 6.2.2.2 Serine phosphorylation of VDAC1 increased following MPTP treatment

Following the observation that several spots were detected by the anti-VDAC1 antibody using 2D-blot analysis, it was hypothesized that these forms might be, at least in part, due to post-translational modifications. Anti-phospho-specific antibodies were then used to observe whether phosphorylated forms would co-localise with spots detected with the anti-VDAC1 antibody.

Figure 6.12A shows an electrophoretogram of 1 mM MPTP treated cells and controls blotted onto a membrane and probed with an anti-phosphoserine antibody. As before (section 5.2.2.1), background staining was high in these blots. However, two faint spots were detected in the controls. More intense spots were detected following MPTP treatment with the apparition of one or two more spots with an acidic shift. The same membranes were stripped to remove the primary and secondary antibodies and re-probed for VDAC1 detection. The control showed two highly stained spots co-localised with phosphoserine. The MPTP treated sample showed one big VDAC1 spot accompanied by 3 small spots with an acidic shift and a trail on the basic side. The AIDA software was used to quantify the signal intensity in the main spot using the anti-phosphoserine and anti-VDAC1 antibodies in treated and control samples. The main spot was used because it was easily detected. Phosphoserine / VDAC1 ratio was 3.8-fold increased following 1 mM MPTP treatment for 24 hours (n = 2, 3.0 and 4.6-fold increase for each replicate).

#### 6.2.2.3 Threonine phosphorylation of VDAC1 decreased following MPTP treatment

Similar analysis to phosphoserine investigation was attempted using an anti-phosphothreonine antibody. The detection of phosphothreonine proved difficult to observe and background staining was high, as previously recorded (section 5.2.2.1).

**A. Co-localisation of phosphoserine and VDAC1 protein****B. Co-localisation of phosphothreonine and VDAC1 protein****Figure 6.12: Co-localisation of phosphorylated residues and VDAC1 using 2D-blot analysis**

Mouse N2a neuroblastomas were differentiated for 16 hours in serum free medium supplemented with 0.3 mM dbcAMP. Following incubation, cells were treated with 1 mM MPTP for 24 hours. Subcellular fractionation was then carried out. 50  $\mu$ g protein from mitochondrial fractions for each treatment were fractionated by 2DE (12 % resolving gel) and then transferred onto a nitrocellulose membrane. Blots were stained with copper to check for protein loading before cutting the blot at the molecular level of VDAC1. Then the membrane was probed with either A. anti-phosphoserine or B. anti-phosphothreonine antibodies at 1 in 500 dilution followed by the ECL detection procedure. Antibodies were then stripped of the blot and membranes were re-probed with anti-VDAC antibody at 1 in 1,000 dilution (refer to section 2.2.11).

However, on few occasions, successful staining was achieved. For example, using pI 7-10 IPG strips, one distinct spot was observed with phosphothreonine detection in both MPTP treated samples and controls (figure 6.12B). This spot had a reduced intensity following MPTP treatment; indeed, the phosphothreonine / VDAC1 ratio was 53 % (n = 1).

Additionally, tyrosine phosphorylation analysis was attempted but was not successful.

#### 6.2.2.4 Potential phosphorylated peptides observed using peptide mass fingerprinting

Parallel to western blot analysis, peptide mass fingerprinting was used to observe the presence of phosphorylated peptides in the trypsinised spot formerly identified as VDAC1 using 2DE (spot 19 in figure 6.1). Two phosphorylated peptides were observed containing threonine and serine phosphorylation sites (Figure 6.13). Both peptides were identified to possess sites predicted to be kinase targets. As described in figure 6.13B, peptide (a) contained 2 sites for pKC, and peptide mass fingerprinting analysis showed that only one of these sites was phosphorylated. Peptide (b) had 3 predicted sites, two for pKC and one for both p38 and creatine kinase I (CKI), and peptide mass fingerprinting analysis showed that two out of the three were phosphorylated in the spot analysed. These data are consistent with antibody-based analyses since they infer the possibility that both serine and threonine phosphorylations are present in the main spot identified as VDAC1.



## 6.3 DISCUSSION

### 6.3.1 Identification of VDAC1 isoforms in the mitochondrial proteome

Following evidence that VDAC1 protein levels were increased following treatment with sub-cytotoxic concentrations of MPTP using a quantitative analysis of the mitochondrial proteome resolved by 2DE, further analysis was carried out on the VDAC protein, concentrating particularly on the VDAC1 isoform.

The mitochondrial proteome resolved using 2DE using pI 3-10 IPG strips and total protein stains (silver stain and SyproRuby dye) revealed only two spots identified as VDAC. Indeed, one spot was identified as VDAC1 with a molecular weight around 30 kDa and pI 8.6 and one spot was identified as VDAC2 with a molecular weight around 32 kDa and pI 7.44 (figure 6.1 and 3.12). VDAC3 was not identified in the proteome profile; this could be because it was hidden by the VDAC1 spot (VDAC3 molecular weight 31 kDa and pI 9), not focused as its pI is very basic, or not successfully identified by peptide mass fingerprinting. The spot representing VDAC1 was intense, particularly compared to the VDAC2 spot, consistent with observations that VDAC1 is the most abundant isoform present on the OMM (Yamamoto *et al.*, 2006).

Because VDAC1 was the isoform showing an upregulation in protein levels (section 5.2.1.1, figure 5.1 and table 5.1), this study concentrated on the VDAC1 isoform. Peptide mass fingerprinting analysis of the VDAC1 spot covered 81 % of the total sequence showing a high confidence of the identity of the spot. However, the sequence compared with by the Mascot database was a total of 296 amino acids. As explained earlier, two splice-variants exist, differing in 13 amino acids and the form found in the OMM lacks the first 13 amino acids of the N-terminus (283 amino acids) (Buettner *et al.*, 2000). Consistent with this comment is the observation that, out of the 12 successful attempts to identify VDAC1 using MALDI-TOF and the Mascot database, none of the 13 first amino acids were present.

### 6.3.2 Changes in VDAC1 protein levels following MPTP treatment

#### 6.3.2.1 Links between increased VDAC1 levels and cell death markers

Increases in VDAC1 protein levels were MPTP concentration- and time-dependent; although the increase was only significant with 1 mM MPTP treatment for 24 hours. Because transient caspase activity was observed at the 2 hour time-point with 1 mM MPTP and 10  $\mu$ M for 24 hours (refer to section 4.2.2.5), it could be argued that VDAC1 levels should have been checked at the 2 hour time-point with 1 mM MPTP and earlier time-points. However, changes in VDAC1 levels with 1 mM MPTP were not significant at 4 hours and it is possible that caspase activation is not linked to VDAC1 levels since transient activity of caspase-3/7 was observed following 10  $\mu$ M MPTP treatment for 24 hours while no changes in VDAC1 levels were observed.

By 24 hours, 1 mM MPTP led to a non-significant reduction (20 %) of mitochondrial membrane potential, while a higher dose, 2 mM MPTP, led to a significant decrease (40 %) (refer to section 4.2.1.5), suggesting that the increase in VDAC1 protein levels preceded a reduction in mitochondrial membrane potential. This agrees with the hypothesis that VDAC may be playing a role in the depolarisation of mitochondria and in the formation of the transition pore (see introduction section 6.1.1.1). Since there was no evidence of apoptotic factors in the present model (following 1 mM MPTP for 24 hours), a potential role of VDAC in apoptotic cell following MPTP is not discussed here.

#### 6.3.2.2 Effects of other inhibitors of the electron transfer chain on VDAC1 levels

The main effects of MPTP are known to occur via the inhibition of complex I, via its metabolite MPP<sup>+</sup> (Langston *et al.*, 1983; Ramsay *et al.*, 1987). To check whether increased VDAC1 protein levels were linked to specific inhibition of complex I or general inhibition of the ETC, the effects of other complex inhibitors on VDAC1 levels were investigated. Treatment with sub-cytotoxic concentrations of another complex I inhibitor, rotenone, also increased VDAC1 levels by around 60 %. Such an increase was also observed in a preliminary study carried out by an undergraduate student in-house (data not published) using the same cell model and analysing mitochondrial extracts following treatment with

sub-cytotoxic concentrations of rotenone. Additionally, Xiong *et al.* (2008) showed similar increases in VDAC following rotenone treatment of human SH-SY5Y neuronal cells.

3-NP and sodium azide, inhibiting complex II and IV, respectively, also resulted in increases in VDAC1 levels, based on duplicate samples, whilst antimycin A (complex III inhibitor) treatment increased VDAC1 levels in one of the two replicates. Since a study undertaken in-house by an undergraduate student using the same model also showed an increase in VDAC1 levels following treatment with antimycin A, it is likely that complex III inhibition leads to increased VDAC1 levels. Thus it can be concluded that general ETC inhibition leads to increases in VDAC1 protein levels in mouse N2a neuroblastoma cells.

Using a similar proteomic approach with post-mortem brain regions of patients with Down syndrome and AD, Yoo and colleagues (2001) have also observed changes in VDAC isoforms. They found that VDAC1 levels were elevated and VDAC2 levels were unchanged in brain patients of Down syndrome compared to controls, similar to the results observed in the present study in the PD model. However, in brains of AD patients, they found that VDAC1 protein levels were decreased, while VDAC2 levels were increased in the frontal cortex and thalamus of patients. The combined results indicate dysregulated levels of VDAC isoforms in neurodegeneration.

### 6.3.2.3 Significance of increased levels of VDAC1

Increased levels of a protein can be due to a number of factors, including (a) upregulation of transcription and/or (b) increased translation and/or (c) decreased degradation of the protein. In the present study, VDAC1 mRNA levels, as shown by semi-quantitative RT-PCR and quantitative real-time PCR, were not significantly increased following treatment with 1 mM MPTP over 24 hours or treatment with sub-cytotoxic concentrations of other complex inhibitors, showing that the increased protein levels were not regulated at the transcriptional level in the present model. This is not in agreement with the work carried out by Xiong *et al.*, (2008), where rotenone treatment of human SH-SY5Y neuronal cells led to increased VDAC mRNA expression; however they did not define precisely which isoform was studied and they used cytotoxic concentrations of rotenone, which could explain the difference with the present study.

Thus, in the present model, increased VDAC1 protein levels could be due to an increase in VDAC1 mRNA translation and/or in a decrease in VDAC1 degradation. Impairment in

proteolytic pathways is one of the hallmarks of PD and other neurodegenerative conditions such as AD and HD (Lee *et al.*, 2004; McNaught *et al.*, 2002; Van Tijn *et al.*, 2007; Hunter *et al.*, 2007). More particularly, MPP<sup>+</sup> treated human SH-SY5Y cells showed a decreased activity of the 20S component of the ubiquitin-proteasome system (Caneda-Ferron *et al.*, 2008); moreover, proteins from the OMM have been found ubiquitinated and thought to be degraded by the proteasome (Neutzner *et al.*, 2007). It is therefore possible that VDAC1 protein levels increased as a result of decreased proteolysis of the protein, although increased translation of the protein could still be accompanying this phenomenon.

Complex I inhibition, as well as inhibition of other complexes from the ETC, could result in two common events: decrease in ATP production by oxidative phosphorylation and increased ROS production (Wu *et al.*, 1990; Chiueh *et al.*, 1993; McGeer and McGeer, 1998; Perez-de la Cruz and Santamaria, 2007). Upregulation of VDAC1 could be linked to these two events as it was observed by inhibiting the four complexes. The channel has been linked to ATP energy stores by its interaction with several molecules, of which the two most interesting for the present project are HK and CK. At normal physiological conditions, VDAC has a high conductance with preference for channelling anionic metabolites (e.g. ATP, ADP and AMP). Following ATP production via oxidative phosphorylation, ATP tends to exit mitochondria via VDAC and ADP enters the organelle to be used as substrate for renewal of ATP production. It is thought that HK and CK bind VDAC to have a direct access to their common substrate, ATP. VDAC-bound hexokinase drives the glycolysis rate, while VDAC-bound creatine kinase drives ATP storage, both kinases competing for the same binding site on VDAC channel as well as competing with pro-apoptotic molecules, preventing apoptosis (Anflous-Pharayyas *et al.*, 2007).

Interestingly, Chalmers-Redman *et al.* (1999) have shown that supplementation of glucose reduced MPP<sup>+</sup> toxicity in PC12 cells. Moreover, when glycolysis was blocked by glucose depletion, MPP<sup>+</sup>-induced toxicity was exacerbated (Basma *et al.*, 1992). This protective effect of glycolysis could be illustrated by a corresponding binding of HK competing with pro-apoptotic molecules and preventing apoptosis. Similarly, another well known protective event that has not been completely explained yet was the protective effect of creatine in neurodegeneration and other diseases. For example, in ischemia, creatine was found to buffer depletion of ATP stores and to delay synaptic failure by preventing muscle and heart cell death (Matthews *et al.*, 1999). Brewer and Wallimann (2000) found that

creatine was protective of glutamate- and  $\beta$ -amyloid-induced toxicity in rat hippocampal neurons, as a model of AD. Ferrante and colleagues (2000) found that creatine was neuroprotective in a mouse model of HD. Thus, creatine has been studied as a potential therapeutic molecule for neurodegenerative diseases in the last decade. It was originally thought to be due to its role in buffering ATP energy (Brewer and Wallimann, 2000) but an additional or combinational effect could be due to the binding of CK to VDAC, preventing pro-apoptotic molecules from interacting with the channel and mitochondrial pore opening. Another common effect of inhibition of the ETC is increased ROS production (Han *et al.*, 2003). Han and colleagues (2003a) have shown that VDAC had a role in the diffusion of  $O_2^{\cdot -}$  from the IMS to the cytoplasm. This diffusion can exacerbate the oxidative damage by extending the effects all over the cell. This could be a molecular event that might contribute to MPTP-induced toxicity.

In general, VDAC1 overexpression has often been linked to cell death in a variety of organisms (Tomasello *et al.*, 2009 as discussed in introduction; Xiong *et al.*, 2008, as discussed previously; and reviewed in Shoshan-Barmatz *et al.*, 2006). It is worth quoting that overexpression of VDAC has also been observed in cell survival conditions, in cancer cells but this could account as a consequence of upregulation of HK, leading to increased cell survival (Shinohara *et al.*, 2000). Thus, in the present model, following electron transfer inhibition and, more particularly, MPTP-induced complex I inhibition, the upregulation of VDAC1 protein levels could be linked to pro-apoptotic events. As illustrated in figure 6.14, several molecular events can lead to the same consequence. This is a very important hypothesis as this upregulation of VDAC1 occurred prior to cell death and could be used as a marker of neurodegeneration. However, such a model still needs to be validated by investigating other molecular events such as HK and CK binding to VDAC1, expression and localisation of Bcl<sub>2</sub> family molecules and cellular state following MPTP-induced toxicity (as opposed to sub-cytotoxicity).

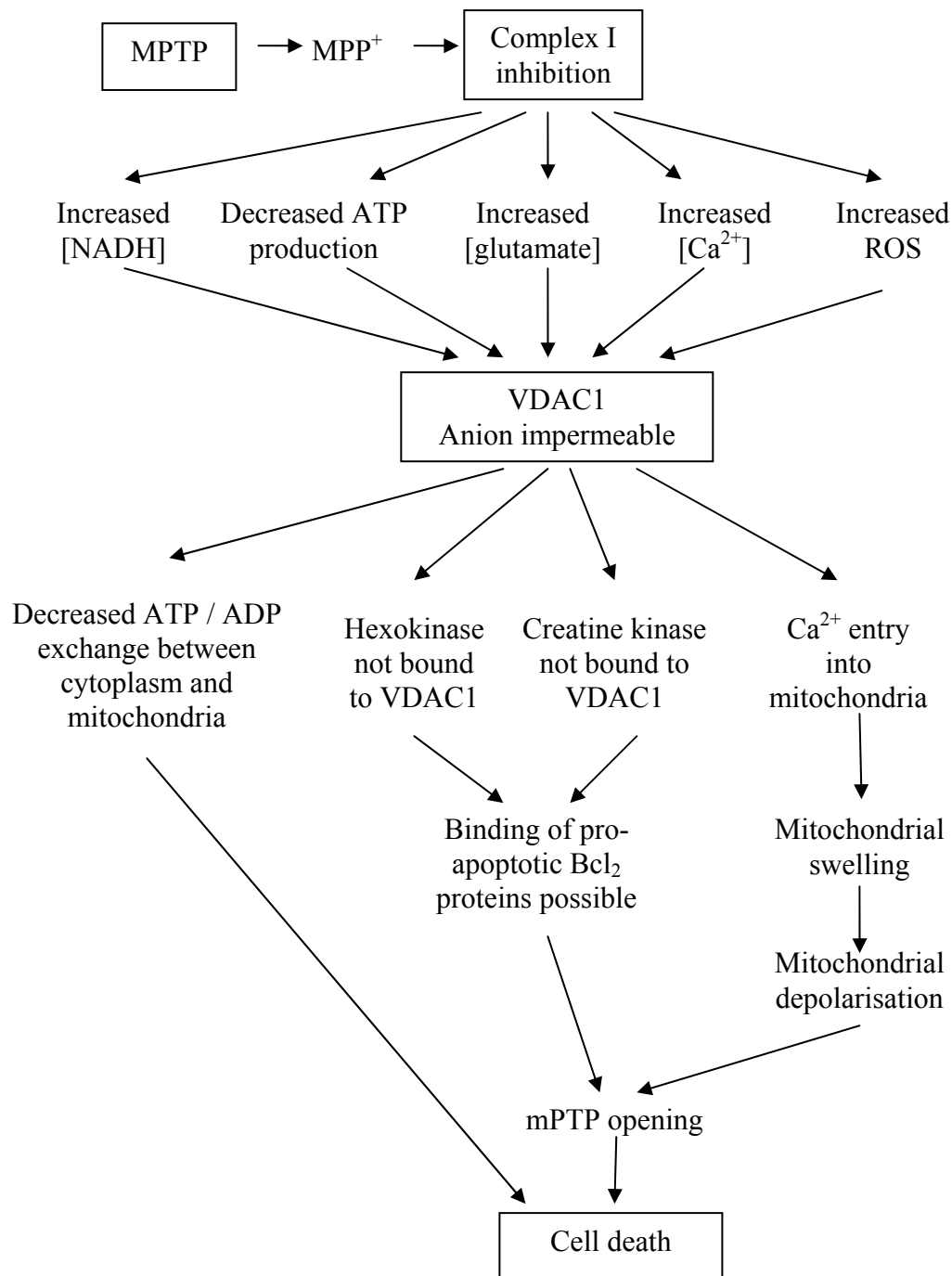


**Figure 6.14: Hypothetic molecular events of MPTP effects leading to cell death**

Additionally, VDAC has been observed to be the target of many signaling kinases, regulating the binding of molecules to the channel (Das *et al.*, 2008; Schwertz *et al.*, 2007). Variations in kinase activities have been observed in MPTP-induced toxicity and in other models of PD (Salinas *et al.*, 2001; De Girolamo *et al.*, 2006; King *et al.*, 2008). Investigating VDAC1 phosphorylation states and uncovering the kinases involved in this process following MPTP-induced toxicity could unravel more particular molecular events involved in MPTP-induced toxicity.

### 6.3.3 Phosphorylation state of VDAC1 following MPTP treatment

An attempt to analyse VDAC1 phosphorylation state was undertaken using 2D-blot analysis. Such analysis was difficult as the anti-phospho-amino acid antibodies were not specific to VDAC1, leading to a high background and necessity to co-localise the VDAC1 spots with spots observed using anti-phosphoserine and anti-phosphothreonine antibodies. Nevertheless, preliminary data indicated an increase in serine phosphorylation and a decrease in threonine phosphorylation on the VDAC protein, but of course the precise phosphorylation sites could not be ascertained using these antibody reagents.

In order to investigate VDAC1 phosphorylation sites, peptide mass fingerprinting was performed to search for phosphopeptides in the peptide mixture. Several phosphorylation sites were detected on two different phosphopeptides. However, no confirmation using post-source decay analysis was obtained so the presence of these peptides and exact site of phosphorylations were not validated. Moreover, the phosphorylated sites shown in these phosphopeptides are predicted sites by consensus sequences and only one of the sites was found *in vivo* in previous studies (the pKC serine phosphorylation site on peptide a; Jaburek *et al.*, 2006).

Nevertheless, these analyses showed that VDAC1 spots were phosphorylated on serine and threonine residues, particularly the main spot originally identified by peptide mass fingerprinting following 2DE.

A few phosphorylation sites and targeting kinases of VDAC1 have been found *in vivo*, related in the literature. Indeed, pKC- $\epsilon$  was found to phosphorylate serine 12 on VDAC1; however, the consequences of this phosphorylation have yet to be resolved (Jaburek *et al.*, 2006). Another kinase shown to phosphorylate VDAC1 is GSK-3 $\beta$ . Two sites have been found to potentially be phosphorylated by this kinase on the VDAC1 sequence, threonine

51 (Pastorino *et al.*, 2005) and serine 136 (Jaburek *et al.*, 2006). Pastorino *et al.* (2005) showed that Akt inhibition led to GSK-3 $\beta$  activation leading to VDAC1 phosphorylation on threonine 51, decreasing the binding of HK to VDAC1. The inverse pathway was also happening, activation of Akt led to inhibition of GSK-3 $\beta$  leading to decreased phosphorylation of VDAC1, increasing the binding of HK to VDAC1. Other consequences of GSK-3 $\beta$  activation were blockade of the transition pore and decrease in ATP production (Das *et al.*, 2008) probably due to a decrease in complex I activity (King *et al.*, 2008). Interestingly, activation of GSK-3 $\beta$  also exacerbated the toxic effects of MPP<sup>+</sup> toxicity in SH-SY5Y cells (King *et al.*, 2008). The latter is consistent with observations in PC12 cells showing that phosphorylation (i.e. activation) of Akt was protective from MPP<sup>+</sup> toxicity (Salinas *et al.*, 2001), probably due to increased hexokinase binding to VDAC1 as shown in rat fibroblasts (Gottlob *et al.*, 2001).

Another signaling kinase, p38 MAPK, is involved in VDAC1 phosphorylation and possibly in PD molecular events. Indeed activation of p38 indirectly increases VDAC1 phosphorylation (Schwartz *et al.*, 2007), and a p38 consensus sequence is present on VDAC1 (figure 6.13Bb). Moreover, p38 inhibition was shown to be protective of the proapoptotic events consequent to VDAC1 overexpression in Human Hela cells (Tomasello *et al.*, 2009). The neurotoxin 6-OHDA, mimicking PD biochemical features, has been shown to cause transient p38 activation concomitant with Bax-dependent apoptosis (Gomez-Lazaro *et al.*, 2008), consistent with the previous observations that inhibition of p38 was protective.

The mode of actions of GSK-3 $\beta$  and p38 in cellular models of PD are consistent with the consequences following VDAC1 phosphorylation via these two kinases, directly or indirectly. Nevertheless, additional research is needed to confirm a role for GSK-3 $\beta$  and/or p38-dependent VDAC1 phosphorylation in MPTP-induced cytotoxicity in mouse N2a neuroblastoma cells. In addition it should be noted that other signaling kinases have been linked to VDAC phosphorylation, such as C-Raf kinase (LeMellay *et al.*, 2002) and cAMP-dependent pKA (Bera *et al.*, 1995), in particular, both known to be involved in the interaction of VDAC with Bcl<sub>2</sub> family proteins.

## **CHAPTER VII:**

# **GENERAL DISCUSSION**

## **7.1 STUDY OF THE MITOCHONDRIAL PROTEOME**

### **7.1.1 Mitochondrial enrichment and purity following subcellular fractionation**

Following subcellular fractionation of mouse N2a neuroblastoma cell extracts, mitochondrial fractions were observed to be enriched over 5-fold. These fractions were found to have negligible contamination by cytosol, nuclei and endoplasmic reticulum. Although some proteins from the ER were detected in the mitochondrial proteome on 2DE, these were mainly proteins known to interact with the mitochondrial membrane.

Mitochondrial fractions were found to be slightly contaminated with lysosomes; however, compared to the mitochondrial enrichment and the low amount of material available from cultured cells, it was decided that this contamination was not an issue in the present study.

2DE analysis also showed that proteins from all mitochondrial sub-localisations were present including from the OMM, for example VDAC isoforms, showing the integrity of the organelle.

### **7.1.2 Mitochondrial proteome resolved on mini-2DE**

Mitochondrial fractions resolved on 2DE showed up to 400 spots (using mini-2D-gels and broad range pI 3-10). Although this number seemed low compared to 1,098 proteins found in a comprehensive study of the mouse mitochondrial proteome (Pagliarini *et al.*, 2008), phosphorylated forms could be observed using ProQ Diamond that were not visualised using total protein stains indicating that more proteins were present in the gel.

### **7.1.3 Limitations of 2DE protocol and further recommendations**

Although 2DE is a powerful tool able to resolve in theory up to 1,000 proteins on a gel electrophoresis, there are still several limitations that need to be addressed.

Due to the large number of hydrophobic proteins found in mitochondria, mainly due to its double membrane composition, the choice of detergent during sample preparation was important. A comprehensive analysis of the effects of different detergents on the mitochondrial proteome showed that CHAPS was the detergent of choice, which was not

expected as other detergents have been shown to solubilise membranes more effectively (Luche *et al.*, 2003).

Another problem was the limited amount of mitochondrial material available from cell culture, which meant that only 3 replicates could be used for the analysis. Additionally, the number of replicates analysed in parallel was also a limiting factor. The number of replicates is an important factor to overcome the low reproducibility that has been observed using the 2DE approach. Several reviews about 2DE reproducibility and analysis planning have been written in an attempt to standardise the approach intra- and inter-laboratories (Moxon *et al.*, 2009; Biron *et al.*, 2006), although each group is still following its own analysis procedure. In the present study, triplicates were used for practicability purposes due to material limitations but it has been proposed that 5 replicates should be the prerequisite (Biron *et al.*, 2006); however, mitochondrial proteome studies have been published using triplicates for each treatment (Fukada *et al.*, 2004). A sensible recommendation for similar analysis would be to increase the number of replicates whenever possible.

#### **7.1.4 Study of the mitochondrial phosphoproteome: limitations and future recommendations**

In parallel to a quantitative analysis of the mitochondrial total proteins, a study of the phosphoproteome was attempted using two different detection approaches. Phospho-amino acid specific antibodies were useful for probing 1D and 2D western blots of mitochondrial proteins. Nevertheless, identification of proteins using the 1D approach was not undertaken due to the poor resolution. 2D western blot analysis allowed alignment with total protein stain in some cases. However, the sensitivity of the antibody was a limiting factor and the background was relatively high. 2D-blot analysis was only successful with one replicate of serine phosphorylation analysis. Therefore, more sensitive antibodies are needed before this approach can be used routinely.

The second approach to study the phosphoproteome used the phosphoprotein specific fluorescent dye ProQ Diamond. The poor resolution of 1D gels and the complexity of the mitochondrial phosphoproteome made it difficult to detect changes between treatments. The 2D approach showed an even more complex profile with multi-phosphorylated forms

of the same protein, although resolution was improved. As for the antibody-based approach, the background of the 2DE profile was high.

As the background was lower using pI 5-8, recommendations for the analysis of the mitochondrial phosphoproteome would be to use such IPG strips in further analyses and/or fractionate samples to enrich phosphoproteins prior to 2DE.

Antibody-based microarrays, allowing the visualisation of the phosphorylation states of a range of molecules, are commercially available. More particularly, future work could, for example, include the use of one of these arrays to study the phosphorylation status of a range of proteins involved in apoptotic and signaling pathways.

## **7.2 MPTP EFFECTS ON MOUSE N2a NEUROBLASTOMA**

### **7.2.1 Cellular effects**

Sub-cytotoxic effects of MPTP on differentiated N2a cells were studied using 1 mM MPTP for 24 hours because, at this concentration, the cells lacked axon-like processes, had a round cell body but were still intact and overall metabolic activity was unaffected (chapter IV). However, although no apparent cell death was observed, the cellular ATP levels were down to 50 % of control values mostly due to a decrease in ATP production via oxidative phosphorylation as a consequence of complex I inhibition. Although some mitochondria were swollen, the majority were still polarised as opposed to following a higher concentration of MPTP (2 mM MPTP for 24 hours) where mitochondria were significantly depolarised.

There was no evidence of caspase-3/7 or caspase-2 activation following exposure to 1 mM MPTP but a transient caspase-3/7 activation was observed at lower concentrations. Overall, although no cell death was observed, metabolic activity and morphology of mitochondria seemed to be showing early signs of being affected by the chosen conditions of MPTP exposure, indicating that the mitochondrial proteome might consequently be altered.

### 7.2.2 MPTP effects on the mitochondrial proteome

Initial studies using 2DE showed that sub-cytotoxic MPTP concentrations modulated the levels of at least 32 proteins. Interestingly, ten of those proteins identified are involved in key mitochondrial and cellular pathways including oxidative phosphorylation, metabolic pathways such as the Krebs cycle and amino acid synthesis (notably aspartate and glutamate transamination), protein folding and an OMM channel.

The change in levels of four of these proteins, VDAC1, GOT2, Hsp60 and Hsc70 were validated by western blotting analysis but the potential involvement of the other proteins (MDH, SDH, ATP synthase subunits, ETF- $\alpha$  and STIP1) has also been discussed in section 5.3.3.

The main molecular events resulting from MPTP-induced toxicity observed in previous studies were ATP depletion (Singer *et al.*, 1988), ROS production (Chiueh *et al.*, 1993), glutamate excitotoxicity (Meredith *et al.*, 2009) and disruption of calcium homeostasis (Chiueh *et al.*, 1993) leading to cell death. Further work is needed to establish the links between complex I inhibition on the IMM to the above mentioned phenomena.

Although ATP depletion could be explained by complex I inhibition and the decrease in proton motive force, in accordance with previous studies (for example Ferrer *et al.*, 2007), the present study showed that ATP synthase subunit levels were also altered. This suggests that complex I inhibition may have led to molecular variations in complex V, further accentuating ATP depletion.

One could expect that, since NADH can not be oxidised via complex I due to its inhibition, metabolic and ETC enzymes would have decreased in activity and levels. However, increased protein levels of ETF $\alpha$ , MDH and FMH suggested that Krebs cycle might be induced to increase ATP production via other means than NADH oxidation by complex I (discussed in section 5.3.3.2) although these processes, if occurring, were not able to completely prevent ATP depletion.

The hypothesis of reversed Krebs cycle would be consistent with increased glutamate levels observed in MPTP-induced toxicity (Meredith *et al.*, 2009; Lange *et al.*, 1997).

Another aspect of MPTP-induced toxicity in the mitochondrial proteome was the elevated levels of chaperones and co-chaperones (Hsc70, Hsp60 and STIP1) and alterations in their phosphorylation states. These changes (validated by western blot analysis in the case of

Hsp60 and Hsc 70) could have a protective role due to anti-apoptotic properties as well as a role in protein folding allowing proper function of proteins (section 5.3.3.1).

These events are links between complex I inhibition by MPTP-induced toxicity and some of the hallmarks of the disease observed elsewhere in the cell such as glutamate excitotoxicity, ATP-dependent processes impairment,  $\text{Ca}^{2+}$ -dependent processes activation, ROS-induced damages and proteolysis impairment. A potential link between mitochondrial events and cytoplasmic events has been described in the present study by the observation of changes in the levels and phosphorylation status of the OMM channel VDAC1, in MPTP-induced toxicity. Indeed, VDAC1 has been observed to channel ATP, ROS,  $\text{Ca}^{2+}$ , NADH and glutamate, all involved in MPTP toxicity (described in section 6.1; Lemasters *et al.*, 2006; Han *et al.*, 2003a; and represented in figure 7.1).

### 7.3 VDAC

#### 7.3.1 The role of VDAC in neurodegeneration

VDAC1 protein levels were increased following sub-cytotoxic concentrations of several electron transfer chain inhibitors, whilst no mRNA changes were observed, suggesting a common effect of electron transfer inhibition on VDAC1 protein levels. Two molecular events are known to be common following inhibition of complexes, ATP depletion and ROS production, both types of molecules channelled through VDAC. From these results, it can be hypothesised that ATP depletion could increase VDAC protein levels, for example due to a need of increased exchange of ATP / ADP between the cytoplasm and the mitochondria; and / or ROS production via the electron transfer chain, particularly  $\text{O}_2^{\bullet-}$  might lead to increased VDAC1 levels as the channel has a role in releasing ROS to the cytoplasm (Han *et al.*, 2003). Interestingly, Xiong *et al.* (2008) showed that hydrogen peroxide could lead to increased levels of VDAC in human SH-SY5Y cells and this could be inhibited by an antioxidant (called Asiatic acid), further suggesting a role of ROS in VDAC levels regulation. Shimada *et al.* (2009) recently showed that the toxicity of paraquat, another complex I inhibitor, was potentiated by VDAC1 over-expression via increased levels of  $\text{O}_2^{\bullet-}$  in Hela cells; both Paraquat-induced cytotoxicity and  $\text{O}_2^{\bullet-}$  increased production were suppressed in VDAC1-knockdown cells.

VDAC1 phosphorylation levels were also modulated following MPTP treatment suggesting that VDAC1 might change its conformation, leading to different molecules binding the channel.

The observation that VDAC1 level and phosphorylation state was changes following MPTP and other complex inhibitor-induced toxicity was an important novel insight into the molecular pathways involved in neurodegenerative diseases, particularly as a mediator molecule between mitochondria and the rest of the cell (figure 7.1).

### **7.3.2 Future recommendations for VDAC studies**

Further investigations on the role of ROS in the regulation of VDAC1 levels, including the effects of antioxidants would be of great interest to further understand the role of VDAC in neurodegeneration and cell death.

It would be useful to study the effects of electron transport inhibitors on global interactions of VDAC with other proteins using, for example, immunoprecipitation techniques. Interactions with the Bcl-2 family of proteins, HK and CK would be of particular interest, but new interactions could be revealed using this approach.

Finally the phosphorylation state of VDAC seems to be an important feature of the channel and further investigation of the phosphorylation status of the channel and molecules binding the channel following treatment with complex inhibitors could help to improve our understanding of the molecular events involved in neurodegeneration. This could not only help to identify new biomarkers of effect but also aid the development of new therapeutic agents by targeting the different phosphorylation states of VDAC (in order to select a conformation of the channel that would prevent the cell death pathway in which VDAC is involved).

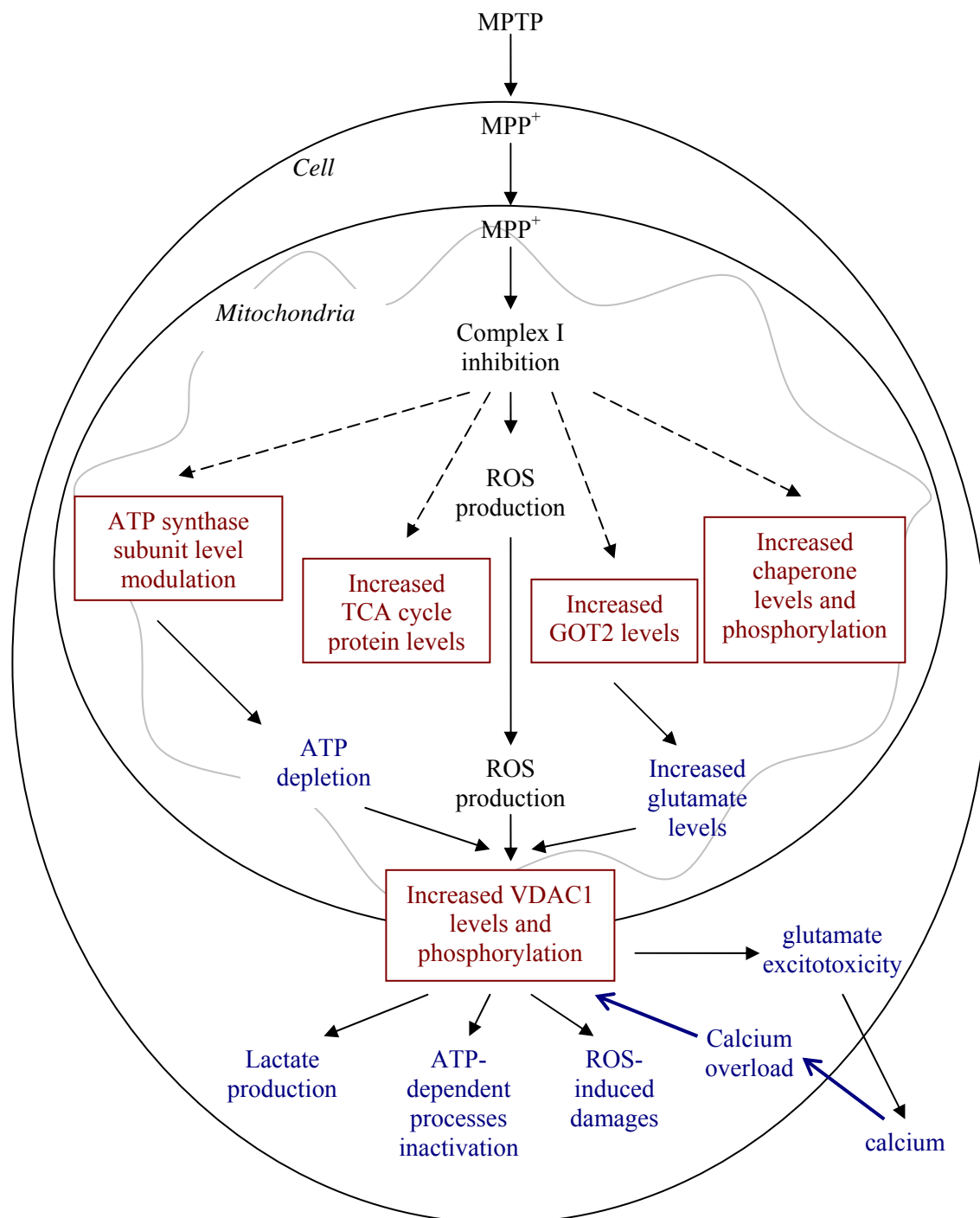


**Figure 7.1: Schematic representation of MPTP effects on mitochondrial processes and cellular consequences**

Mitochondrial protein regulated by MPTP-induced toxicity.

Potential consequences of mitochondrial markers previously observed also found as consequences of MPTP-induced toxicity in the literature.

A detailed description can be found in the text.

## 7.4 CONCLUSION

In conclusion, the present project used a range of cellular and molecular approaches to study the effects of sub-cytotoxic concentrations of MPTP on the mitochondrial proteome from cultured cells. Indeed the study of the mitochondrial fraction from mouse N2a cells using a proteomic approach allowed the observation of markers in MPTP-induced toxicity.

- 32 mitochondrial proteins were potentially involved in MPTP-induced toxicity, of which 10 were identified by peptide mass fingerprinting, suggesting the involvement of chaperones, components of the Krebs cycle and amino acid synthesis pathway, electron transfer proteins and an OMM protein in MPTP-induced toxicity (VDAC1).
- Altered levels of Hsc70, Hsp60, GOT2 and VDAC1 were validated as potential markers of MPTP-induced toxicity.
- Changes in the mitochondrial phosphoproteome were observed, particularly phosphorylation of chaperones, suggesting a role of altered protein kinase activity in mitochondrial dysfunction.
- Further investigations of the effects of complex inhibitors on VDAC1 protein levels and phosphorylation states, suggested an important role of the channel as a modulator between the mitochondria and the rest of the cell.

A continued understanding on the role of VDAC in neurodegeneration and other pathologies could make the channel a potential target of therapy.

# **CHAPTER VIII**

## **REFERENCES**

- Abou-Sleiman, P.M., Muqit, M.M. and Wood NW. (2006) Expanding insights of mitochondrial dysfunction in Parkinson's disease. *Nat. Rev. of Neurosci.* **7** (3): 207-19.
- Ackrell, B.A. (2002) Cytopathies involving mitochondrial complex II. *Mol. Aspects Med.* **23** (5): 369-84. Review.
- Adams, J.D. Jr, Klaidman, L.K. and Leung, A.C. (1993) MPP+ and MPDP+ induced oxygen radical formation with mitochondrial enzymes. *Free Radic. Biol. Med.* **15** (2): 181-6.
- Aebersold, R.H., Leavitt, J., Saavedra, R.A., Hood, L.E. and Kent, S.B. (1987) Internal amino acid sequence analysis of proteins separated by one- or two-dimensional gel electrophoresis after in situ protease digestion on nitrocellulose. *Proc. Natl. Acad. Sci. U.S.A.* **84** (20): 6970-4.
- Almeida, A. and Medina, J.M. (1998) A rapid method for the isolation of metabolically active mitochondria from rat neurons and astrocytes in primary culture. *Brain Res. Brain Res. Protoc.* **2** (3): 209-14.
- Amazzal, L., Lapôte, A., Quignon, F. and Bagrel D. (2007) Mangiferin protects against 1-methyl-4-phenylpyridinium toxicity mediated by oxidative stress in N2A cells. *Neurosci. Lett.* **418** (2): 159-64.
- Anderson, N.G. and Anderson, L. (1982) The Human Protein Index. *Clin. Chem.* **28** (4 Pt 2): 739-48.
- Anflous-Pharayra, K., Cai, Z.J. and Craigen, W.J. (2007) VDAC1 serves as a mitochondrial binding site for hexokinase in oxidative muscles. *Biochim. Biophys. Acta.* **1767** (2): 136-42.
- Antos, N., Stobienia, O., Budzińska, M. and Kmita, H. (2001) Under conditions of insufficient permeability of VDAC1, external NADH may use the TOM complex channel to cross the outer membrane of *Saccharomyces cerevisiae* mitochondria. *J. Bioenerg. Biomembr.* **33** (2): 119-26.
- de Araújo, M.E. and Huber, L.A. (2007) Subcellular fractionation. *Methods Mol. Biol.* **357**: 73-85.
- Atamna, H. and Frey, W.H. 2<sup>nd</sup> (2007). Mechanisms of mitochondrial dysfunction and energy deficiency in Alzheimer's disease. *Mitochondrion.* **7** (5): 297-310. Review.
- Aubry, L. and Klein, G. (2006) Purification techniques of subcellular compartments for analytical and preparative purposes. *Methods Mol. Biol.* **346**: 171-85.
- Augusti-Tocco, G. and Sato, G. (1969) Establishment of functional clonal lines of neurons from mouse neuroblastoma. *Proc. Natl. Acad. Sci. USA.* **64** (1): 311-5.
- Bailey, S.M., Landar, A. and Darley-Usmar, V. (2005) Mitochondrial proteomics in free radical research. *Free Radic. Biol. Med.* **38** (2): 175-88. Review.
- Baines, C.P., Kaiser, R.A., Sheiko, T., Craigen, W.J. and Molkentin, J.D. (2007) Voltage-dependent anion channels are dispensable for mitochondrial-dependent cell death. *Nat Cell Biol.* **9** (5): 550-5.
- Baron, M., Kudin, A.P. and Kunz, W.S. (2007) Mitochondrial dysfunction in neurodegenerative disorders. *Biochem. Soc. Trans.* **35** (Pt 5):1228-31. Review.
- Barzilai, A. and Melamed, E. (2003) Molecular mechanisms of selective dopaminergic neuronal death in Parkinson's disease. *Trends Mol. Med.* **9** (3):126-32. Review.
- Barzilai, A., Zilkha-Falb, R., Daily, D., Stern, N., Offen, D., Ziv, I., Melamed, E. and Shirvan, A. (2000) The molecular mechanism of dopamine-induced apoptosis: identification and characterization of genes that mediate dopamine toxicity. *J. Neural. Transm. Suppl.* (60): 59-76.
- Basma, A.N., Heikkila, R.E., Saporito, M.S., Philbert, M., Geller, H.M. and Nicklas, W.J. (1992) 1-Methyl-4-(2'-ethylphenyl)-1,2,3,6-tetrahydropyridine-induced toxicity in PC12 cells is enhanced by preventing glycolysis. *J. Neurochem.* **58** (3): 1052-9.

- Basso, M., Giraud, S., Corpillo, D., Bergamasco, B., Lopiano, L. and Fasano, M. (2004) Proteome analysis of human substantia nigra in Parkinson's disease. *Proteomics* **4** (12): 3943-52.
- Beal, M.F. (2001) Experimental models of Parkinson's disease. *Nat. Rev. Neurosci.* **2** (5), 325-34. Review.
- Beck, K.E. (2004) Changes in the cytoskeleton and signalling pathways in differentiated human neuroblastoma cells following MPP<sup>+</sup> exposure. *phD thesis*, Nottingham Trent University.
- Bender, A., Krishnan, K.J., Morris, C.M., Taylor, G.A., Reeve, A.K., Perry, R.H., Jaros, E., Hersheson, J.S., Betts, J., Klopstock, T., Taylor, R.W. and Turnbull, D.M. (2006) High levels of mitochondrial DNA deletions in substantia nigra neurons in aging and Parkinson disease. *Nat. Genet.* **38** (5): 515-7.
- Bennett, M.C, Diamond, D.M., Stryker, S.L., Parks, J.K. and Parker, W.D. Jr. (1992) Cytochrome oxidase inhibition: a novel animal model of Alzheimer's disease. *J. Geriatr. Psychiatry. Neurol.* **5** (2): 93-101.
- Bera, A.K., Ghosh, S. and Das, S. (1995) Mitochondrial VDAC can be phosphorylated by cyclic AMP-dependent protein kinase. *Biochem. Biophys. Res. Commun.* **209** (1): 213-7.
- Bezard, E., Gross, C.E., Fournier, M.C., Dovero, S., Bloch, B. and Jaber, M. (1999) Absence of MPTP-induced neuronal death in mice lacking the dopamine transporter. *Exp. Neurol.* **155** (2): 268-73.
- Bilsland, J., Roy, S., Xanthoudakis, S., Nicholson, D.W., Han, Y., Grimm, E., Hefti, F. and Harper, S. J. (2002). Caspase Inhibitors Attenuate 1-Methyl-4-Phenylpyridinium Toxicity in Primary Cultures of Mesencephalic Dopaminergic Neurons. *J. Neurosci.* **22** (7), 2637-2649.
- Biron, D.G., Brun, C., Lefevre, T., Lebarbenchon, C., Loxdale, H.D., Chevenet, F., Brizard, J.P. and Thomas, F. (2006) The pitfalls of proteomics experiments without the correct use of bioinformatics tools. *Proteomics* **6** (20): 5577-96. Review.
- Blum, D., Torch, S., Lamberg, N., Nissou, M.F., Benabid, A.L., Sadoul, R. and Verna, J.M. (2001). Molecular Pathways involved in the Neurotoxicity of 6-OHDA, Dopamine and MPTP: Contribution of the Apoptotic Theory in Parkinson's Disease. *Prog. Neurobiol.* **65** (2), 135-72. Review.
- Bogaerts, V., Theuns, J. and van Broeckhoven, C. (2008) Genetic findings in Parkinson's disease and translation into treatment: a leading role for mitochondria? *Genes Brain Behav.* **7** (2): 129-51. Review.
- Bolender, N., Sickmann, A., Wagner, R., Meisinger, C. and Pfanner, N. Multiple pathways for sorting mitochondrial precursor proteins. *EMBO Rep.* **9** (1): 42-9. Review.
- Boujrad, H., Gubkina, O., Robert, N., Krantic, S. and Susin, S.A. (2007) AIF-mediated programmed necrosis: a highly regulated way to die. *Cell Cycle* **6** (21): 2612-9. Review.
- Bové, J., Prou, D., Perier, C. and Przedborski, S. (2005) Toxin-induced models of Parkinson's disease. *NeuroRx* **2** (3): 484-94.
- Bradford M.M. (1976) A rapid and sensitive method for the quantitation of microgram quantities of protein utilizing the principle of protein-dye binding, *Anal Biochem* **72**, 248-254
- Brewer, G.J. and Wallimann, T.W. (2000) Protective effect of the energy precursor creatine against toxicity of glutamate and beta-amyloid in rat hippocampal neurons. *J. Neurochem.* **74** (5): 1968-78.
- Bronisz, A., Gajkowska, B. and Domańska-Janik, K. (2002) PKC and Raf-1 inhibition-related apoptotic signalling in N2a cells. *J. Neurochem.* **81** (6): 1176-84.
- Brooks, W.J., Jarvis, M.F. and Wagner, G.C. (1989) Astrocytes as a primary locus for the conversion MPTP into MPP<sup>+</sup>. *J. Neural. Transm.* **76** (1): 1-12.

- Brouillet, E., Jacquard, C., Bizat, N. and Blum, D. 3-Nitropropionic acid: a mitochondrial toxin to uncover physiopathological mechanisms underlying striatal degeneration in Huntington's disease. *J. Neurochem.* **95** (6): 1521-40. Review.
- Brown, T.P., Rumsby, P.C., Capleton, A.C., Rushton, L. and Levy, L.S. (2006) Pesticides and Parkinson's disease--is there a link? *Environ. Health Perspect.* **114** (2): 156-64.
- Buettner, R., Papoutsoglou, G., Scemes, E., Spray, D.C. and Dermietzel, R. (2000) Evidence for secretory pathway localization of a voltage-dependent anion channel isoform. *Proc. Natl. Acad. Sci. U S A.* **97** (7): 3201-6.
- Butterfield, D.A., Abdul, H.M., Newman, S and Reed, T. (2006) Redox proteomics in some age-related neurodegenerative disorders or models thereof. *NeuroRx.* **3** (3): 344-57. Review.
- Cada, A., Gonzalez-Lima, F., Rose, G.M. and Bennett, M.C. (1995) Regional brain effects of sodium azide treatment on cytochrome oxidase activity: a quantitative histochemical study. *Metab. Brain Dis.* **10** (4): 303-20.
- Caneda-Ferrón, B., De Girolamo, L.A., Costa, T., Beck, K.E., Layfield, R. and Billett, E.E. (2008) Assessment of the direct and indirect effects of MPP+ and dopamine on the human proteasome: implications for Parkinson's disease aetiology. *J. Neurochem.* **105** (1): 225-38.
- Cappello, F., de Macario, E.C., Marasà, L., Zummo, G and Macario, A.J. (2008) Hsp60 expression, new locations, functions and perspectives for cancer diagnosis and therapy. *Cancer Biol. Ther.* **7** (6): 801-9. Review.
- Cappelletti, G., Pedrotti, B., Maggioni, M.G. and Maci R (2001). Microtubule assembly is directly affected by MPP(+)in vitro. *Cell Biol. Int.* **25** (10), 981-4.
- Cardone, M.H., Roy, N., Stennicke, H.R., Salvesen, G.S., Franke, T.F., Stanbridge, E., Frisch, S. and Reed, J.C. (1998) Regulation of cell death protease caspase-9 by phosphorylation. *Science* **282** (5392): 1318-21.
- Cardoso, S.M., Moreira, P.I., Agostinho, P., Pereira, C. and Oliveira, C.R. (2005) Neurodegenerative pathways in Parkinson's disease: therapeutic strategies. *Cur. Drug Targets CNS Neurol. Disord.* **4** (4): 405-19. Review.
- Cassarino, D.S. and Bennett, J.P. Jr (1999) An evaluation of the role of mitochondria in neurodegenerative diseases: mitochondrial mutations and oxidative pathology, protective nuclear responses, and cell death in neurodegeneration. *Brain Res. Brain Res. Rev.* **29** (1): 1-25. Review.
- Cassarino, D.S., Parks, J.K., Parker, W.D. Jr and Bennett, J.P. Jr (1999) The parkinsonian neurotoxin MPP+ opens the mitochondrial permeability transition pore and releases cytochrome c in isolated mitochondria via an oxidative mechanism. *Biochim. et Biophys. Acta.* **1453** (1): 49-62.
- Chandler, J.M., Cohen, G.M. and MacFarlane, M. (1998) Different subcellular distribution of caspase-3 and caspase-7 following Fas-induced apoptosis in mouse liver. *J. Biol. Chem.* **273** (18): 10815-8.
- Chandra, D., Choy, G. and Tang DG (2007) Cytosolic accumulation of HSP60 during apoptosis with or without apparent mitochondrial release: evidence that its pro-apoptotic or pro-survival functions involve differential interactions with caspase-3. *J. Biol. Chem.* **282** (43): 31289-301.
- Chang, M.H., Karageorgos, L.E., Meikle, P.J. (2002) CD107a (LAMP-1) and CD107b (LAMP-2). *J. Biol. Regul. Homeost. Agents* **16** (2): 147-51. Review.
- Chang, J.H. and Prasad, K.N. (1976) Differentiation of mouse neuroblastoma cells in vitro and in vivo induced by cyclic adenosine monophosphate (cAMP). *J. Pediatr. Surg.* **11** (5):847-58.

- Chee, J.L., Guan, X.L., Lee, J.Y., Dong, B., Leong, S.M., Ong, E.H., Liou, A.K. and Lim, T.M. (2005) Compensatory caspase activation in MPP<sup>+</sup>-induced cell death in dopaminergic neurons. *Cell. Mol. Life Sci.* **62** (2): 227-38.
- Chiba, K., Peterson, L.A., Castagnoli, K.P., Trevor, A.J. and Castagnoli, N. Jr. (1985) Studies on the molecular mechanism of bioactivation of the selective nigrostriatal toxin 1-methyl-4-phenyl-1,2,3,6-tetrahydropyridine. *Drug Metab. Dispos.* **13** (3): 342-7.
- Chinnery, P.F. and Schon, E.A. (2003) Mitochondria. *J. Neurol. Neurosurg. Psychiatr.* **74** (9): 1188-99. Review.
- Chiueh, C.C., Miyake, H. and Peng, M.T. (1993) Role of dopamine autoxidation, hydroxyl radical generation, and calcium overload in underlying mechanisms involved in MPTP-induced parkinsonism. *Adv. Neurol.* **60**: 251-8.
- Coles, C.J., Edmondson, D.E. and Singer, T.P. (1979) Inactivation of succinate dehydrogenase by 3-nitropropionate. *J. Biol. Chem.* **254** (12): 5161-7.
- Colombini, M. (2009) The published 3D structure of the VDAC channel: native or not? *Trends Biochem. Sci.* **34** (8): 382-9.
- Conejero-Goldberg, C., Davies, P. and Ulloa, L. (2008) Alpha7 nicotinic acetylcholine receptor: a link between inflammation and neurodegeneration. *Neurosci. Biobehav. Rev.* **32** (4): 693-706. Review.
- Cossarizza, A., Baccarani-Contri, M., Kalashnikova, G. and Franceschi, C. (1993) A new method for the cytofluorimetric analysis of mitochondrial membrane potential using the J-aggregate forming lipophilic cation 5,5',6,6'-tetrachloro-1,1',3,3'-tetraethylbenzimidazolcarbocyanine iodide (JC-1). *Biochem. Biophys. Res. Commun.* **197** (1): 40-5.
- Cox, B. and Emili, A. (2006) Tissue subcellular fractionation and protein extraction for use in mass-spectrometry-based proteomics. *Nat. Protoc.* **1** (4): 1872-8.
- D'Amato, R.J., Alexander, G.M., Schwartzman, R.J., Kitt, C.A., Price, D.L. and Snyder, S.H. (1987) Evidence for neuromelanin involvement in MPTP-induced neurotoxicity. *Nature* **327** (6120): 324-6.
- Dani, D. and Dencher, N.A. (2008) Native-DIGE: a new look at the mitochondrial membrane proteome. *Biotechnol. J.* **3** (6): 817-22.
- Das, S., Wong, R., Rajapakse, N., Murphy, E. and Steenbergen, C. (2008) Glycogen synthase kinase 3 inhibition slows mitochondrial adenine nucleotide transport and regulates voltage-dependent anion channel phosphorylation. *Circ. Res.* **103** (9):983-91.
- Datta, S.R., Dudek, H., Tao, X., Masters, S., Fu, H., Gotoh, Y., Greenberg, M.E. (1997) Akt phosphorylation of BAD couples survival signals to the cell-intrinsic death machinery. *Cell* **91** (2): 231-41.
- Davis, G.C., Williams, A.C., Markey, S.P., Ebert, M.H., Caine, E.D., Reichert, C.M., Kopin, I.J. (1979) Chronic Parkinsonism secondary to intravenous injection of meperidine analogues. *Psychiatry Res.* **1** (3):249-54.
- De Girolamo, L.A. and Billett, E.E. (2006) Role of extracellular-regulated kinase and c-jun NH(2)-terminal kinase in 1-methyl-4-phenyl-1,2,3,6-tetrahydropyridine-induced neurofilament phosphorylation. *J. Neurosci. Res.* **83** (4): 680-693.
- De Girolamo, L.A., Hargreaves, A. and Billett, E.E. (2001). Protection from MPTP-induced Neurotoxicity in Differentiating Mouse N2a neuroblastoma cells. *J. Neurochem.* **76**, 3, 650.

- De Girolamo, L.A., Billett, E.E. and Hargreaves, A. (2000). Effects of Methyl-4-Phenyl-1,2,3,6-Tetrahydropyridine on Differentiating Mouse N2a Neuroblastoma Cells. *J. Neurochem.* **75** (1): 133-40.
- De Iuliis, A., Grigoletto, J., Recchia, A., Giusti, P. and Arslan, P. (2005) A proteomic approach in the study of an animal model of Parkinson's disease. *Clin. Chim. Acta.* **357** (2): 202-9.
- Denton, T. and Howard, B.D. (1984) Inhibition of dopamine uptake by N-methyl-4-phenyl-1,2,3,6-tetrahydropyridine, a cause of parkinsonism. *Biochem. Biophys. Res. Commun.* **119** (3): 1186-90.
- Deocaris, C.C., Kaul, S.C. and Wadhwa, R. (2006) On the brotherhood of the mitochondrial chaperones mortalin and heat shock protein 60. *Cell Stress Chaperones.* **11** (2): 116-28. Review.
- Deumens, R., Blokland, A. and Prickaerts, J. (2002) Modeling Parkinson's disease in rats: an evaluation of 6-OHDA lesions of the nigrostriatal pathway. *Exp. Neurol.* **175** (2): 303-17. Review.
- Diaz-Corrales, F.J., Asanuma, M., Miyazaki, I., Miyoshi, K. and Ogawa, N. (2005) Rotenone induces aggregation of gamma-tubulin protein and subsequent disorganization of the centrosome: relevance to formation of inclusion bodies and neurodegeneration. *Neuroscience* **133** (1): 117-35.
- Di Monte, D., Jewell, S.A., Ekström, G., Sandy, M.S. and Smith, M.T. (1986) 1-Methyl-4-phenyl-1,2,3,6-tetrahydropyridine (MPTP) and 1-methyl-4-phenylpyridine (MPP+) cause rapid ATP depletion in isolated hepatocytes. *Biochem. Biophys. Res. Commun.* **137** (1): 310-5.
- Donaire, V., Niso, M., Morán, J.M., García, L., González-Polo, R.A., Soler, G., Fuentes, J.M. (2005) Heat shock proteins protect both MPP(+) and paraquat neurotoxicity. *Brain Res. Bull.* **67** (6): 509-14.
- Dowling J.E. (2001) *Neurons and networks: an introduction to behavioral neuroscience*, Harvard University Press, 2<sup>nd</sup> edition, pp32-41.
- Druzhyna, N.M., Hollensworth, S.B., Kelley, M.R., Wilson, G.L. and Ledoux, S.P. (2003) Targeting human 8-oxoguanine glycosylase to mitochondria of oligodendrocytes protects against menadione-induced oxidative stress. *Glia.* **42** (4): 370-8.
- Du, Y., Dodel, R.C., Bales, K.R., Jemmerson, R., Hamilton-Byrd, E. and Paul, S.M. (1997) Involvement of a caspase-3-like cysteine protease in 1-methyl-4-phenylpyridinium-mediated apoptosis of cultured cerebellar granule neurons. *J. Neurochem.* **69** (4): 1382-8.
- Duan, H., Chinnaiyan, A.M., Hudson, P.L., Wing, J.P., He, W.W. and Dixit, V.M. (1996) ICE-LAP3, a novel mammalian homologue of the *Caenorhabditis elegans* cell death protein Ced-3 is activated during Fas- and tumor necrosis factor-induced apoptosis. *J. Biol. Chem.* **271** (3): 1621-5.
- Dupuis, L., Gonzalez de Aguilar, J.L., Oudart, H., de Tapia, M., Barbeito, L., Loeffler, J.P. (2004) Mitochondria in amyotrophic lateral sclerosis: a trigger and a target. *Neurodegener. Dis.* **1** (6): 245-54. Review.
- Eguchi, Y., Shimizu, S. and Tsujimoto, Y. (1997) Intracellular ATP levels determine cell death fate by apoptosis or necrosis. *Cancer Res.* **57** (10): 1835-40.
- Englard, S. and Seifter, S. (1990) Precipitation techniques. *Methods Enzymol.* **182**: 285-300.
- Fan, G.H., Zhou, H.Y., Yang, H., Chen, S.D. (2006) Heat shock proteins reduce alpha-synuclein aggregation induced by MPP(+) in SK-N-SH cells. *FEBS Letters* **580** (13): 3091-8.
- Fawcett, A (1994) *Textbook of Histology*, Chapman and Hall, 12th edition.
- Fernández-Vizarra, E., López-Pérez, M.J. and Enriquez, J.A. (2002) Isolation of biogenetically competent mitochondria from mammalian tissues and cultured cells. *Methods* **26** (4): 292-7.

- Ferrante, R.J., Andreassen, O.A., Jenkins, B.G., Dedeoglu, A., Kuemmerle, S., Kubilus, J.K., Kaddurah-Daouk, R., Hersch, S.M. and Beal, M.F. (2000) Neuroprotective effects of creatine in a transgenic mouse model of Huntington's disease. *J. Neurosci.* **20** (12): 4389-97.
- Ferrer, I., Perez, E., Dalfó, E. and Barrachina, M. (2007) Abnormal levels of prohibitin and ATP synthase in the substantia nigra and frontal cortex in Parkinson's disease. *Neurosci. Lett.* **415** (3): 205-9.
- Fitzgerald, J.C. and Plun-Favreau, H. (2008) Emerging pathways in genetic Parkinson's disease: autosomal-recessive genes in Parkinson's disease--a common pathway? *FEBS J.* **275** (23): 5758-66. Review.
- Flaskos, J., McLean, W.G., Fowler, M.J. and Hargreaves, A.J. (1998) Tricresyl phosphate inhibits the formation of axon-like processes and disrupts neurofilaments in cultured mouse N2a and rat PC12 cells. *Neurosci. Lett.* **242** (2): 101-4.
- Fornai, F., Schlüter, O.M., Lenzi, P., Gesi, M., Ruffoli, R., Ferrucci, M., Lazzeri, G., Busceti, C.L., Pontarelli, F., Battaglia, G., Pellegrini, A., Nicoletti, F., Ruggieri, S., Paparelli, A. and Südhof, T.C. (2005) Parkinson-like syndrome induced by continuous MPTP infusion: convergent roles of the ubiquitin-proteasome system and alpha-synuclein. *Proc. Natl. Acad. Sci. U.S.A.* **102** (9): 3413-8.
- Forno, L.S., Langston, J.W., DeLanney, L.E. and Irwin, I. (1988) An electron microscopic study of MPTP-induced inclusion bodies in an old monkey. *Brain Res.* **448** (1): 150-7.
- Freyaldenhoven, T.E. and Ali, S.F. (1996) Heat shock proteins protect cultured fibroblasts from the cytotoxic effects of MPP<sup>+</sup>. *Brain Res.* **735** (1): 42-9.
- Fujiki, Y., Hubbard, A.L., Fowler, S. and Lazarow, P.B. (1982) Isolation of intracellular membranes by means of sodium carbonate treatment: application to endoplasmic reticulum. *J. Cell Biol.* **93** (1): 97-102.
- Fukada, K., Zhang, F., Vien, A., Cashman, N.R. and Zhu, H. (2004) Mitochondrial proteomic analysis of a cell line model of familial amyotrophic lateral sclerosis. *Mol. Cell. Proteomics* **3** (12): 1211-23.
- Fukae, J., Mizuno, Y. and Hattori, N. (2007) Mitochondrial dysfunction in Parkinson's disease. *Mitochondrion* **7** (1-2): 58-62. Review.
- Fukui, H. and Moraes, C.T. (2008) The mitochondrial impairment, oxidative stress and neurodegeneration connection: reality or just an attractive hypothesis? *Trends Neurosci.* **31** (5): 251-6. Review.
- Fukushima, T., Decker, R.V., Anderson, W.M. and Spivey, H.O. (1989) Substrate channeling of NADH and binding of dehydrogenases to complex I. *J. Biol. Chem.* **264** (28): 16483-8.
- Gabalton, T. and Huynen, M.A. (2004) Shaping the mitochondrial proteome. *Biochim. Biophys. Acta.* **1659** (2-3): 212-20. Review.
- Gandhi, S. and Wood, N.W. (2005) Molecular pathogenesis of Parkinson's disease. *Hum. Mol. Genet.* **14** Spec No. 2: 2749-2755. Review.
- Garcia-Calvo, M., Peterson, E.P., Leiting, B., Ruel, R., Nicholson, D.W. and Thornberry, N.A. (1998) Inhibition of human caspases by peptide-based and macromolecular inhibitors. *J. Biol. Chem.* **273** (49): 32608-13.
- Garrido, C., Galluzzi, L., Brunet, M., Puig, P.E., Didelot, C. and Kroemer, G. (2006) Mechanisms of cytochrome c release from mitochondria. *Cell Death Differ.* **13** (9): 1423-33. Review.
- Gaucher, S.P., Taylor, S.W., Fahy, E., Zhang, B., Warnock, D.E., Ghosh, S.S. and Gibson, B.W. (2004) Expanded coverage of the human heart mitochondrial proteome using multidimensional liquid chromatography coupled with tandem mass spectrometry. *J. Proteome Res.* **3** (3): 495-505.

- Golbe, L.I., Miller, D.C., Duvoisin, R.C. (1990), Autosomal dominant Lewy-body Parkinson's disease. *Adv. Neurol.* **53**: 287-92.
- Goldberg, M., Harel, A. and Gruenbaum, Y. (1999) The nuclear lamina: molecular organization and interaction with chromatin. *Crit. Rev. Eukaryot. Gene Expr.* **9** (3-4): 285-93. Review.
- Golshani-Hebroni, S.G. and Bessman, S.P. (1997) Hexokinase binding to mitochondria: a basis for proliferative energy metabolism. *J. Bioenerg. Biomembr.* **29** (4): 331-8. Review.
- Golstein, P. and Kroemer, G. (2007) Cell death by necrosis: towards a molecular definition. *Trends Biochem. Sci.* **32** (1): 37-43. Review
- Gomez-Lazaro, M., Galindo, M.F., Concannon, C.G., Segura, M.F., Fernandez-Gomez, F.J., Llecha, N., Comella, J.X., Prehn, J.H. and Jordan, J. (2008) 6-Hydroxydopamine activates the mitochondrial apoptosis pathway through p38 MAPK-mediated, p53-independent activation of Bax and PUMA. *J. Neurochem.* **104** (6): 1599-612.
- Görg, A., Postel, W. and Günther S. (1988) The current state of two-dimensional electrophoresis with immobilized pH gradients. *Electrophoresis.* **9** (9):531-46. Review.
- Gottlob, K., Majewski, N., Kennedy, S., Kandel, E., Robey, R.B. and Hay, N. (2001) Inhibition of early apoptotic events by Akt/PKB is dependent on the first committed step of glycolysis and mitochondrial hexokinase. *Genes Dev.* **15** (11): 1406-18.
- Govorun, V.M., Archakov, A.I. (2002) Proteomic technologies in modern biomedical science. *Biochemistry* **67** (10): 1109-23. Review.
- Greene, L.A. and Tischler, A.S. (1976) Establishment of a noradrenergic clonal line of rat adrenal pheochromocytoma cells which respond to nerve growth factor. *Proc. Nat. Acad. Sci. U.S.A.* **73** (7): 2424-8.
- Greenamyre, J.T. and Hastings, TG. (2004) Biomedicine. Parkinson's--divergent causes, convergent mechanisms. *Science* **304** (5674): 1120-2.
- Grover, G.J., Marone, P.A., Koetzner, L., Seto-Young, D. (2008) Energetic signalling in the control of mitochondrial F1F0 ATP synthase activity in health and disease. *Int. J. Biochem. Cell Biol.* **40** (12): 2698-701.
- Gupta, M., Gupta, B.K., Thomas, R., Bruemmer, V., Sladek, J.R. Jr, Felten, D.L. (1986) Aged mice are more sensitive to 1-methyl-4-phenyl-1,2,3,6-tetrahydropyridine treatment than young adults. *Neurosci. Lett.* **70** (3): 326-31.
- Hajnoczky, G, Csordás, G. and Yi, M. (2002) Old players in a new role: mitochondria-associated membranes, VDAC, and ryanodine receptors as contributors to calcium signal propagation from endoplasmic reticulum to the mitochondria. *Cell Calcium.* **32** (5-6): 363-77. Review.
- Hald, A. and Lotharius, J. (2005) Oxidative stress and inflammation in Parkinson's disease: is there a causal link? *Exp. Neurol.* **193** (2): 279-90. Review.
- Halestrap, A.P. (2009) What is the mitochondrial permeability transition pore? *J. Mol. Cell Cardiol.* **46** (6): 821-31. Review.
- Halestrap, A.P., McStay, G.P. and Clarke, S.J. (2002) The permeability transition pore complex: another view. *Biochimie* **84** (2-3): 153-66. Review
- Halestrap, A.P., Doran, E., Gillespie, J.P., O'Toole, A. (2000) Mitochondria and cell death. *Biochem. Soc. Trans.* **28** (2): 170-7. Review.
- Han, Y.H., Kim, S.H., Kim, S.Z., Park, W.H. (2008a) Antimycin A as a mitochondrial electron transport inhibitor prevents the growth of human lung cancer A549 cells. *Oncol. Rep.* **20** (3): 689-93.

- Han, S.I., Kim, Y.S. and Kim, T.H. (2008b) Role of apoptotic and necrotic cell death under physiologic conditions. *B.M.B Rep.* **41** (1): 1-10. Review.
- Han, D., Antunes, F., Canali, R., Rettori, D. and Cadenas, E. (2003a) Voltage-dependent anion channels control the release of the superoxide anion from mitochondria to cytosol. *J. Biol. Chem.* **278** (8): 5557-63.
- Han, B.S., Noh, J.S., Gwag, B.J. and Oh, Y.J. (2003b) A Distinct Death Mechanism is induced by 1-methyl-4-phenylpyridinium or by 6-hydroxydopamine in Cultured Rat Cortical Neurons: Degradation and Dephosphorylation of tau. *Neurosci. Lett.* **341**, 99-102.
- Hara, M.R., Cascio, M.B. and Sawa, A. (2006) GAPDH as a sensor of NO stress. *Biochim. Biophys. Acta.* **1762** (5):502-9. Review.
- Harris, W., Sachana, M., Flaskos, J. and Hargreaves, A.J. (2009) Neuroprotection from diazinon-induced toxicity in differentiating murine N2a neuroblastoma cells. *Neurotoxicology.* **30** (6): 958-64.
- Hartl, F.U. and Hayer-Hartl, M. (2009) Converging concepts of protein folding in vitro and in vivo. *Nat. Struct. Mol. Biol.* **16** (6): 574-81. Review.
- Hartley, A., Stone, J.M., Heron, C., Cooper, J.M. and Schapira AH (1994) Complex I inhibitors induce dose-dependent apoptosis in PC12 cells: relevance to Parkinson's disease. *J. Neurochem.* **63** (5): 1987-90.
- Hartmann, A., Hunot, S., Michel, P.P., Muriel, M.P., Vyas, S., Faucheux, B.A., Mouatt-Prigent, A., Turmel, H., Srinivasan, A., Ruberg, M., Evan, G.I., Agid, Y. and Hirsch, E.C. (2000) Caspase-3: A vulnerability factor and final effector in apoptotic death of dopaminergic neurons in Parkinson's disease. *Proc. Natl. Acad. Sci. U.S.A.* **97** (6): 2875-80.
- Hayashi, T. and Su, T.P. (2007) Sigma-1 receptor chaperones at the ER-mitochondrion interface regulate Ca(2+) signaling and cell survival. *Cell* **131** (3): 596-610.
- He, X.J., Yamauchi, H., Uetsuka, K. and Nakayama, H. (2008) Neurotoxicity of MPTP to migrating neuroblasts: studies in acute and subacute mouse models of Parkinson's disease. *Neurotoxicology* **29** (3): 413-20.
- Henchcliffe, C. and Beal, M.F. (2008) Mitochondrial biology and oxidative stress in Parkinson disease pathogenesis. *Nat. Clin. Pract. Neurol.* **4** (11): 600-9. Review.
- Holdorff, B. (2002) Friedrich Heinrich Lewy (1885-1950) and his work. *J. Hist. Neurosci.* **11** (1): 19-28.
- Howell, N., Elson, J.L., Chinnery, P.F. and Turnbull, D.M. (2005) mtDNA mutations and common neurodegenerative disorders. *Trends Genet.* **21** (11): 583-6. Review.
- Hu, L.F., Wang, S., Shi, X.R., Yao, H.H., Sun, Y.H., Ding, J.H., Liu, S.Y. and Hu G. (2005) ATP-sensitive potassium channel opener iptakalim protected against the cytotoxicity of MPP+ on SH-SY5Y cells by decreasing extracellular glutamate level. *J. Neurochem.* **94** (6): 1570-9.
- Huang, Y., Cheung, L., Rowe, D., Halliday, G. (2004) Genetic contributions to Parkinson's disease. *Brain Res. Brain Res. Rev.* **46** (1): 44-70. Review.
- Huber, L.A., Pfaller, K. and Vietor, I. (2003) Organelle proteomics: implications for subcellular fractionation in proteomics. *Circ. Res.* **92** (9) :962-8. Review.
- Hunter, J.M., Lesort, M. and Johnson, G.V. (2007) Ubiquitin-proteasome system alterations in a striatal cell model of Huntington's disease. *J. Neurosci. Res.* **85** (8): 1774-88.
- Hsu, Y.T., Wolter, K.G. and Youle, R.J. (1997) Cytosol-to-membrane redistribution of Bax and Bcl-X(L) during apoptosis. *Proc. Natl. Acad. Sci. U.S.A.* **94** (8): 3668-72.

- Izzo, G., Guerrieri, F. and Papa, S. (1978) On the mechanism of inhibition of the respiratory chain by 2-heptyl-4-hydroxyquinoline-N-oxide. *FEBS Lett.* **93** (2): 320-2
- Jabůrek, M., Costa, A.D., Burton, J.R., Costa, C.L. and Garlid, K.D. (2006) Mitochondrial PKC epsilon and mitochondrial ATP-sensitive K<sup>+</sup> channel copurify and coreconstitute to form a functioning signaling module in proteoliposomes. *Circ. Res.* **99** (8): 878-83.
- Jana, M., Jana, A., Pal, U. and Pahan, K.A (2007) Simplified method for isolating highly purified neurons, oligodendrocytes, astrocytes, and microglia from the same human fetal brain tissue. *Neurochem. Res.* **32** (12) :2015-22.
- Jin, J., Li, G.J., Davis, J., Zhu, D., Wang, Y., Pan, C., Zhang, J. (2006) Identification of novel proteins interacting with both a-synuclein and DJ-1. *Mol. Cell Proteomics* **6** (5): 845-59.
- Jin, J., Meredith, G.E., Chen, L., Zhou, Y., Xu, J., Shie, F.S., Lockhart, P. and Zhang, J. (2005). Quantitative proteomic analysis of mitochondrial proteins: relevance to Lewy body formation and Parkinson's disease. *Brain Research. Mol. Brain Res.* **134** (1): 119-38.
- Johannessen, J.N., Adams, J.D., Schuller, H.M., Bacon, J.P. and Markey, S.P. (1986) 1-Methyl-4-phenylpyridine (MPP<sup>+</sup>) induces oxidative stress in the rodent. *Life Sci.* **38** (8): 743-9.
- Kajta, M. (2004) Apoptosis in the central nervous system: mechanisms and protective strategies. *Pol. J. Pharmacol.* **56** (6): 689-700. Review
- Kanamatsu, T., Otsuki, T., Tokuno, H., Nambu, A., Takada, M., Okamoto, K., Watanabe, H., Umeda, M. and Tsukada, Y. (2007) Changes in the rates of the tricarboxylic acid (TCA) cycle and glutamine synthesis in the monkey brain with hemiparkinsonism induced by intracarotid infusion of 1-methyl-4-phenyl-1,2,3,6-tetrahydropyridine (MPTP): studies by non-invasive <sup>13</sup>C-magnetic resonance spectroscopy. *Brain Res.* **21**; 1181:142-8.
- Kasraie, S., Houshmand, M., Banoei, M.M., Ahari, S.E., Panahi, M.S., Shariati, P., Bahar, M. and Moin, M. (2008) Investigation of tRNA(Leu/Lys) and ATPase 6 genes mutations in Huntington's disease. *Cell Mol. Neurobiol.* **28** (7): 933-8.
- Kidd, P.M. (2005) Neurodegeneration from mitochondrial insufficiency: nutrients, stem cells, growth factors, and prospects for brain rebuilding using integrative management. *Alternative Medicine Review* **10** (4): 268-93. Review.
- Kim, Y.S., Jung, M.H., Choi, M.Y., Kim, Y.H., Sheverdin, V., Kim, J.H., Ha, H.J., Park, D.J., Kang, S.S., Cho, G.J., Choi, W.S. and Chang, S.H. (2009) Glutamine attenuates tubular cell apoptosis in acute kidney injury via inhibition of the c-Jun N-terminal kinase phosphorylation of 14-3-3. *Crit. Care Med.* **37** (6): 2033-44.
- King, T.D., Clodfelder-Miller, B., Barksdale, K.A. and Bijur, G.N. (2008) Unregulated mitochondrial GSK3beta activity results in NADH: ubiquinone oxidoreductase deficiency. *Neurotox. Res.* **14** (4): 367-82.
- Kmita, H., Antos, N., Wojtkowska, M. and Hryniewiecka, L. (2004) Processes underlying the upregulation of Tom proteins in *S. cerevisiae* mitochondria depleted of the VDAC channel. *J. Bioenerg. Biomembr.* **36** (2): 187-93.
- Kopin, I.J. (1987) MPTP: an industrial chemical and contaminant of illicit narcotics stimulates a new era in research on Parkinson's disease. *Environ. Health Perspect.* **75**: 45-51. Review.
- Krajewski, S., Tanaka, S., Takayama, S., Schibler, M.J., Fenton, W. and Reed, J.C. (1993) Investigation of the subcellular distribution of the bcl-2 oncoprotein: residence in the nuclear envelope, endoplasmic reticulum, and outer mitochondrial membranes. *Cancer Res.* **53** (19): 4701-14.

- Kraytsberg, Y., Kudryavtseva, E., McKee, A.C., Geula, C., Kowall, N.W. and Khrapko, K. (2006) Mitochondrial DNA deletions are abundant and cause functional impairment in aged human substantia nigra neurons. *Nature Genetics* **38** (5): 518-20.
- Kruft, V., Eubel, H., Jansch, L., Werhahn, W. and Braun, H.P. (2001) Proteomic approach to identify novel mitochondrial proteins in Arabidopsis. *Plant Physiol.* **127** (4):1694-710.
- Kroemer, G., Galluzzi, L., Vandenabeele, P., Abrams, J., Alnemri, E.S., Baehrecke, E.H., Blagosklonny, M.V., El-Deiry, W.S., Golstein, P., Green, D.R., Hengartner, M., Knight, R.A., Kumar, S., Lipton, S.A., Malorni, W., Nuñez, G., Peter, M.E., Tschopp, J., Yuan, J., Piacentini, M., Zhivotovsky, B., Melino, G. (2009). Nomenclature Committee on Cell Death. Classification of cell death: recommendations of the Nomenclature Committee on Cell Death 2009. *Cell Death Differ.* **16** (1): 3-11.
- Kroemer, G., Galluzzi, L. and Brenner, C. (2007) Mitochondrial membrane permeabilization in cell death. *Physiol. Rev.* **87** (1): 99-163. Review.
- Kulich, S.M., Horbinski, C., Patel, M. and Chu, C.T. (2007) 6-Hydroxydopamine induces mitochondrial ERK activation. *Free Radic. Biol. Med.* **43** (3): 372-83.
- Lai J.C. and Clark, J.B. (1979) Preparation of synaptic and nonsynaptic mitochondria from mammalian brain. *Methods in Enzymology* **55**: 51-60.
- Lane, E.L., Handley, O.J., Rosser, A.E. and Dunnett, S.B. (2008) Potential cellular and regenerative approaches for the treatment of Parkinson's disease. *Neuropsychiatr. Dis. Treat.* **4** (5): 835-45.
- Lange, K.W., Kornhuber, J. and Riederer, P. (1997) Dopamine/glutamate interactions in Parkinson's disease. *Neurosci. Biobehav. Rev.* **21** (4): 393-400. Review.
- Langston, J.W., Ballard, P., Tetrud, J.W. and Irwin I. (1983). Chronic Parkinsonism in humans due to a product of meperidine-analog synthesis. *Science* **219** (4587), 979-80.
- Lavedan, C., Buchholtz, S., Nussbaum, R.L., Albin, R.L. and Polymeropoulos, M.H. (2002) A mutation in the human neurofilament M gene in Parkinson's disease that suggests a role for the cytoskeleton in neuronal degeneration. *Neurosci. Lett.* **322** (1): 57-61.
- Lawen, A., Ly, J.D., Lane, D.J., Zarschler, K., Messina, A. and De Pinto, V. (2005) Voltage-dependent anion-selective channel 1 (VDAC1)--a mitochondrial protein, rediscovered as a novel enzyme in the plasma membrane. *Int. J. Biochem. Cell Biol.* **37** (2): 277-82. Review.
- Le, W.D., Xu, P., Jankovic, J., Jiang, H., Appel, S.H., Smith, R.G., Vassilatis, D.K. (2003) Mutations in NR4A2 associated with familial Parkinson disease. *Nat. Genet.* **33** (1):85-9. Erratum in: *Nat Genet.* **33** (2):214.
- Lee, C.S., Park, W.J., Ko, H.H. and Han, E.S. (2006) Differential involvement of mitochondrial permeability transition in cytotoxicity of 1-methyl-4-phenylpyridinium and 6-hydroxydopamine. *Mol. Cell Biochem.* **289** (1-2): 193-200.
- Lee, H.J., Khoshaghideh, F., Patel, S. and Lee, S.J. (2004). Clearance of  $\alpha$ -synuclein Oligomeric intermediates via the Lysosomal Degradation Pathways. *J. Neurosci.* **24** (8), 1888-1896.
- Lee, Y.M., Park, S.H., Chung, K.C. and Oh, Y.J. (2003) Proteomic analysis reveals upregulation of calreticulin in murine dopaminergic neuronal cells after treatment with 6-hydroxydopamine. *Neurosci. Lett.* **352** (1): 17-20.
- Lemasters, J.J. and Holmuhamedov, E. (2006) Voltage-dependent anion channel (VDAC) as mitochondrial governor--thinking outside the box. *Biochim. Biophys. Acta.* **1762** (2): 181-90. Review.
- Le Mellay, V., Troppmair, J., Benz, R. and Rapp, U.R. (2002) Negative regulation of mitochondrial VDAC channels by C-Raf kinase. *BMC Cell Biol.* **3**: 14.

- Leroy, E., Boyer, R., Auburger, G., Leube, B., Ulm, G., Mezey, E., Harta, G., Brownstein, M.J., Jonnalagada, S., Chernova, T., Dehejia, A., Lavedan, C., Gasser, T., Steinbach, P.J., Wilkinson, K.D. and Polymeropoulos, M.H. (1998) The ubiquitin pathway in Parkinson's disease. *Nature*. **395** (6701): 451-2.
- Leung, H. and Mok, V. (2005) Parkinson's disease: aetiology, diagnosis, and management. *Hong Kong Med. J.* **11** (6): 476-89.
- Levitt, P., Pintar, J.E. and Breakefield, X.O. (1982) Immunocytochemical demonstration of monoamine oxidase B in brain astrocytes and serotonergic neurons. *Proc. Natl. Acad. Sci. U.S.A.* **79** (20): 6385-9.
- Liebler, D.C. (2002) Introduction to Proteomic: Tools for the New Biology, *Human Press Inc.*, USA.
- Liu, B., Xie, J.X., Tsang, L.L., Rowlands, D.K, Ho, L.S., Gou, Y.L., Chung, Y.W. and Chan, H.C. (2008) Bak Foong protects dopaminergic neurons against MPTP-induced neurotoxicity by its anti-apoptotic activity. *Cell Biol. Int.* **32** (1): 86-92.
- Lizotte, E., Tremblay, A., Allen, B.G. and Fiset, C. (2005) Isolation and characterization of subcellular protein fractions from mouse heart. *Anal. Biochem.* **345** (1): 47-54.
- Lopez, M.F. and Melov, S. (2002) Applied proteomics: mitochondrial proteins and effect on function. *Circ.Res.* **90** (4): 380-9. Review.
- Lopez, M.F., Berggren, K., Chernokalskaya, E., Lazarev, A., Robinson, M. and Patton, W.F. (2000) A comparison of silver stain and SYPRO Ruby Protein Gel Stain with respect to protein detection in two-dimensional gels and identification by peptide mass profiling. *Electrophoresis.* **21** (17): 3673-83.
- Luche, S., Santoni, V. and Rabilloud, T. (2003) Evaluation of nonionic and zwitterionic detergents as membrane protein solubilizers in two-dimensional electrophoresis. *Proteomics.* **3** (3): 249-53.
- Marcelli, M., Cunningham, G.R., Haidacher, S.J., Padayatty, S.J., Sturgis, L., Kagan, C. and Denner, L. (1998) Caspase-7 is activated during lovastatin-induced apoptosis of the prostate cancer cell line LNCaP. *Cancer Res.* **58** (1): 76-83.
- Magen, D., Georgopoulos, C., Bross, P., Ang, D., Segev, Y., Goldsher, D., Nemirovski, A., Shahar, E., Ravid, S., Luder, A., Heno, B., Gershoni-Baruch, R., Skorecki, K. and Mandel, H. (2008) Mitochondrial hsp60 chaperonopathy causes an autosomal-recessive neurodegenerative disorder linked to brain hypomyelination and leukodystrophy. *Am. J. Hum. Genet.* **83** (1): 30-42.
- Martin, D.P., Schmidt, R.E., DiStefano, P.S., Lowry, O.H., Carter, J.G. and Johnson, E.M. Jr. (1988) Inhibitors of protein synthesis and RNA synthesis prevent neuronal death caused by nerve growth factor deprivation. *J. Cell Biol.* **106** (3):829-44.
- Mastro, R and Hall, M. (1999) Protein delipidation and precipitation by tri-n-butylphosphate, acetone, and methanol treatment for isoelectric focusing and two-dimensional gel electrophoresis. *Anal. Biochem.* **273** (2): 313-5.
- Matthews, R.T., Ferrante, R.J., Klivenyi, P., Yang, L., Klein, A.M., Mueller, G., Kaddurah-Daouk, R. and Beal, M.F. (1999) Creatine and cyclocreatine attenuate MPTP neurotoxicity. *Exp. Neurol.* **57** (1): 142-9.
- Matsumine, H., Saito, M., Shimoda-Matsubayashi, S., Tanaka, H., Ishikawa, A., Nakagawa-Hattori, Y., Yokochi, M., Kobayashi, T., Igarashi, S., Takano, H., Sanpei, K., Koike, R., Mori, H., Kondo, T., Mizutani, Y., Schäffer, A.A., Yamamura, Y., Nakamura, S., Kuzuhara, S., Tsuji, S. and Mizuno, Y. (1997) Localization of a gene for an autosomal recessive form of juvenile Parkinsonism to chromosome 6q25.2-27. *Am. J. Hum. Genet.* **60** (3): 588-96.

- Mazzio, E.A., Reams, R.R. and Soliman, K.F. (2004) The role of oxidative stress, impaired glycolysis and mitochondrial respiratory redox failure in the cytotoxic effects of 6-hydroxydopamine in vitro. *Brain Res.* **1004** (1-2): 29-44.
- Mazzio, E. and Soliman, K.F. (2003) The role of glycolysis and gluconeogenesis in the cytoprotection of neuroblastoma cells against 1-methyl 4-phenylpyridinium ion toxicity. *Neurotoxicology* **24** (1): 137-47.
- McGeer, E.G. and McGeer, P.L. (1998). The importance of inflammatory mechanisms in Alzheimer disease. *Exp. Gerontol.* **33** (5): 371-8. Review.
- McGeer, P.L., Itagaki, S., Boyes, B.E. and McGeer, E.G. (1988) Reactive microglia are positive for HLA-DR in the substantia nigra of Parkinson's and Alzheimer's disease brains. *Neurology* **38** (8): 1285-91.
- McKenna, M.C., Stevenson, J.H., Huang, X. and Hopkins, I.B. (2000) Differential distribution of the enzymes glutamate dehydrogenase and aspartate aminotransferase in cortical synaptic mitochondria contributes to metabolic compartmentation in cortical synaptic terminals. *Neurochem. Int.* **37** (2-3): 229-41. Review.
- McNaught, K.P., Mytilineou, C., JnoBaptiste, R., Yabut, J., Shashidaran, P., Jenner, P. and Olanow, C.W. (2002). Impairment of the Ubiquitin-proteasome System causes Dopaminergic Cell Death and Inclusion Body Formation in Ventral Mesencephalic Cultures. *Journal of Neurochemistry* . **81**, 301-306.
- McNaught, K.S. and Jenner, P. (2001) Proteasomal function is impaired in substantia nigra in Parkinson's disease. *Neurosci. Lett.* **297** (3): 191-4.
- Meimaridou, E., Gooljar, S.B. and Chapple, J.P. (2009) From hatching to dispatching: the multiple cellular roles of the Hsp70 molecular chaperone machinery. *J. Mol. Endocrinol.* **42** (1): 1-9. Review.
- Meredith, G.E., Totterdell, S., Beales, M. and Meshul, C.K. (2009) Impaired glutamate homeostasis and programmed cell death in a chronic MPTP mouse model of Parkinson's disease. *Exp. Neurol.* **219** (1): 334-40.
- Merril, C.R., Switzer, R.C. and Van Keuren, M.L. (1979) Trace polypeptides in cellular extracts and human body fluids detected by two-dimensional electrophoresis and a highly sensitive silver stain. *Proc. Natl. Acad. Sci. U.S.A.* **76** (9): 4335-9.
- Miller, Karl J. (1998) Overview of the Pathway.
- Mitra, S. and Finkbeiner, S. (2008) The ubiquitin-proteasome pathway in Huntington's disease. *Scientific WorldJournal.* **8**: 421-33. Review.
- Mizuno, Y., Sone, N. and Saitoh, T. (1987) Effects of 1-methyl-4-phenyl-1,2,3,6-tetrahydropyridine and 1-methyl-4-phenylpyridinium ion on activities of the enzymes in the electron transport system in mouse brain. *J. Neurochem.* **48** (6): 1787-93.
- Mootha, V.K., Bunkenborg, J., Olsen, J.V., Hjerrild, M., Wisniewski, J.R., Stahl, E., Bolouri, M.S., Ray, H.N., Sihag, S., Kamal, M., Patterson, N., Lander, E.S., Mann, M. (2003) Integrated analysis of protein composition, tissue diversity, and gene regulation in mouse mitochondria. *Cell.* **115** (5): 629-40.
- Mosmann, T. (1983) Rapid colorimetric assay for cellular growth and survival: application to proliferation and cytotoxicity assays. *J. Immunol. Methods* **65** (1-2): 55-63.
- Moxon, J.V., Padula, M.P., Herbert, B.R., Golledge, J. (2009) Challenges, current status and future perspectives of proteomics in improving understanding, diagnosis and treatment of vascular disease. *Eur. J. Vasc. Endovasc. Surg.* **38** (3): 346-55. Review.

- Moyes, C.D., Schulte, P.M. and Hochachka, P.W. (1992) Recovery metabolism of trout white muscle: role of mitochondria. *Am. J. Physiol.* **262** (2 Pt 2): R295-304.
- Murray, J., Yonally, S., Aggeler, R., Marusich, M.F. and Capaldi, R.A. (2004) Focused proteomics: towards a high throughput monoclonal antibody-based resolution of proteins for diagnosis of mitochondrial diseases. *Biochim. Biophys. Acta.* **1659** (2-3): 206-11.
- Nakamura, M., Yamada, M., Ohsawa, T., Morisawa, H., Nishine, T., Nishimura, O., and Toda, T. (2006) Phosphoproteomic profiling of human SH-SY5Y neuroblastoma cells during response to 6-hydroxydopamine-induced oxidative stress. *Biochim. Biophys. Acta.* **1763** (9): 977-89.
- Narotzky, R. and Bondareff, W. (1974) Biogenic amines in cultured neuroblastoma and astrocytoma cells. *J. Cell Biol.* **63** (1): 64-70.
- Neutzner, A., Youle, R.J. and Karbowski, M. (2007) Outer mitochondrial membrane protein degradation by the proteasome. *Novartis Found Symp.* **287**: 4-14; discussion 14-20. Review.
- Nicklas, W.J., Vyas, I. and Heikkila, R.E. (1985) Inhibition of NADH-linked oxidation in brain mitochondria by 1-methyl-4-phenyl-pyridine, a metabolite of the neurotoxin, 1-methyl-4-phenyl-1,2,5,6-tetrahydropyridine. *Life Sci.* **36** (26): 2503-8.
- Niquet, J., Seo, D.W. and Wasterlain, C.G. (2006) Mitochondrial pathways of neuronal necrosis. *Biochem. Soc. Trans.* **34** (Pt 6): 1347-51.
- Novikova, L., Garris, B.L., Garris, D.R. and Lau, Y.S. (2006) Early signs of neuronal apoptosis in the substantia nigra pars compacta of the progressive neurodegenerative mouse 1-methyl-4-phenyl-1,2,3,6-tetrahydropyridine/probenecid model of Parkinson's disease. *Neuroscience.* **140** (1): 67-76.
- Obata, T. and Yamanaka, Y. (2001) Nitric oxide enhances MPP(+)-induced hydroxyl radical generation via depolarization activated nitric oxide synthase in rat striatum. *Brain Res.* **902** (2): 223-8.
- O'Farrell, P.H. (1975) High resolution two-dimensional electrophoresis of proteins. *J. Biol. Chem.* **250** (10): 4007-21.
- Olanow, C.W., Perl, D.P., DeMartino, G.N. and McNaught, K.P. (2004). Lewy-Body formation is an Aggresome-related Process: a Hypothesis. *Lancet Neurol.* **3** (8), 496-503, Review.
- Olanow, C.W. and Tatton, W.G. (1999) Etiology and pathogenesis of Parkinson's disease. *Annu. Rev. Neurosci.* **22**: 123-44. Review.
- Orrenius, S. (2004) Mitochondrial regulation of apoptotic cell death. *Toxicology Letters* **149** (1-3): 19-23. Review.
- Ott, M., Norberg, E., Zhivotovsky, B. and Orrenius, S. (2009) Mitochondrial targeting of tBid/Bax: a role for the TOM complex? *Cell Death Differ.* **16** (8): 1075-82.
- Pagliarini, D.J., Calvo, S.E., Chang, B., Sheth, S.A., Vafai, S.B., Ong, S.E., Walford, G.A., Sugiana, C., Boneh, A., Chen, W.K., Hill, D.E., Vidal, M., Evans, J.G., Thorburn, D.R., Carr, S.A., Mootha, V.K. A mitochondrial protein compendium elucidates complex I disease biology. *Cell* **134** (1): 112-23.
- Palacino, J.J., Sagi, D., Goldberg, M.S., Krauss, S., Motz, C., Wacker, M., Klose, J. and Shen, J. (2004) Mitochondrial dysfunction and oxidative damage in parkin-deficient mice. *J. Biol. Chem.* **279** (18): 18614-22.
- Parcellier, A., Tintignac, L.A., Zhuravleva, E. and Hemmings, B.A. (2008) PKB and the mitochondria: AKTing on apoptosis. *Cell. Signal.* **20** (1):21-30. Review.
- Parone, P.A., James, D. and Martinou, J.C. (2002) Mitochondria: regulating the inevitable. *Biochimie* **84** (2-3): 105-11. Review.

- Pastorino, J.G., Hoek, J.B. and Shulga, N. (2005) Activation of glycogen synthase kinase 3beta disrupts the binding of hexokinase II to mitochondria by phosphorylating voltage-dependent anion channel and potentiates chemotherapy-induced cytotoxicity. *Cancer Res.* **65** (22): 10545-54.
- Patton, W.F. (2002) Detection technologies in proteome analysis. *J. Chromatogr. B Analyt. Technol. Biomed. Life Sci.* **771** (1-2): 3-31. Review.
- Paulson, L., Martin, P., Nilsson, C.L., Ljung, E., Westman-Brinkmalm, A., Blennow, K. and Davidsson, P. (2004) Comparative proteome analysis of thalamus in MK-801-treated rats. *Proteomics* **4** (3): 819-25.
- Perez-De La Cruz, V. and Santamaria, A. (2007) Integrative hypothesis for Huntington's disease: a brief review of experimental evidence. *Physiol. Res.* **56** (5): 513-26. Review.
- Pertoft, H. (2000) Fractionation of cells and subcellular particles with Percoll. *J. Biochem. Biophys. Methods.* **44** (1-2): 1-30. Review.
- Petit-Paitel, A., Brau, F., Cazareth, J. and Chabry, J. (2009) Involvement of cytosolic and mitochondrial GSK-3beta in mitochondrial dysfunction and neuronal cell death of MPTP/MPP-treated neurons. *PLoS One* **4** (5): e5491.
- Pieczenik, S.R. and Neustadt, J. (2007) Mitochondrial dysfunction and molecular pathways of disease. *Exp. Mol. Pathol.* **83** (1): 84-92
- Prashad, N. and Rosenberg, R.N. (1978) Induction of cyclic AMP-binding proteins by dibutyryl cyclic AMP in mouse neuroblastoma cells. *Biochim. Biophys. Acta.* **539** (4): 459-69.
- Premkumar, A. and Simantov, R. (2002) Mitochondrial voltage-dependent anion channel is involved in dopamine-induced apoptosis. *J. Neurochem.* **82** (2): 345-52.
- Pridgeon, J.W., Olzmann, J.A., Chin, L.S., Li, L. (2007) PINK1 protects against oxidative stress by phosphorylating mitochondrial chaperone TRAP1. *PLoS Biol.* **5** (7): e172.
- Przedborski, S., Jackson-Lewis, V., Naini, A.B., Jakowec, M., Petzinger, G., Miller, R. and Akram, M. (2001) The parkinsonian toxin 1-methyl-4-phenyl-1,2,3,6-tetrahydropyridine (MPTP): a technical review of its utility and safety. *J. Neurochem.* **76** (5): 1265-74. Review.
- Przedborski, S. and Vila, M. (2001) The last decade in Parkinson's disease research. Basic sciences. *Adv. Neurol.* **86**: 177-86. Review.
- Rabilloud, T., Luche, S., Santoni, V. and Chevallet M. (2007) Detergents and chaotropes for protein solubilization before two-dimensional electrophoresis. *Methods Mol. Biol.* **355**: 111-9.
- Quigney, D.J., Gorman, A.M. and Samali, A. (2003) Heat shock protects PC12 cells against MPP+ toxicity. *Brain Res.* **993** (1-2): 133-9.
- Raggiacchi, R., Lorenzetto, C., Diodato, E., Caricasole, A., Gotta, S. and Terstappen, G.C. (2006) Detection of phosphorylation patterns in rat cortical neurons by combining phosphatase treatment and DIGE technology. *Proteomics* **6** (3): 748-56.
- Ramsay, R.R., Kowal, A.T., Johnson, M.K., Salach, J.I. and Singer, T.P. (1987) The inhibition site of MPP+, the neurotoxic bioactivation product of 1-methyl-4-phenyl-1,2,3,6-tetrahydropyridine is near the Q-binding site of NADH dehydrogenase. *Arch. Biochem. Biophys.* **259** (2): 645-9.
- Ramsay, R.R., Salach, J.I. and Singer, T.P. (1986) Uptake of the neurotoxin 1-methyl-4-phenylpyridine (MPP+) by mitochondria and its relation to the inhibition of the mitochondrial oxidation of NAD+-linked substrates by MPP+. *Biochem. Biophys. Res. Commun.* **134** (2): 743-8.
- Reifschneider, N.H., Goto, S., Nakamoto, H., Takahashi, R., Sugawa, M., Dencher, N.A. and Krause, F. (2006) Defining the mitochondrial proteomes from five rat organs in a physiologically significant context using 2D blue-native/SDS-PAGE. *J. Proteome Res.* **5** (5): 1117-32.

- Rosenfeld, J., Capdevielle, J., Guillemot, J.C. and Ferrara, P. (1992) In-gel digestion of proteins for internal sequence analysis after one- or two-dimensional gel electrophoresis. *Anal. Biochem.* **203** (1): 173-9.
- Rossi, D. and Gaidano, G. (2003) Messengers of cell death: apoptotic signaling in health and disease. *Haematologica* **88** (2): 212-8. Review.
- Rostovtseva, T.K. and Bezrukov, S.M. (2008) VDAC regulation: role of cytosolic proteins and mitochondrial lipids. *J. Bioenerg. Biomembr.* **40** (3): 163-70.
- Roth, M., Zhong, J., Tamm, M. and Szilard, J. (2009) Mesothelioma cells escape heat stress by upregulating Hsp40/Hsp70 expression via mitogen-activated protein kinases. *J. Biomed. Biotechnol.* **2009**: 451084.
- Rozenal, R., Gebhard, D., Padin, C., Urban, M., Wu, J.Y., Spray, D.C. and Chiu, F.C. (1995) Purification of cell populations from human fetal brain using flow cytometric techniques. *Brain Res. Dev. Brain Res.* **85** (2): 161-70.
- Rubinsztein, D.C. (2006) The roles of intracellular protein-degradation pathways in neurodegeneration. *Nature.* **443** (7113): 780-6. Review.
- Salach, J.I., Singer, T.P., Castagnoli, N. Jr and Trevor, A. (1984) Oxidation of the neurotoxic amine 1-methyl-4-phenyl-1,2,3,6-tetrahydropyridine (MPTP) by monoamine oxidases A and B and suicide inactivation of the enzymes by MPTP. *Biochem. Biophys. Res. Commun.* **125** (2): 831-5.
- Salinas, M., Martín, D., Alvarez, A. and Cuadrado, A. (2001) Akt1/PKBalpha protects PC12 cells against the parkinsonism-inducing neurotoxin 1-methyl-4-phenylpyridinium and reduces the levels of oxygen-free radicals. *Mol. Cell. Neurosci.* **17** (1): 67-77.
- Sanz, E., Quintana, A., Battaglia, V., Toninello, A., Hidalgo, J., Ambrosio, S., Valoti, M., Marco, J.L., Tipton, K.F., Unzeta, M. (2008) Anti-apoptotic effect of Mao-B inhibitor PF9601N [N-(2-propynyl)-2-(5-benzyloxy-indolyl) methylamine] is mediated by p53 pathway inhibition in MPP(+)-treated SH-SY5Y human dopaminergic cells. *J. Neurochem.* **105**: 2404-417.
- Sawada, H. and Shimohama, S. (1999) MPP(+) and glutamate in the degeneration of nigral dopaminergic neurons. *Parkinsonism Relat. Disord.* **5** (4): 209-15.
- Schapira, A.H. (2006) Mitochondrial disease. *Lancet* **368** (9529): 70-82.
- Schapira, A.H., Cooper, J.M., Dexter, D., Clark, J.B., Jenner, P., Marsden, C.D. (1990) Mitochondrial complex I deficiency in Parkinson's disease. *J. Neurochem.* **54** (3): 823-7.
- Scheffler, N.K., Miller, S.W., Carroll, A.K., Anderson, C., Davis, R.E., Ghosh, S.S. and Gibson, B.W. (2001) Two-dimensional electrophoresis and mass spectrometric identification of mitochondrial proteins from an SH-SY5Y neuroblastoma cell line. *Mitochondrion* **1** (2): 161-79.
- Schubert, D., Humphreys, S., Baroni, C. and Cohn, M. (1969) In vitro differentiation of a mouse neuroblastoma. *Proc. Natl. Acad. Sci. U.S.A.* **64** (1): 316-23
- Schwartz, H., Carter, J.M., Abdudurehman, M., Russ, M., Buerke, U., Schlitt, A., Müller-Werdan, U., Prondzinsky, R., Werdan, K. and Buerke, M. (2007) Myocardial ischemia/reperfusion causes VDAC phosphorylation which is reduced by cardioprotection with a p38 MAP kinase inhibitor. *Proteomics.* **7** (24): 4579-88.
- Seniuk, N.A., Tatton, W.G. and Greenwood, C.E. (1990) Dose-dependent destruction of the coeruleus-cortical and nigral-striatal projections by MPTP. *Brain Res.* **10;527**(1):7-20. Erratum in: *Brain Res.* (1990) **535** (2): 360. *Brain Res.* (1991) **552** (2): 357.
- Shimada, H., Hirai, K.I., Simamura, E., Hatta, T., Iwakiri, H., Mizuki, K., Hatta, T., Sawasaki, T., Matsunaga, S., Endo, Y. and Shimizu S. (2009) Paraquat toxicity induced by voltage-dependent anion channel 1 acting as an NADH-dependent oxidoreductase. *J. Biol. Chem.* **284** (42): 28642-9.

- Shimizu, S., Matsuoka, Y., Shinohara, Y., Yoneda, Y. and Tsujimoto, Y. (2001) Essential role of voltage-dependent anion channel in various forms of apoptosis in mammalian cells. *J. Cell Biol.* **152** (2): 237-50.
- Shimoke, K., Kudo, M., Ikeuchi, T. (2003) MPTP-induced reactive oxygen species promote cell death through a gradual activation of caspase-3 without expression of GRP78/Bip as a preventive measure against ER stress in PC12 cells. *Life Sci.* **73** (5): 581-93.
- Shindo, H., Thomas, T.P., Larkin, D.D., Karihaloo, A.K., Inada, H., Onaya, T., Stevens, M.J. and Greene, D.A. (1996) Modulation of basal nitric oxide-dependent cyclic-GMP production by ambient glucose, myo-inositol, and protein kinase C in SH-SY5Y human neuroblastoma cells. *J. Clin. Invest.* **97** (3): 736-45.
- Shinohara, Y., Ishida, T., Hino, M., Yamazaki, N., Baba, Y. and Terada, H. (2000) Characterization of porin isoforms expressed in tumor cells. *Eur. J. Biochem.* **267** (19): 6067-73.
- Shoshan-Barmatz, V., Israelson, A., Brdiczka, D. and Sheu, S.S. (2006) The voltage-dependent anion channel (VDAC): function in intracellular signalling, cell life and cell death. *Curr. Pharm. Des.* **12** (18): 2249-70. Review.
- Singer, T.P., Ramsay, R.R., McKeown, K., Trevor, A. and Castagnoli, N.E. Jr (1988) Mechanism of the neurotoxicity of 1-methyl-4-phenylpyridinium (MPP+), the toxic bioactivation product of 1-methyl-4-phenyl-1,2,3,6-tetrahydropyridine (MPTP). *Toxicology* **49** (1): 17-23. Review.
- Smith, C.U.M. (2002). *Elements of Molecular Neurobiology*. Third edition, John Wiley & Sons LTD, chapters 1, 15, 21.
- Song, X., Perkins, S., Jortner, B.S. and Ehrich, M. (1997) Cytotoxic effects of MPTP on SH-SY5Y human neuroblastoma cells. *Neurotoxicology* **18** (2): 341-53.
- Sriram, K., Pai, K.S., Boyd, M.R. and Ravindranath, V. (1997) Evidence for generation of oxidative stress in brain by MPTP: in vitro and in vivo studies in mice. *Brain Res.* **749** (1): 44-52.
- Stasyk, T. and Huber, L.A. (2004) Zooming in: fractionation strategies in proteomics. *Proteomics.* **4** (12): 3704-16. Review.
- Suen, D.F., Norris, K.L., Youle, R.J. (2008) Mitochondrial dynamics and apoptosis. *Genes Dev.* **22** (12): 1577-90. Review.
- Szabados, T., Dul, C., Majtényi, K., Hargitai, J., Péntzes, Z., Urbanics, R. (2004) A chronic Alzheimer's model evoked by mitochondrial poison sodium azide for pharmacological investigations. *Behav. Brain Res.* **154** (1): 31-40.
- Takahashi, N., Miner, L.L., Sora, I., Ujike, H., Revay, R.S., Kostic, V., Jackson-Lewis, V., Przedborski, S. and Uhl, G.R. (1997) VMAT2 knockout mice: heterozygotes display reduced amphetamine-conditioned reward, enhanced amphetamine locomotion, and enhanced MPTP toxicity. *Proc. Natl. Acad. Sci. U.S.A.* **94** (18): 9938-43.
- Taylor, S.W., Fahy, E., Zhang, B., Glenn, G.M., Warnock, D.E., Wiley, S., Murphy, A.N., Gaucher, S.P., Capaldi, R.A., Gibson, B.W. and Ghosh, S.S. (2003a) Characterization of the human heart mitochondrial proteome. *Nat. Biotechnol.* **21** (3): 281-6.
- Taylor, S.W., Fahy, E. and Ghosh, S.S. (2003b) Global organellar proteomics. *Trends Biotech.* **21** (2): 82-8. Review.
- Teller, J.K., Fahien, L.A. and Valdivia, E. (1990) Interactions among mitochondrial aspartate aminotransferase, malate dehydrogenase, and the inner mitochondrial membrane from heart, hepatoma, and liver. *J. Biol. Chem.* **265** (32): 19486-94.
- Tetrud, J.W. and Langston, J.W. (1992) Tremor in MPTP-induced parkinsonism. *Neurology* **42** (2): 407-10.

- Thornberry, N.A., Rano, T.A., Peterson, E.P., Rasper, D.M., Timkey, T., Garcia-Calvo, M., Houtzager, V.M., Nordstrom, P.A., Roy, S., Vaillancourt, J.P., Chapman, K.T. and Nicholson, D.W. (1997) A combinatorial approach defines specificities of members of the caspase family and granzyme B. Functional relationships established for key mediators of apoptosis. *J. Biol. Chem.* **272** (29): 17907-11.
- Tomasello, F., Messina, A., Lartigue, L., Schembri, L., Medina, C., Reina, S., Thoraval, D., Crouzet, M., Ichas, F., De Pinto, V., De Giorgi, F. (2009) Outer membrane VDAC1 controls permeability transition of the inner mitochondrial membrane in cellulo during stress-induced apoptosis. *Cell Res.* **9** (12): 1363-76
- Towbin, H., Staehelin, T. and Gordon, J. (1979). Electrophoretic transfer of proteins from polyacrylamide gels to nitrocellulose sheets: Procedure and some applications. *Proceedings of the National Academy of Sciences USA* **76** (9), 4350-4354.
- Tsuji, T., Shiozaki, A., Kohno, R., Yoshizato, K. and Shimohama, S. (2002) Proteomic profiling and neurodegeneration in Alzheimer's disease. *Neurochem. Res.* **27** (10): 1245-53.
- Tsujimoto, Y. and Shimizu S. (2002) The voltage-dependent anion channel: an essential player in apoptosis. *Biochimie* **84** (2-3): 187-93. Review.
- Turski, L., Bressler, K., Rettig, K.J., Löschnann, P.A. and Wachtel, H. (1991) Protection of substantia nigra from MPP+ neurotoxicity by N-methyl-D-aspartate antagonists. *Nature* **349** (6308): 414-8.
- Twig, G., Hyde, B., Shirihai, O.S. (2008) Mitochondrial fusion, fission and autophagy as a quality control axis: the bioenergetic view. *Biochim. Biophys. Acta.* **1777** (9): 1092-7. Review.
- Valente, E.M., Abou-Sleiman, P.M., Caputo, V., Muqit, M.M., Harvey, K., Gispert, S., Ali, Z., Del Turco, D., Bentivoglio, A.R., Healy, D.G., Albanese, A., Nussbaum, R., González-Maldonado, R., Deller, T., Salvi, S., Cortelli, P., Gilks, W.P., Latchman, D.S., Harvey, R.J., Dallapiccola, B., Auburger, G., Wood, N.W. (2004) Hereditary early-onset Parkinson's disease caused by mutations in PINK1 *Science.* **304** (5674): 1158-60.
- Van Duijn, C.M., Dekker, M.C., Bonifati, V., Galjaard, R.J., Houwing-Duistermaat, J.J., Snijders, P.J., Testers, L., Breedveld, G.J., Horstink, M., Sandkuijl, L.A., van Swieten, J.C., Oostra, B.A. and Heutink, P. (2001) Park7, a novel locus for autosomal recessive early-onset parkinsonism, on chromosome 1p36. *Am. J. Hum. Genet.* **69** (3): 629-34.
- Vander Heiden, M.G., Li, X.X., Gottleib, E., Hill, R.B., Thompson, C.B., Colombini, M. (2001) Bcl-xL promotes the open configuration of the voltage-dependent anion channel and metabolite passage through the outer mitochondrial membrane. *J. Biol. Chem.* **276** (22): 19414-9.
- Van Laar, V.S. and Berman, S.B. (2009) Mitochondrial dynamics in Parkinson's disease. *Exp. Neurol.* **218** (2): 247-56. Review.
- Van Laar, V.S., Dukes, A.A., Cascio, M. and Hastings, T.G. (2008) Proteomic analysis of rat brain mitochondria following exposure to dopamine quinone: implications for Parkinson disease. *Neurobiol. Dis.* **29** (3): 477-89.
- Van Tijn, P., de Vrij, F.M., Schuurman, K.G., Dantuma, N.P., Fischer, D.F., van Leeuwen, F.W. and Hol, E.M. (2007) Dose-dependent inhibition of proteasome activity by a mutant ubiquitin associated with neurodegenerative disease. *J. Cell. Sci.* **120** (Pt 9): 1615-23.
- Villa, R.F., Arnaboldi, R., Ghigini, B. and Gorini, A. (1994) Parkinson-like disease by 1-methyl-4-phenyl-1,2,3,6-tetrahydropyridine (MPTP) toxicity in *Macaca fascicularis*: synaptosomal metabolism and action of dihydroergocriptine. *Neurochem. Res.* **19** (3): 229-36.
- Von Ahnen, O., Waterhouse, N.J., Kuwana, T., Newmeyer, D.D. and Green, D.R. (2000) The 'harmless' release of cytochrome c. *Cell Death Differ.* **7** (12): 1192-9. Review.

- Vyssokikh, M.Y. and Brdiczka, D. (2003) The function of complexes between the outer mitochondrial membrane pore (VDAC) and the adenine nucleotide translocase in regulation of energy metabolism and apoptosis. *Acta Biochim Pol.* **50** (2): 389-404. Review.
- Wasinger, V.C., Cordwell, S.J., Cerpa-Poljak, A., Yan, J.X., Gooley, A.A., Wilkins, M.R., Duncan, M.W., Harris, R., Williams, K.L., Humphery-Smith, I. (1995) Progress with gene-product mapping of the Mollicutes: *Mycoplasma genitalium*. *Electrophoresis.* **16** (7): 1090-4.
- Watabe, M. and Nakaki, T. (2007) ATP depletion does not account for apoptosis induced by inhibition of mitochondrial electron transport chain in human dopaminergic cells. *Neuropharmacology* **52** (2): 536-41.
- Weissman, J.S., Hohl, C.M., Kovalenko, O., Kashi, Y., Chen, S., Braig, K., Saibil, H.R., Fenton, W.A. and Horwich, A.L. (1995) Mechanism of GroEL action: productive release of polypeptide from a sequestered position under GroES. *Cell* **83** (4): 577-87.
- Werner, C.J., Heyny-von Haussen, R., Mall, G. and Wolf, S. (2008) Proteome analysis of human substantia nigra in Parkinson's disease. *Proteome Sci.* **14**; 6:8.
- Wu, E.Y., Smith, M.T., Bellomo, G. and Di Monte, D. (1990) Relationships between the mitochondrial transmembrane potential, ATP concentration, and cytotoxicity in isolated rat hepatocytes. *Arch. Biochem. Biophys.* **282** (2): 358-62.
- Xiong, Y., Ding, H., Xu, M. and Gao, J. (2009) Protective effects of asiatic acid on rotenone- or H<sub>2</sub>O<sub>2</sub>-induced injury in SH-SY5Y cells. *Neurochem. Res.* **34** (4): 746-54.
- Xu, L., Voloboueva, L.A., Ouyang, Y., Emery, J.F. and Giffard, R.G. (2009) Overexpression of mitochondrial Hsp70/Hsp75 in rat brain protects mitochondria, reduces oxidative stress, and protects from focal ischemia. *J. Cereb. Blood Flow Metab.* **29** (2): 365-74.
- Yamamoto, T., Yamada, A., Watanabe, M., Yoshimura, Y., Yamazaki, N., Yoshimura, Y., Yamauchi, T., Kataoka, M., Nagata, T., Terada, H. and Shinohara Y. (2006) VDAC1, having a shorter N-terminus than VDAC2 but showing the same migration in an SDS-polyacrylamide gel, is the predominant form expressed in mitochondria of various tissues. *J. Proteome Res.* **5** (12): 3336-44.
- Yang, L., Sun, M., Sun, X.M., Cheng, G.Z., Nicosia, S.V. and Cheng, J.Q. (2007) Akt attenuation of the serine protease activity of HtrA2/Omi through phosphorylation of serine 212. *J. Biol. Chem.* **282** (15):10981-7.
- Yang, L., Matthews, R.T., Schulz, J.B., Klockgether, T., Liao, A.W., Martinou, J.C., Penney, J.B. Jr, Hyman, B.T. and Beal, M.F. (1998) 1-Methyl-4-phenyl-1,2,3,6-tetrahydropyridine neurotoxicity is attenuated in mice overexpressing *Bcl-2*. *J. Neurosci.* **18** (20): 8145-52.
- Ye, C., Zhang, Y., Wang, W., Wang, J. and Li, H. (2008) Inhibition of neurite outgrowth and promotion of cell death by cytoplasmic soluble mutant huntingtin stably transfected in mouse neuroblastoma cells. *Neurosci. Lett.* **442** (1): 63-8.
- Yoo, B.C., Fountoulakis, M., Cairns, N. and Lubec, G. (2001) Changes of voltage-dependent anion-selective channel proteins VDAC1 and VDAC2 brain levels in patients with Alzheimer's disease and Down syndrome. *Electrophoresis* **22** (1): 172-9.
- Yuan, J., Lipinski, M. and Degtarev, A. (2003) Diversity in the mechanisms of neuronal cell death. *Neuron.* **40** (2): 401-13. Review.
- Zaid, H., Abu-Hamad, S., Israelson, A., Nathan, I., Shoshan-Barmatz, V. (2005) The voltage-dependent anion channel-1 modulates apoptotic cell death. *Cell Death Differ.* **12** (7): 751-60.
- Zang, L.Y. and Misra, H.P. (1992) Superoxide radical production during the autoxidation of 1-methyl-4-phenyl-2,3-dihydropyridinium perchlorate. *J. Biol. Chem.* **267** (25): 17547-52.

Zhang, F., Lin, X.J., Ji, L.N., Du, H.N., Tang, L., He, J.H., Hu, J. and Hu, H.Y. (2008) Assembly of alpha-synuclein fibrils in nanoscale studied by peptide truncation and AFM. *Biochem. Biophys. Res. Commun.* **368** (2): 388-94.

Zhang, L., Shimoji, M., Thomas, B., Moore, D.J., Yu, S.W., Marupudi, N.I., Torp, R., Torgner, I.A., Ottersen, O.P., Dawson, T.M. and Dawson, V.L. (2005) Mitochondrial localization of the Parkinson's disease related protein DJ-1: implications for pathogenesis. *Hum. Mol. Gen.* **14** (14): 2063-73.

Zhang, L., Pelech, S. and Uitto, V.J. (2004) Bacterial GroEL-like heat shock protein 60 protects epithelial cells from stress-induced death through activation of ERK and inhibition of caspase 3. *Exp. Cell Res.* **292** (1): 231-40.

Zhao, X., Li, Q., Zhao, L. and Pu, X. (2007) Proteome analysis of the substantia nigra and striatal tissue in mouse MPTP model of Parkinson's disease. *Proteomics Clin. Appl.* **1**: 1556-1569.

Zhou, X.W., Winblad, B., Guan, Z. and Pei, J.J. (2009) Interactions Between Glycogen Synthase Kinase 3beta, Protein Kinase B, and Protein Phosphatase 2A in Tau Phosphorylation in Mouse N2a Neuroblastoma Cells. *J. Alzheimers Dis.* In Press.

Zhou, Y., Gu, G., Goodlett, D.R., Zhang, T., Pan, C., Montine, T.J., Montine, K.S., Aebersold, R.H. and Zhang, J. (2004) Analysis of alpha-synuclein-associated proteins by quantitative proteomics. *J. Biol. Chem.* **279** (37): 39155-64.

**Database Web sites referenced in the text:**

[www.expasy.org/tools](http://www.expasy.org/tools)

<http://www.matrixscience.com>

<http://www.uniprot.org>